Basics of Abdominal, Gynaecological, Obstetrics and Small Parts Ultrasound

Rajendra K. Diwakar
Editor

Springer

Basics of Abdominal, Gynaecological, Obstetrics and Small Parts Ultrasound

Rajendra K. Diwakar
Editor

Basics of Abdominal, Gynaecological, Obstetrics and Small Parts Ultrasound

Springer

Editor
Rajendra K. Diwakar
Department of Radio-diagnosis
C.C.M. Medical College & Hospital
Durg
India

ISBN 978-981-10-4872-2 ISBN 978-981-10-4873-9 (eBook)
https://doi.org/10.1007/978-981-10-4873-9

Library of Congress Control Number: 2017961727

Printed on acid-free paper

This Springer imprint is published by Springer Nature
The registered company is Springer Nature Singapore Pte Ltd.
The registered company address is: 152 Beach Road, #21-01/04 Gateway East, Singapore 189721, Singapore

This book is dedicated to
my late father Mr. K. C. Diwakar
and
my late mother Smt. K. B. Diwakar

Preface

This is yet another attempt by me in writing a book. More than three decades of experience in the field of ultrasound practice prompted me to venture for this book. I thought that it would be most appropriate to bring out a short book for the newcomer radiologists, residents in radiodiagnosis, obstetricians and gynaecologists engaged in practising sonography, who are keen to have knowledge or who intend to improve their diagnostic capabilities for better management of patients. This book, I hope, will be able to provide answers to so many frequently asked questions. Those who are engaged in basic ultrasound can use this concise book to improve their skill and as a ready reference in case of any doubt or when a difficult situation is faced at the time of conducting the ultrasound examination. This book cannot replace textbooks. Nonetheless, if only a few feel that they have benefitted by reading this book, the purpose of bringing out this book will be fulfilled.

Durg, India — Rajendra K. Diwakar

Acknowledgements

To my granddaughter Reya, my son-in-law Peiyush and my daughter Prachi who inspired me to begin writing a book which has seen the light of the day.

To my wife Kirti whose constant encouragement was the sole driving force for me to bring out this book as early as possible.

To my son Rakesh who acquainted me with the use of a laptop.

To Dr. Shiv Chandrakar, chairman, and Dr. Mrs. Sunita Chandrakar, director, C.C.M. Medical College, Durg, for their support.

To Dr. M. K. Dwivedi for his valuable guidance to complete the book.

To all my friends, my well-wishers and my patients for everything they have contributed in bringing out this book.

Last but not the least, to Springer for encouraging me by accepting the book for publication.

Contents

1 Introduction and Physics of Ultrasound 1
R.K. Diwakar

2 Abdominal Ultrasound 13
M.K. Dwivedi

3 Gynaecologic Ultrasound 57
R.K. Diwakar

4 Obstetric Ultrasound 77
R.K. Diwakar

5 Colour Doppler Sonography in Obstetrics 121
M.K. Dwivedi

6 Chromosomal Abnormalities 127
M.K. Dwivedi

7 Ultrasound of Small Parts and Superficial Organs 133
R.K. Diwakar

8 Neonatal Cranial Ultrasound 147
R.K. Diwakar

9 Ultrasound-Guided Biopsy, Aspiration and Fine Needle Aspiration Cytology 153
M.K. Dwivedi

Appendix A 155

Appendix B 157

About the Editor

Dr. Rajendra Kumar Diwakar
MBBS, MD (Radiology), 1976

Working Experience:

1. Senior Specialist, Dept. of Radiodiagnosis, JLN Hospital & Research Centre, Bhilai Steel Plant, Steel Authority of India Ltd., Bhilai, Durg (CG), India, from 1977 to 1992
2. Visiting Consultant, Radiodiagnosis, C.C.M. Hospital, Nehru Nagar, Bhilai, Durg (CG), India, 2000–2010
3. Present Assignment: Assistant Professor, Dept. of Radiodiagnosis, C.C.M. Medical & Hospital, Kachandur, Durg (CG), India, 2013 till today

Rajendra K. Diwakar is the recipient of the prestigious Dr. Ashok Mukherjee Memorial Oration Award in 1988 in the Annual Congress of the Indian Radiological and Imaging Association, India. He was honoured with the Dr. D. C. Sen Gold Medal in 1987. He has published many scientific papers in various national and international journals.

He has worked as senior radiologist for 12 years in JLN Hospital & Research Centre, Bhilai Steel Plant, Sail, Bhilai, in the Department of Radiodiagnosis. At present, he is a faculty member and assistant professor in the Department of Radiodiagnosis in Chandulal Chandrakar Memorial Medical College & Hospital, Durg (CG), India.

About the Contributor

Dr. M. K. Dwivedi
Assistant Professor, Dept. of Radiodiagnosis
CM Medical College & Hospital, Kachandur, Durg (CG), India-490024
MD (Radiology), 1988, Govt. Medical College, Jabalpur, Rani Durgavati University, Jabalpur (M.P.), India

Major Scientific Papers Published

1. Management of severe hemoptysis due to pulmonary tuberculosis by bronchial artery embolisation. IJRI, 1999; vol 9 (4).165–168
2. CT findings of descending necrotising mediastinitis. IJRI, 2001; vol 11(3):131–134
3. Efficacy of partial splenic artery embolisation in the management of hypersplenism. IJRI, 2002; vol 12 (3). 371–374
4. Efficacy of fallopian tubal catheterization in treatment of infertility. IJRI, 2005; vol 1(4). 521–523

Working Experience:

Director and Head of the Department of Radiodiagnosis, JLN Hospital & Research Centre, Bhilai Steel Plant, Steel Authority of India Ltd., Bhilai, Durg (CG), India.490020 [1989-2016]

Introduction and Physics of Ultrasound

1

R.K. Diwakar

Abstract

The detection and display of acoustic energy reflected from interfaces within the body form the basis of all ultrasound applications. Knowledge of ultrasound physics, range of frequency of transducer and propagation of sound waves in human tissue are essential to choose the proper ultrasound probe of suitable frequency to perform high-quality two-dimensional greyscale and flow parameters. The images that are free from artefacts avoid pitfalls and error in diagnosis, thus increasing the examination skills and diagnostic capabilities and maximum gain from the state-of-the-art ultrasound technology.

The sound energy used in diagnostic ultrasonography is free from any biological hazards. However, because of the thermal effect and the risk of cavitation, it is recommended that the proper frequency of ultrasound transducer should be used keeping the examination time as minimal as possible without affecting the quality of the examination. The American Society in Ultrasound Medicine recommendations are adhered to.

Medical ultrasound or diagnostic ultrasound or sonography is synonym. It is also called greyscale imaging, 2D imaging or B-mode imaging. The high-frequency sound waves, in the range of 2–20 MHz, are used as a source of energy. They are sent inside the human body, and the returning signals are received to produce an image on the monitor or screen of ultrasound equipment. Interpretation of the image is used in making a diagnosis.

R.K. Diwakar
Department of Radio-Diagnosis, C.C.M. Medical College & Hospital, Durg, Chhattisgarh, India
e-mail: rkdiwakar49@yahoomail.co.in

Medical ultrasound uses the principle of propagation and reflection of sound waves. We have noticed that in a hall or a well or in front of a mountain, if the sound is produced, we hear the same sound after sometime as it comes back to us after striking the object. This is called echo (Fig. 1.1). This principle is used in sonar to locate the submarine or a sunken ship in the bottom of the sea or to find out the depth of the sea.

The propagation velocity of sound wave in common body tissue [1] is shown in the graph (Fig. 1.2).

The high-frequency sound waves which are inaudible to human ears are sent inside the body,

R.K. Diwakar (ed.), *Basics of Abdominal, Gynaecological, Obstetrics and Small Parts Ultrasound*,
https://doi.org/10.1007/978-981-10-4873-9_1

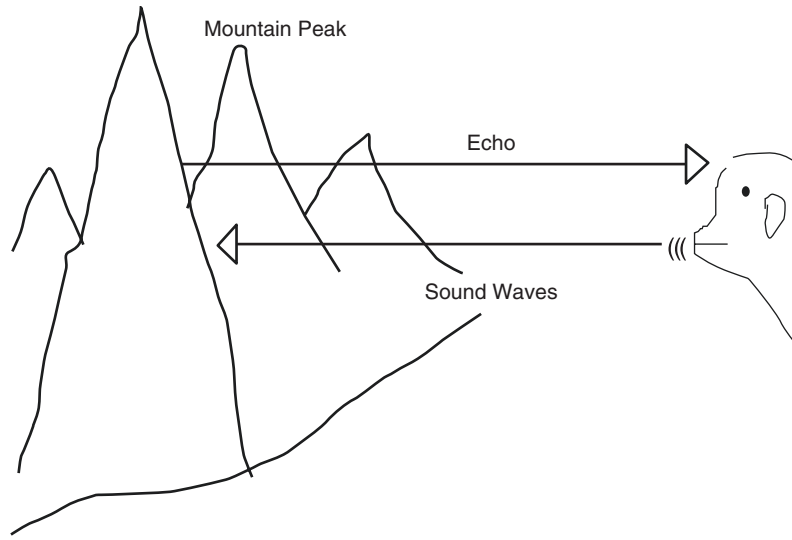

Fig. 1.1 Reflection of sound wave producing echo

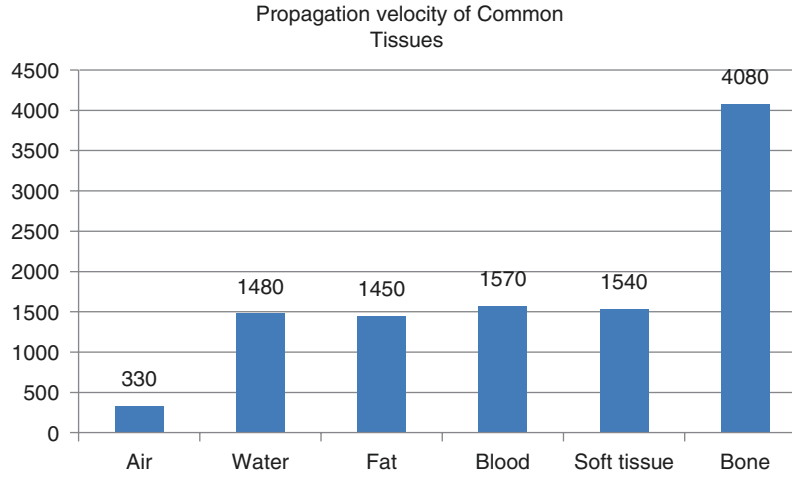

Fig. 1.2 Propagation velocity of sound wave in different body tissue

and returning sound waves received are sent to the computer for analysis to produce an image on the monitor of the ultrasound equipment. Sound below 2 MHz and above 20 MHz cannot be heard by the human ears. The ultrasound machine uses the sound waves in the range of 2–20 MHz. With higher frequency of sound waves, the penetration or depth is reduced. In other words higher-frequency probe is required for thinner patient or paediatric patients and for sonography of small parts or superficial organs such as thyroid, breast, testes and parotid gland and for colour Doppler study of vascular system. The lower-frequency probe is needed for thick or obese patient (for focus at a depth of 10 cm or more).

In the beginning the ultrasound machine used to be big in size. The technical developments and advancement in the computers in the past made it possible today to have as small as portable or laptop ultrasound machine with good resolution and software for calculation of different parameters.

As sound passes through the tissue, it loses energy through the transfer of energy to the body tissue. The sound wave propagates by reflection, refraction or scattering in the body tissue having different physical properties (acoustic interfaces) (Fig. 1.3).

As the acoustic energy moves through a uniform medium, the energy is transferred to the transmitting medium as heat. Attenuation is the result of the combined effects of absorption, scattering and reflections and is measured in decibel. Attenuation value for normal tissues is shown in the graph (Fig. 1.4).

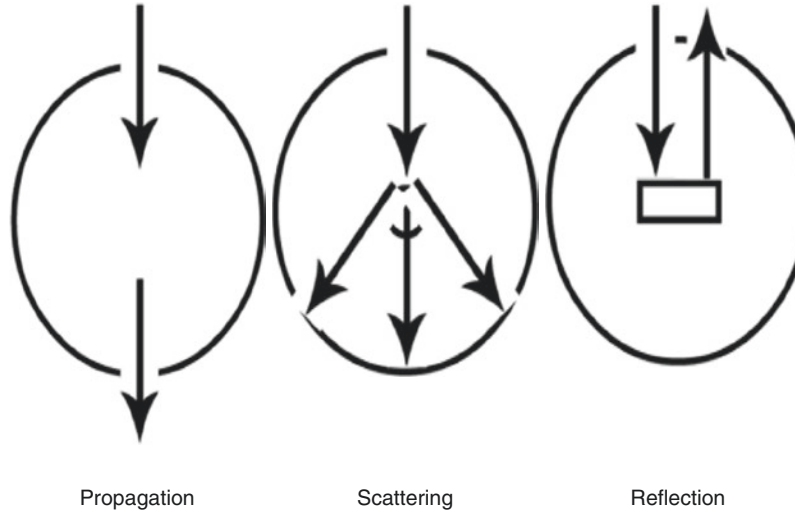

Fig. 1.3 Transmission of sound wave

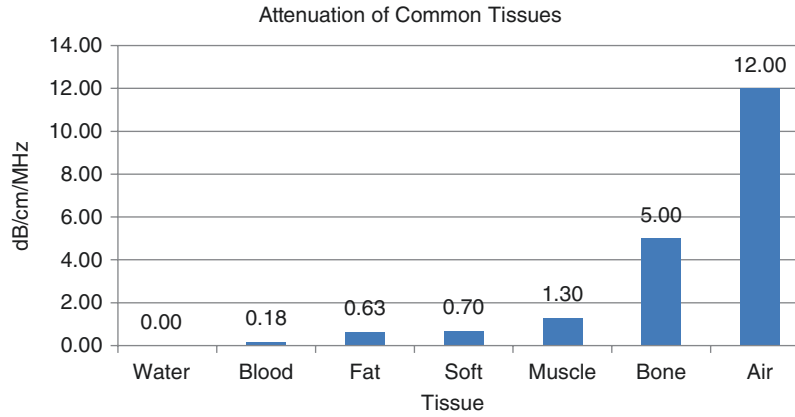

Fig. 1.4 Attenuation of sound wave in different body tissue

1.1 Ultrasound Equipment

The ultrasound equipment has a probe or transducer to produce high-frequency acoustic energy. After travelling inside the body, they are reflected from different interfaces of tissues within the body to generate high-resolution, two-dimensional greyscale images as well as flow parameters (in duplex system or colour Doppler equipment) which are displayed on the monitor of the equipment. Familiarity with these images and their interpretation enables one to make a diagnosis.

The propagation velocity of sound in human body is assumed to be 1540 m/s. The sound waves travel through different interfaces of the body tissue. The sound waves are reflected, refracted and scattered, or there is impedance. The acoustic impedance is produced by high density of the structure like bone, calculus or calcification so that almost all of the incident energy is reflected. The area posterior to such structures is seen black/echo-free; this is called posterior shadowing. The instrument has a transmitter and receiver of sound waves, i.e. the transducer. Ultrasound signals may be displayed in several ways [2] on the monitor in different modes as shown below.

1. *A-mode* (*amplitude mode*) in the form of oscilloscope. It was used in the earliest A-mode devices. However, it is still used in A-mode ultrasound of the eye (Fig. 1.5).
2. *Real-time greyscale or B-mode display* (*brightness mode*) provides two-dimensional (2D) image in the ultrasound of abdomen, pelvis and obstetric-gynaecologic applications (Fig. 1.6).
3. *M-mode* (motion mode) *ultrasound* displays echo amplitude and shows the position of moving reflectors. It is used for echocardiography and vascular study (Fig. 1.7).

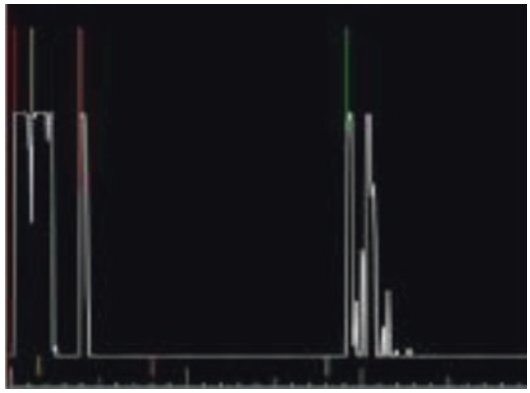

Fig. 1.5 A-mode display for eye ultrasound

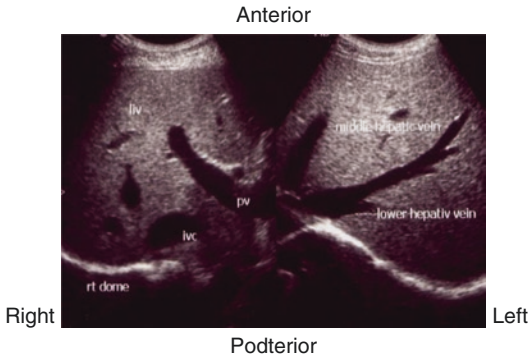

Fig. 1.6 B-mode/2D image in ultrasound

The image is stored on video. It can be printed on the film by laser or optical camera. The image can be recorded on thermal paper also. The quality of image depends on proper adjustment of brightness and contrast, lack of which results in unsatisfactory hard copy.

The ultrasound machines can broadly be classified into three types:

1. Black and white ultrasound machine for greyscale imaging having a convex or linear transducer
2. Colour ultrasound machine with convex, micro-convex or linear probe
3. Ultrasound equipments with 3D and 4D facility (Fig. 1.8)

The colour USG machines have facility for black and white ultrasound and also the colour imaging and flow studies.

The USG machine may have a single transducer (Fig. 1.9) or multiple transducers (Fig. 1.10). Certain models of ultrasound equipment may have multi-frequency probe, i.e. combination of 3, 3.5 and 5 MHz probe. Transvaginal probe may be in the range of 6–12 MHz (Fig. 1.11).

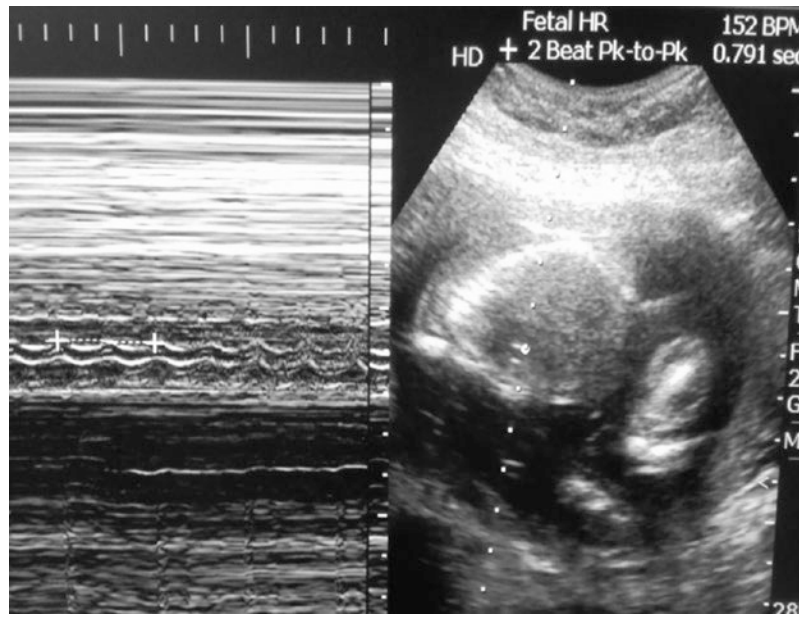

Fig. 1.7 M-mode recording for foetal heart calculation

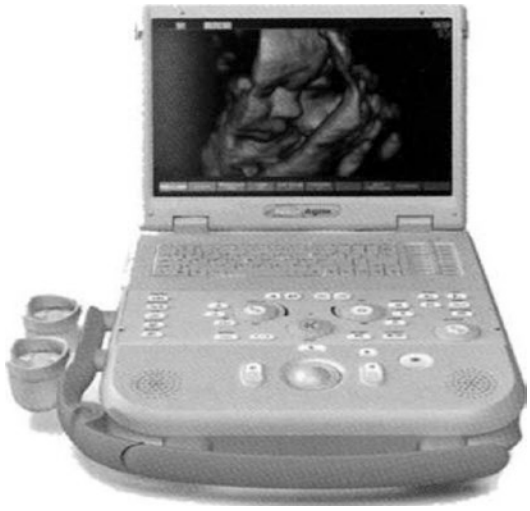

Fig. 1.8 Laptop colour USG with 3D image of foetal face

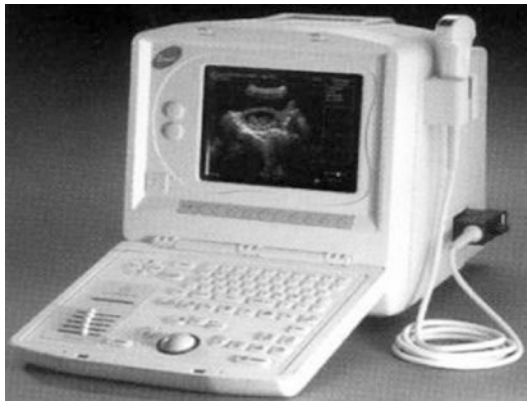

Fig. 1.9 Portable USG unit with single probe

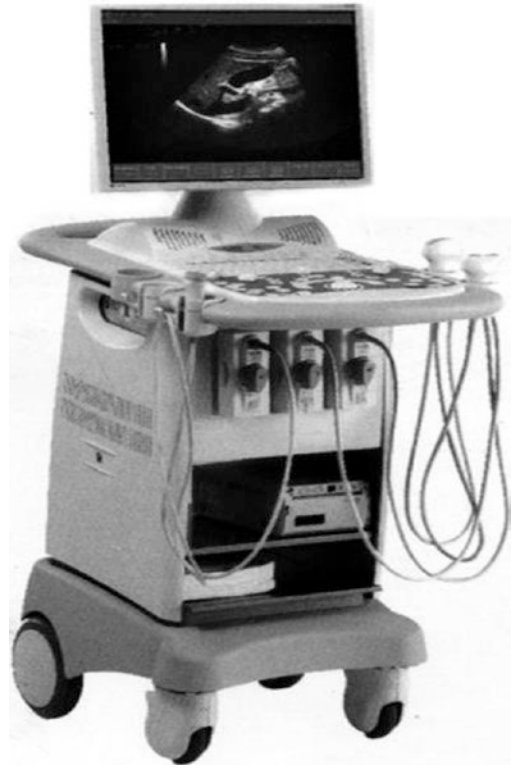

Fig. 1.10 Ultrasound equipment with multiple probes

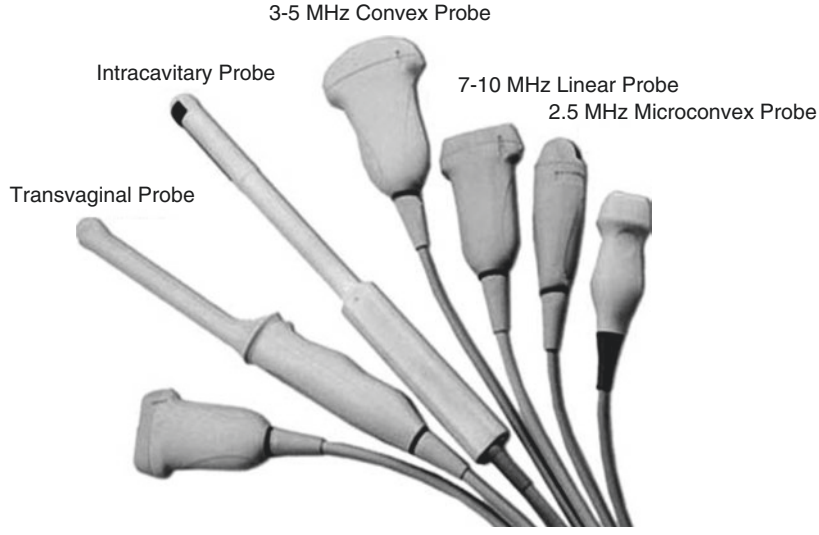

Fig. 1.11 Different shape and frequency of ultrasound probes with transvaginal probe

1.2 Frequency of Ultrasound Transducer

The frequency of the ultrasound transducer for various USG examinations is shown in Table 1.1.

The depth focus differs at various frequencies of transducer:

1. 2–2.5 MHz = 12–15 cm
2. 3–3.5 MHz = 9–10 cm
3. 5–7 MHz = 5–7 cm
4. 7 MHz = 2–3 cm
5. 10 MHz = 1–2 cm
6. 12 MHz = 1 cm

The arrangement of piezoelectric material in the transducer is called array. It may be linear array, curved array, phased array or annular array.

Linear array produces a rectangular shape image, while curved array produces a sector image (truncated cone shape).

Phased array transducer is used for the heart and intercostal scanning for liver/spleen since it is smaller in size.

Annular array transducer produces a uniform and highly focused beam.

The piezoelectric property of a material is the unique ability to respond to the action of an electric field by changing shape and also having the property of generating electric potentials when compressed. The naturally occurring piezoelectric material is quartz crystal. However, man-made piezoelectric crystal is having a mixture of lead zirconate, titanate and epoxy. The crystal is designed to vibrate in thickness mode or radial mode to produce high-frequency sound waves.

Table 1.1 Frequency of probe for different applications

Abdomen	3–3.5 MHz
Paediatrics	5 MHz
Breast	5–7 MHz
Eye, small parts (thyroid, parathyroid, testis)	7–10 MHz
Colour Doppler	5–10 MHz
Transvaginal sonography	6–12 MHz
Intracavitary probe	6–12 MHz
Paediatric echocardiography	1.8 MHz
Echocardiography adult	2–2.5 MHz

The resolution of ultrasound is described as its ability to resolve two objects adjacent to each other. The axial resolution applies to distinguish two objects that are along the direction of the beam. The lateral resolution applies to distinguish two objects that are perpendicular to the beam axis.

The near-field or Fresnel zone is near to the transducer, while the far-field or Fraunhofer zone is away from the transducer. The lateral resolution decreases rapidly in the depth as the beam begins to diverge in the far field. Hence, divergence is decreased by increasing the frequency. The major advantages of high frequency are that the beam is less divergent and generally produces less blurring giving better details.

1.2.1 Imaging Artefacts

Many imaging artefacts are induced by errors in scanning technique or improper use of the instrument and are preventable. Artefacts may suggest the presence of structures that are not present resulting in misdiagnosis, or they may cause important findings to be obscured.

Reverberation artefacts arise when the ultrasound signals reflect repeatedly between highly reflective interfaces that are usually not near the transducer. Reverberations may give false impression of solid structures in areas where only fluid is present.

Refraction causes bending of the sound beam so that targets not along the axis of the transducer are insonated. This may result in errors of measurements.

Shadowing results when there is a marked reduction in the intensity of ultrasound deep to a strong reflector or attenuator, and there may be partial or complete loss of information (Figs. 1.12, 1.13 and 1.14).

Another common cause of loss of image information is improper adjustment of system gain and TGC settings. Poor scanning angles, inadequate penetration, improper selection of transducer frequency and poor resolution may result in loss of significant information.

Doppler ultrasound. Conventional B-mode imaging uses pulse-echo transmission, detection

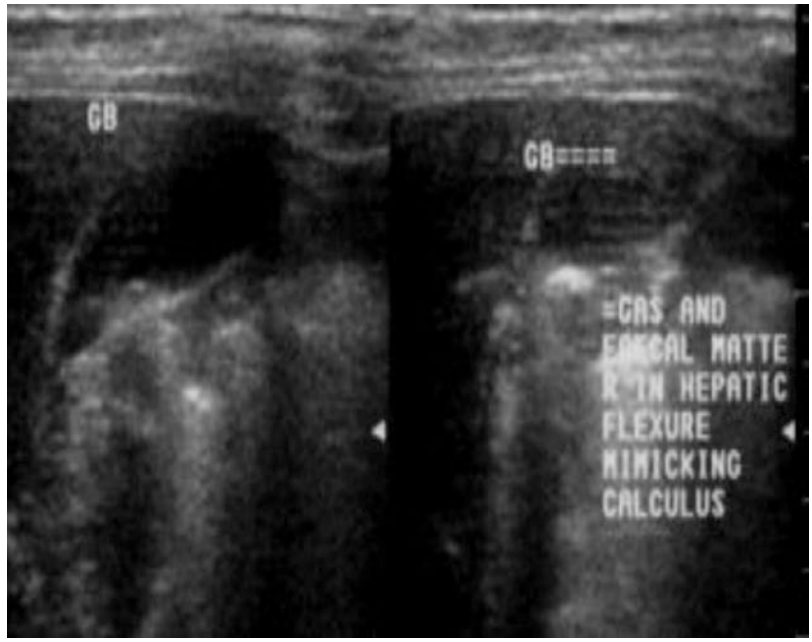

Fig. 1.12 Faecolith and gas in hepatic flexure mimicking a calculus, however, posterior shadowing is not remarkable

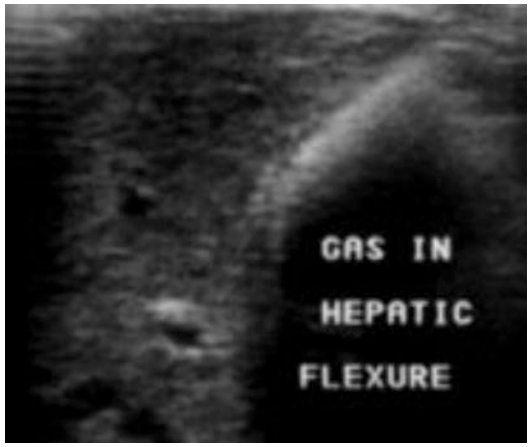

Fig. 1.13 Gas-distended hepatic flexure obscuring gall bladder

and display techniques. Brief pulses of ultrasound energy emitted by transducer are reflected from acoustic interfaces within the body. Precise timing allows determination of the depth from which the echo originates [3]. When pulsed wave ultrasound is reflected from an interface, the backscattered (reflected) signal contains amplitude, phase and frequency information [3]. When high-frequency sound impinges on a stationary interface, the reflected ultrasound has essentially the same frequency or wavelength as the transmitted sound. If, however, the reflecting interface is moving with respect to the sound beam emitted from the transducer, there is a change in the frequency of the sound, scattered by the moving object. This change in frequency is the result of *Doppler effect* [3]. The angle between the axis of flow and the incident ultrasound beam is called the *Doppler angle*. At Doppler angle of 90°, there is no relative movement of the target towards or away from the transducer (this is used in duplex instruments); no Doppler frequency shift is detected. Doppler measurements can be made at angles of less than 60°. (This is used in colour flow instruments.) The most common form of Doppler ultrasound to be used for radiologic applications is colour flow Doppler imaging [4] as shown in Figs. 1.15 and 1.16.

Harmonic imaging uses the same array transducers as conventional imaging, and only software changes are needed for this particular ultrasound system to suppress echoes from solid tissue as well as from red blood cells so that a microbubble of contrast agent in tissue vasculature can be identified.

Power mode Doppler (Figs. 1.17 and 1.18) is much less angle dependent without aliasing having a homogenous background colour, and there is increased sensitivity for flow detection, while

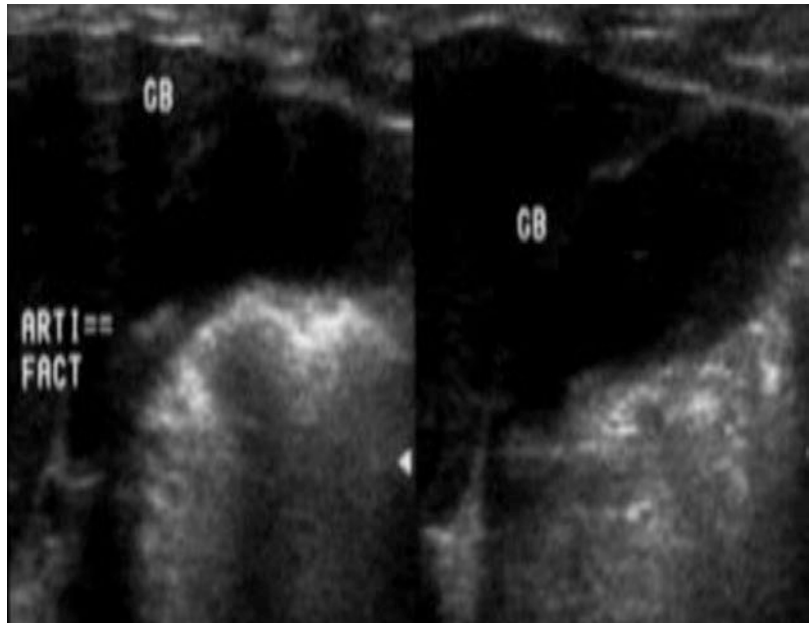

Fig. 1.14 Colonic contents superimposed on posterior wall of gall bladder giving false impression of calculi in the gall bladder

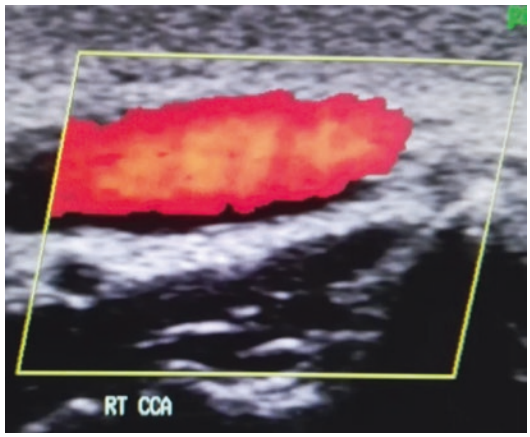

Fig. 1.15 Colour flow in common carotid artery

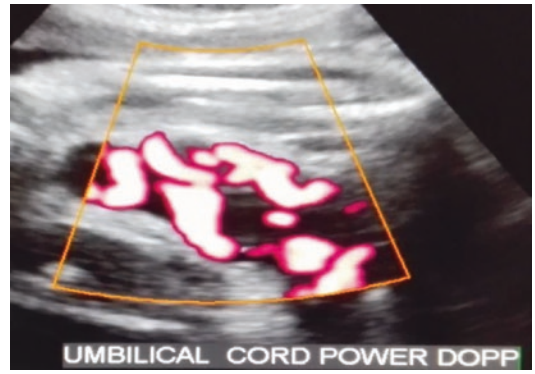

Fig. 1.17 Umbilical cord in power Doppler mode

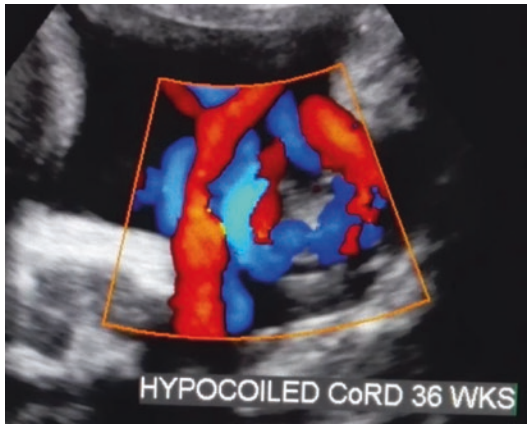

Fig. 1.16 Colour flow image of umbilical cord

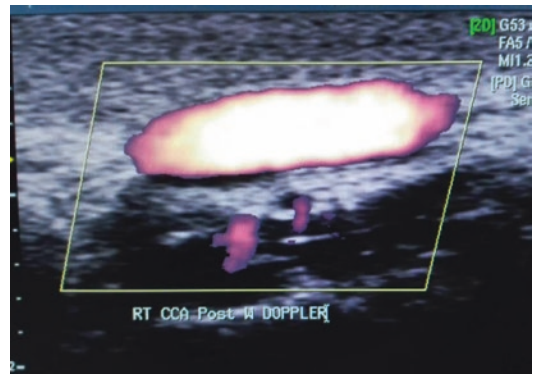

Fig. 1.18 Power Doppler carotid artery

colour flow Doppler imaging is angle dependent with aliasing and artefacts caused by noise and provides information related to flow direction and velocity.

In greyscale imaging, the lesion or abnormality depending on the echogenic property of the surrounding normal tissue can be divided into three types:

1. Hyper-echogenic (solid lesion, abscess, calcification/calculus, bone).
2. Hypo-echogenic/echo-free (fluid, cyst, haemorrhage after liquefaction).
3. Iso-echogenic having echogenic texture equal to surrounding tissues (uterine fibroid).
4. Complex echotexture: a lesion having complex echotexture may reveal combination of hypo-echogenic and different grades of hyper-echogenic texture and/or calcification or areas of haemorrhage.

1.3 Biological Hazards of Sonography

Ultrasound machines using sound waves as a source of energy in the range of 2–20 MHz are considered to be safe in various experiments by different workers. Diagnostic ultrasound has been in use since the 1950s. No adverse biological effects have ever been reported [5]. Therefore, ultrasound is considered to be hazard-free, safe and comparatively less expensive investigation which provides quick information which is important in making a decision for the management of patient. The ultrasound examination can be repeated safely whenever indicated. In ultrasound most of the sound energy is converted into heat resulting in tissue heating. The recommendations to decrease heating body tissue in ultrasound exposure are as follows [5]:

1. Use specific application as per body part.
2. Keep power low.
3. Focus at specific depth.
4. Use of fewer ultrasound pulse per second (PRF).
5. Decrease pulse length.
6. Use of appropriate transducer.
7. Increase receiver gain rather than power.

1.3.1 The Safety of Ultrasound [5, 6]

Diagnostic ultrasound uses the transducers which emit energies less than 20 m W/cm^2 which is far below the arbitrary hazard level of ultrasound exposures to tissues more than 100 m W/cm^2. However, specialised ultrasonographic investigations such as pulsed Doppler or transvaginal colour Doppler using energy output reaching up to 100 m W/cm^2 should be used for the shortest possible duration due to the concern of the proximity of the transducer to the foetus.

In general, ultrasound exposure at intensities usually produced by diagnostic ultrasound instruments has not been found to cause any harmful biological effects on the foetus or pregnant woman. It is the responsibility of the operator to complete the examination in shortest possible time. It is also required that the operator is adequately trained and is fully aware of the equipment. The principle of ALARA (as low as reasonably achievable) should be used to obtain necessary diagnostic information [6].

1.4 Preparation of Patient for Ultrasound Examination

The biggest advantage of sonography is that no specific preparation is required for the examination of small parts such as the eye, breast, neonatal brain, echocardiography and colour Doppler study of vascular system of the limbs, neck, aorta, kidneys, placenta, umbilical cord, etc. Overnight fasting, avoiding the morning tea/coffee and ingesting of three to four glasses of water 1–2 h before the ultrasound examination to produce moderate distension of urinary bladder are all that is required for satisfactory abdominal ultrasound examination. The overnight fasting is needed for the gall bladder distension so that its proper evaluation can be done. Whenever, there is unsatisfactory distension of the gall bladder, the patient is instructed to have fat-free diet on the previous day, and a repeat examination next day is required. Sonographic evaluation is not possible in some patients, and then CT has to be recommended.

For pelvic ultrasound, moderate distension of urinary bladder is essential to produce clear image because the bowel containing gas is displaced out of the imaging area. It should be remembered that in the air, the sound waves are conducted in the forward direction, and the sound waves returning towards the probe are reduced so that the quality of image is adversely affected.

The patients for obstetric sonography can take morning breakfast and tea/coffee so that the blood sugar level in the mother as well as in the foetus is maintained. This is important after the first trimester pregnancy when the foetal movements are evaluated for biophysical profile.

Precaution is taken to avoid over-distension of urinary bladder, because it may result in compression of the uterus, and sometimes the gestational sac in early pregnancy may be compressed and is not visualised. The over-distension of urinary bladder may also result in elongation of uterine cervix especially in cases being evaluated for incompetence of cervix.

1.4.1 Positions of Patient and Transducer for Ultrasound Examination

The patient lies supine on the examination table/couch. Proper exposure of the body part to be examined is done by removing the clothes, and a thin layer of jelly is spread on the skin of the part to be examined. The patient is asked to take normal respiration.

For ultrasound examination of the abdomen, patient lies supine, and the examination is usually begun from upper abdomen. First the liver is scanned. Portal vein and common bile duct (CBD) are seen. Both lobes of liver and its segments are evaluated including the domes of diaphragm. Then the gall bladder and intrahepatic biliary radicles (IHBR) are viewed. The pancreas is visualised in both the coronal and longitudinal plane with patient in supine position. The patient is asked to turn to left side, and by keeping the probe in the right flank, the right kidney is seen. The patient is then asked to lie on its right side, and the left kidney and spleen are examined. Both the poles of the kidney should be visualised clearly and should be evaluated for the presence of a mass. The presence of marked gases in the colon may result in obscuration of renal area and non-visualisation of the kidneys. In such a situation, imaging of kidneys is done in prone position by placing the transducer below the 12th rib on the sides of vertebrae, i.e. renal area as per surface anatomy. Then the patient is asked to lie in supine position again, and the pelvic ultrasound is carried out.

Pelvic ultrasound should be done only after good distension of the urinary bladder which helps in keeping the bowel out of the imaging area, and a clear image of the organs can be obtained. The prostate in males and the uterus, ovaries and adnexa in females are visualised. The uterine fundus is visualised clearly if there is proper distension of urinary bladder. Urinary bladder itself is evaluated for wall thickness, its lumen and part of the pelvic ureters especially when they are dilated. In the next step, the small intestine, the large gut, the peritoneal cavity and the retroperitoneal spaces can be evaluated.

The position of transducer on the body surface for ultrasound examination of different body parts is shown in the following diagram (Fig.1.19):

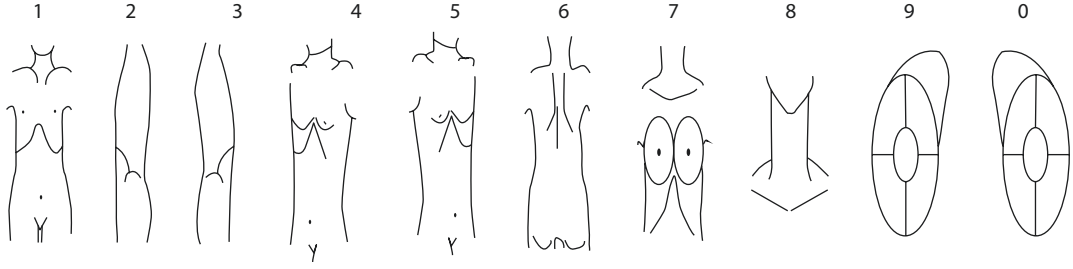

Fig. 1.19 Different positions of transducer on patient for ultrasound examination. (1) Supine, (2) left lateral, (3) right lateral, (4) right oblique, (5) left oblique, (6) subcostal, (7) breast, (8) neck, (9 and 10) quadrants of both breasts

The imaging of various organs in different positions is done in longitudinal as well as transverse plane to have a good quality of image which is free from artefacts. The stomach and urinary bladder distended with fluid serve as a window for transmission of sound waves.

The patients for abdominal and pelvic ultrasound are instructed to take good quantity of water (200–300 mL), an hour or 2, before the examination and to hold urine, so that there is good distension of urinary bladder. In patients having in-dwelling catheter in the urinary bladder, either the catheter is clamped for 1–2 h prior to ultrasound or 200–300 mL of normal saline, is instilled into the urinary bladder through the catheter. The water ingestion resulting in distension of the stomach allows good propagation of sound waves and visualisation of the pancreas.

In black and white sonography, the solid organs like the liver, pancreas, spleen, prostate, uterus, ovaries and lymph nodes are seen having a fine granular appearance which is called the echogenic texture of the organ. Such organs are called *echogenic.* The echogenicity may be homogenous or heterogenous. The hollow organs containing fluid such as the stomach, gall bladder, urinary bladder, the blood vessels like abdominal aorta, the veins and common bile duct are seen as black. These structures are called *hypo-echogenic or sonolucent or echo-free*. The structure having the echogenic property equal to the surrounding tissue is called *iso-echogenic*. This is especially seen in small-size fibroid which may be missed in USG if the uterine contour or displacement of endometrial echo-complex is not properly evaluated. In some cases, magnetic resonance imaging (MRI) may be required to detect small-size iso-echogenic uterine leiomyoma.

1.4.2 3D and 4D Sonography

Three-dimensional ultrasound (3-DUS) imaging is a new technology that allows imaging from volume sonographic data rather than conventional planar data. Volume data are generally obtained by acquiring many slices of conventional ultrasound data, identifying the location of the slice in space and reconstructing it into a volume.

The 3-DUS has definite advantages over 2-DUS especially in obstetrics to allow to understand more clearly the foetal anomalies, foetal face, cleft lip/palate, micrognathia, midface hypoplasia and asymmetric facies. In CNS, the volume has been rotated so that the sagittal, coronal and axial views are displayed. The level of the neural tube defect can be more accurate than 2-DUS. The images of extremities are often remarkably lifelike as the foetus matures. Evaluation of foetuses with skeletal dysplasias can be enhanced using 3-DUS as an adjunct to 2-DUS. Measurement of the liver and lung may assist in identifying IUGR and pulmonary hypoplasia, respectively.

The distinct advantage of 3-DUS is its ability to examine structures from planes not possible with 2-DUS because of transducer-positioning limitations and foetal positioning.

Limitations and problems of 3D and 4D ultrasound scanning:

1. In obese patients or in pregnancy with oligohydramnios, the quality of images may be poor in resolution and quality.
2. Excessive foetal movements may also result in poor resolution.
3. Non-visualisation of foetal face if it is opposed to uterine wall or the foetus in prone position.
4. Three-dimensional image may be difficult to obtain in the last 1 month of pregnancy.
5. 4D scan can be used complimentary to 2D or B-mode ultrasound.

References

1. Chivers RC, Parry RJ. Ultrasonic velocity and attenuation in mammalian tissues. J Acoust Soc Am. 1978;63:940–53.
2. Merrit CRB, Hykes DL, Hedrik WR, et al. Medical diagnostic ultrasound instrumentation and clinical interpretation. Topics in Radiology/Council report. JAMA. 1991;265:1155–9.
3. Merritt CRB. Doppler US. The basics. Radiographics. 1991;11:109–11.
4. Merritt CRB. Doppler color flow imaging. J Clin Ultrasound. 1987;15:591–7.
5. American Institute of Ultrasound in Medicine. Medical ultrasound safety. Rockville: American Institute of Ultrasound in Medicine; 1993.
6. Merrit CRB, Kremkau FW, Hobbins JC. Diagnostic ultrasound: bioeffects and safety. Ultrasound Obstet Gynaecol. 1992;2:366–74.

Abdominal Ultrasound

2

M.K. Dwivedi

Abstract

A good orientation of ultrasound anatomy is a prerequisite for optimal examination. A good preparation of patient is helpful in optimising the gain. In a serious patient, in non-cooperative patients or in ICU, the examination becomes challenging because it has to be accomplished quickly. In paediatric patients mild sedation may be required. In infants mother may be asked to feed the baby. Examination in sagittal plane or coronal plane or through subcostal or intercostal area is done to avoid artefacts and to have good quality images. Visualisation of kidneys from the flank becomes difficult in the presence of gases in the bowel; then scanning from posterior surface along 12th rib is done to clearly visualise both the poles of kidneys.

It is important to have good orientation of ultrasound anatomy to find out variation from normal and to identify the disease/lesion.

2.1 Liver [1, 2]

Liver is located behind the lower ribs on the right side in the right upper quadrant of the abdomen. Its imaging is done by placing the transducer in the intercostal spaces of the lower ribs or by placing the probe in the subcostal area. Liver is seen as organ with homogenous texture. Functionally, the liver is divided into three lobes: the right, the left and the caudate lobes. The right lobe of the liver is separated from the left by the main lobar fissure which passes through the gall bladder fossa to the inferior vena cava. The caudate lobe is situated on the posterior aspect of the liver between IVC and the fissure for ligamentum venosum. The left intersegmental fissure divides the left lobe into medial and lateral segment. The branches of the hepatic artery accompany the portal vein. The confluence of the splenic vein and the superior mesenteric vein, near the head of the pancreas, forms the portal vein which runs towards the liver. Main portal vein is seen as linear black tubular structure of 10–15 mm in

M.K. Dwivedi
Department of Radio-Diagnosis, C.C.M. Medical College & Hospital, Durg, Chhattisgarh, India
e-mail: mahendra_van@yahoo.com

R.K. Diwakar (ed.), *Basics of Abdominal, Gynaecological, Obstetrics and Small Parts Ultrasound*,
https://doi.org/10.1007/978-981-10-4873-9_2

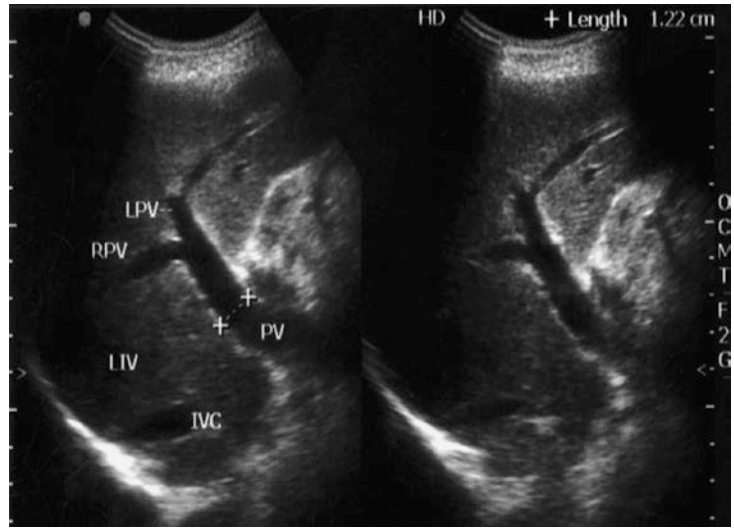

Fig. 2.1 Main portal vein dividing into the right and left branch

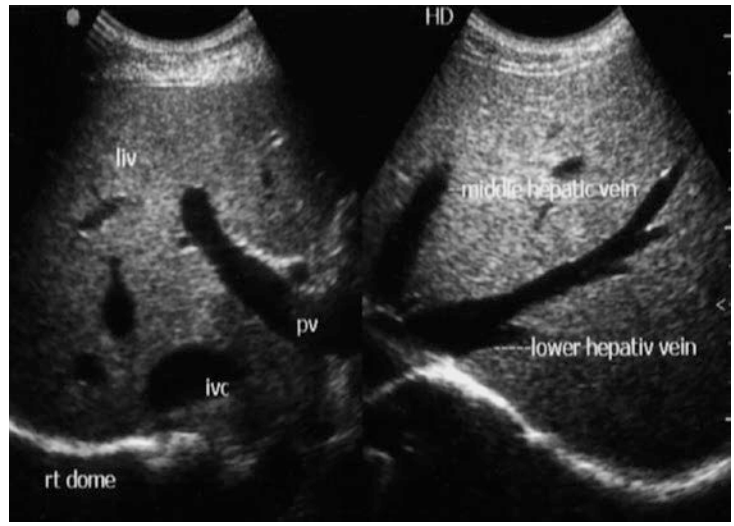

Fig. 2.2 Normal anatomy of the liver with venous vascular structures

diameter entering into the liver through the porta hepatis, traverses anteriorly into the liver substance and divides into the right and left portal vein. Smaller branches of the portal vein are usually not seen (Fig. 2.1). Three hepatic veins, namely, the upper, the middle and the lower, join the inferior vena cava at the level of the right diaphragm (Fig. 2.2).

The common bile duct (CBD), which runs anterior to the portal vein (Fig. 2.3), is joined by the pancreatic duct at the second part of the duodenum to open into the second part of the duodenum on hepaticopancreatic papilla.

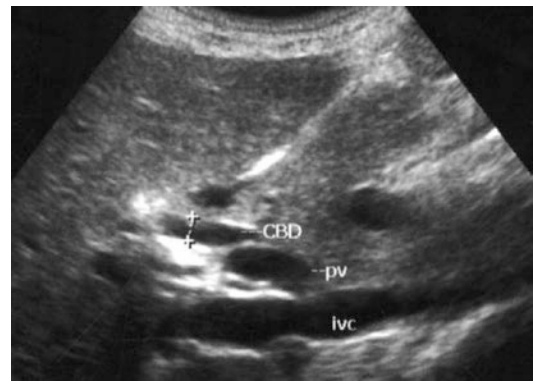

Fig. 2.3 Inferior vena cava (IVC) posterior to the portal vein

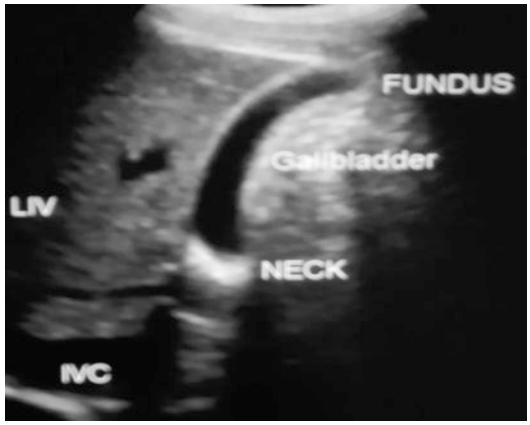

Fig. 2.4 Fundus, body and neck of GB

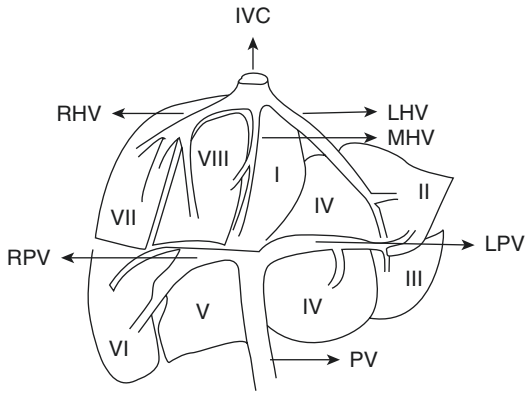

Fig. 2.5 Couinaud's segments of the liver

The distended gall bladder is a thin wall pear-shaped structure with echo-free lumen. It is seen in the liver and located anterior to the common bile duct (Fig. 2.4).

The liver is divided into functional segments (Couinaud's anatomy) [3, 4] longitudinally into four sections; each of this section is transverse by an imaginary plane through the right main and left main portal pedicles. Thus eight segments are available for hepatic lesion localisation for the convenience of the surgeon. This is illustrated in Figs. 2.5 and 2.6 and Table 2.1.

Table 2.1 Hepatic anatomy

Couinaud	Traditional
Segment I	Caudate lobe
Segment II	Lateral segment of the left lobe (superior)
Segment III	Lateral segment of the left lobe (inferior)
Segment IV	Medial segment of the left lobe
Segment V	Anterior segment of the right lobe (inferior)
Segment VI	Posterior segment of the right lobe (inferior)
Segment VII	Posterior segment of the right lobe (superior)
Segment VIII	Anterior segment of the right lobe (superior)

From Rumack CM, Wilson SR, Charboneau JW. In Diagnostic Ultrasound, 2nd edition, chapter 4, Liver; p-90.1998. Mosby-Year Book, Inc. Missouri.

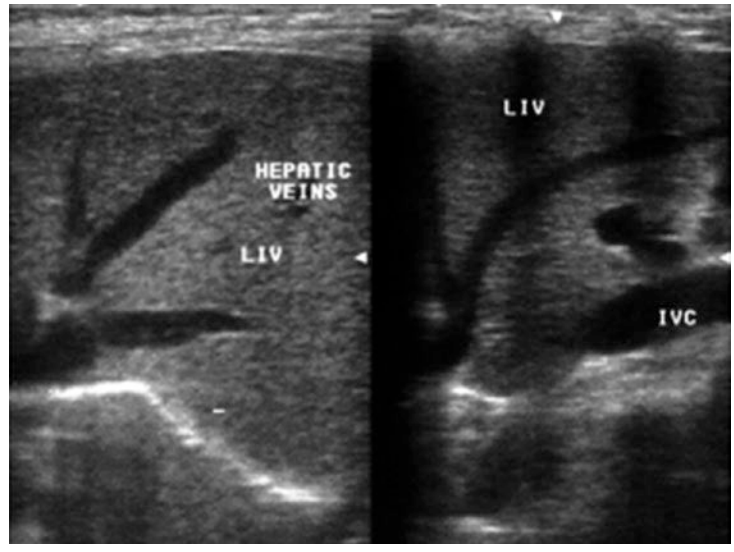

Fig. 2.6 Three hepatic veins joining IVC at the level of right dome of the diaphragm

Hepatomegaly: An accurate assessment of liver enlargement is difficult. However, the enlargement of the liver measures the right lobe of the liver in the mid-clavicular line more than 13 cm. The normal liver is homogenous in echotexture and hyperechoic or iso-echoic to the normal renal cortex.

In hepatitis in most cases, the liver appears normal. However, hepatomegaly and thickening of the gall bladder wall are associated findings in hepatitis.

The hepatic lesions may be solid or cystic.

Hepatic cysts are well-defined fluid-filled spaces having an epithelial lining. Hepatic cysts may be single (Fig. 2.7) or multiple (Fig. 2.8). Colour flow may be seen in hepatic cyst (Fig. 2.9). Abscesses, parasitic cysts and post-traumatic cysts are therefore not true cysts.

Sonography is extremely helpful in the detection of liver abscesses. Amoebic liver abscess is most common in the right lobe of the liver, round or oval in shape with fine internal echoes (Fig. 2.10). It has to be differentiated from pyogenic liver abscess (Fig. 2.11) and hydatic cyst

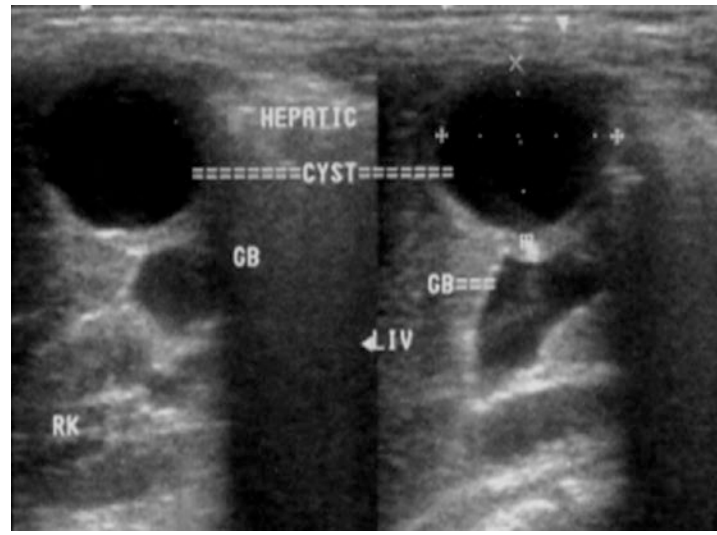

Fig. 2.7 Simple hepatic cyst anterior to the gall bladder

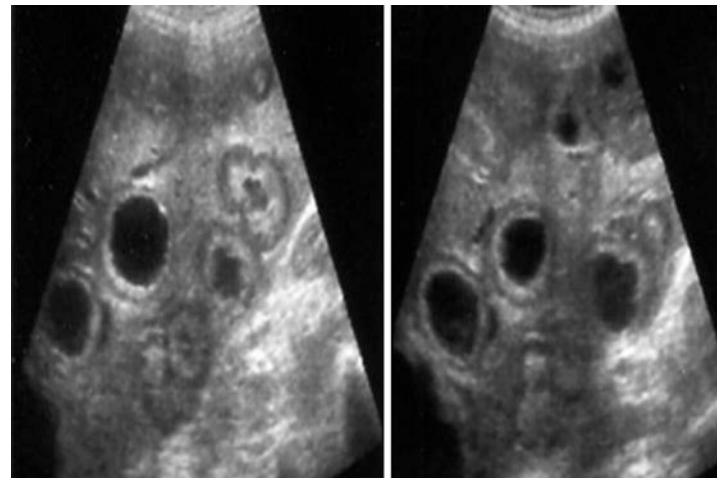

Fig. 2.8 Multiple hepatic cysts

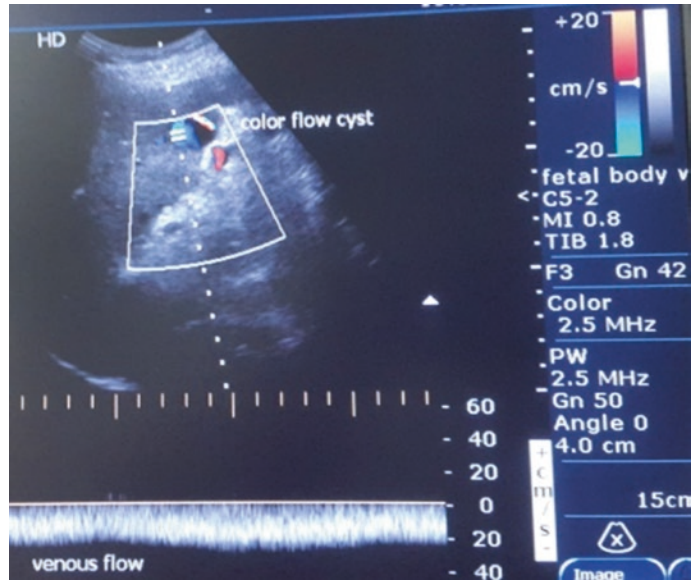

Fig. 2.9 Cyst in the liver showing colour flow in Doppler interrogation

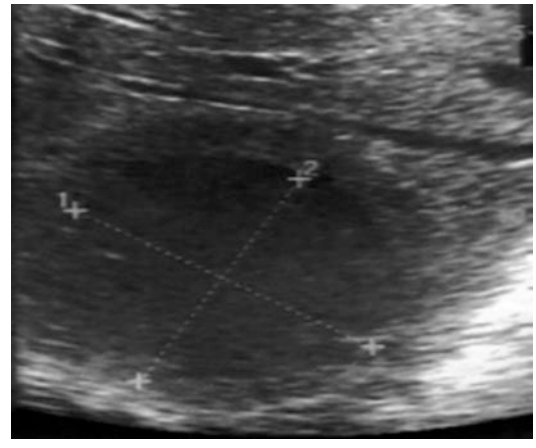

Fig. 2.10 Amoebic liver abscess with thick wall

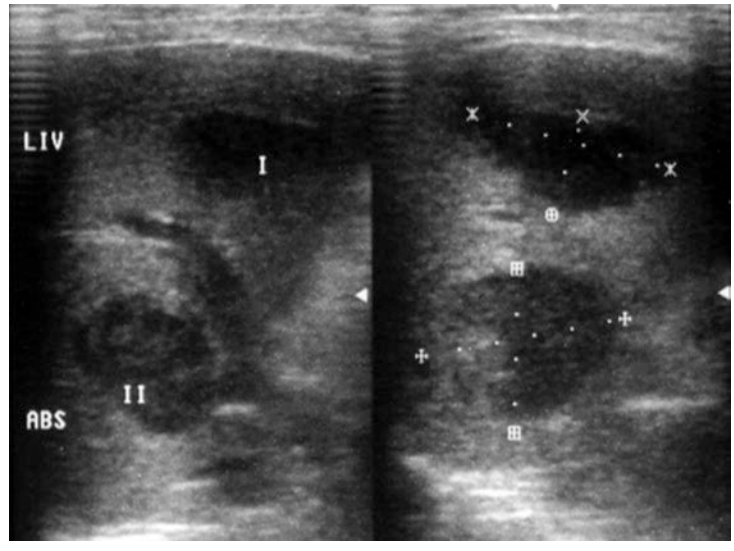

Fig. 2.11 Two liver abscesses (pyogenic) with ill-defined margins

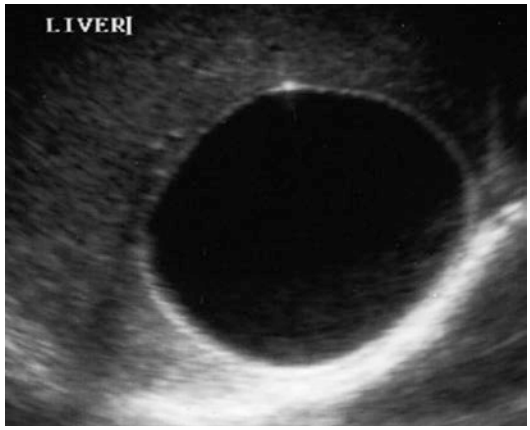

Fig. 2.12 Hydatid cyst in the right lobe liver, no daughter cysts or internal echoes

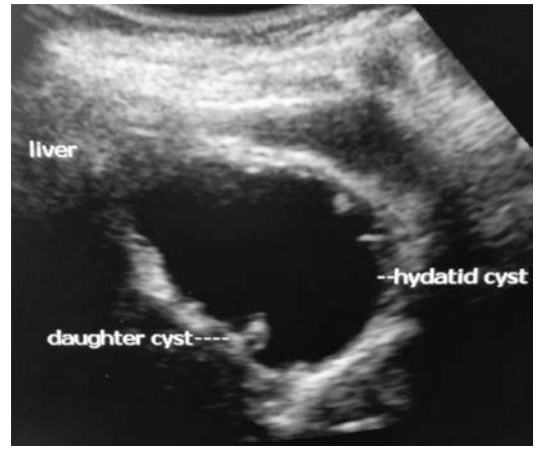

Fig. 2.13 Hepatic hydatid cyst with daughter cysts attached to the wall

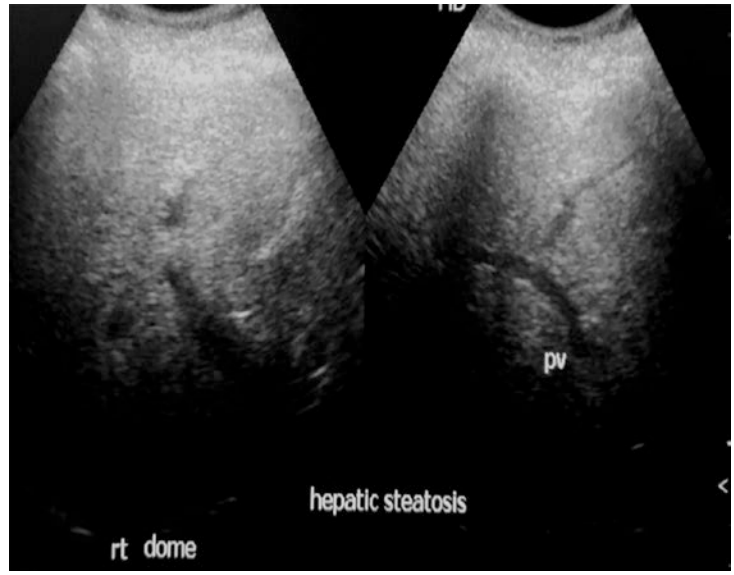

Fig. 2.14 Generalised increase in echogenicity of liver parenchyma in moderate steatosis

(Fig. 2.12). Early pyogenic abscess may appear solid. Drainage of liver abscess under ultrasound guidance is a common procedure now. Follow-up of liver abscess with sonography about its size is quite useful.

Hydatid cyst is most prevalent in sheep and cattle-raising countries notably in the Middle East, Australia and the Mediterranean. The cyst wall consists of an external membrane about 1 mm thick (the ectocyst). The host forms a dense connective tissue capsule around the cyst (the pericyst). The inner germinal layer (the endocyst) gives rise to brood capsules that enlarge to form protoscolices [5].

Lewall [6] proposed four groups:

- Simple cysts containing no internal architecture except sand (Fig. 2.12)
- Cysts with detached endocysts
- Cysts with daughter cysts (Fig. 2.13)
- Densely calcified masses

Fatty liver changes (hepatic steatosis) may be diffuse (Fig. 2.14) or focal (Fig. 2.15). It is an

acquired reversible disorder of metabolism [7]. Diffuse steatosis may be:

1. Mild: minimal diffuse increase in echogenicity of liver parenchyma with normal visualisation of diaphragm and intrahepatic vessel borders
2. Moderate diffuse increase in echogenicity with slightly impaired visualisation of diaphragm and intrahepatic vessels
3. Severe with marked increase in echogenicity of the liver with features of portal hypertension such as ascites, splenomegaly and varices

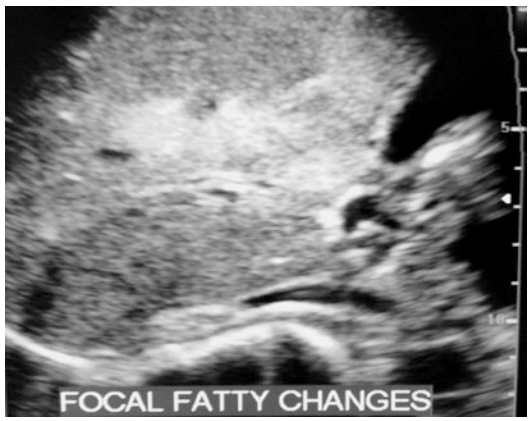

Fig. 2.15 Focal hepatic steatosis in the right lobe of the liver

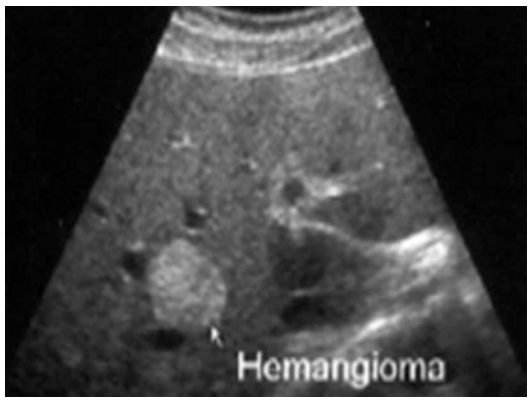

Fig. 2.16 Haemangioma of the liver located near the hepatic vein

Cavernous haemangioma is the homogenously hyperechoic lesion located in close vicinity of a hepatic vein (Fig. 2.16).

Focal nodular hyperplasia (FNH) is the second most common liver mass after haemangioma. It may have the echogenicity equal to the normal liver; therefore, displacement of neighbouring vascular structures gives a clue about its presence.

2.1.1 Hepatic Haematoma

The predominant site of hepatic blunt trauma is the right lobe (Fig. 2.17) and the posterior segment in particular. Initially, the haematoma is echogenic, becoming hypoechoic within a week and indistinct margins after 2–3 weeks. Haemoperitoneum may be an associated finding.

Hepatic carcinoma (Fig. 2.18) and metastasis are usually multiple solid lesions of the liver having variable sizes (Figs. 2.19 and 2.20) and having propensity towards venous invasion, portal vein being involved in most of the cases.

Occasionally, a mass is seen in the porta hepatis resulting in CBD obstruction and dilatation of intrahepatic biliary radicles (Figs. 2.21 and 2.22).

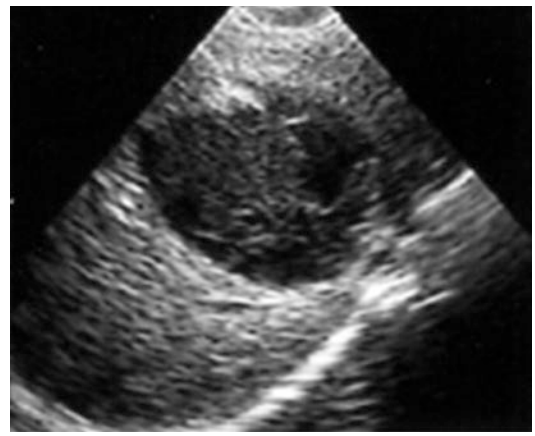

Fig. 2.17 Hepatic haematoma of some duration, hypoechoic than the surrounding parenchyma

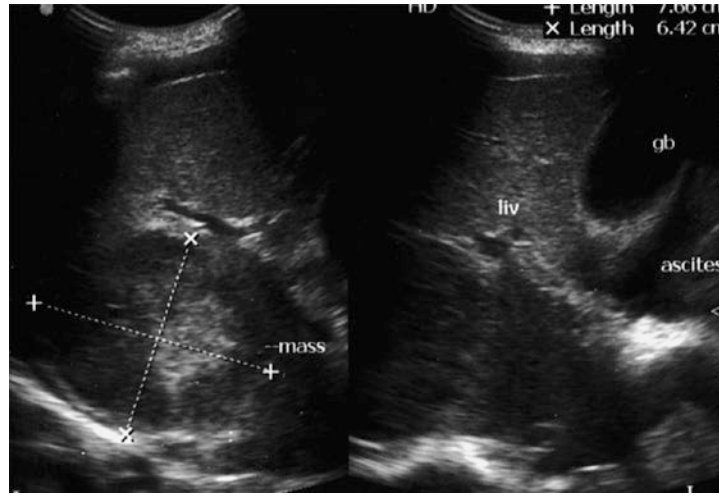

Fig. 2.18 Hepatic carcinoma in the right lobe of the liver in subdiaphragmatic location with anterior displacement of the portal vein and ascites posterior to the gall bladder (GB)

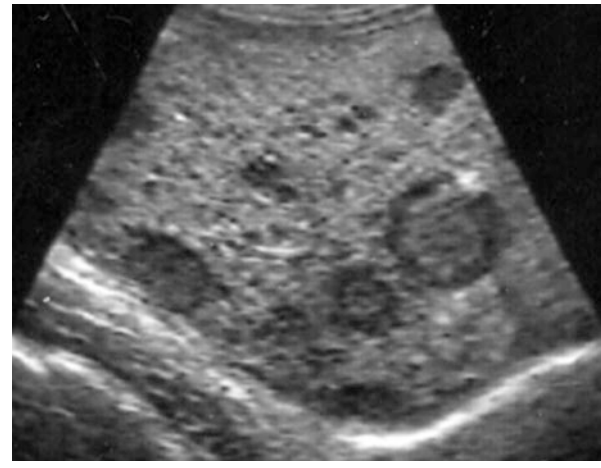

Fig. 2.19 Multiple hepatic metastases

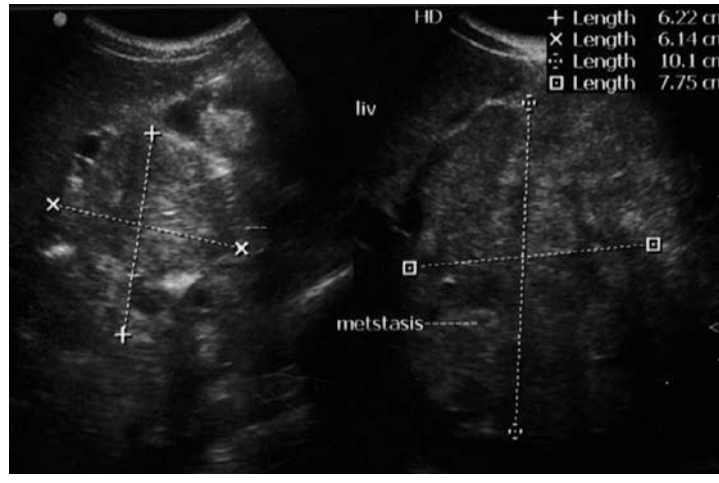

Fig. 2.20 A large primary hepatic tumour with multiple hepatic metastases

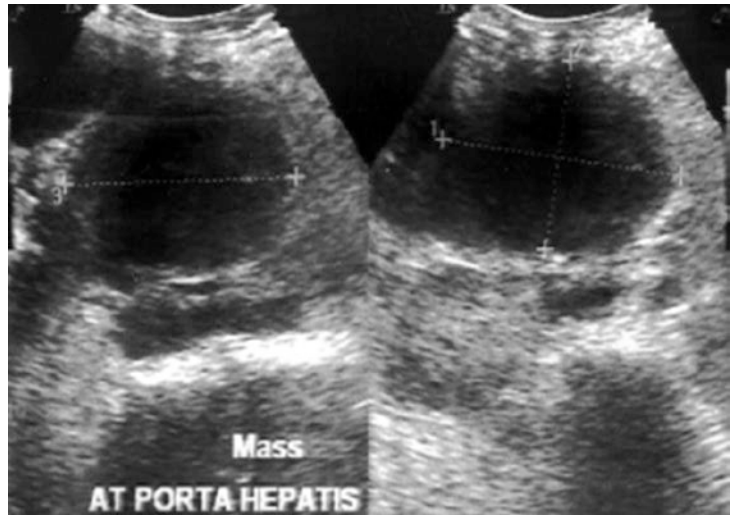

Fig. 2.21 Mass at the porta hepatis

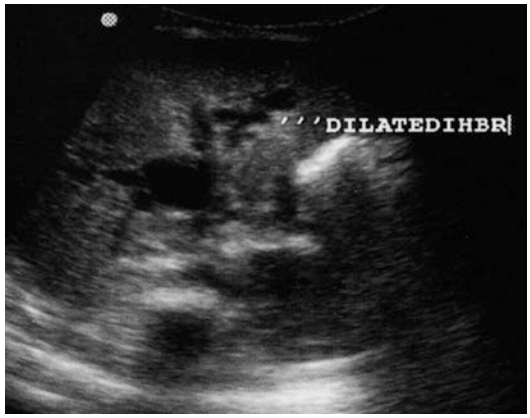

Fig. 2.22 Dilated CBD and intrahepatic biliary radicles (IHBR)

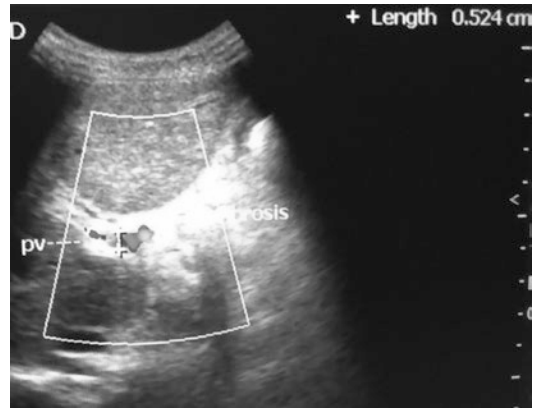

Fig. 2.23 Narrowing of the portal vein in liver cirrhosis

2.1.2 Portal Hypertension and Liver Cirrhosis [8, 9]

The diameter of normal portal vein is 12–15 mm. An increase of less than 20% in diameter of the portal vein with deep inspiration indicates portal hypertension. The calibre of the portal vein initially may be increased >15 mm in portal hypertension, and with development of portosystemic shunts, the portal vein calibre may decrease (Fig. 2.23).

The normal mean portal venous flow velocity is 15–18 cm/s (Fig. 2.24).

In portal hypertension, this becomes monophasic. With increasing severity of portal hypertension, flow becomes biphasic and finally

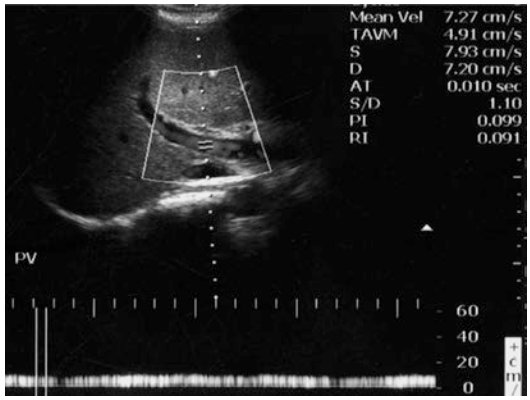

Fig. 2.24 Normal portal vein Doppler waveform

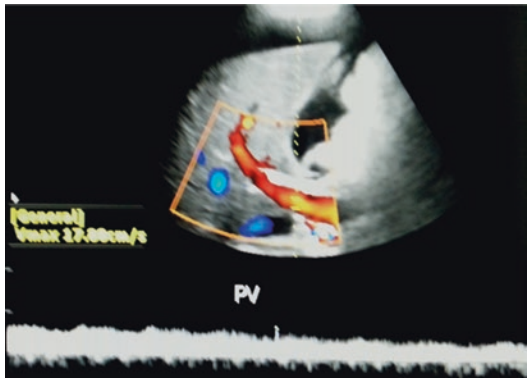

Fig. 2.25 Portal vein colour flow and Doppler waveform in liver cirrhosis

hepatofugal (away from the liver). Kawasaki et al. [8] reported a prevalence of spontaneous hepatofugal flow of 6.1% in cirrhotic patients (Fig. 2.25).

Ascites is present surrounding the liver (Fig. 2.26), in the hepatorenal recess (Morrison's pouch) (Fig. 2.27), in the peritoneal cavity in between the intestinal loops and in female patients posterior to the uterus.

In the presence of gross ascites, the cirrhotic liver is seen bright and echogenic with nodular surface (Fig. 2.28).

Cavernous malformation of the portal vein may be seen in terminal stages of liver cirrhosis (Fig. 2.29).

Dilated hepatic veins are visualised in the liver joining the inferior vena cava which may also be distended in patient of cardiac failure (Fig. 2.30).

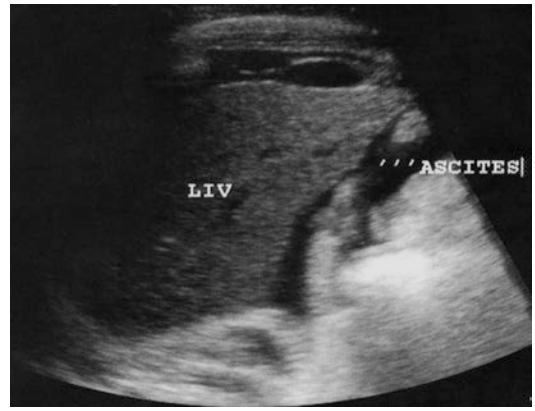

Fig. 2.26 Ascites surrounding the liver

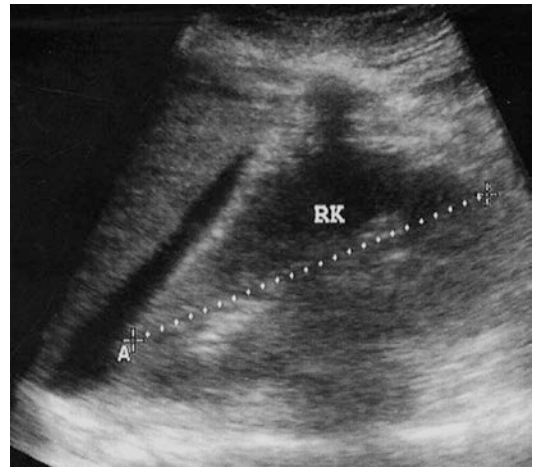

Fig. 2.27 Ascitic fluid in the hepatorenal recess (Morrison's pouch)

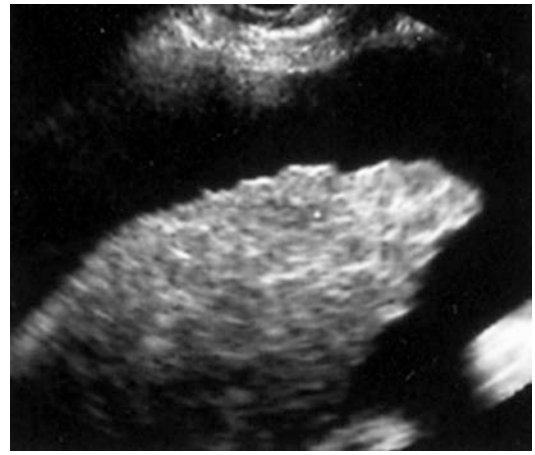

Fig. 2.28 Bright echogenic cirrhotic liver with nodular surface and ascites around it

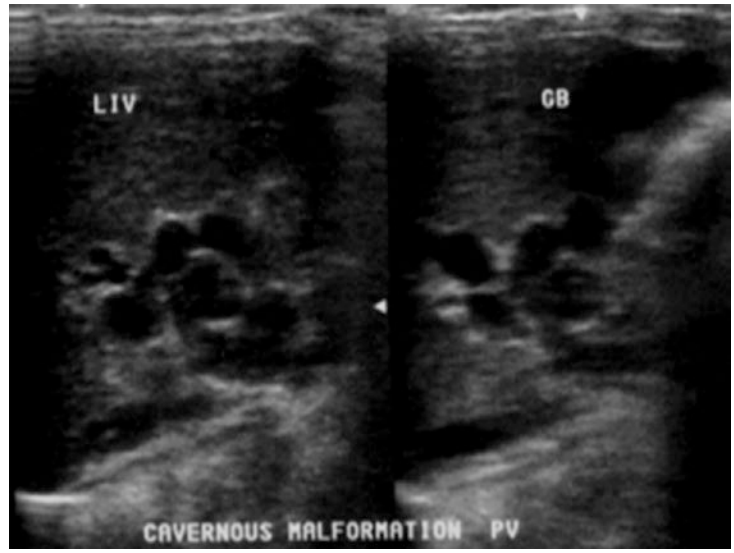

Fig. 2.29 Cavernous malformation of the portal vein in liver cirrhosis

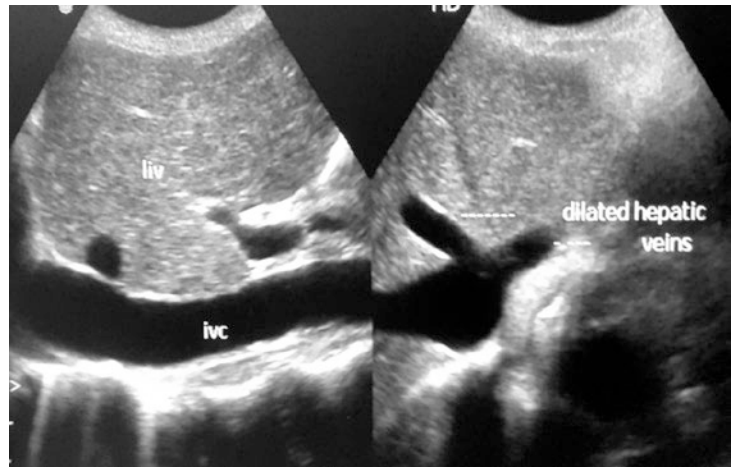

Fig. 2.30 The dilated hepatic veins and inferior vena cava (IVC) in cardiac decompensation

2.1.3 Gall Bladder and Biliary System [10, 11]

Abstract It is seen in the liver area anterior to CBD. It is a pear shaped and appears black as it contains bile which is echo-free (Fig. 2.31). The GB should be seen in all adult patients after a physiological distension following 8–10 h fast. The position and size of the gall bladder are very variable. In general, the transverse diameter is not more than 5 cm. If it is no longer ovoid but rounded in shape, the gall bladder is likely to be obstructed/hydropic. The gall bladder wall is pencil line thick (less than 3 mm) and is well

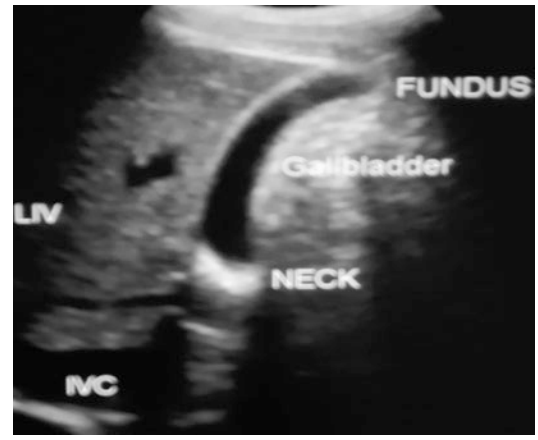

Fig. 2.31 Fundus, body and neck of the gall bladder, inferior vena cava (IVC) and liver (Liv)

demarcated. Sometimes, a fold is seen in the gall bladder between the body and neck which should not be mistaken for disease (Fig. 2.32).

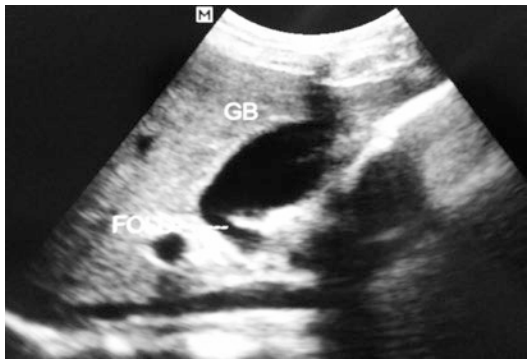

Fig. 2.32 Junctional fold at the gall bladder neck

Anomalous location of the gall bladder, single or multiple septa in the gall bladder and duplication anomalies are detected occasionally.

The most common disease of the gall bladder is calculus (Fig. 2.33). The gall bladder may contain echogenic bile or sludge in patients who undergo prolonged fasting as well as in patients with biliary obstruction at the level of the gall bladder, cystic duct or CBD. The biliary sludge should not be mistaken for gall bladder growth. The biliary sludge is usually present along posterior wall within the gall bladder lumen (Fig. 2.34), and it may shift towards fundus of the gall bladder with change in patient's position to left lateral decubitus/sitting posture. Similarly, a calculus

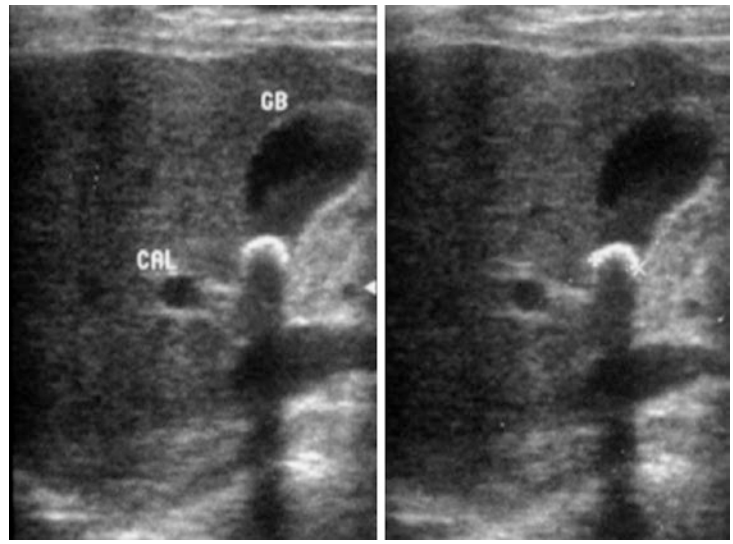

Fig. 2.33 Crescent-shaped single GB calculus with posterior shadowing

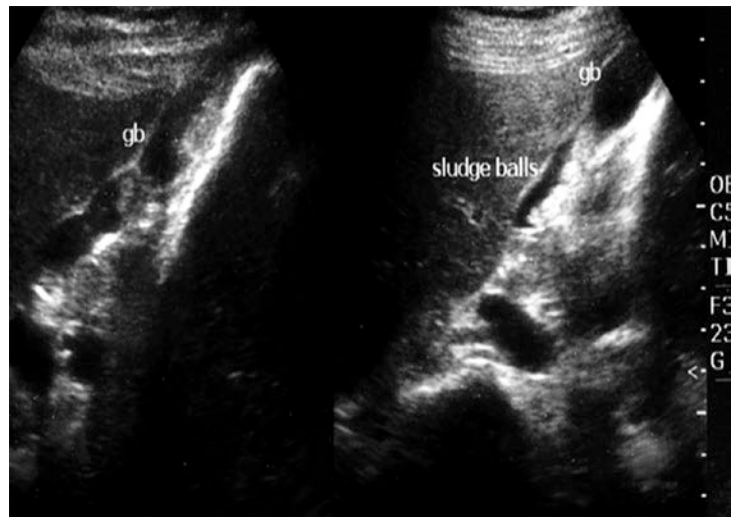

Fig. 2.34 Biliary sludge along the posterior wall of the gall bladder

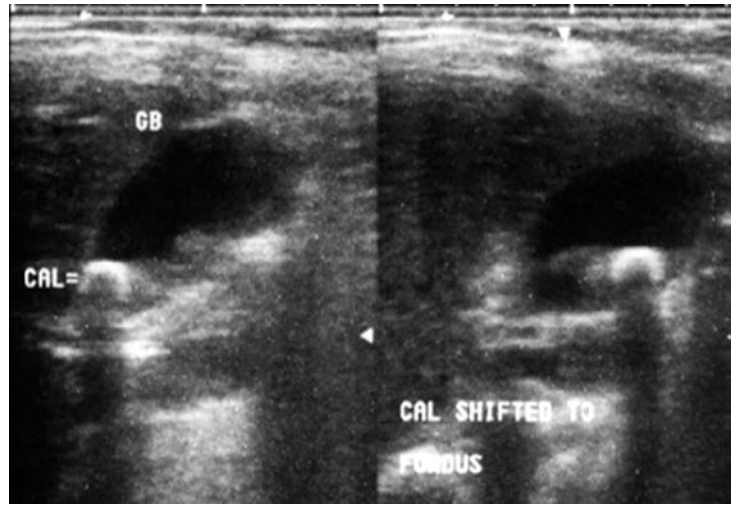

Fig. 2.35 Shifting of calculus from the neck to the body of the gall bladder with change in patient's posture

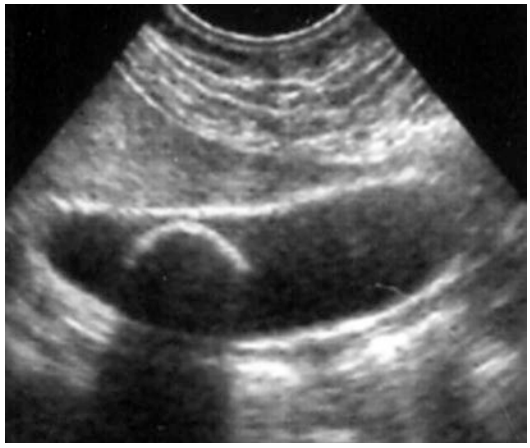

Fig. 2.36 Large calculus in GB with posterior shadow and without significant thickening of the wall

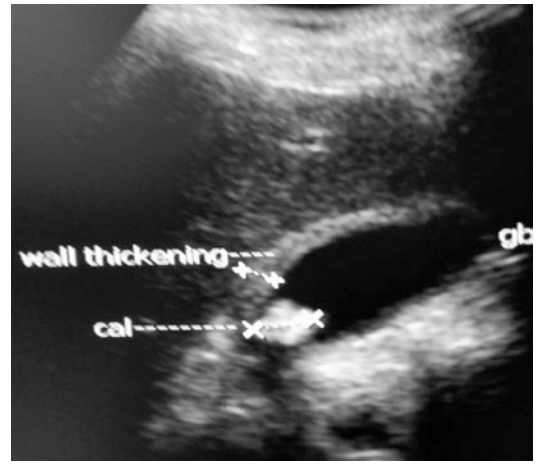

Fig. 2.37 Gall bladder calculus with thickening of the wall

may be impacted at GB neck or may demonstrate its mobility with change in patient's position (Fig. 2.35).

Non-visualisation of the gall bladder may due to (1) post-meal contraction, (2) congenital absence, (3) being shrunken and loaded with multiple calculi and (4) cholecystectomy being done.

Cholelithiasis: The accuracy of gall bladder ultrasound is reported to be 95% in detection of gallstones. Highly reflective echo from the calculus with prominent posterior shadow is the primary role of cholecysto-sonography (Figs. 2.36, 2.37, 2.38 and 2.39). Posterior shadow may be absent in small size stones. The movement of gallstone within its lumen

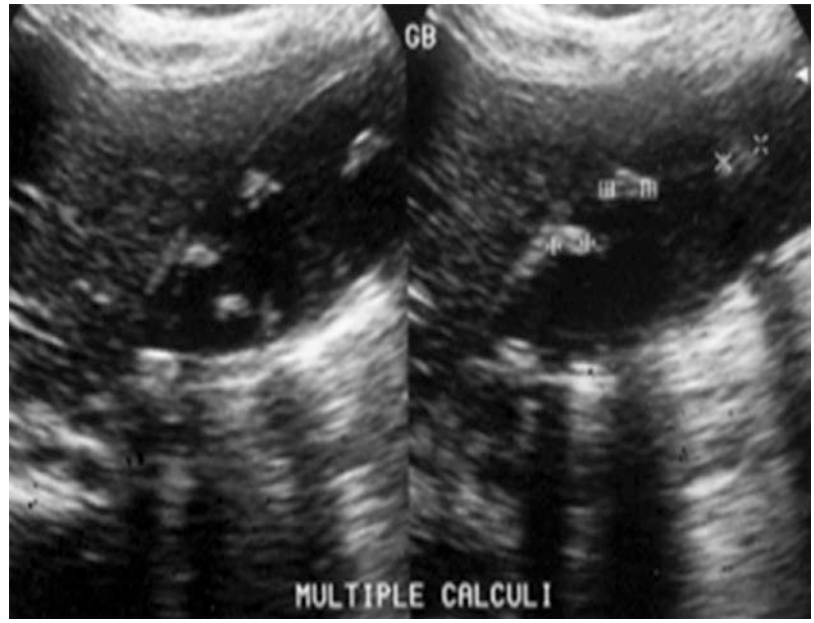

Fig. 2.38 Multiple gall bladder calculi (cholelithiasis) with posterior shadow

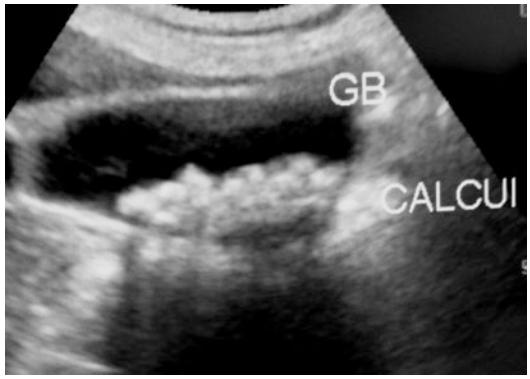

Fig. 2.39 Multiple gall bladder calculi with posterior shadow

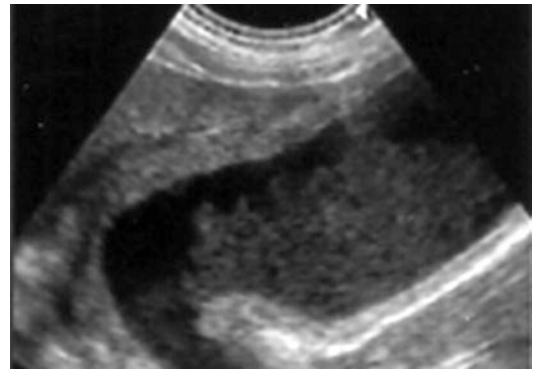

Fig. 2.41 Biliary sludge mimicking a growth with thickening of the GB wall

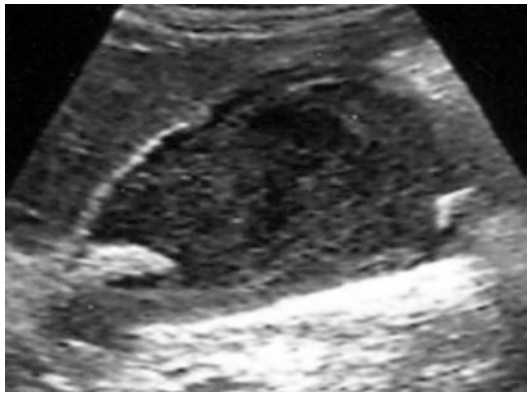

Fig. 2.40 Gall bladder lumen filled with biliary sludge, a calculus in fundus with thickening of the wall

can be seen by repositioning of patient. However, the gallstone impacted in the neck will not show a change in its position. Rarely one may see sludge balls or tumefactive biliary sludge as mobile mass in the gall bladder (Figs. 2.40 and 2.41).

Mucocele of the gall bladder with or without stone resulting in markedly enlarged gall bladder (Figs. 2.42 and 2.43).

The gall bladder growth is always attached to the gall bladder wall, and diffuse thickening of the gall bladder wall (>3 mm) is seen in 50–75% of the patients. Many times, moderate to big size calculus is detected as a coincidence

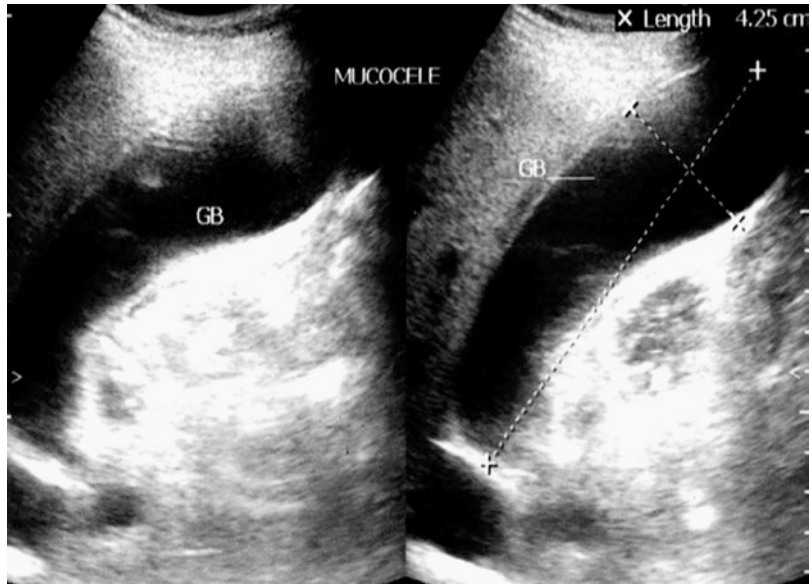

Fig. 2.42 Markedly enlarged gall bladder in mucocele

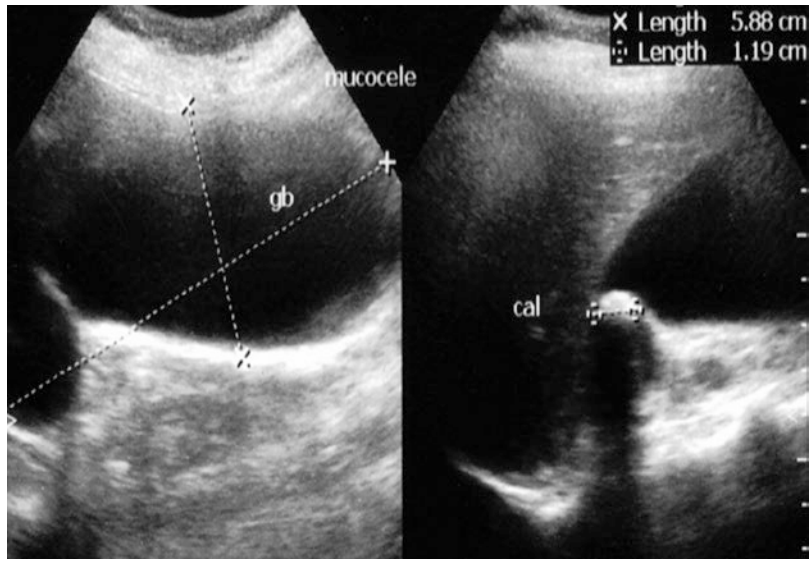

Fig. 2.43 Mucocele of the gall bladder with a calculus

in a patient having no complaints (Figs. 2.44, 2.45 and 2.46). Such calculus is labelled as silent stone. It should always be remembered that hepatic dysfunction may also result in thickening of the gall bladder wall. Gallstones may be a coexistent finding in carcinoma of the gall bladder.

Acute cholecystitis: Signs of acute cholecystitis include gall stones, focally tender gall bladder (sonographic Murphy's sign), impacted gallstone, diffuse wall thickening and sludge and GB dilatation. Complications of acute cholecystitis include emphysematous and gangrenous cholecystitis with perforation.

Irregular thickening of the gall bladder wall in the absence of calculus suggests acalculous cholecystitis (Fig. 2.47). Follow-up study in such cases is useful to demonstrate progressive thickening of the GB wall.

Pseudo gall bladder wall thickening may be caused by oedema in the gall bladder fossa in acute pancreatitis or viral hepatitis (Fig. 2.48) or ascites (Fig. 2.49).

Chronic cholecystitis: Two thirds of patients with gallstones have chronic cholecystitis with complaints of recurrent biliary colic. Thickening of the gall bladder is often present. The gall

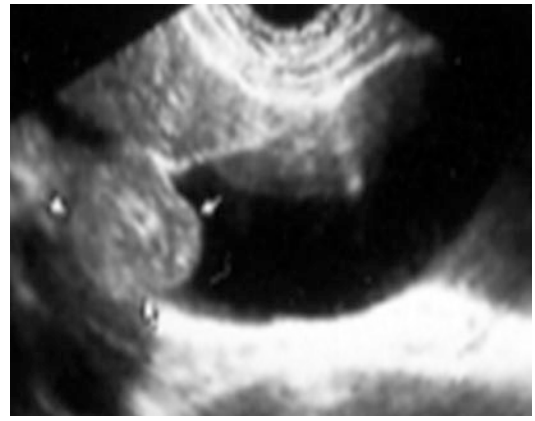

Fig. 2.46 Growth in the gall bladder neck

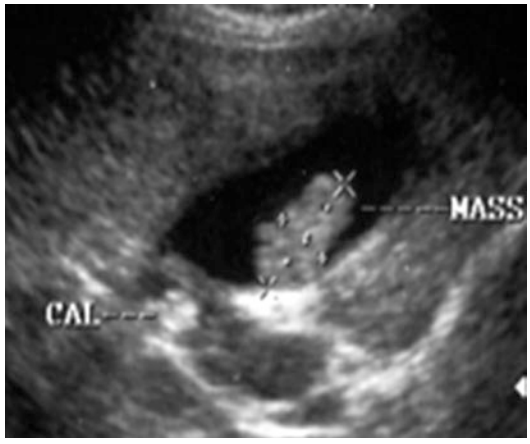

Fig. 2.44 Gall bladder growth and a calculus in the neck

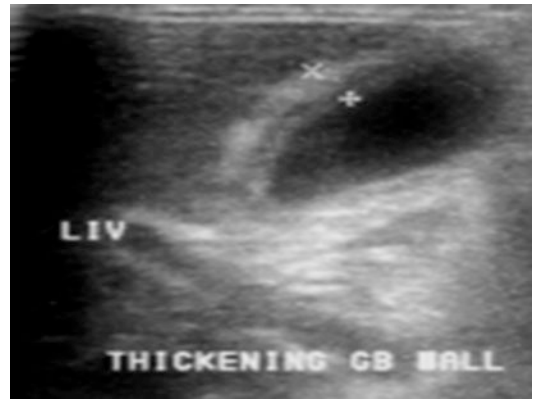

Fig. 2.47 Thickening of the GB wall in acalculous cholecystitis

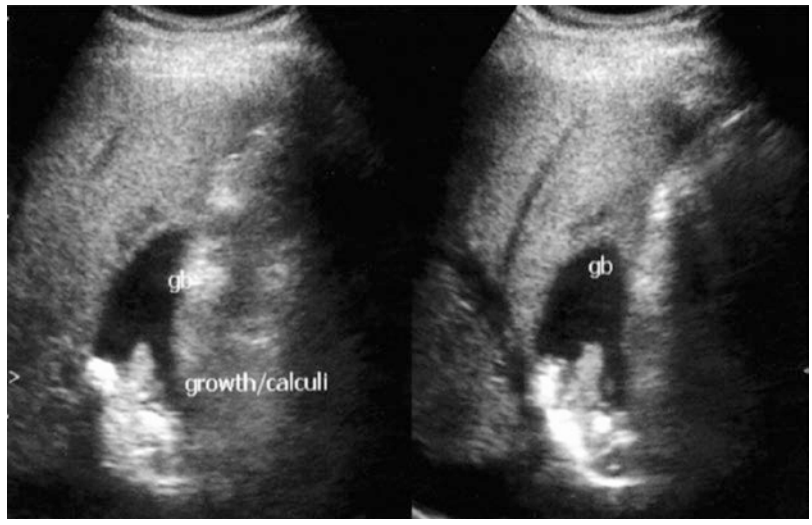

Fig. 2.45 Gall bladder growth with multiple calculi in the neck

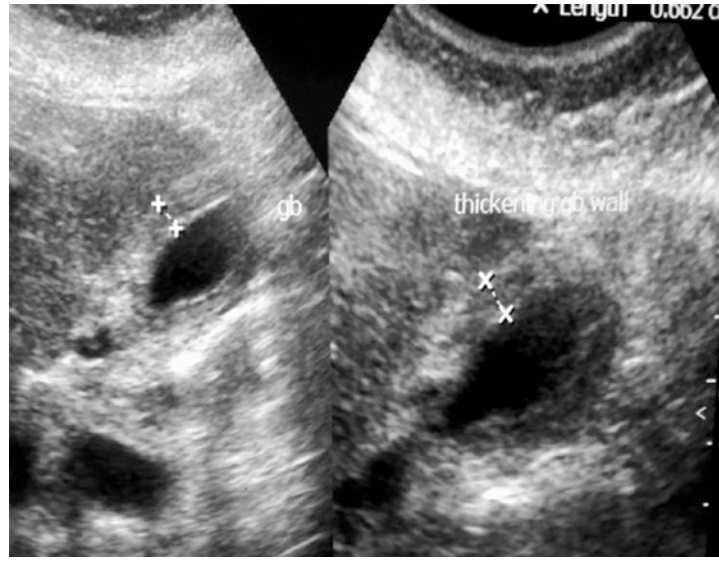

Fig. 2.48 Thickening of the gall bladder wall in hepatic parenchymal disease

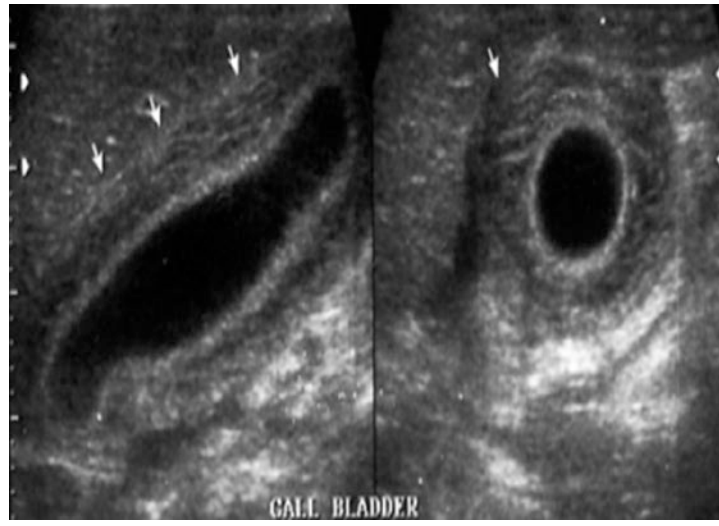

Fig. 2.49 Pseudo-thickening of the GB wall in ascites

bladder may be studded with a number of calculi so that its lumen is not visualised (mountain peak appearance) (Fig. 2.50).

The presence of shadowing posterior to the gall bladder fossa is helpful in diagnosis.

Non-visualisation of the gall bladder suggests obliterated lumen, physiologic contraction (post-meal), contractions from acute severe hepatitis, sludge iso-echogenic to the liver obscuring margins of the gall bladder, absence of the gall bladder, unusual position of the gall bladder (hydrops) and technical error. Gall bladder fossa filled with poorly defined heterogenous echoes resulting in

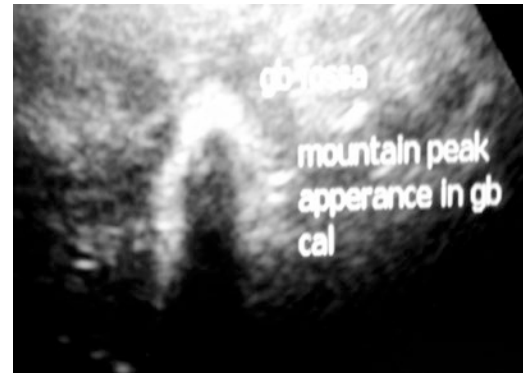

Fig. 2.50 "Mountain peak appearance" of GB lumen filled with calculi

non-visualisation of its lumen suggests gall bladder carcinoma.

Single (Figs. 2.51, 2.52 and 2.53) or multiple polyp or multiple papilloma may occasionally be detected in the gall bladder lumen.

Occasionally, USG may reveal a roundworm in the gall bladder.

2.1.4 Biliary System [10, 11]

Intrahepatic bile ducts are considered dilated if their diameter is more than 40% of the accompanying portal veins (Figs. 2.54 and 2.55).

The common hepatic ducts join the cystic duct to form the CBD which leaves the port-hepatis. Normal cystic duct is 2 mm in diameter and is seen only in 50% of the patients. However, it is easily visualised when there is CBD obstruction. CBD of 0.5 mm diameter suggests CBD dilatation.

CBD stones can be picked up (Figs. 2.56 and 2.57). Calculus in CBD can be missed especially when it is not dilated.

Choledochal cyst has been subdivided into various types:

Type I: Cystic fusiform dilatation of the CBD with an anomalous junction of the pancreaticobiliary system (most common form) (Figs. 2.58 and 2.59).

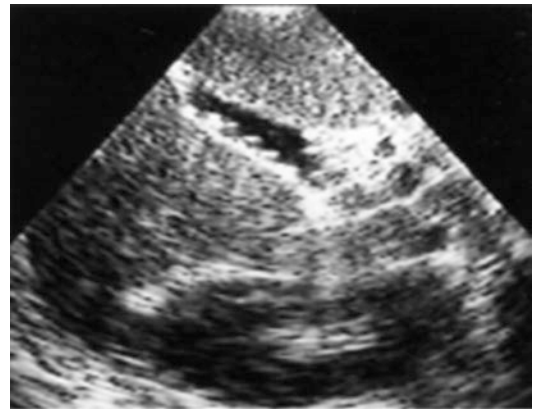

Fig. 2.52 Multiple polyps in both walls of the gall bladder

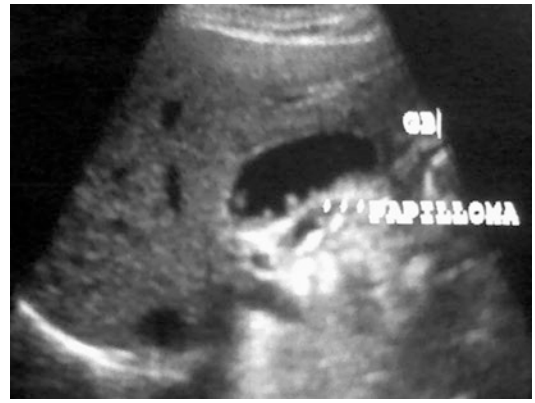

Fig. 2.53 Multiple papilloma in the gall bladder

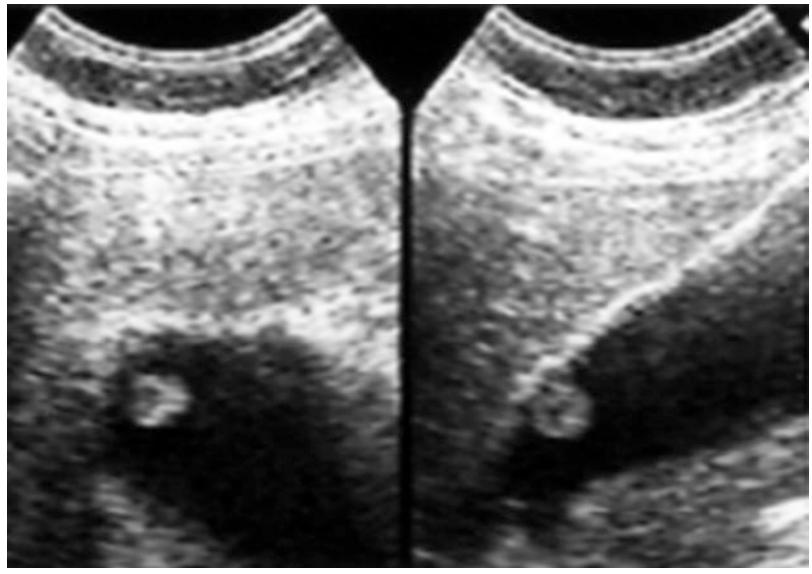

Fig. 2.51 Single polyp attached to the fundus and anterior wall of the gall bladder

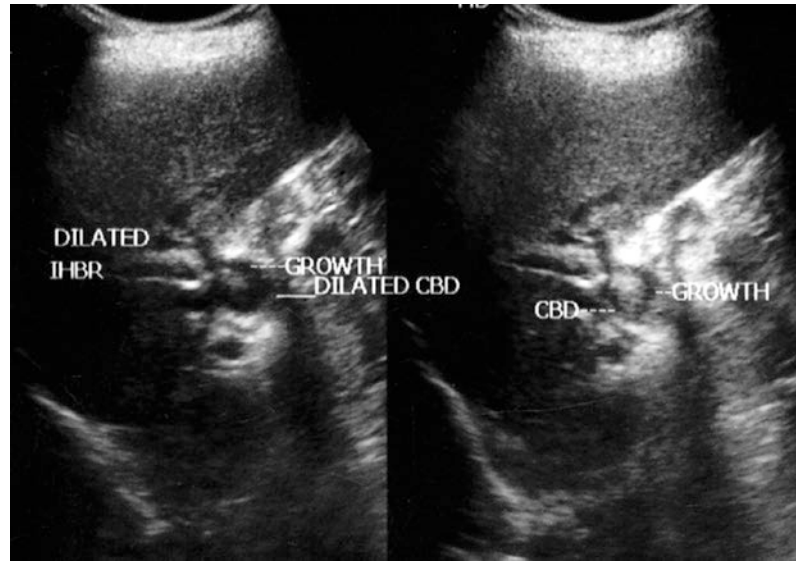

Fig. 2.54 A growth in dilated CBD, IHBR are also dilated

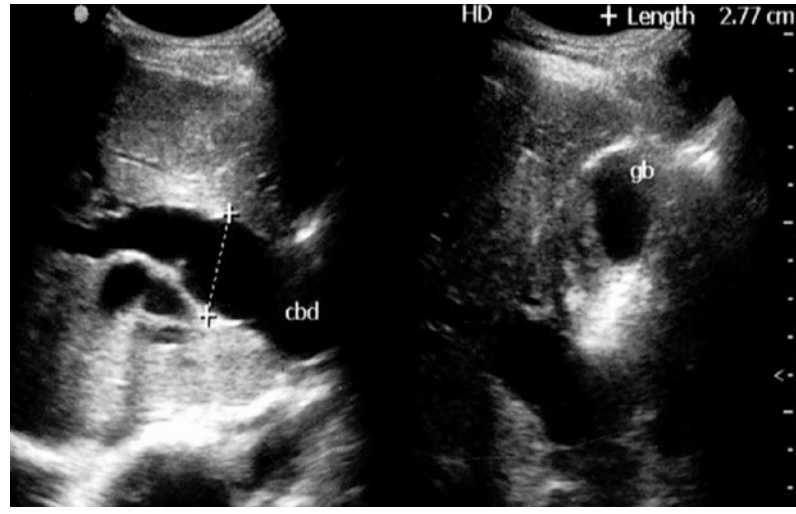

Fig. 2.55 Markedly dilated CBD

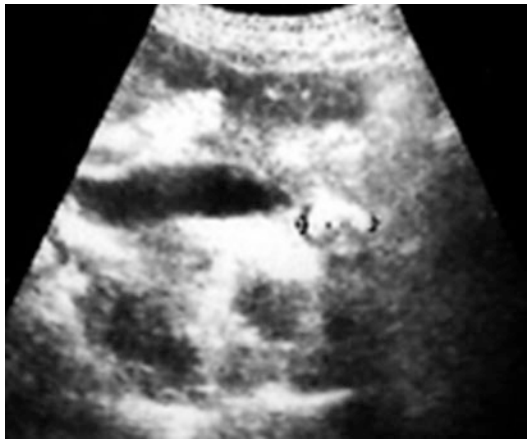

Fig. 2.56 Dilated CBD with calculus in terminal CBD

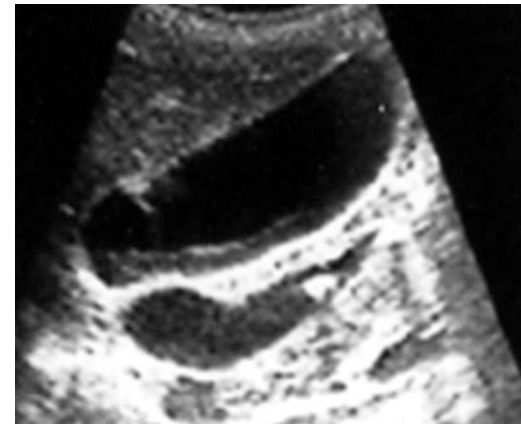

Fig. 2.57 Biliary sludge along posterior wall of the gall bladder with calculus in dilated CBD

Type II: A diverticulum protruding from the wall of the CBD

Type III: A choledochocele or herniation of the CBD into the duodenum

Gall bladder function can be evaluated 2 h after giving a fatty meal, and contraction of the gall bladder by 2 mm or greater suggests normal gall bladder function. However, negative results in a questionable situation must be evaluated by CT.

2.1.5 Pancreas

Abstract Ultrasound is most widely used and least expensive means of visualising the pancreas. The purpose is to differentiate a normal from abnormal pancreas and pancreatitis from malignancy. Ultrasound-guided FNAC has significantly improved the diagnostic accuracy.

Anatomical relationship of the pancreas has been depicted in Fig. 2.60.

It is seen best in epigastrium in the transverse plane when the stomach is distended with fluid.

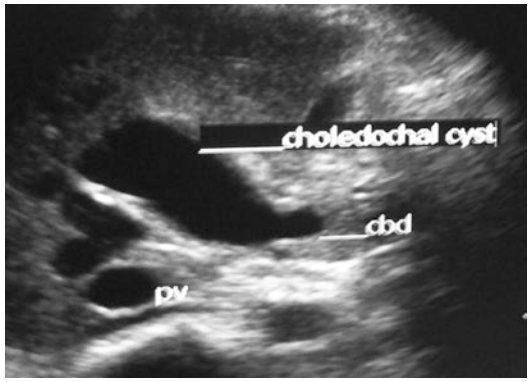

Fig. 2.58 CBD obstruction with choledochal cyst type I

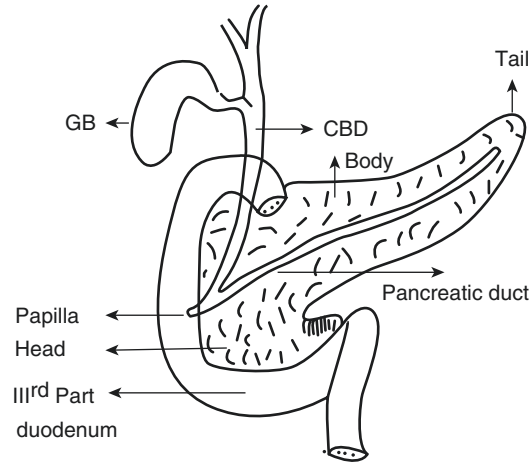

Fig. 2.60 Anatomical relationship of the pancreas

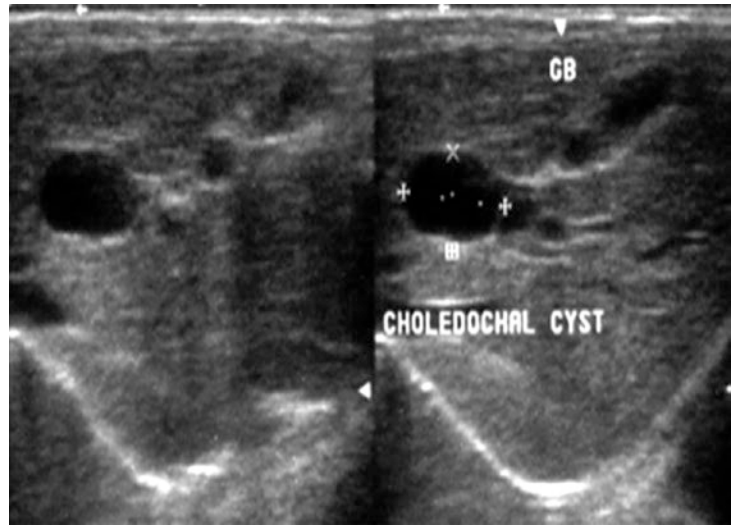

Fig. 2.59 Choledochal cyst type I in a paediatric patient

The superior mesenteric artery courses posterior to the neck of the pancreas separating the head from the body. The left lateral border of the vertebral column is the arbitrary plane demarcating the body and tail of the pancreas. Occasionally, the head, body and tail of the pancreas may be seen in one frame (Figs. 2.61, 2.62 and 2.63). Pancreas in elderly people may be smaller but this has no clinical significance.

The echogenicity of the pancreas is divided into four grades:

Grade I: Equal to the liver
Grade II: Slightly greater than the liver
Grade III: Definitely greater than the liver
Grade IV: As echogenic as retroperitoneal fat

Normal pancreas has Grade I and/or Grade II echogenicity.

The AP diameter of the head more than the transverse diameter of vertebral body suggests enlargement. The pancreatic duct 2–3 mm in diameter is seen in upper portion of the pancreas.

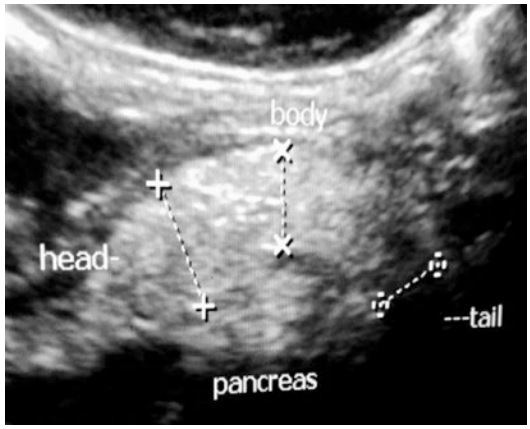

Fig. 2.61 Head, body and tail of the pancreas in coronal plane

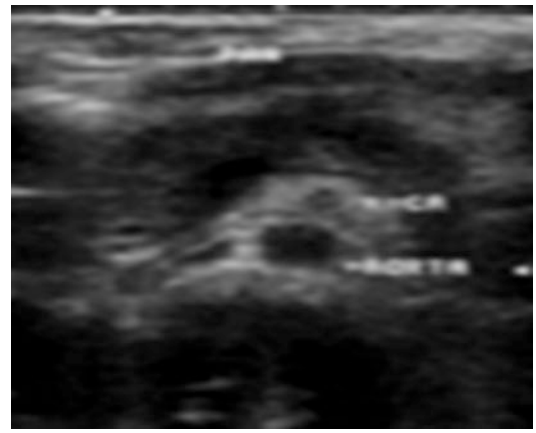

Fig. 2.63 Umbrella-like pancreas anterior to the abdominal aorta and celiac axis in coronal plane

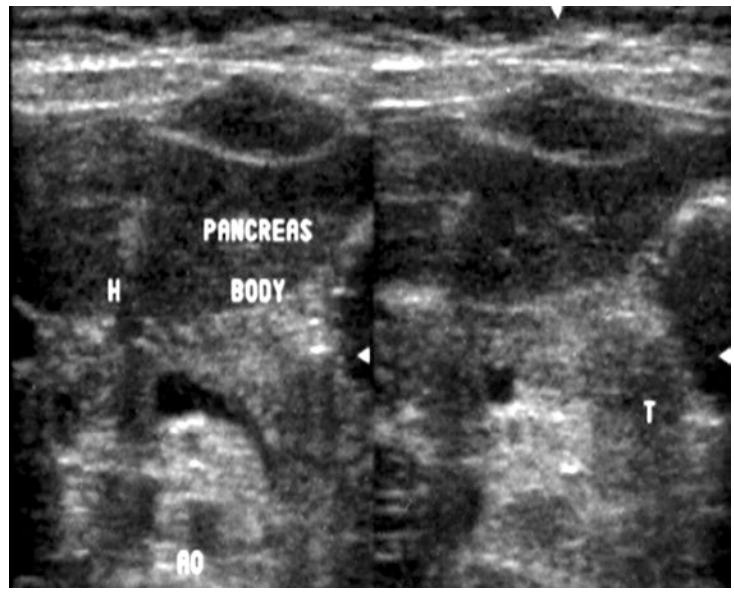

Fig. 2.62 Tail of the pancreas visualised better in the image taken at a different plane for the head and body

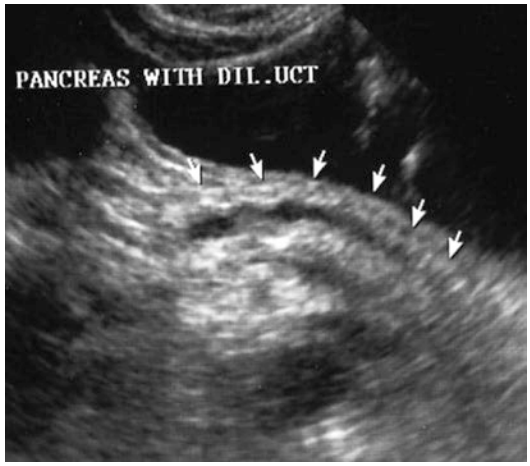

Fig. 2.64 Dilated pancreatic duct seen through distended stomach

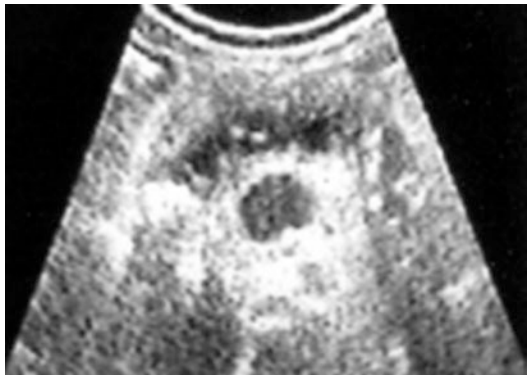

Fig. 2.65 Multiple calculi in dilated pancreatic duct

The dilated pancreatic duct is more easily visualised (Fig. 2.64). If the pancreatic duct is seen in its entire length, it should be considered abnormal and the presence of a small mass should always be looked for.

Causes of pancreatic duct dilatation include (1) tumours of the head of the pancreas or ampulla of Vater, (2) calculus in the pancreatic duct (Fig. 2.65), (3) chronic pancreatitis (Fig. 2.66) and (4) post-operative strictures following Whipple's operation or partial pancreatectomy.

The splenic vein runs on postero-inferior aspect of the pancreas to join the superior mesenteric vein posterior to the neck of the pancreas to form portal vein. The medial portion of the pancreatic head tapers to form the uncinate process. The echogenicity of the pancreas is equal to the liver. Fatty infiltration of the pancreas increases its echogenicity.

Acute pancreatitis: USG findings depend on the severity of disease [12].

(a) Mild forms consist of interstitial oedema limited to the gland with no or slight peripancreatic inflammation (Grade I) (Fig. 2.67).
(b) More severe cases show fat necrosis, parenchymal necrosis and haemorrhage (Grade II).
(c) More severe peripancreatic inflammatory changes with pseudocyst suggest Grade III acute pancreatitis (Fig. 2.68).

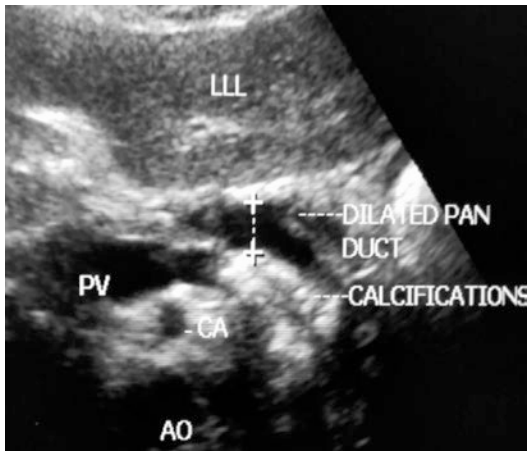

Fig. 2.66 Dilated pancreatic duct with pancreatic calcifications in chronic pancreatitis

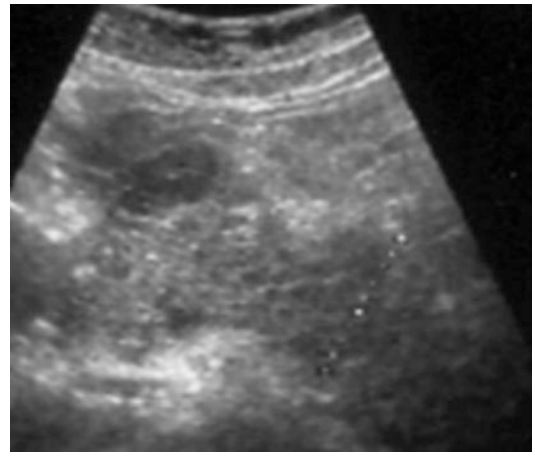

Fig. 2.67 Enlargement of the pancreas with poor definition in acute pancreatitis

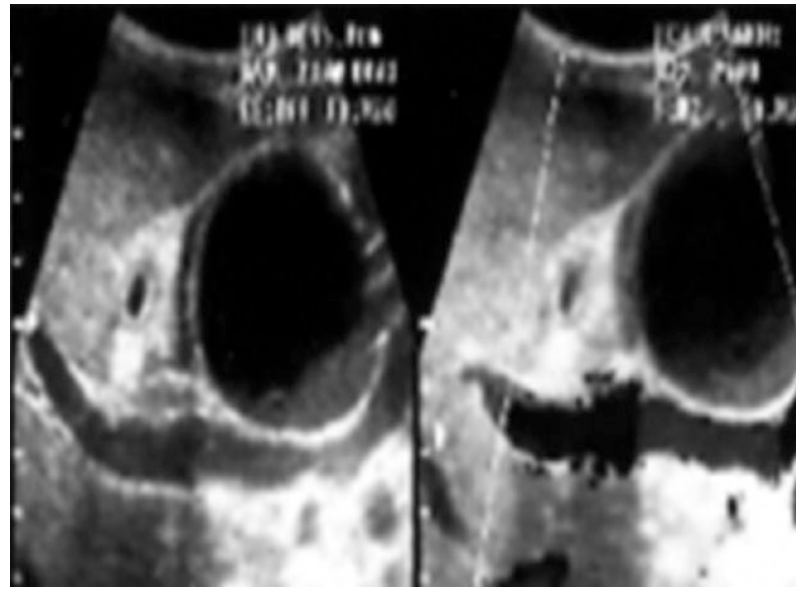

Fig. 2.68 Pseudocyst in the head of the pancreas

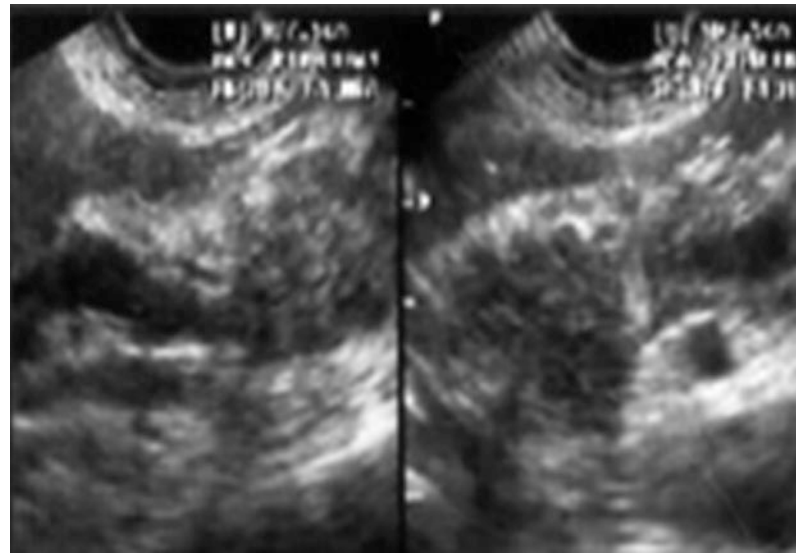

Fig. 2.69 Mass in the head of the pancreas with dilated common bile duct

Pseudocyst formation is an attempt to enclose the active inflammation. Pseudocyst may attain an enormous size and may become multilocular.

Chronic pancreatitis [13] usually results from repeated bouts of mild pancreatitis resulting from high alcohol intake or biliary tract disease. The USG findings include change in size and shape of the pancreas, focal masses, calcifications, pancreatic duct dilatation and pseudocyst formation. Pancreatic calculi often multiple in numbers are seen in the pancreatic duct.

In pancreatic malignancy [14], USG may reveal a poorly defined, homogenous or inhomogenous mass in the pancreas or pancreatic fossa. Compression of the adjacent structure may be an associated finding. The size of the head of the pancreas disproportionate to the body and the tail must be investigated for a mass (Fig. 2.69).

CT/MRI is a better diagnostic tool for pancreatic malignancy as it can do the staging of cancer at the same time.

2.1.6 Spleen [15]

It is seen below the left dome of the diaphragm through the intercostal space of the left lower ribs. The shape of the spleen is variable. The echogenicity of the spleen is lesser than the liver. Spleen becomes more echogenic when it enlarges. Normal spleen size is 12 cm length x breadth 7 cm × thickness 5 cm. The spleen is capable of growing to enormous size. During examination of the spleen, lesions in the neighbouring organs such as the kidney, adrenals, tail of the pancreas and stomach should be scanned carefully to avoid mistakes in the diagnosis.

The normal splenic vein 2–3 mm in diameter is seen in the splenic hilum (Fig. 2.70). The tortuous splenic vein and its dilated tributaries in the splenic pulp are seen in portal hypertension (Fig. 2.71).

The most common applications of ultrasound of spleen include diagnosis of splenomegaly [15] and evaluation of splenic trauma in blunt abdominal injury. The subcapsular and pericapsular haematomas of the spleen can be diagnosed with high accuracy. In splenic abscess filled with pus, CT may be more helpful.

Splenic infarction is seen as triangular (wedge shape) echo-poor area with its broad base away from the centre of the organ.

Nonparasitic cyst (Figs 2.72 and 2.73) may occasionally be found in the spleen.

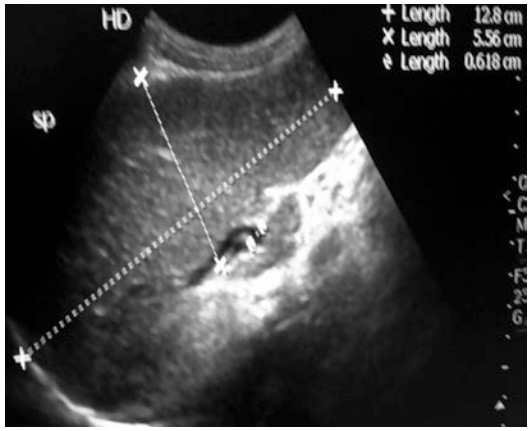

Fig. 2.70 Splenomegaly with dilated splenic vein

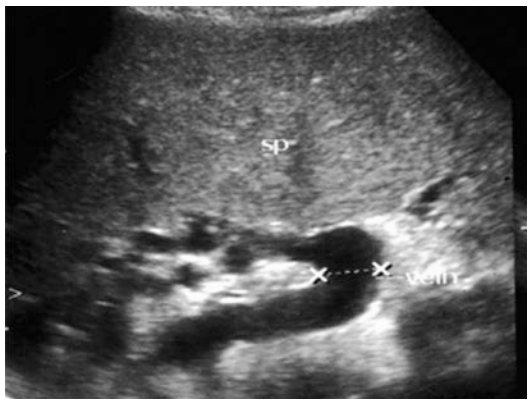

Fig. 2.71 Dilated and tortuous splenic vein and its branches in portal hypertension

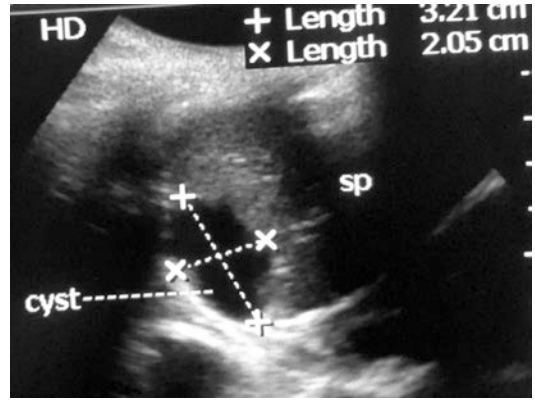

Fig. 2.72 Cystic lesion in the upper pole of the spleen

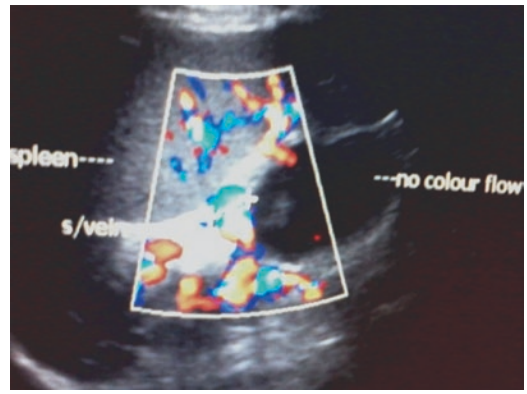

Fig. 2.73 No colour flow in nonparasitic cystic lesion located near splenic hilum, dilated splenic vein and increased vascularity in splenic pulp

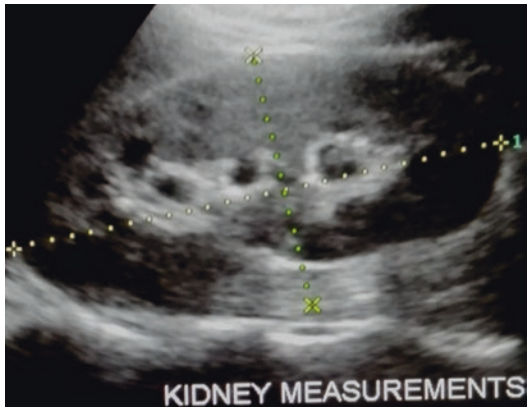

Fig. 2.74 Measurements for kidney size: *1* length, *AP* anteroposterior (xx)

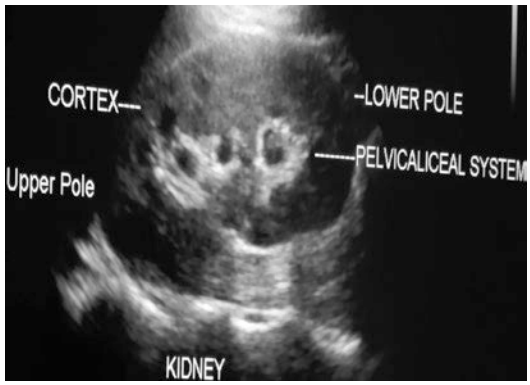

Fig. 2.75 Normal kidney as visualised in 2D sonography

2.2 Ultrasound of the Kidney, Urinary Bladder and Prostate

Abstract The KUB ultrasound is dependent on body habitus, operator experience and type of equipment. High-resolution real-time sector scanner should be used. The patient should fast 6 h before the examination to limit bowel gas. The patient position may be supine, oblique, lateral decubitus and occasionally prone position. A non-dilated ureter may be impossible to visualise because of overlying bowel gas.

2.2.1 Kidneys

The kidneys are seen as bean-shaped structure. The size of each kidney is about 11 cm long, 2.5 cm thick and 5 cm wide (Fig. 2.74). The outline of the kidney is well demarcated. The renal parenchyma is composed of cortex and medullary pyramids. The normal echogenicity of renal cortex is less than the adjacent liver and spleen. The abnormal renal function correlates well with increased echogenicity of the renal cortex. The calices and renal pelvis constitute the pelvicaliceal system (Fig. 2.75). The renal pelvis continues downwards as ureter. The renal sinus is usually about one third of the kidney.

The calculus is the most common disease of urinary system [16, 17]. The calculus may be seen in the calices (Figs. 2.76, 2.77 and 2.78) or

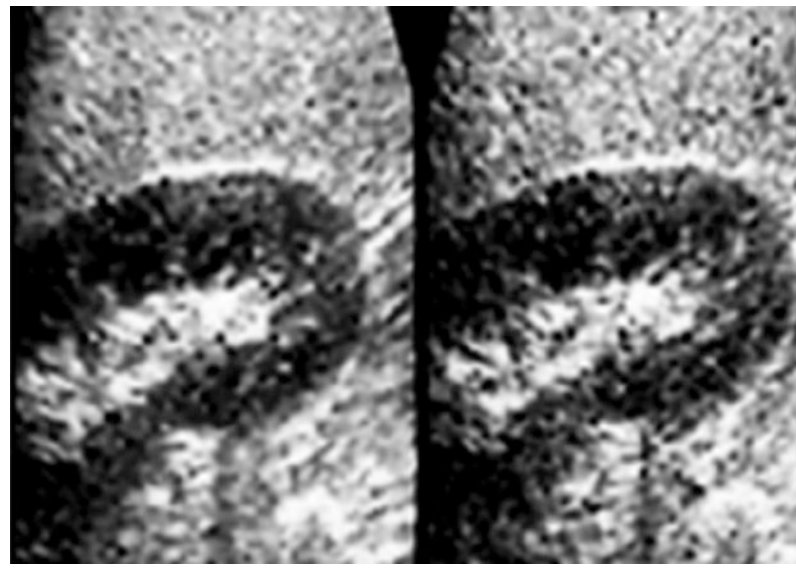

Fig. 2.76 Calculus in lower calyx with posterior shadow and no hydronephrosis

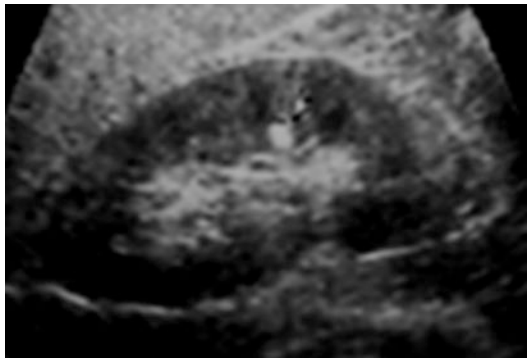

Fig. 2.77 Calculus in the middle calyx right kidney

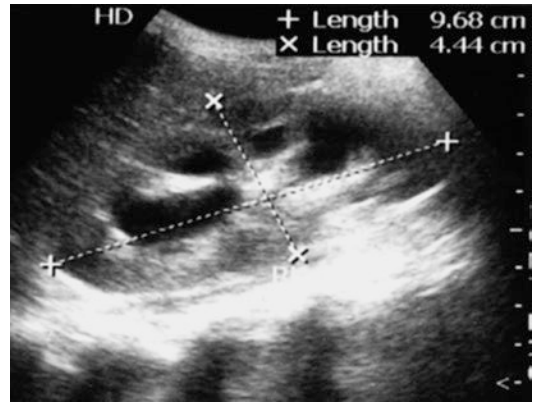

Fig. 2.79 Mild hydronephrosis (caliectasis) right kidney

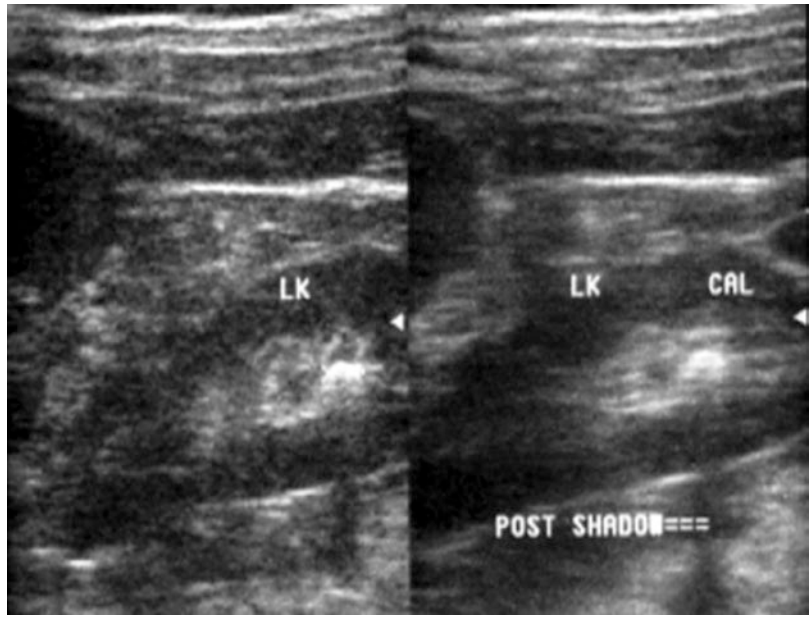

Fig. 2.78 Calculus in the lower calyx left kidney with posterior shadow, no obstructive changes

the renal pelvis or in the ureter or in the urinary bladder. The calculus in the kidney and UB is easy to identify. The calculus in proximal ureter or pelvic ureter may be picked up after gaining some experience in USG. The size of the calculus may vary from few millimetres to few centimetres. They may be single or multiple. The stones of less than 5 mm size may pass spontaneously.

The hydronephrosis secondary to calculus may be mild to severe in degree, or there may be an associated large hydronephrotic sac.

The hydronephrosis secondary to calculus may be mild (Figs. 2.79 and 2.80) to severe in degree, or there may be an associated large hydronephrotic sac (Figs. 2.81 and 2.82).

Sonographic grading of hydronephrosis [18]: The most common system used by Society of Fetal Ultrasound is as follows:

Grade 0: No dilatation, caliceal walls opposed to each other

Grade I: Dilatation of the renal pelvis without dilatation of calices, no parenchymal atrophy

Grade II: Mild dilatation of the renal pelvis and calices (pelvi-caliceal pattern is retained), no parenchymal atrophy

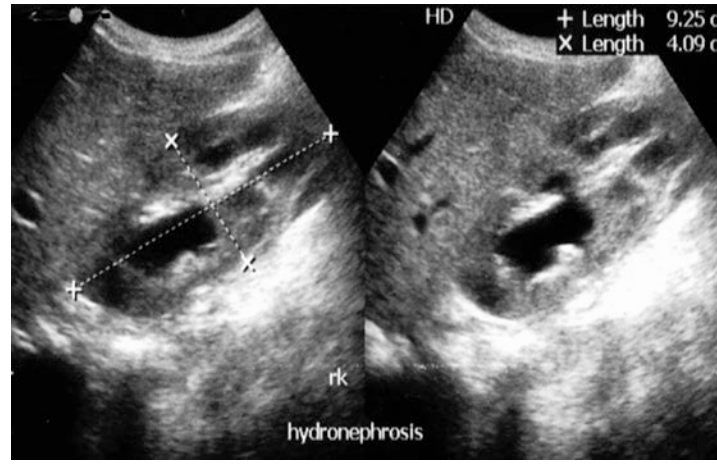

Fig. 2.80 Mild hydronephrosis with a calculus in the upper calyx of the right kidney

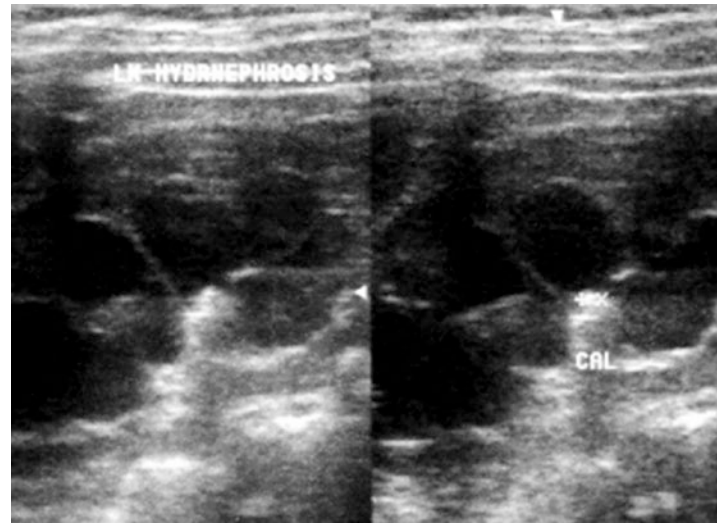

Fig. 2.81 Calculus in the renal pelvis with Grade III hydronephrosis

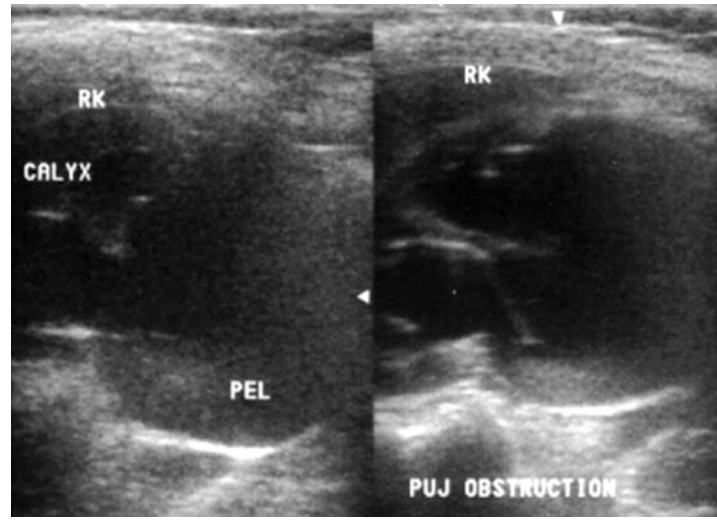

Fig. 2.82 Severe hydronephrosis of the right kidney with PUJ obstruction and thinning of the renal cortex

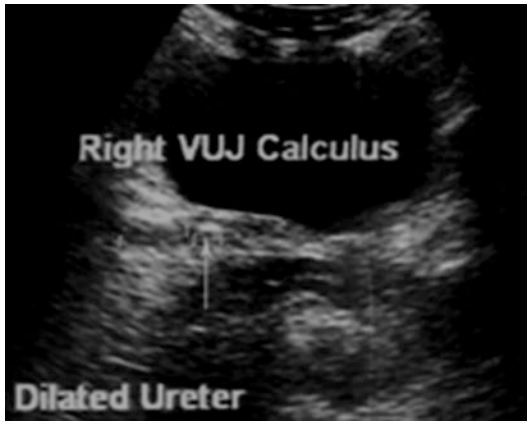

Fig. 2.83 Calculus at right VU junction with dilated pelvic ureter

Grade III: Moderate dilatation of the renal pelvis and calices, blunting of fornices and flattening of papillae and mild cortical thinning

Grade IV: Gross dilatation of the renal pelvis and calices, renal atrophy seen as cortical thinning

Each ureter is about 30–34 cm long and 2–4 mm in diameter. The normal ureter is difficult to visualise in its entire length due to superimposed bowel gas, while dilated ureter is easy to identify. However, normal proximal ureter and portion of the pelvic ureter can be identified (Figs. 2.83, 2.84 and 2.85). Both ureters may be dilated in chronic cystitis (Fig. 2.86).

The urinary bladder is located in the pelvis. Its wall is smooth and of uniform thickness (1–2 mm).

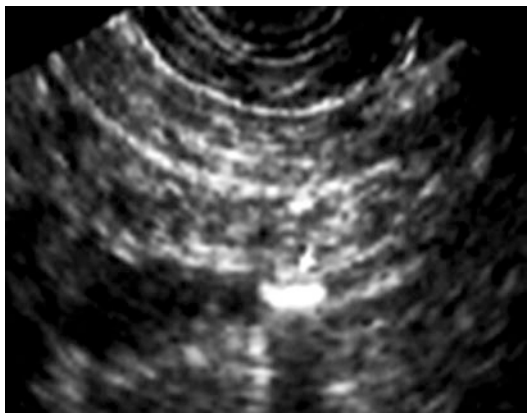

Fig. 2.84 Calculus in dilated ureter with posterior shadow

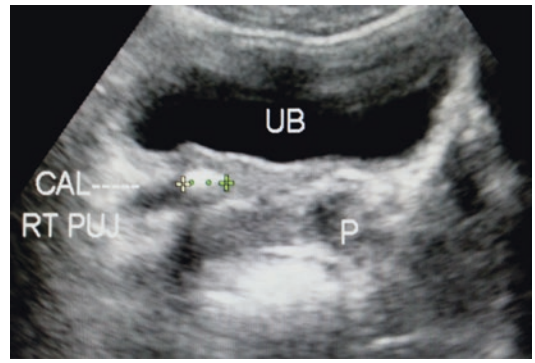

Fig. 2.85 Calculus at the right vesico-ureteric junction

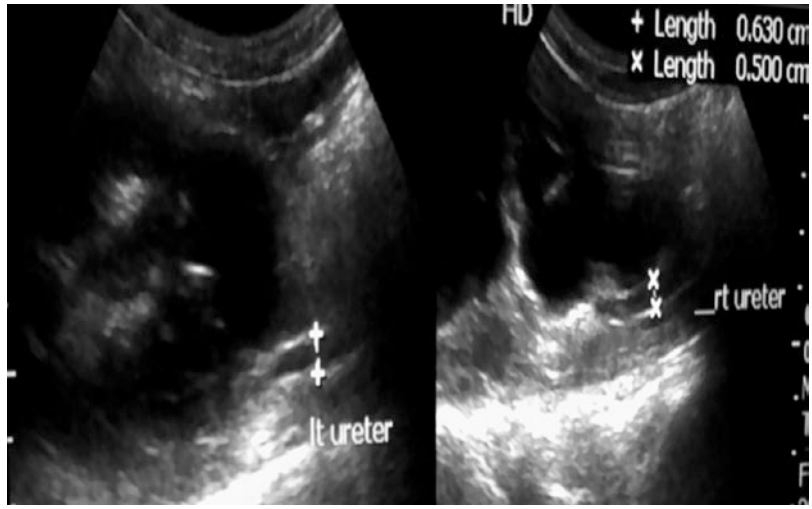

Fig. 2.86 Dilated bilateral pelvic ureter in chronic cystitis

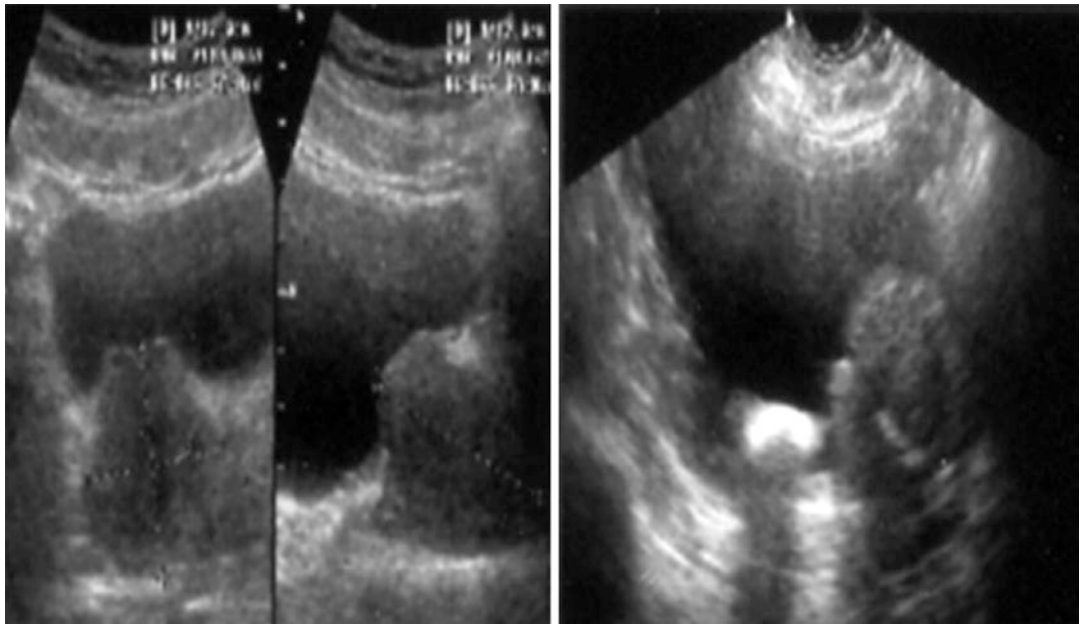

Fig. 2.87 Enlarged median lobe in BPH with associated vesical calculus

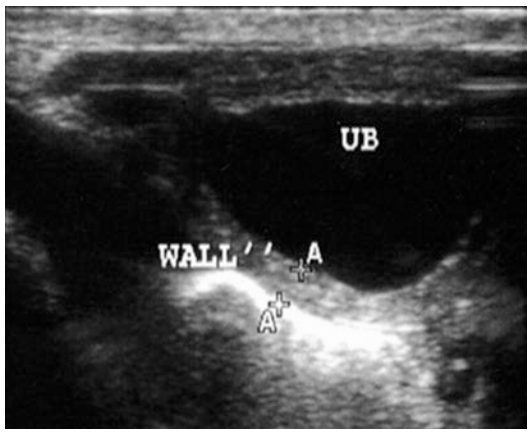

Fig. 2.88 Thickening of the UB wall in chronic cystitis

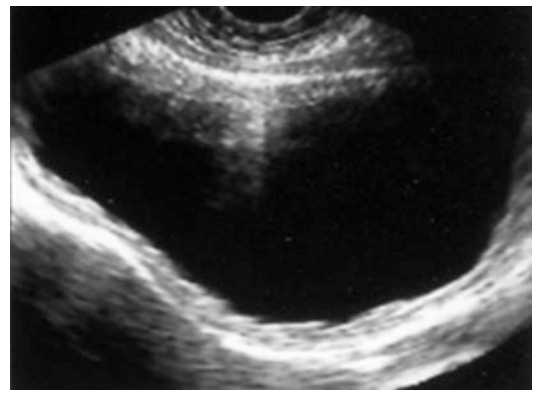

Fig. 2.89 Diffuse thickening of the UB wall in cystitis

The wall thickness varies with the degree of distension of UB. The volume of the urinary bladder after voiding (PVR) can be determined by the formula: length × width × AP dimension × 0.52 = volume in mL.

Vesical calculus is fairly easy to pick up at USG (Fig. 2.87).

In chronic cystitis, irregular shape and thickening of the UB wall (Figs. 2.88 and 2.89) with coarse trabeculations inside (Fig. 2.90) and increased PVR are the usual sonographic findings.

Echogenic urine in the urinary bladder is seen in pyuria (Fig. 2.91).

Growth in the urinary bladder often invades into the bladder wall and neighbouring pelvic planes at the time when the diagnosis is made (Figs. 2.92 and 2.93). CT is a better choice for the evaluation of growth in the urinary bladder.

Despite remarkable improvements in the diagnostic accuracy, some of the pitfalls of

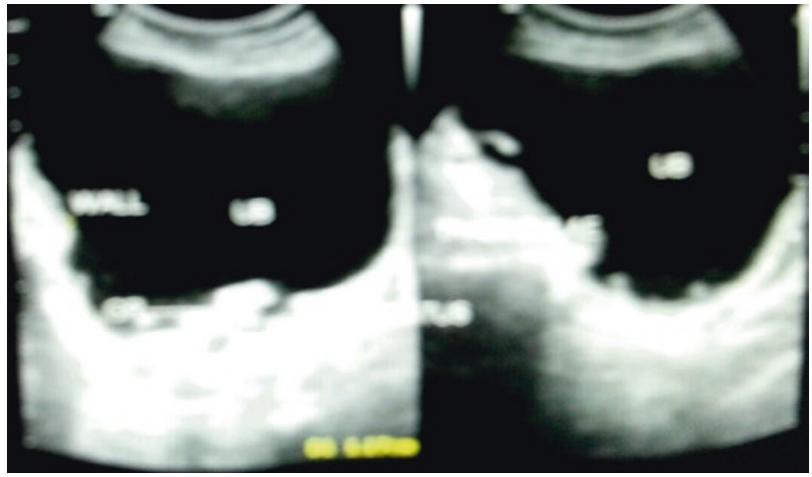

Fig. 2.90 Coarse trabeculae in chronic cystitis

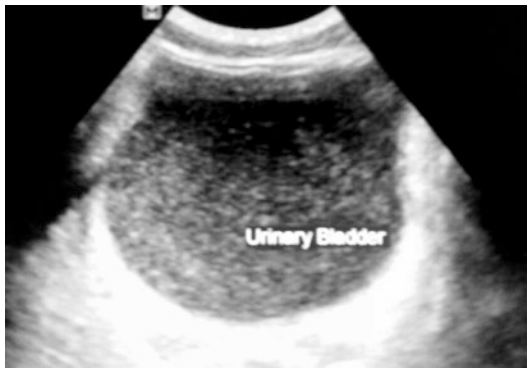

Fig. 2.91 Fine echogenicity in the bladder in pyuria

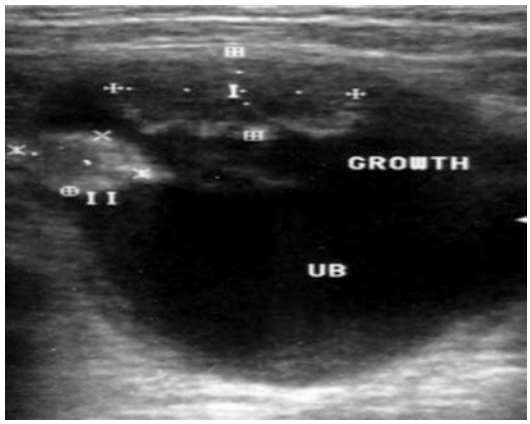

Fig. 2.92 Growth in UB at 9–12 o'clock position

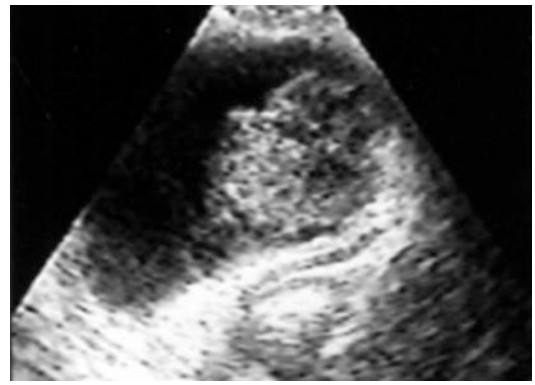

Fig. 2.93 Growth in the base and left wall of UB at 4–6 o'clock position

ultrasonographic tests for evaluation of the bladder as a possible source of haematuria still remain. Smaller lesions (smaller than 0.5 cm) and lesions located in the dome or bladder neck are more difficult to visualise sonographically. Tumour configuration is also an important factor: plaque-like lesions are almost certainly harder to detect than polypoid ones [19].

The cyst in the renal cortex is seen usually as a coincidental finding. The benign cyst has well-defined thin wall, and it contains clear (echo-free) fluid (Fig. 2.94). The benign cysts are more often seen in patients beyond 60 years of age as a senile change and are usually asymptomatic (Fig. 2.95). The cysts of more than 5 cm size, having solid area or haemorrhage inside with the presence of pain in flank or ureteric colic-like symptoms, need attention and proper management.

Adult polycystic disease of the kidney (Fig. 2.96) shows the presence of multiple cysts of variable sizes in the cortex in both kidneys with non-distension of the renal pelvis [20].

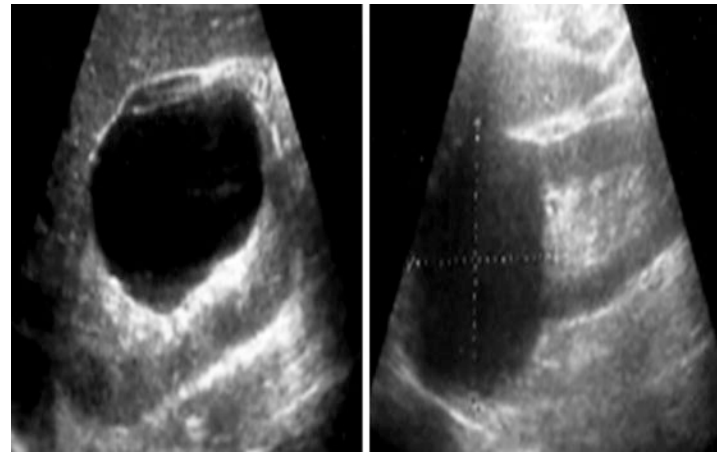

Fig. 2.94 Benign cyst in the upper pole of the right kidney

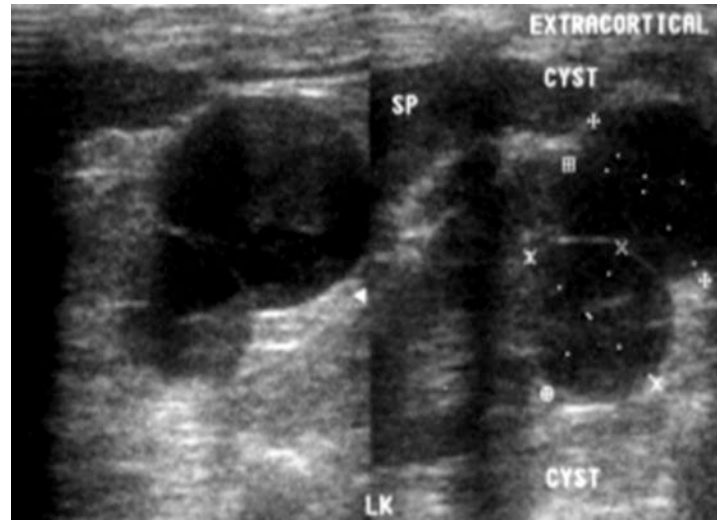

Fig. 2.95 Extracortical cyst at the lower pole of the left kidney

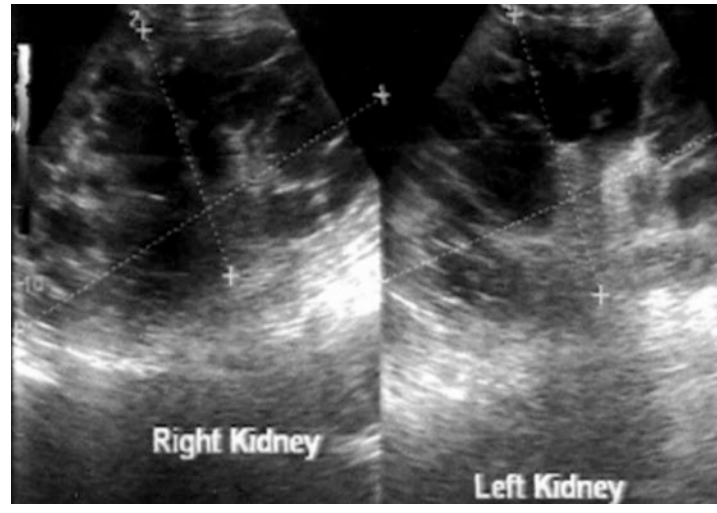

Fig. 2.96 Adult polycystic disease of the kidney

Polycystic disease

1. Autosomal recessive polycystic kidney disease (ARPCK) depending on the age of onset in individual is divided into four types: perinatal, neonatal, infantile and juvenile. USG reveal massively enlarged and echogenic kidneys with lack of cortico-medullary differentiation. Occasionally, macroscopic cysts will be noted.
2. Autosomal dominant polycystic kidney disease (ADPCK) results in a large number of bilateral cortical and medullary renal cysts which vary considerably in size and are often asymmetric. Sonography may reveal cysts with thick wall and internal echoes when complicated by haemorrhage or infection. Dystrophic calcification in cyst wall or stones may be seen.

Multicystic dysplastic kidney disease (*MCDK*) is usually unilateral and involves the whole kidney. Sonography reveals multiple noncommunicating cysts, absence of normal renal parenchyma and normal renal sinus and focal echogenic areas of primitive mesenchymal or tiny cysts.

Perinephric haematoma (Fig. 2.97) shows obscuration of renal outline and large haematoma may result into renal tamponade.

Angiomyolipoma is a highly vascular benign tumour of the kidney (Fig. 2.98) in which biopsy or aspiration cytology should not be done and CT angiography may be needed to establish the diagnosis.

The renal mass lesions are usually solid (Fig. 2.99). There may be calcification or cystic areas within the mass. Renal biopsy or ultrasound-guided aspiration cytology is needed to confirm malignancy. Colour flow study within the mass is helpful.

Ultrasound is the first diagnostic tool for evaluation of renal parenchymal disease [21]. Renal cortex is slightly more echogenic than the medulla (Fig. 2.100). This differentiation is lost

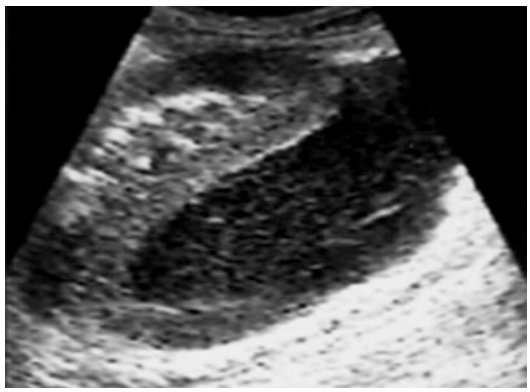

Fig. 2.97 Perinephric haematoma

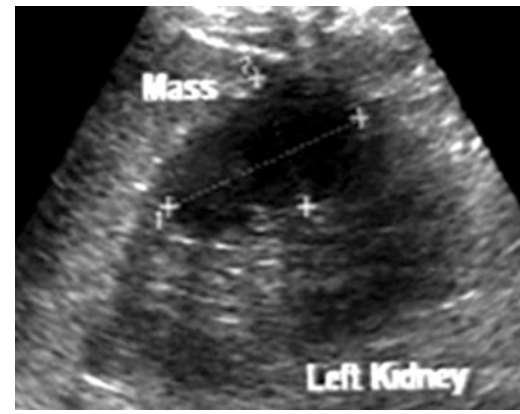

Fig. 2.99 Renal mass in the left kidney

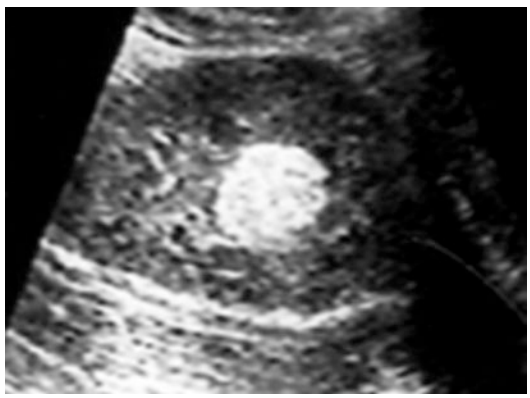

Fig. 2.98 Angiomyolipoma of the kidney

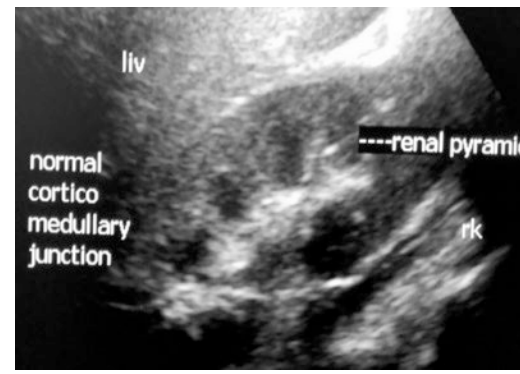

Fig. 2.100 Renal cortex and pyramids in the normal kidney

in renal parenchymal disease (Figs. 2.101 and 2.102). All medical diseases of the kidney, nephritis, glomerulonephritis and those associated with systemic diseases are considered as renal parenchymal diseases.

The comparison of echogenicity of the renal cortex with liver parenchyma and with pelvi-caliceal system of the kidney is used to classify the renal parenchymal disease into four grades:

Grade I: Increased echogenicity of the renal cortex equal to liver parenchyma
Grade II: Echogenicity of the renal cortex more than liver parenchyma
Grade III: Echogenicity of the renal cortex equal to pelvi-caliceal system
Grade IV: Echogenicity of the renal cortex more than the pelvi-caliceal system

The kidneys may become small in size (contracted kidneys) in terminal stage.

Grade I and Grade II sonographic changes of bilateral renal parenchymal disease (Fig. 2.103) may revert to normal after proper management, while Grade III and Grade IV changes are irreversible (prognostic significance).

Nephrotic syndrome in paediatric patients reveals that the kidneys are enlarged in size with markedly increased anteroposterior dimension

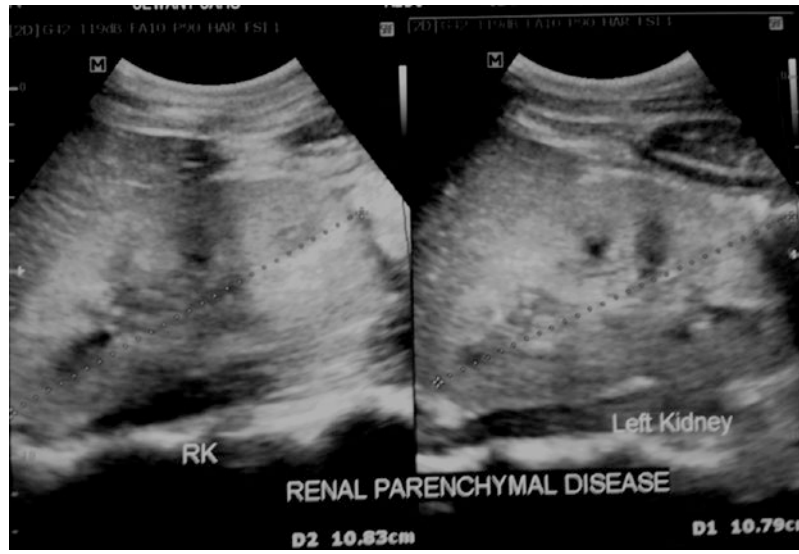

Fig. 2.101 Loss of cortico-medullary differentiation in renal parenchymal disease (Grade III)

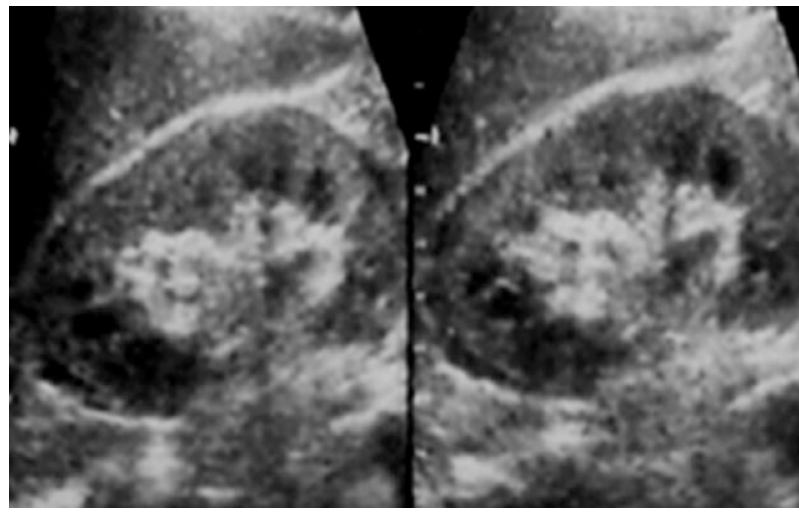

Fig. 2.102 Acute pyelonephritis with swollen renal pyramids and increased echogenicity of renal cortex equal to echogenicity of the liver

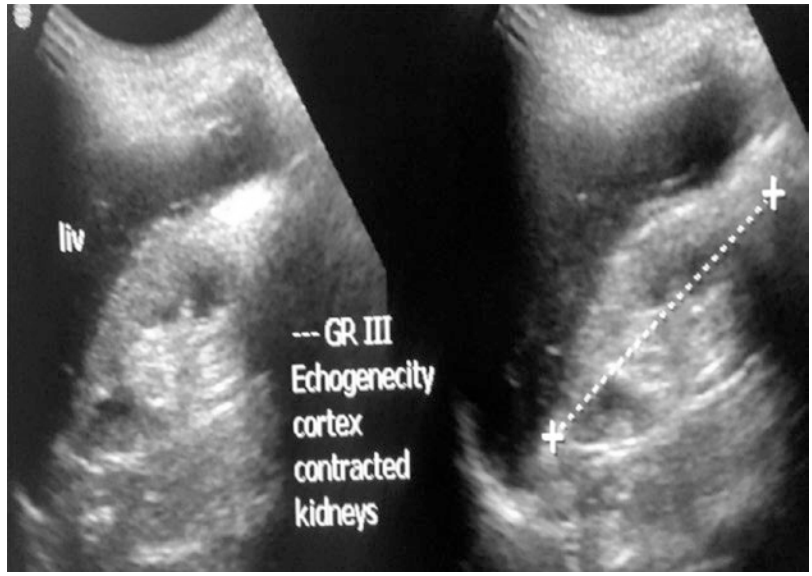

Fig. 2.103 Echogenicity of the renal cortex more than liver parenchyma and less than pelvicaliceal system (Grade III renal parenchymal disease)

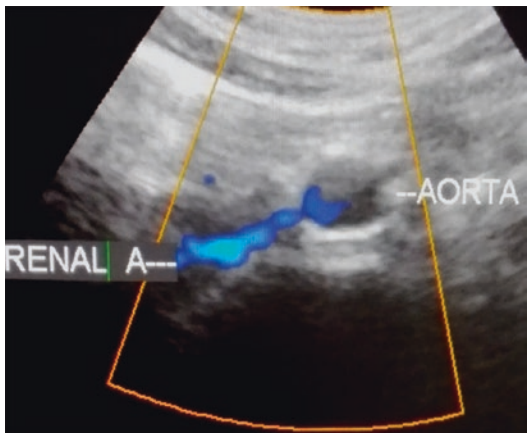

Fig. 2.104 Right renal artery origin from the abdominal aorta in colour Doppler

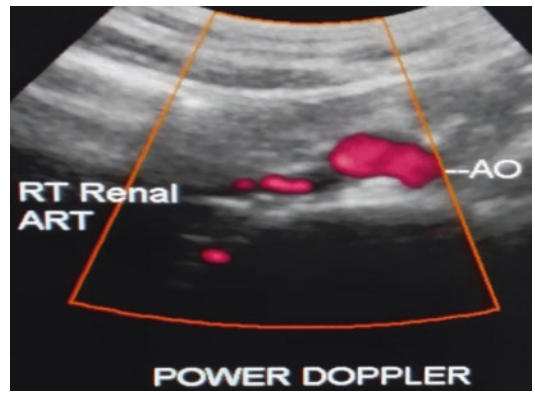

Fig. 2.105 Origin of the right renal artery from the aorta in power Doppler mode

and swollen renal pyramids. Echogenicity of renal cortex is increased with coexistent ascites.

In renal hypertension, colour Doppler study of intrarenal vasculature and detection of abnormal Doppler signals at or just distal to stenosis is more rewarding as the evaluation of main arteries as a screening technique has not proved to be successful. Therefore, intra-arterial digital subtraction angiography or MR angiography is being used to improve detection rate of renal hypertension. Colour flow mapping of renal artery is shown in Figs. 2.104, 2.105 and 2.106.

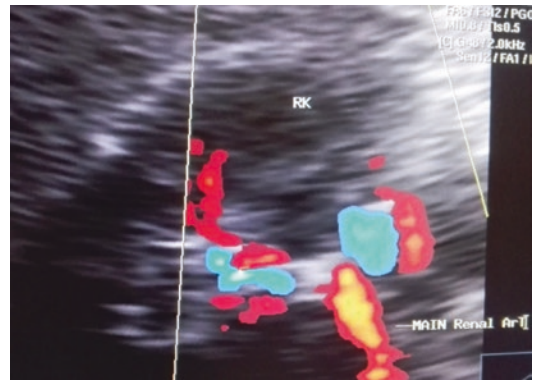

Fig. 2.106 Main renal artery in colour flow mapping

Doppler in Renal Artery Stenosis (RAS)

Significant controversy persists about the role of Doppler ultrasound in the diagnosis of RAS [grey]. The lack of the normal early systolic peak in segmental renal artery is the best predictor of renal artery stenosis with luminal narrowing of greater than 60% (Stavros).

The use of Doppler in diagnosis of RAS [22] is because of its ability to identify a focal area of increased peak systolic velocity (PSV) (Fig. 2.107) at the anatomic site of stenosis and to demonstrate a decrease in the rate of systolic acceleration distal to a stenosis. Studies have suggested that a PSV >100 cm/s or RAR >3.5 (ratio of peak systolic renal artery velocity to peak systolic aortic velocity) has sensitivities of 79–91% and specificities of 73–92% for haemodynamically significant RAS (>50–60%) diameter reduction [22].

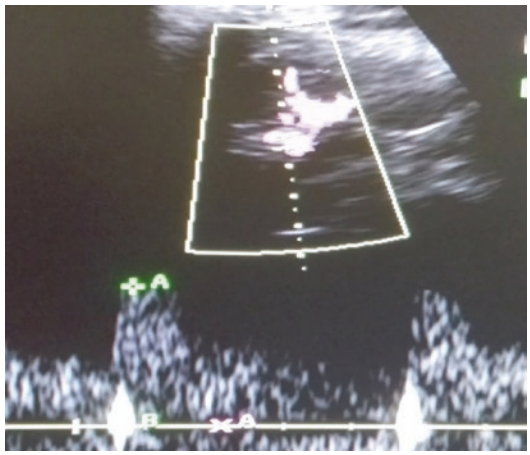

Fig. 2.107 Doppler waveform in normal renal artery

Obstructive Uropathy

Platt et al. [23] found an elevated mean RI of 0.77 in acutely obstructed kidney when no pyelectasis is observed. However, RI of >0.7 is found in hydronephrosis.

In unilateral pyelocaliectasis, the resistance index ratio (RIR) of 1.1 or more (RI of obstructed kidney divided by RI of non-obstructed kidney) suggests obstruction [24].

Hepatorenal Syndrome

It is defined as unexplained kidney failure in a patient with liver disease who does not have clinical, laboratory or anatomic evidence of other known cause of kidney failure. The hallmark change is intrarenal vasoconstriction [25, 26] reflected as an elevated RI.

Ectopic Kidney

The kidney may be located in ectopic position from the pelvis to its ascent into the renal fossa (Figs. 2.108 and 2.109).

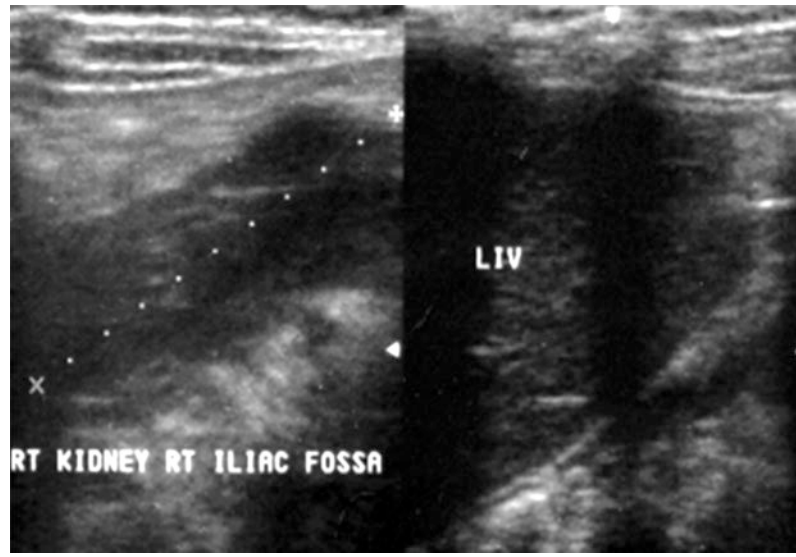

Fig. 2.108 Absence of the right kidney in sub-hepatic area, with ectopic location in the right iliac fossa

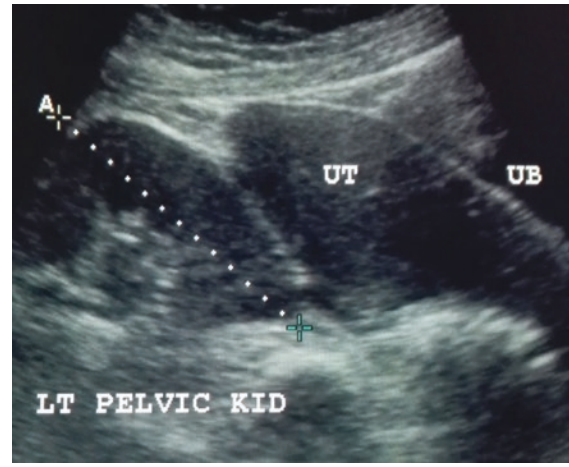

Fig. 2.109 Ectopic location of the left kidney in the pelvis, uterus (ut) and urinary bladder (UB)

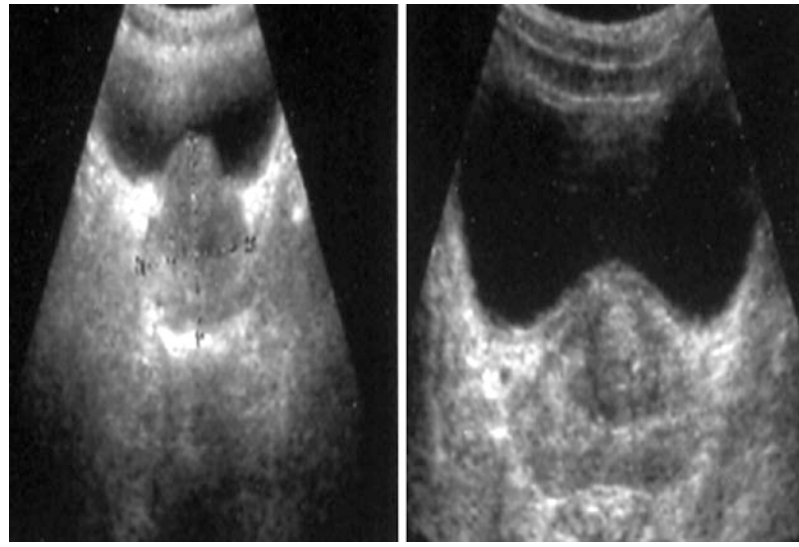

Fig. 2.110 Prostatomegaly (BPH) with enlarged median lobe jutting into the bladder base

Suprarenal glands are located at the upper pole of the kidney and normal adrenal glands are difficult to visualise in ultrasound. The tumours of adrenal glands can be missed by ultrasonography unless they attain a bigger size. CT/MRI is extremely useful in such situations.

2.2.2 Prostate [27–29]

The transabdominal approach through the urinary bladder is quite accurate for assessing the size and the enlargement of the prostate (hypertrophy). However, for detection of prostatic tumour, the usefulness of transabdominal sonography is limited where transrectal technique and colour USG are more useful.

The sonographic anatomy of the prostate is described as the peripheral zone and the inner gland which encompasses the transitional and central zones and the periurethral glandular area. However, the concept of median lobe and its enlargement in benign prostatic hypertrophy (BPH) still holds good (Figs. 2.110 and 2.111). The outline of the prostate is well defined. Normal prostate has iso-echoic texture.

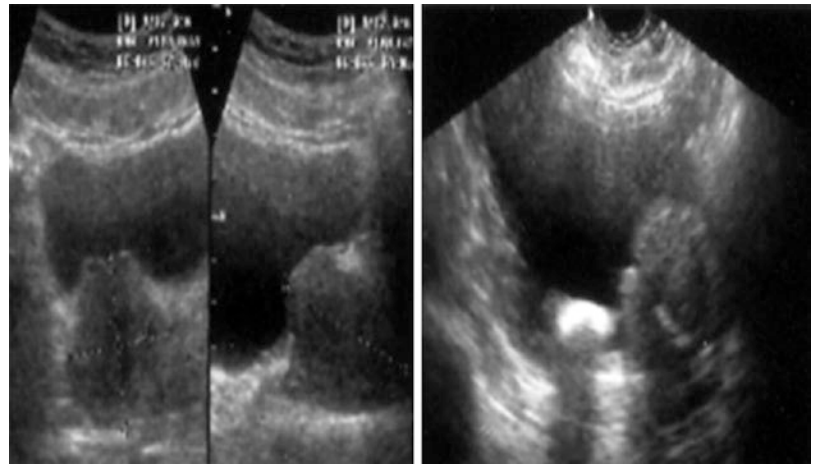

Fig. 2.111 Enlarged median lobe in BPH with associated vesical calculus

The normal prostate weighs less than 20 grammes in younger patient. At age 50, its weight less than 40 g is considered normal. The weight of the prostate is determined by the formula: Length (L) × Width (W) × Height (H) × 0.52 = Weight in grammes/volume in mL.

Prostatic enlargement can be divided into mild, moderate and severe depending on the weight of the prostate:

Mild = below 40 g
Moderate = 40–60 g
Severe = above 60 g

Transurethral resection (TUR) of the prostate is considered to be more rewarding in cases where the prostatic weight is less than 60 g. Prostatic hyperplasia may be observed again after a gap of few months or years post-TUR.

Post-void residual volume of 5–10 mL is normal. PVR of 20 mL or more is considered to be significant (Fig. 2.112).

Twenty percent of the men above 40 years and 43% of the men above 60 years may have benign prostatic hypertrophy (BPH). There is no clear relation between prostatic volume and symptoms. The international prostate symptom score has been developed to decide treatment options.

Prostate-specific antigen (PSA) levels are used for screening of prostate cancer. All men above the age of 50 should have routine yearly PSA and digital rectal examination and prostate ultrasound.

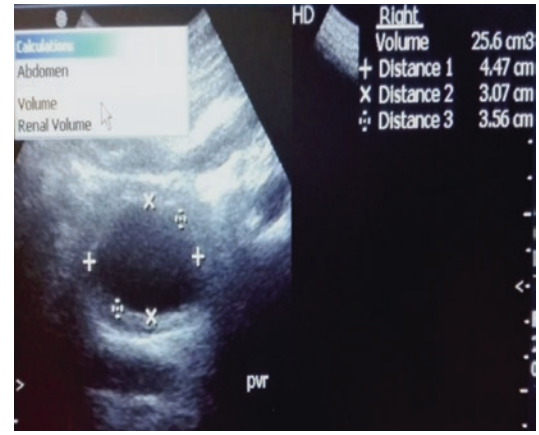

Fig. 2.112 Measurements of UB after voiding (*PVR* post-void residue)

The normal PSA levels are [30]:

Ages 40–49 = 0–2.5.
Ages 50–59 = 0–3.5.
Ages 60–69 = 0–4.5.
Ages 70–79 = 0–6.5.

PSA determination of 0–4 ng/mL is normal and above 10 ng/mL is abnormal. Transrectal ultrasound (TRUS) acts as a diagnostic technique for staging of prostate cancer.

Sonography in chronic prostatitis may reveal focal masses of different degrees of echogenicity, capsular thickening or irregularity, periurethral glandular thickening and distended seminal vesicles.

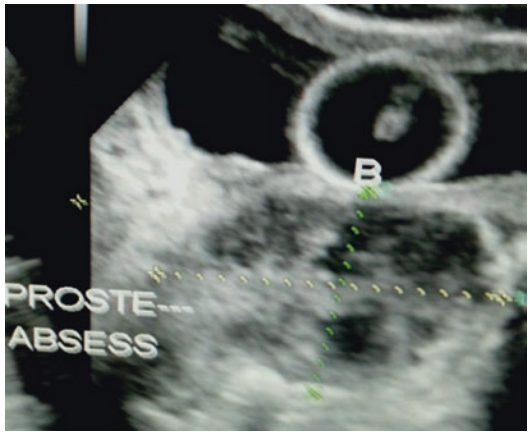

Fig. 2.113 Heterogenous texture of the prostate with thickening of capsule in prostatic abscess

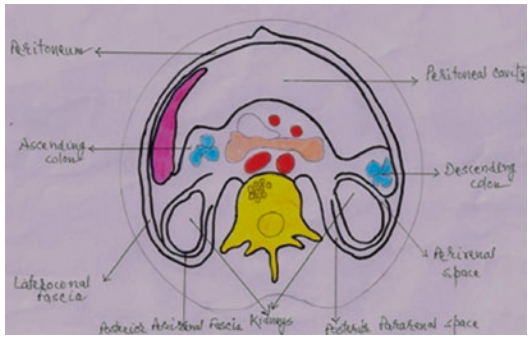

Fig. 2.114 Retroperitoneal spaces (From Wikipedia, free encyclopaedia)

Prostatic abscess reveals anechoic mass with or without internal echoes which is difficult to differentiate from carcinoma (Fig. 2.113).

Retroperitoneum [31]

Retroperitoneum contains a variable amount of fibrous and fatty tissue. The fascia divides it into a number of spaces (Fig. 2.114). The most common pathology is the presence of a mass.

USG signs include displacement of normal structures, direct invasion of neighbouring organs, asymmetry of normal structures and loss of retroperitoneal details. With USG, it can be determined whether it is solid/cystic/vascular, fixed/free, presence of air/calcium and its size. Only enlarged lymph nodes can be detected with USG.

CT usually is the imaging procedure of choice for evaluating retroperitoneum.

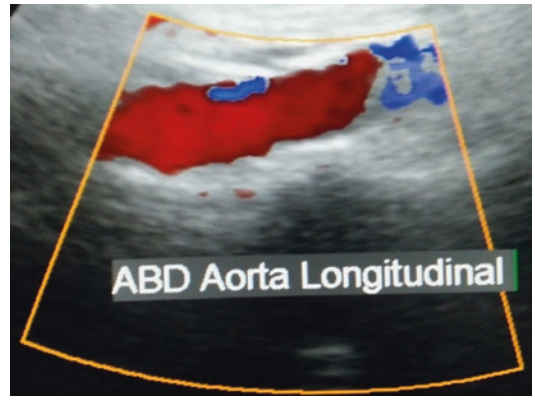

Fig. 2.115 Colour flow in the proximal abdominal aorta in long section

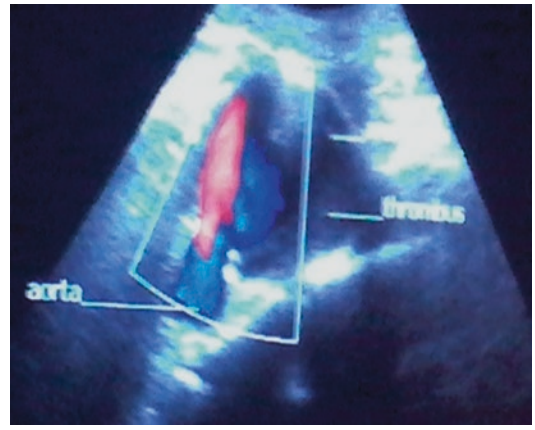

Fig. 2.116 Aortic aneurysm with thrombus partially blocking the aortic lumen

Abdominal aorta: It is located slightly left to midline in the upper abdomen to lower abdomen where it divides into the right common iliac artery and the left common iliac artery. Its pulsations can be seen. Celiac axis and renal arteries can be visualised in upper portion of the abdominal aorta. The normal diameter is 2.3 cm in males and 1.9 cm in females. The indications for aortic USG are visualisation of the entire abdominal aorta (Fig. 2.115) and its branches, detection of atheromatous stenosis, aneurysm (Fig. 2.116) and dissection and evaluation of adjacent organs. Spectral Doppler analysis provides valuable information in regard to velocity and flow pattern.

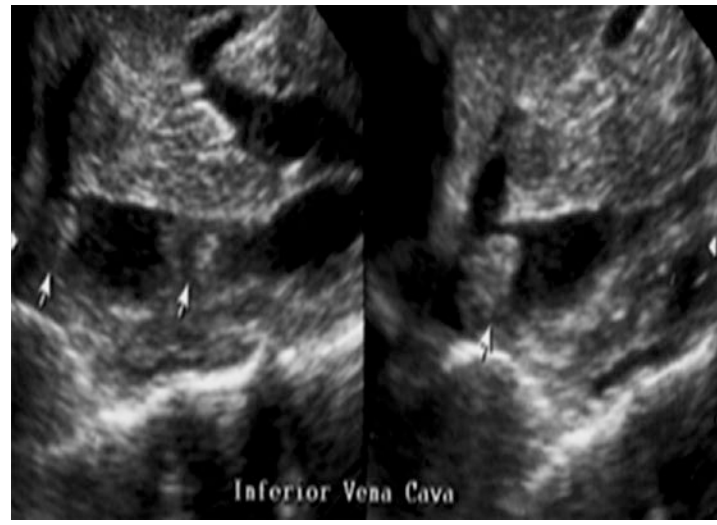

Fig. 2.117 Tumour thrombus in IVC in subdiaphragmatic area

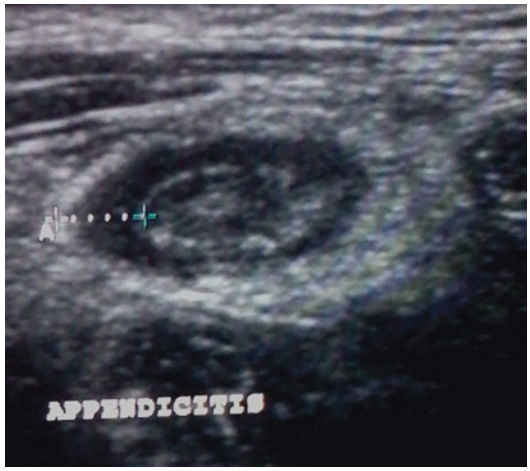

Fig. 2.118 Thickening of appendicular wall in coronal plane in acute appendicitis

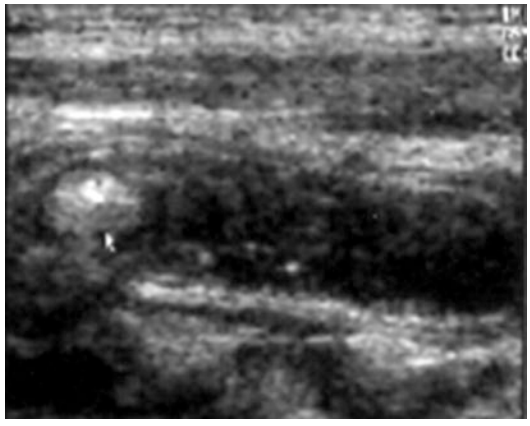

Fig. 2.119 Dilated appendix with faecal mass in acute appendicitis

Inferior vena cava (IVC) is viewed in the upper abdomen where its intrahepatic portion is seen. The remainder of the vessel is inconsistently seen due to bowel gas. With deep inspiration IVC dilates and with deep expiration its diameter decreases. Cardiac failure and fluid overload increase the diameter of IVC and hepatic veins. IVC may reveal a tumour thrombus (Fig. 2.117) in a patient of malignancy.

2.2.3 USG of Appendix [32]

The right iliac fossa can be evaluated for appendix. The normal appendix is difficult to visualise. The position of the appendix is variable which poses difficulty in its imaging. However, acute appendicitis with graded compression can be diagnosed keeping in view the thickness of wall 3 mm and greater (Fig. 2.118), diameter of appendix 6 mm and more, presence of appendicolith (Fig. 2.119) or fluid around appendix. False-positive diagnosis could be higher than expected; therefore it is better to have CT for more reliable and confident diagnosis.

Colour flow imaging reveals increased vascularity in appendicular wall (Figs. 2.120 and 2.121).

Figure 2.122 reveals appendicular abscess.

In acute appendicitis, echogenic fluid containing dilated small intestinal loops due to ileus may be visualised in the right lower of the abdomen (Fig. 2.123).

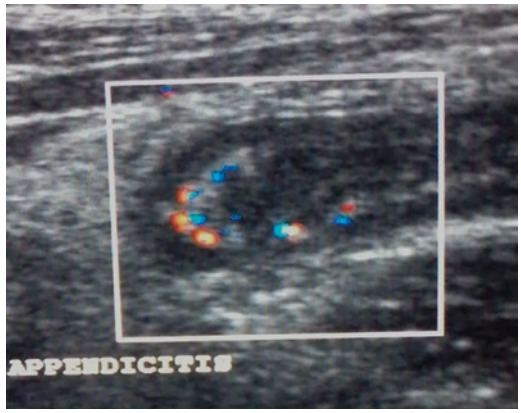

Fig. 2.120 Hypervascularity and thickening of the wall in acute appendicitis

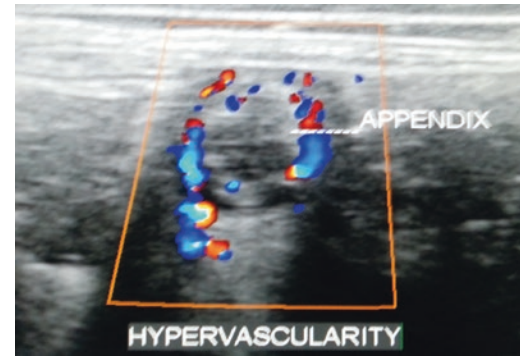

Fig. 2.121 Hypervascularity in appendicular wall in cross-section image in appendicitis

Fig. 2.122 Enlarged appendix with abscess

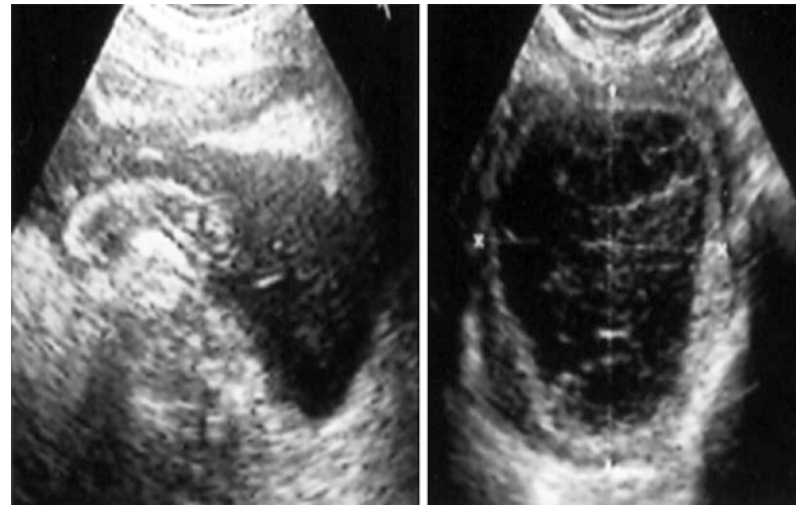

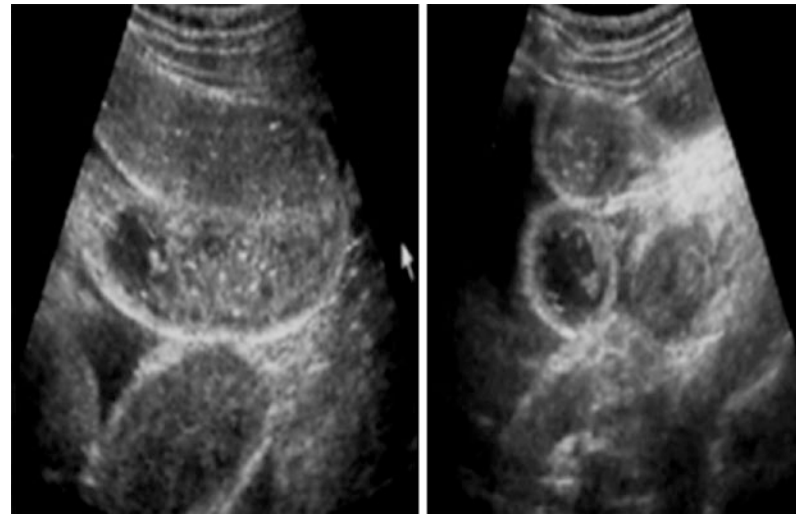

Fig. 2.123 Dilated intestinal loops with fluid in peritoneal cavity in acute appendicitis

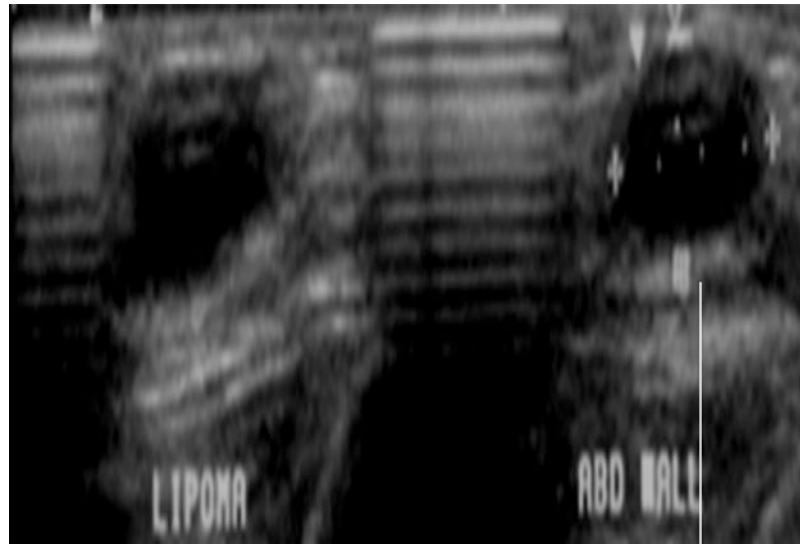

Fig. 2.124 Lipoma in the anterior abdominal wall

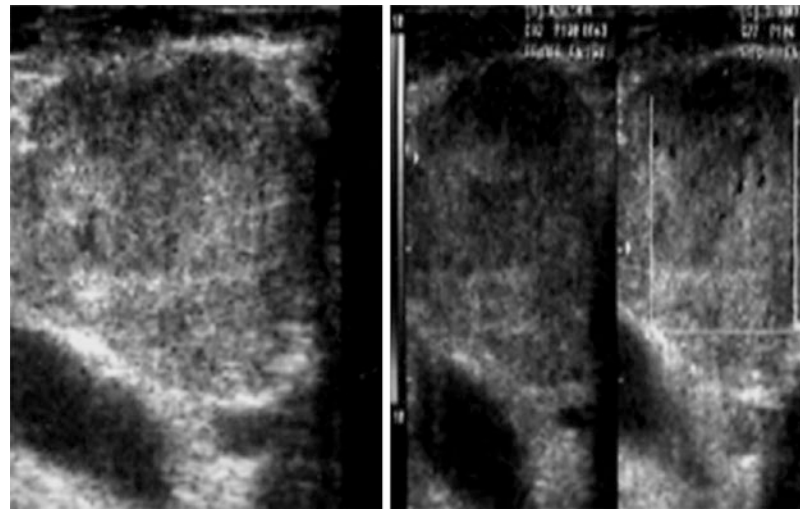

Fig. 2.125 Enlarged (Virchow's) lymph node in right subclavicular area

Anterior abdominal wall [33]: Imaging of anterior abdominal wall with 6–8 MHz linear probe may reveal lipoma (Fig. 2.124), neurofibroma, haematoma or abscess.

Occasionally USG is recommended to detect lymphadenopathy (Figs. 2.125, 2.126 and 2.127). However, the main object is to differentiate abscess/solid mass lesion from cystic lesion in case of doubt.

2.2.4 Detection of Pleural Effusion [34]

The thorax can be examined by direct intercostal/subcostal approach. Most pleural fluid is anechoic separating the parietal and visceral pleura (Figs. 2.128 and 2.129). The quantity of pleural fluid can be estimated by measuring the maximum perpendicular distance between the

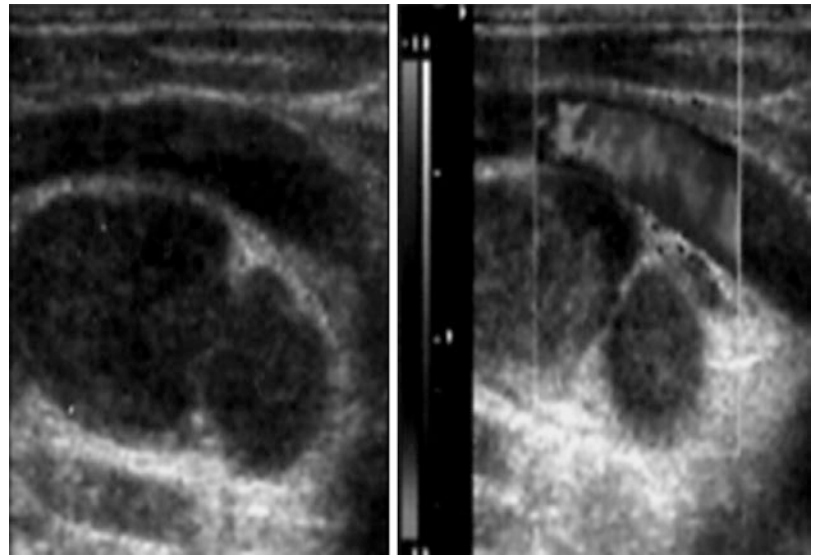

Fig. 2.126 Enlarged tubercular lymph node in the neck

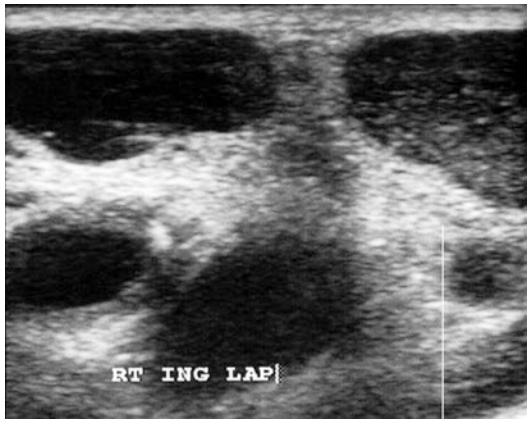

Fig. 2.127 Multiple enlarged lymph nodes in the right inguinal region

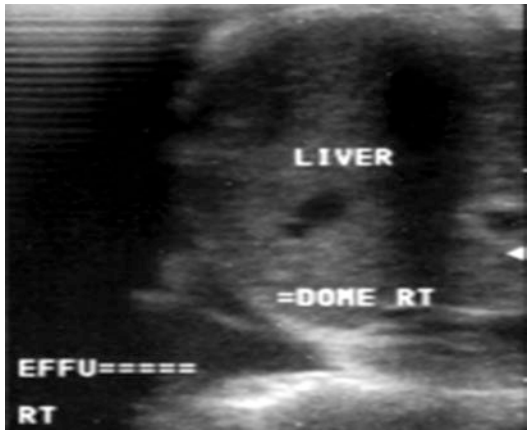

Fig. 2.128 Small pleural effusion in costo-diaphragmatic recess

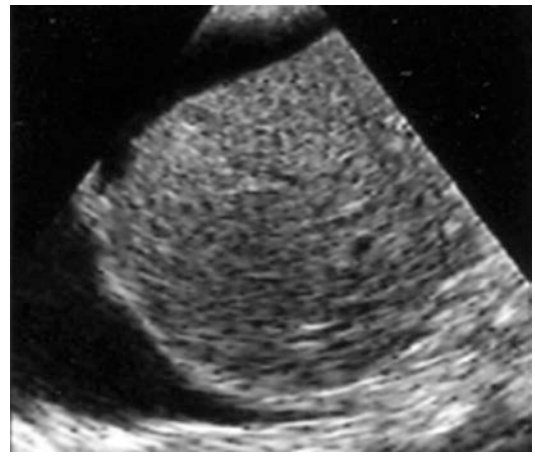

Fig. 2.129 Pleural effusion above the right diaphragm and ascites anterior to the liver

lung surface and chest wall with patient in supine position. A 20 mm width has a mean volume of 380 mL + 130 mL. A 40 mm width corresponds to about 1000 mL + 330 mL. It is possible to differentiate between pleural thickening and pleural fluid. Encysted pleural collection can be differentiated from pulmonary consolidation or mass. Ultrasound-guided pleural aspiration and fine needle aspiration cytology (FNAC) are now an established practice in most of the centres.

Occasionally pleural effusion with multiple septa may be found (Fig. 2.130).

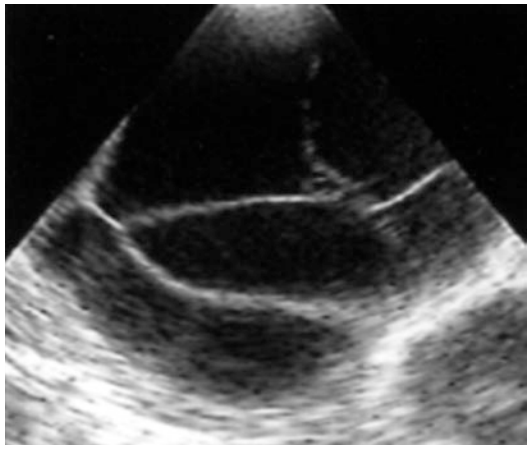

Fig. 2.130 Pleural effusion with multiple septa

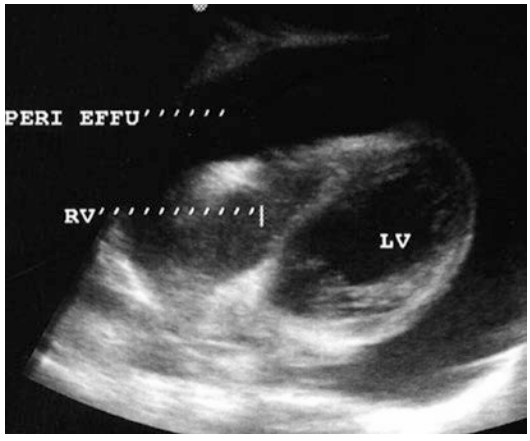

Fig. 2.131 Large pericardial effusion in a patient of disseminated lupus erythematosus

USG through subcostal approach may reveal pericardiac effusion (Fig. 2.131).

References

1. Marks WM, Filly RA, Callen PW. Ultrasonic anatomy of the liver: a review with new applications. J Clin Ultrasound. 1979;7:137–46.
2. Couinaud C. Le foie. In Etudes Anatomiques et Chirugicales. Paris: Masson et Cie; 1957.
3. Lafortune M, Madore F, Patriquin HB, Breton G. Segmental anatomy of the liver: a sonographic approach to Counidaud nomenclature. Radiology. 1991;181:443–8.
4. Neederau C, Sonnenberg A, Muller JE, et al. Sonographic measurement of the normal liver, spleen, pancreas and portal vein. Radiology. 1983;149:537–40.
5. Gharbi HA, Hassine W, Brauner MW, et al. Ultrasound examination of the hydatid liver. Radiology. 1981;139:459–63.
6. Lewall DB, Corkell SJ. Hepatic echinococcal cysts: sonographic appearance and classification. Radiology. 1985;155:773–5.
7. Wilson SR, Rosen IE, Chin-Sang HB, et al. Fatty infiltration of the liver: an imaging challenge. J Can Assoc Radiol. 1982;33:227–32.
8. Patriquin H, Lafortune M, Burns PN, et al. Duplex Doppler examination in portal hypertension. AJR. 1987;149:71–6.
9. Kawasaki T, Motiyasu F, Nishida O, et al. Analysis of hepato-fugal flow in portal venous system using ultrasonic Doppler duplex system. Am J Gastroenterol. 1989;84:937–41.
10. Laing FC, Jeffrey RB Jr, Wing VW. Biliary dilatation: defining the level and cause by real-time ultrasound. Radiology. 1986;160:39–42.
11. Behan M, Kazam E. Sonography of the common bile duct: value of right anterior oblique view. AJR. 1978;130:701–9.
12. Freeny PC. Classification of pancreatitis. Radiol Clin N Am. 1989;27:1–3.
13. Alpern MB, Sandler MA, Kellman GM, et al. Chronic pancreatitis: ultrasonic features. Radiology. 1985;155:215–9.
14. Wiill FS. Pancreatic tumours and overview of pancreatic disease. In: Weills FS, editor. Ultrasound diagnosis of digestive disease. New York: Springer; 1996. p. 481–510.
15. Frank K, Linhart P, Kortsik C, et al. Sonographic determination of spleen size: normal dimensions in adults with a healthy spleen. Ultraschall Med. 1986;7(3):134–7.
16. Middleton WD, Dodds WJ, Lawson TL, et al. Renal calculi: sensitivity for detection with US. Radiology. 1988;167:239–23.
17. Spirnak JP, Resnick M, Banner MP. Calculus disease of the urinary tract, general considerations. In: Pollack HM, editor. Clinical urography, An atlas and textbook of urologic imaging. Philadelphia: WB Saunders; 1990. p. 1752–8.
18. Fernbach SK, Maizels M, Conway JJ. Ultrasound grading of hydronephrosis: introduction to the system used by the Society for Fetal Urology. Pediatr Radiol. 1994;23(6):478–80.
19. Ozden E, Turgut AT, Turkolmez K, Resorlu B, Safak M. Effect of bladder carcinoma location on detection rates by ultrasonography and computed tomography. Urology. 2007;69:889–92.
20. Levine E. Acquired cystic kidney disease. Radiol Clin N Am. 1196;34(5):947–64.

21. Davidson AJ. Chronic parenchymal disease. In: Pallack HM, editor. Clinical urography, An atlas and textbook of urologic imaging. Philadelphia: WB Saunders; 1990. p. 2277–88.
22. Stavros AT, Parker SH, Yakes WF, et al. Segmental stenosis of the renal artery: pattern recognition of tardus and parvus abnormality with duplex sonography. Radiology. 1992;184:487–92.
23. Kohler TR, Zierler RE, Martin RL. Non invasive diagnosis of renal artery stenosis by Ultrasound Duplex scanning. J Vasc Surg. 1986;4:450–6.
24. Platt JF, Rubin JM, Ellis JH, et al. Duplex Doppler US of the kidney differentiation of obstructive from non-obstructive dilatation. Radiology. 1989;171:515–7.
25. Killer MS, Korsvih HE, Weiss RM. Diuretic Doppler sonography with correlative scintigraphy in children with hydronephrosis. Sco. Pediatr Radiol. 1992;35:4972.
26. Gentiline P, Laffe G, Buzzeli G. Functional renal alteration in chronic liver disease. Digestion. 1980;20:73–78.27.
27. Mc Neal JE. The zonal anatomy of the prostate. Prostate. 1981;2:35–49.
28. Bree RL. The prostate. In: Rumack CM, Wilson SR, Charbonean JW, editors. Diagnostic ultrasound, vol. 1. 2nd ed. St. Louis: Mosby Year Book; 1988. p. 399–429.
29. Jacobson H, Torp-Pedersen S, Juul N. Ultrasonic evaluation of age-related human prostatic growth and development of benign prostatic hyperplasia. Scand J Urol Nephrol. 1988;107(Suppl):26–31.
30. Oesterling JE, Jacobson SJ, Cooner WH. The use of age-specific reference ranges for serum prostate specific antigen in men of 60 years old or older. J Urol. 1995;153(4):1160–3.
31. Downey DB. The Retroperitoneum and great vessels, Chap 12. In: Rumack CM, Wilson SR, Charbonean JW, editors. Diagnostic ultrasound. 2nd ed. St. Louis: Mosby; 1998. p. 453–80.
32. Jeffrey RB, Jain KA, Ngheim HV. CT-sonographic diagnosis of acute appendicitis: interpretative pitfalls. Am J Roentgenol. 1994;162:55–9.
33. Engel JW, Deitch EE. Sonography of the anterior abdominal wall. AJR. 1981;137:73–7.
34. Yu C-J, Yang P-C, Chang D-B, et al. Diagnostic and therapeutic use of chest sonography: value in critically ill patient. AJR. 1992;159:695–701.

Gynaecologic Ultrasound

3

R.K. Diwakar

Abstract

Sonography has become indispensable in the evaluation of gynaecological disease. The trans-abdominal and transvaginal sonography are well-established techniques and complementary to each other, for assessing the female pelvic organs. Good distension of the urinary bladder displaces the bowel out of the pelvis so that the entire uterus including the fundus, ovaries and adnexa are clearly visualised, while the empty urinary bladder is required for transvaginal sonography. Images in the sagittal and coronal planes are obtained. Transvaginal sonography provides greater detail of the internal characteristics of a pelvic mass because of the higher frequency of the transducer.

3.1 Gynaecologic Sonography

The USG of the pelvis in female includes visualisation of the uterus, ovaries and adnexa (Fig. 3.1). The uterus is seen in long section (Fig. 3.2), and rotating the probe by 90°, the coronal section is obtained (Fig. 3.3). The endometrial complex is seen in the midline in the upper portion of the uterus in the long section. It measures 1–2 mm in thickness. The uterine cervix, the vagina and the pouch of Douglas (posterior to uterus) can be seen. The upper portion of the vagina is usually visible in USG. The ovaries are located on either sides of the uterus, and their position varies with the degree of urinary bladder distension. Posterior to the uterus, the rectum is located which usually contains gas and faecal matter. On the either sides of the uterus, the adnexa (pelvic muscles and connective tissue) are visualised. The normal fallopian tubes and broad ligament are not visualised. However, in the presence of pelvic ascites, the broad ligament is visualised (Fig. 3.4) [1].

US characteristics of benign and malignant ovarian masses is shown in Table 3.1

The dilated tubes (hydrosalpinx) forming part of complex adnexal mass are seen.

In retroverted uterus, the cervix and uterine fundus are seen at the same level (Fig. 3.5).

Transvaginal sonography (TVS) (Fig. 3.6) can be done in the absence of urinary bladder distension

R.K. Diwakar
Department of Radio-Diagnosis, C.C.M. Medical College & Hospital, Durg, Chhattisgarh, India
e-mail: rkdiwakar49@yahoomail.co.in

R.K. Diwakar (ed.), *Basics of Abdominal, Gynaecological, Obstetrics and Small Parts Ultrasound*,
https://doi.org/10.1007/978-981-10-4873-9_3

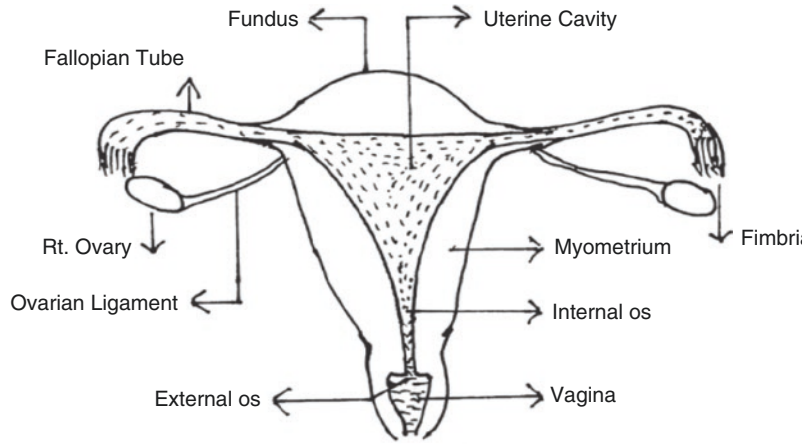

Fig. 3.1 Anatomy of the uterus, ovaries and fallopian tubes

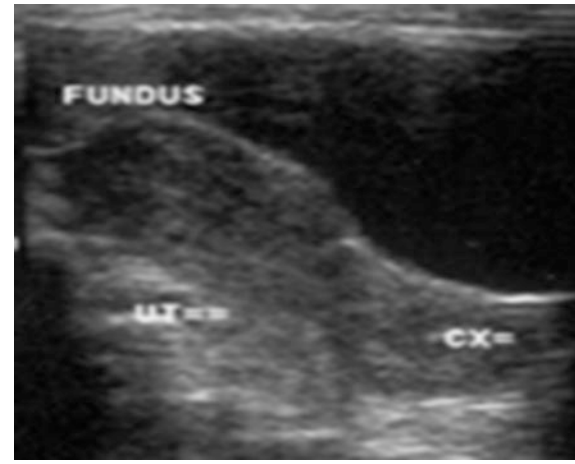

Fig. 3.2 Longitudinal scan of the uterus showing fundus and cervix, normal thin endometrial echo complex seen in the midline in the upper portion of the uterus

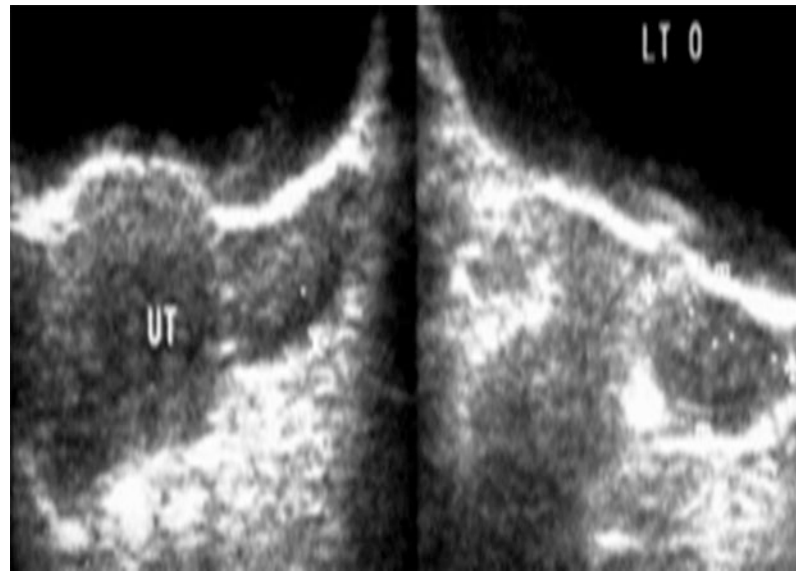

Fig. 3.3 USG in coronal plane showing the uterus and left ovary

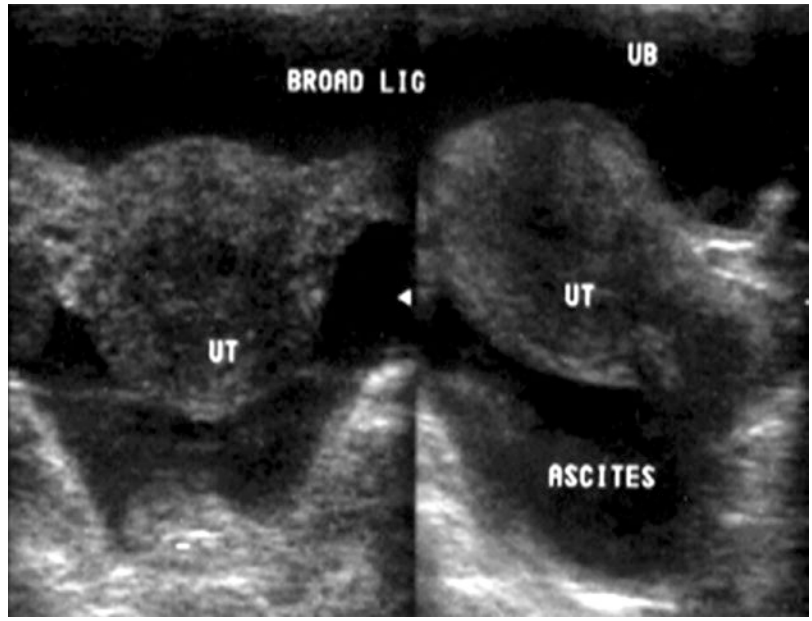

Fig. 3.4 Broad ligament on sides of the uterus visualised only in the presence of ascites

Table 3.1 Ovarian masses, benign vs. malignant [23]

US characteristics	Benign disease	Malignant disease
Size	Small <5 cm	Large >10 cm
External contour	Thin wall, well-defined borders	Thick wall, ill-defined/irregular borders
Internal features	Purely cystic, thin septations	Solid/complex. Thick/irregular septations, echogenic nodule
Doppler	High-resistance or no flow, avascular nodules	Low-resistance flow, vascular nodule
Associated findings		Ascites, peritoneal implants

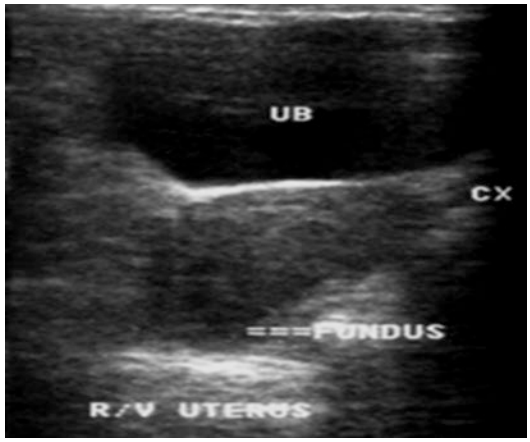

Fig. 3.5 Posteriorly directed fundus of the retroverted uterus

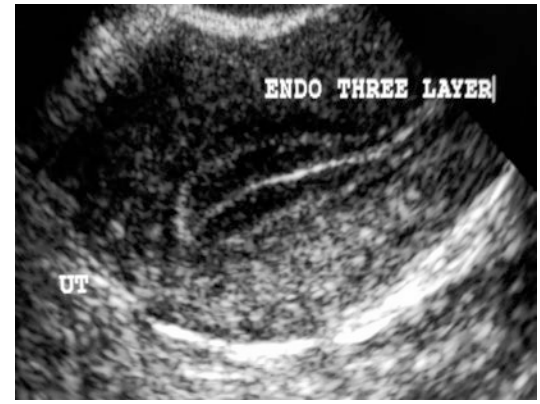

Fig. 3.6 Three-layer appearance of the endometrium in TVS

or in obese patients with better evaluation of the retroverted uterus, better distinction between the adnexal mass and bowel loops and greater detail of the internal characteristics of a pelvic mass [2]. It can be used, if necessary, after the initial transabdominal pelvic sonography. Andolf and Jorgensen [3] found no significant difference in the diagnostic outcome between the techniques.

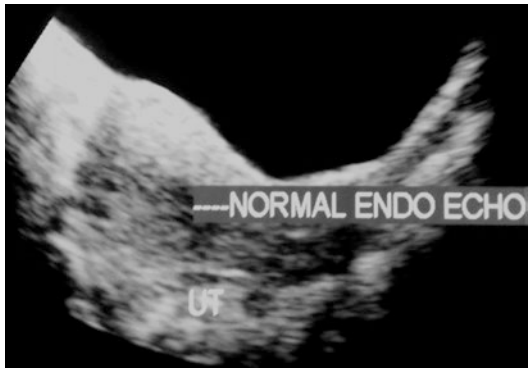

Fig. 3.7 Normal location and thickness of endometrial echo

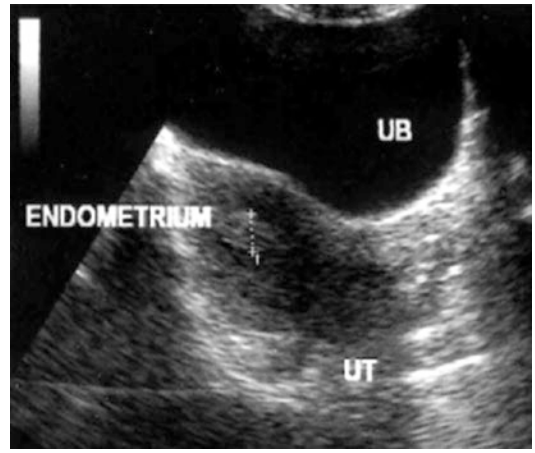

Fig. 3.8 Mild thickening of the endometrium

The normal nulliparous uterus measures 8 cm (*L*) × 5 cm (width) × 4 cm (AP diameter). After menopause the uterus atrophies and it measures 3.5–6.5 cm (*L*) × 1.2–1.8 cm (AP). Multiparity increases the normal size by more than 1 cm in each dimension [4].

The sonographic appearance of the endometrium varies during menstrual cycle [5]. The normal endometrium is 2–3 mm in thickness and located in the midline in the upper portion of the uterus (Fig. 3.7). The hypoechoic thickening in proliferative phase may reach 4–8 mm, while the hyperechoic thickening in secretory phase measures 7–14 mm [5].

The causes of endometrial thickening are [5]:

1. Early intrauterine pregnancy
2. Incomplete abortion
3. Ectopic pregnancy
4. Retained products
5. Trophoblastic disease
6. Adhesions
7. Hyperplasia
8. Polyps
9. Carcinoma

Endometrial thickening of 4 mm and more than 8 mm in the bleeding and asymptomatic postmenopausal woman (Fig. 3.8), respectively, requires endometrial sampling [6].

The infantile or prepubertal uterus measures 2–3.3 cm in length and 0.5–1.0 cm in AP diameter [1] (Fig. 3.9).

Leiomyoma (fibroid) of uterus occurs 20–30% over the age of 30 years [7]. Leiomyomas may be single (Fig. 3.10) or multiple (Fig. 3.11). The size may vary from small to very large. They may be hypoechogenic in texture. Intramural fibroids are most common (Fig. 3.12); submucosal fibroids produce symptoms most frequently,

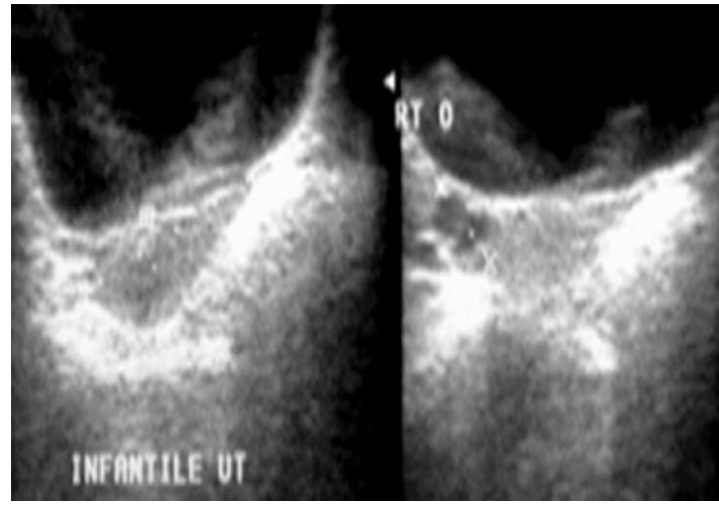

Fig. 3.9 Small dimensions of the uterus and ovaries (infantile uterus) in a girl of 16 years, no menarche

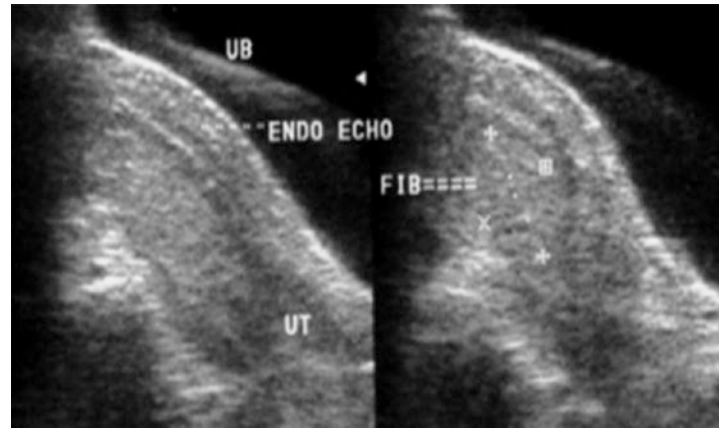

Fig. 3.10 Anterior displacement of endometrial echo by an intramural fibroid

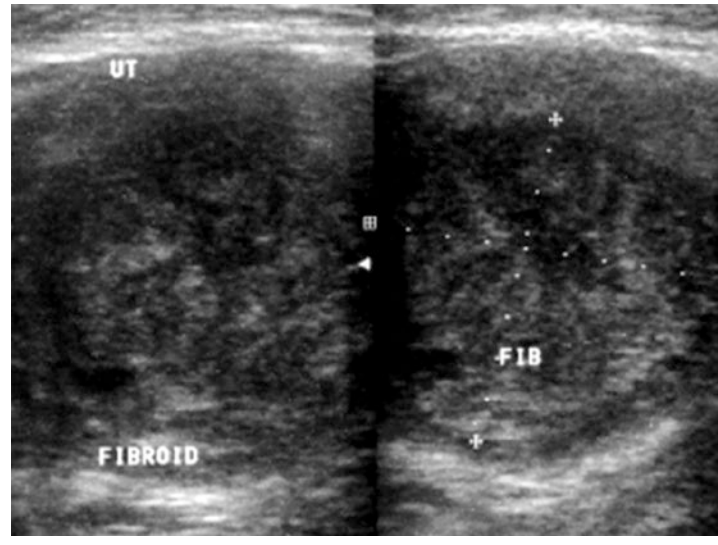

Fig. 3.11 Multiple intramural fibroids with inhomogenous echotexture

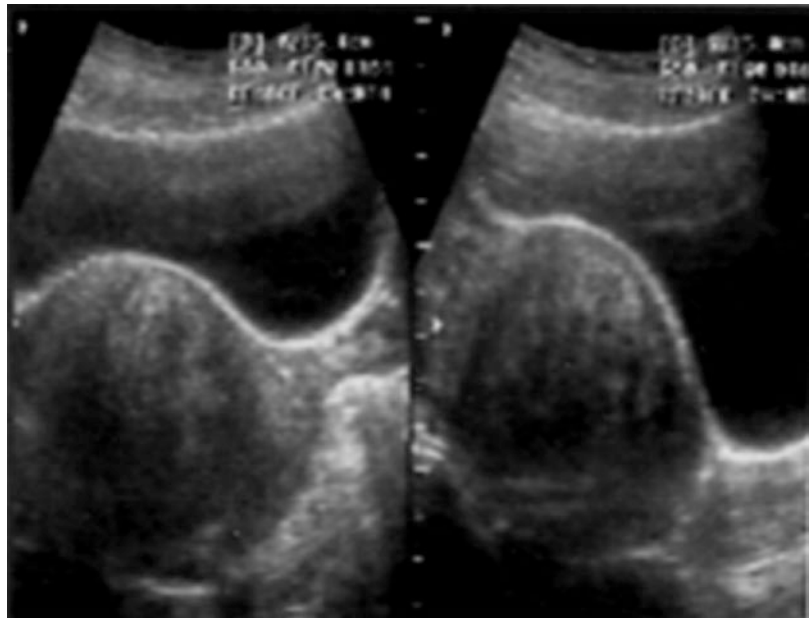

Fig. 3.12 Intramural fibroid with fine foci of calcifications

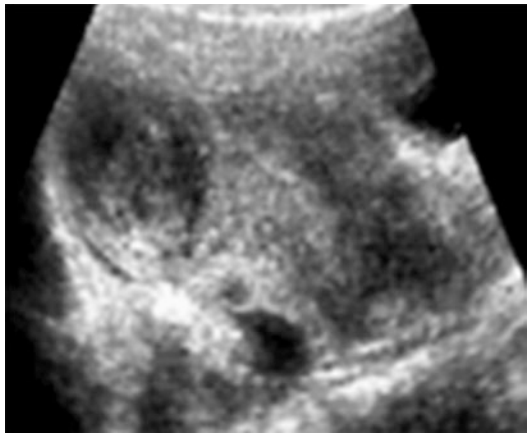

Fig. 3.13 Subserosal fibroid at the fundus of the uterus

and subserous (Fig. 3.13) fibroids may present as an adnexal mass. Calcifications and cystic degeneration (areas of necrosis) are associated findings. Fibroid may produce displacement of endometrial echo (Fig. 3.10). Many patients may remain asymptomatic. A rapid increase in size, especially in a postmenopausal patient, should raise the possibility of sarcomatous change [8].

Some of the small fibroids may produce a bulge in the uterine wall (Fig. 3.14), while others having echogenicity equal to the surrounding myometrium (isoechogenic) can be diagnosed with MRI [9].

Approximately 8% of leiomyoma may arise in the cervix (Fig. 3.15). The pedunculated fibroid may prolapse into the vagina. The cervical stump after hysterectomy may simulate a mass. The normal cervix and cervical polyps are demonstrated best by TVS.

Adenomyosis may be diffuse or nodular in form. It is characterised by the presence of endometrial glands within the myometrium showing as small cystic lesions [10].

Endometritis may reveal thick and irregular endometrium with or without fluid in its cavity.

Endometrial adhesions (synechiae) appear as bridging bands of tissue in the endometrial cavity and are demonstrated best by sonohysterography where fluid is instilled into the endometrial cavity [11].

Endometriosis is the presence of functioning endometrial tissue outside the uterus. It may be diffuse or localised. The women are affected usually during the reproductive years. The localised form consists of a unilocular or multilocular cystic mass (chocolate cyst) containing diffuse homogenous low-level internal echoes better appreciated on TVS [12].

Endometrial polyp seen as a focal, round echogenic mass in the cavity [13] is easily visualised in TVS (Fig. 3.16). The polyp is identified more easily when the fluid within the endometrial cavity is present (Fig. 3.17) or when the fluid is instilled into the endometrial cavity in sonohysteroscopy.

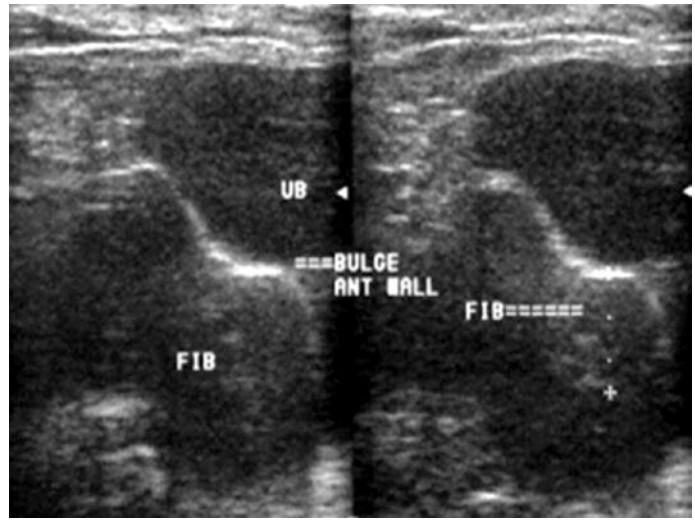

Fig. 3.14 A bulge in the anterior wall of the lower segment of the uterus by a fibroid

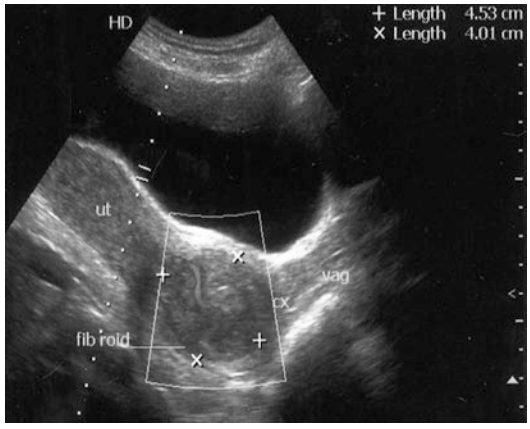

Fig. 3.15 Increased AP dimension of the lower segment of the uterus with a fibroid near the cervix

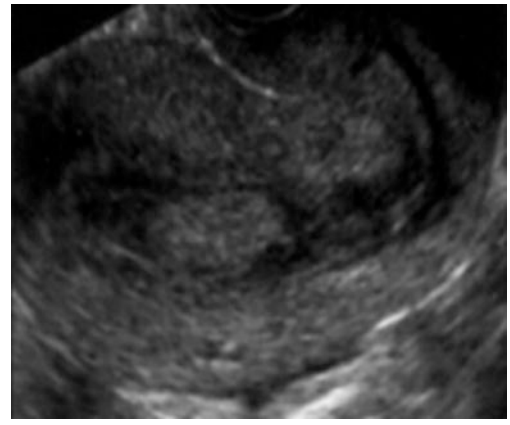

Fig. 3.16 Polyp in the endometrial cavity in TVS

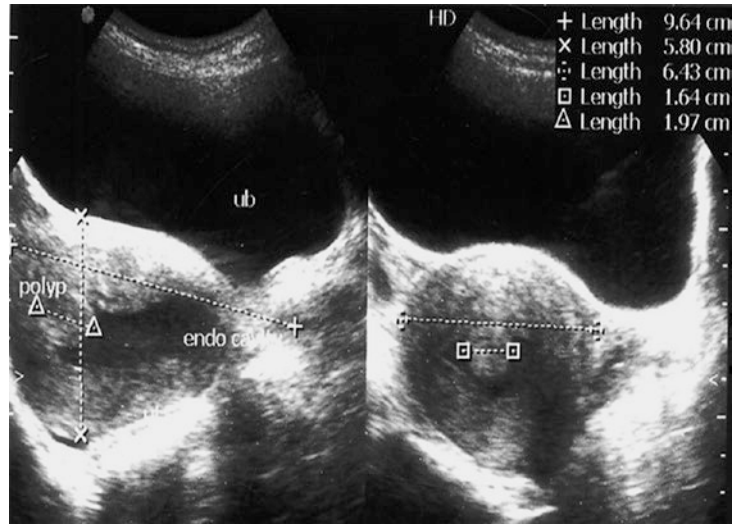

Fig. 3.17 Endometrial polyp in the fluid-distended endometrial cavity

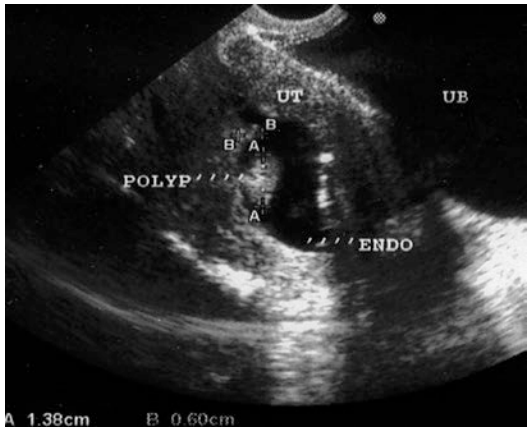

Fig. 3.18 Two endometrial polyps in the endometrial cavity distended with infusion of normal saline through Foley's catheter (SIS)

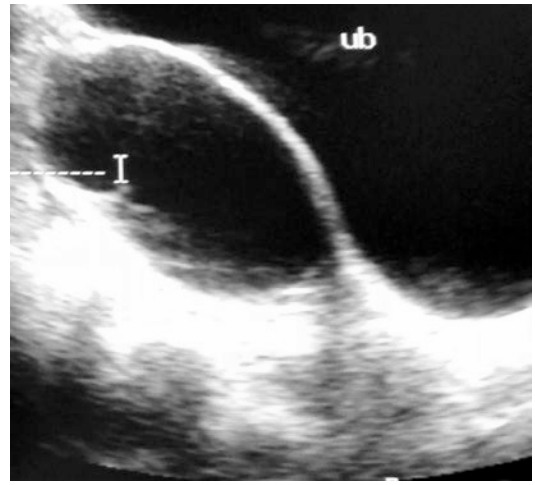

Fig. 3.21 Collection of blood in the uterus (haematometra)

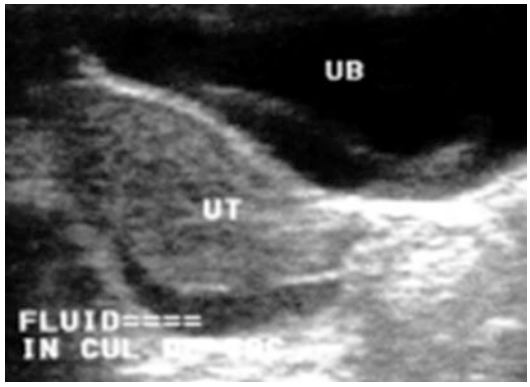

Fig. 3.19 Fluid in the cul-de-sac in PID

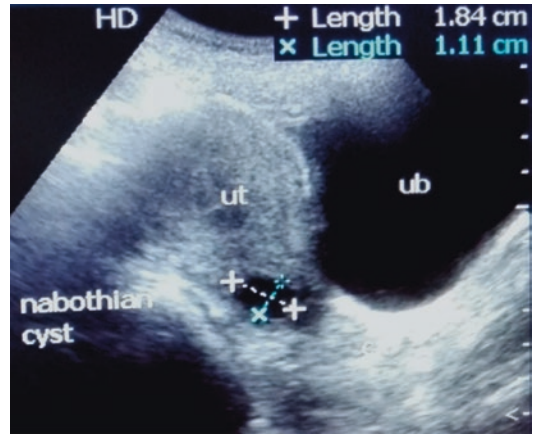

Fig. 3.22 Nabothian cyst in the cervix uterus

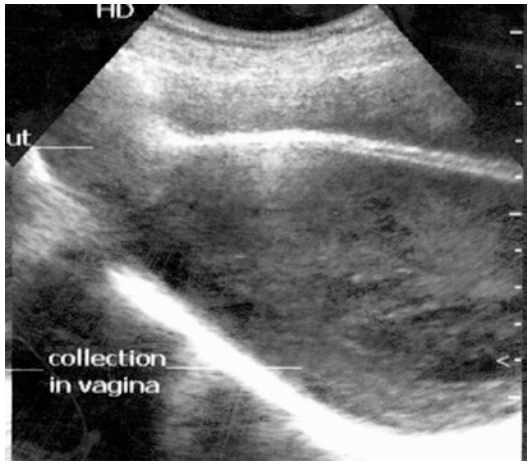

Fig. 3.20 Blood collection in vagina (haematocolpos), uterus (ut) displaced anteriorly

Saline infusion sonography (SIS) causes distension of the endometrial cavity resulting in better visualisation of the endometrial polyp (Fig. 3.18).

Collection of fluid in the pouch of Douglas or cul-de-sac is a common finding in pelvic inflammatory disease (Fig. 3.19) [14].

Haematocolpos shows distended vagina with echogenic material in young patient with imperforate hymen (Fig. 3.20). The haematometra is a blood-filled endometrial cavity (Fig. 3.21) [15].

Nabothian cysts are seen in the cervix (Fig. 3.22), may be multiple (Fig. 3.23) and may contain internal echoes caused by haemorrhage or infection. Multiple cysts may be the cause of benign enlargement of the cervix [16].

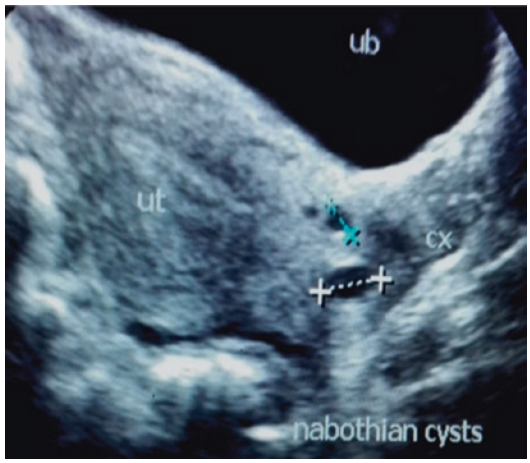

Fig. 3.23 Multiple nabothian cysts of variable sizes

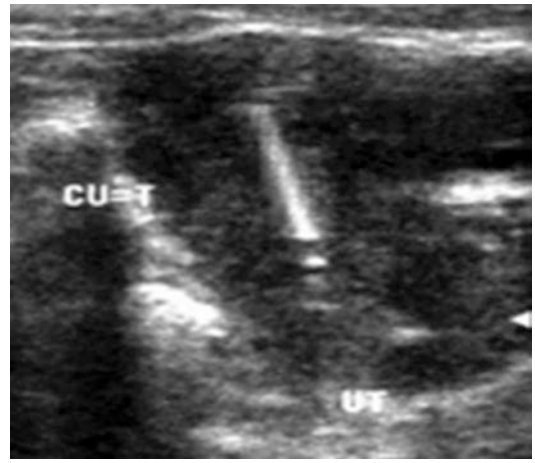

Fig. 3.24 Intrauterine contraceptive device (Cu-T) in situ in the uterus

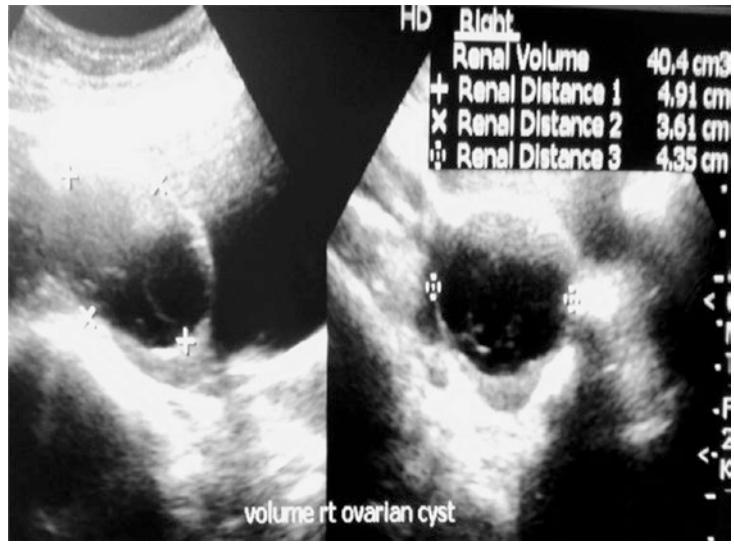

Fig. 3.25 Measurement of the volume of cyst in the right ovary

Patients of carcinoma cervix are rarely referred for sonography. Only big size growth can be detected by ultrasound.

Pelvic USG is commonly used for the presence and location of Cu-T (Fig. 3.24) and also to find out myometrial penetration [17]. When no device is seen in the uterus, abdominal radiograph may reveal a peritoneal position anywhere from the pelvis to diaphragm.

Ovaries: The normal ovaries are visualised laterally or posterolaterally to the uterus. They may be seen high in the pelvis or in the cul-de-sac (pouch of Douglas). The normal ovaries have relatively homogeneous texture. The follicles are seen in the peripheral area, i.e. in the cortex of the ovary. Normally, follicles appear 10 days after the beginning of the menstrual cycle increasing gradually in size reaching up to 2–2.5 cm at the time of ovulation. The other follicles become atrophic.

The ovarian volume in ml is calculated by the formula for an ellipse: the ovarian size length × width × height in cm × 0.52 (Fig. 3.25). The upper limit of ovarian volume at menarche is 8 mL, in adult is 22 mL and in

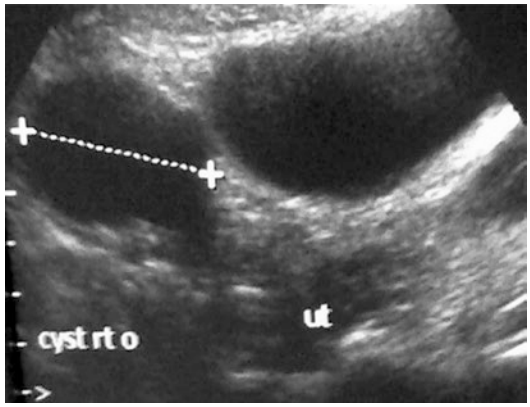

Fig. 3.26 Unilocular cyst in the right ovary

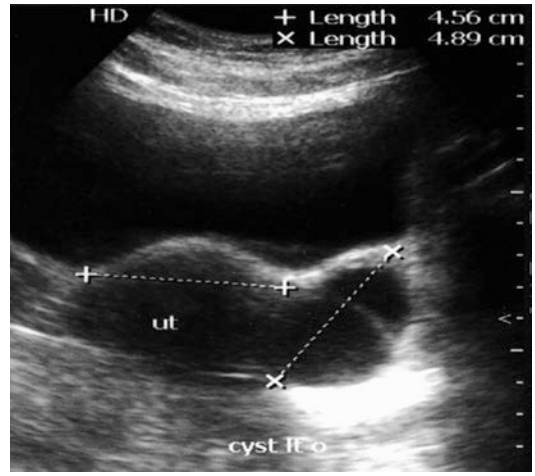

Fig. 3.28 Cyst in the left ovary with two loculi

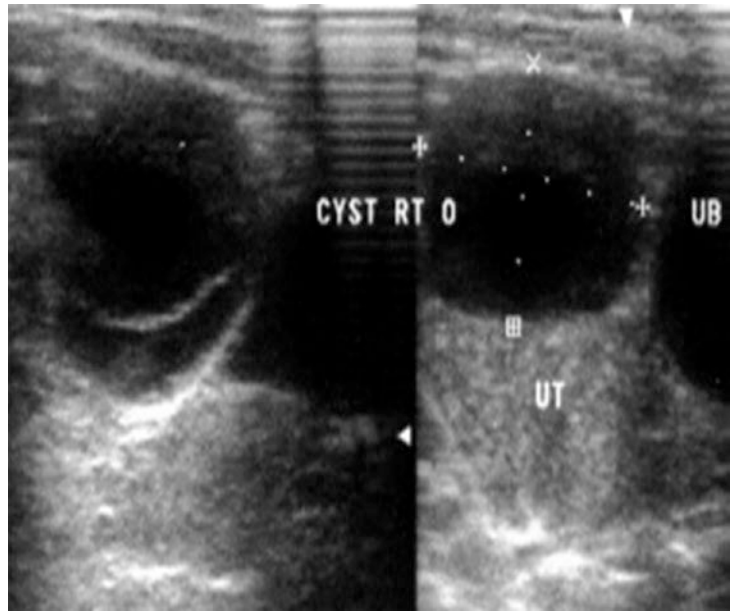

Fig. 3.27 Larger size ovarian cyst with septa (bilocular)

postmenopausal women is 8 mL. Cohen et al. [18] assessed 866 normal ovaries by transabdominal sonography and reported a mean ovarian volume of 9.8 =/−5.8 cc with an upper limit of 21.9 cc.

Cysts of different sizes can be seen in the ovaries (Figs. 3.26, 3.27, 3.28 and 3.29). Surgery is required for cysts of 5 cm or greater in size and if containing internal septa and/or nodule [6] (Fig. 3.30).

Polycystic ovarian disease (PCOD) [19] results due to chronic anovulation and is a common cause of infertility. Ultrasound findings are the bilaterally enlarged ovaries with multiple cysts of 5–8 mm

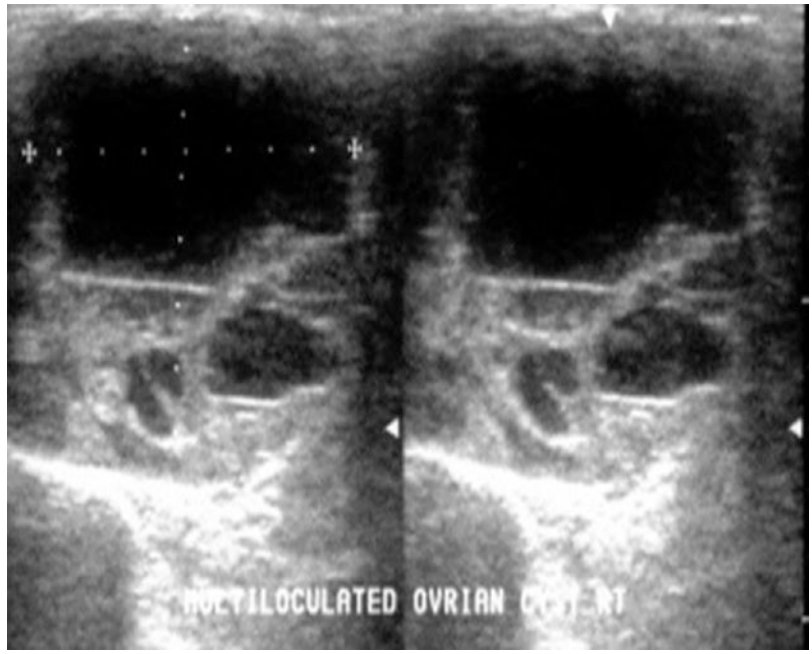

Fig. 3.29 Multiloculated ovarian cyst

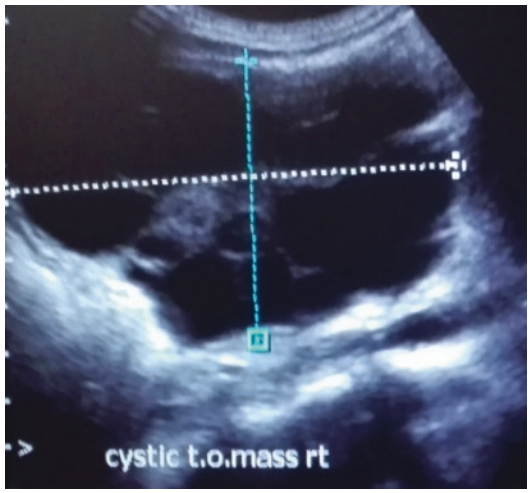

Fig. 3.30 Cystic tubo-ovarian mass with multiple septa and loculi

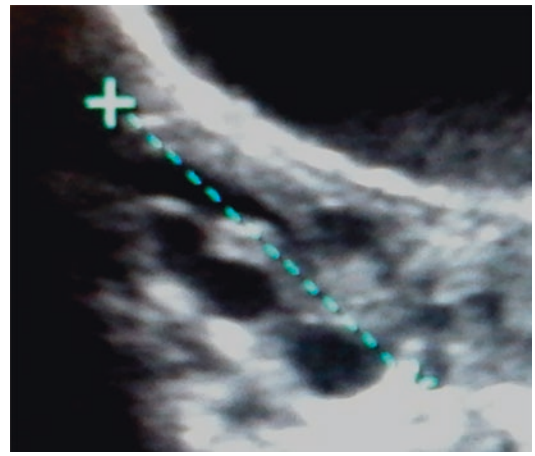

Fig. 3.31 Multiple cysts in the ovary in PCOD

size located peripherally in the ovaries (Figs. 3.31 and 3.32).

Follicular formation refers to the continuous process occurring throughout reproductive life. Each month only one follicle, the preovulatory or dominant follicle, achieves complete maturation, releasing ultimately the oocyte, i.e. ovulation [7]. Typically five follicles, maybe up to 11 follicles, become visible in sonography (Fig. 3.33). The dominant follicle reaches the pre-ovulation diameter of 20–23 mm (Fig. 3.34). The dominant follicle grows by 2–3 mm per day. The non-dominant follicles rarely exceed 11 mm in diameter [20]. The oocyte as such cannot be visualised within

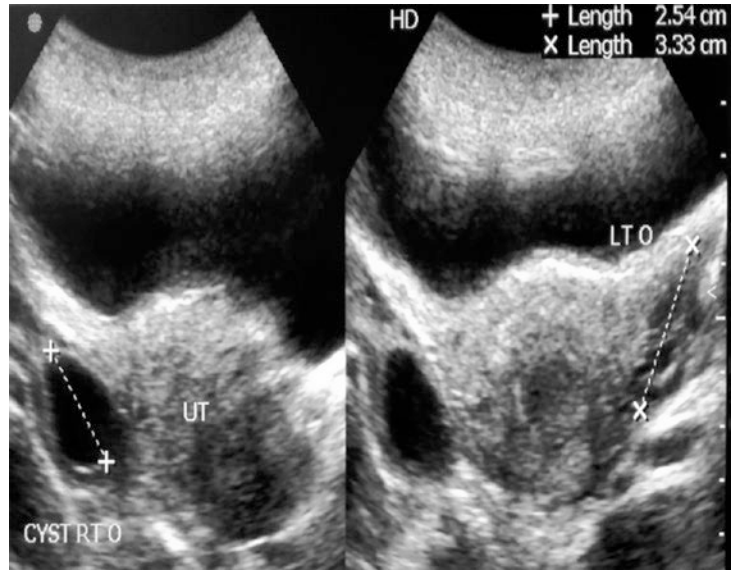

Fig. 3.32 Unilocular cyst in the right ovary, small multiple cysts in the left ovary in PCOD

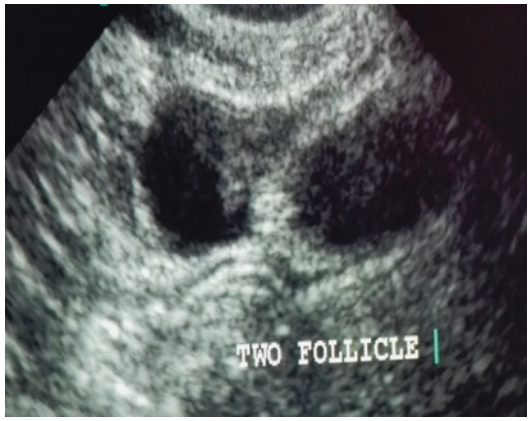

Fig. 3.33 Two follicles in the ovary seen in TVS

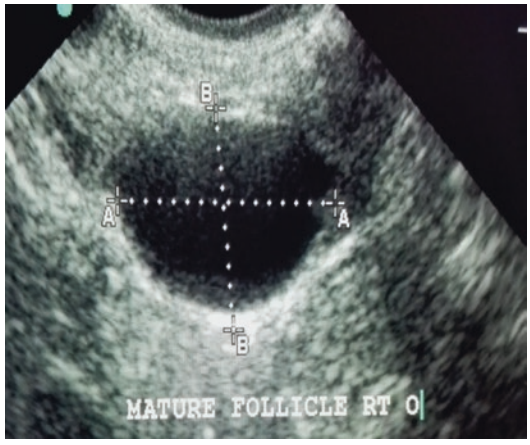

Fig. 3.34 Dominant follicle of 2.5 cm in the right ovary

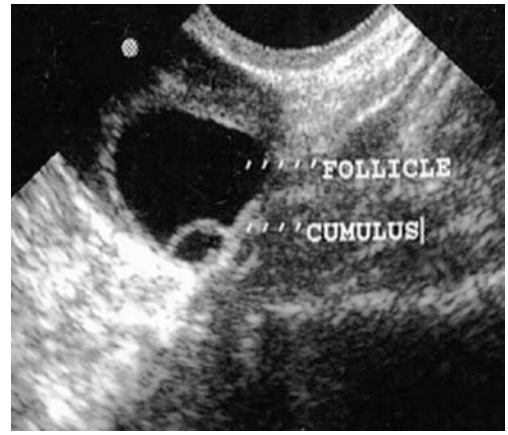

Fig. 3.35 Cumulus oophorous seen prior to follicle rupture

the Graafian follicle; however, a 1 mm internal protrusion, i.e. cumulus oophorus (Fig. 3.35), indicates maturity of the follicle, and its visualisation predicts ovulation within 36 h [21].

Pelvic inflammatory disease (PID) [22] at USG is seen as thickening of endometrium or fluid in cul-de-sac (Figs. 3.36 and 3.37), enlarged ovaries with multiple cysts, fluid-filled fallopian tubes (hydrosalpinx or pyosalpinx), tubo-ovarian complex (fusion of the inflamed dilated tube and ovary) (Fig. 3.38) or tubo-ovarian abscess (Fig. 3.39). In chronic PID extensive fibrosis and adhesions lead to formation of ill-defined mass with obscuration of margins of the pelvic organs (Figs. 3.40 and 3.41) [23].

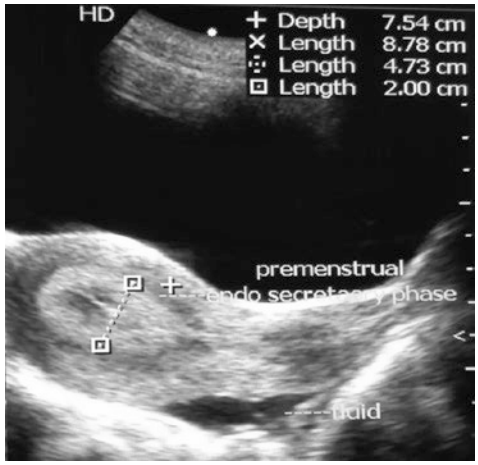

Fig. 3.36 Thickening of the endometrium in a premenstrual young girl with fluid in the cul-de-sac

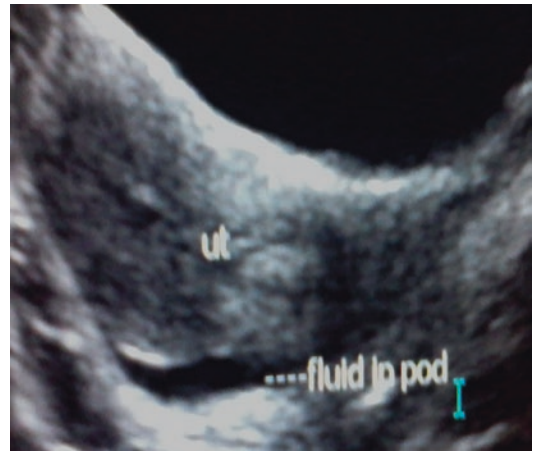

Fig. 3.37 Fluid in the pouch of Douglas in PID

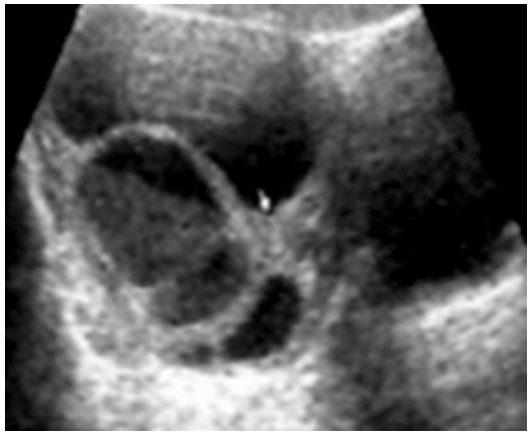

Fig. 3.38 Hydrosalpinx with debris and cyst in the ovary

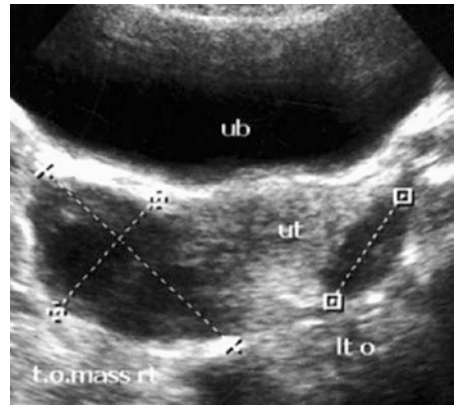

Fig. 3.40 Right tubo-ovarian mass, unilocular cyst left ovary

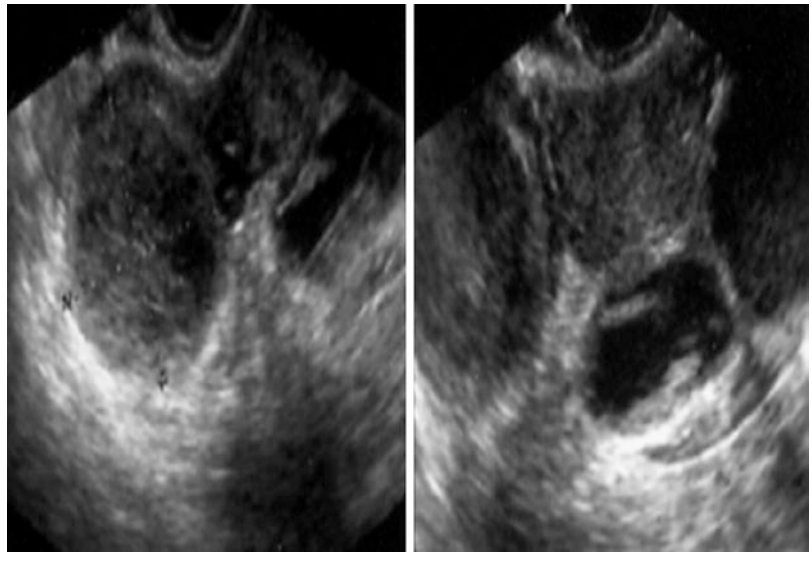

Fig. 3.39 Tubo-ovarian abscess with complex echotexture

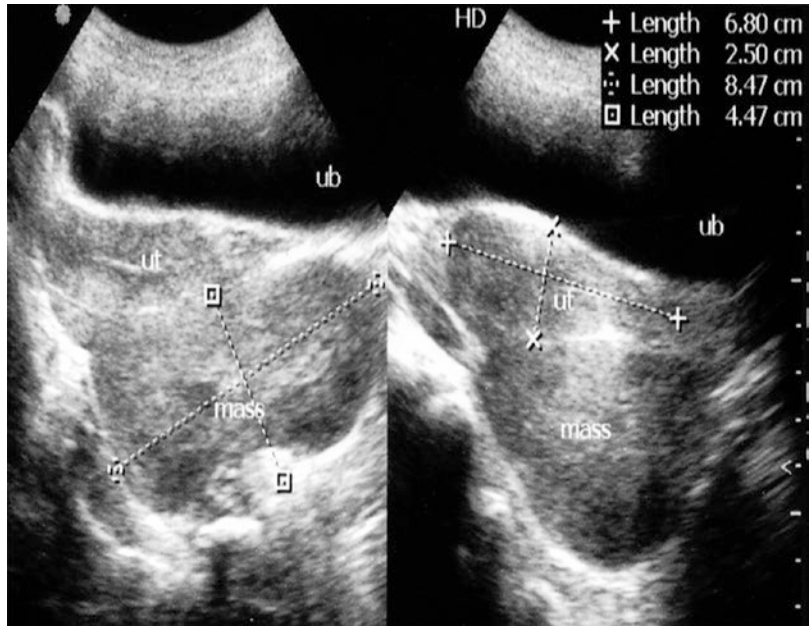

Fig. 3.41 Mass in the left adnexa posterolateral to the uterus

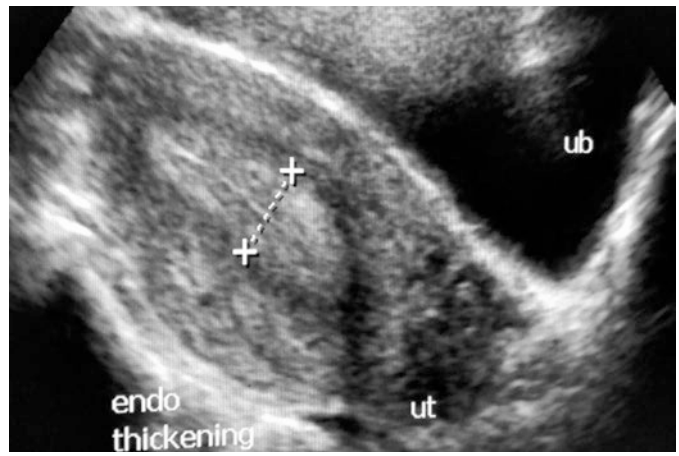

Fig. 3.42 Thickened endometrium

Recommendations for postmenopausal women: endometrial thickness (double layer) [24] (Fig. 3.42):

1. <4 mm: Bleeding = no biopsy (probably atrophic)
   No bleeding = normal
2. 5–8 mm: Bleeding = biopsy
   No bleeding = probably normal, no biopsy
3. >8 mm: Sequential hormone—rescan early or late in cycle = if still >8 mm = biopsy
   All other hormone regimen = biopsy

Cystic teratoma or dermoid cysts constitute about 15–25% of ovarian neoplasm (Figs. 3.43 and 3.44) and are virtually always benign. The USG appearance may vary from completely cystic to solid mass with dermoid plug (mural nodule) [25], tip of the iceberg sign [26], dermoid mesh [27] (multiple linear hyper-echogenic interfaces floating within the cystic mass) or a fat-fluid or hair-fluid level.

The location of the centre of the gestational sac relative to the midpoint axis of the uterus can be used as an easy method to differentiate

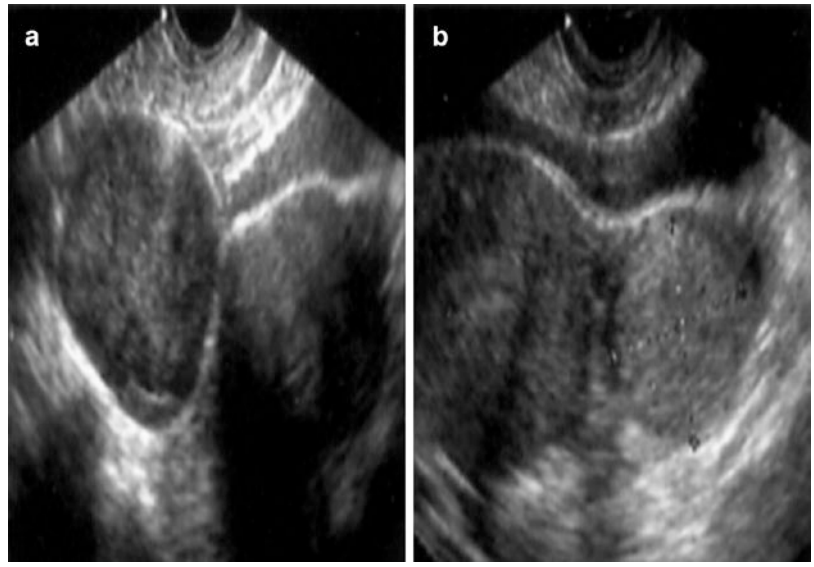

Fig. 3.43 Dermoid cyst (**a**) in the right ovary and (**b**) in the left ovary in two different patients

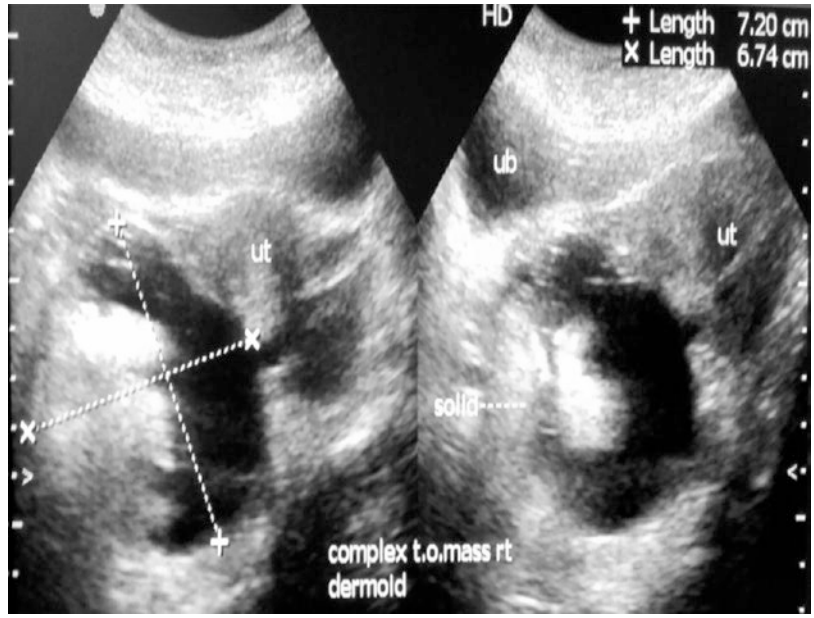

Fig. 3.44 Dermoid cyst right ovary containing hyper-echogenic solid area with posterior shadow

between normal intrauterine pregnancy (IUP) and caesarean scar pregnancy (CSP) between 5 and 10 weeks of gestation [28] (Fig. 3.45).

Retained products of conception are seen as a heterogenous mass, but it may be caused by blood clots or infected or necrotic material without the presence of placental tissue being found (Fig. 3.46) [29]. Occasionally, definitive placental tissue may be identified (Fig. 3.47).

Ovarian cancer: It usually presents as an adnexal mass. Well-defined anechoic lesions are more likely to be benign, whereas lesions with irregular walls, thick and irregular septations, mural nodules and solid echogenic ele-

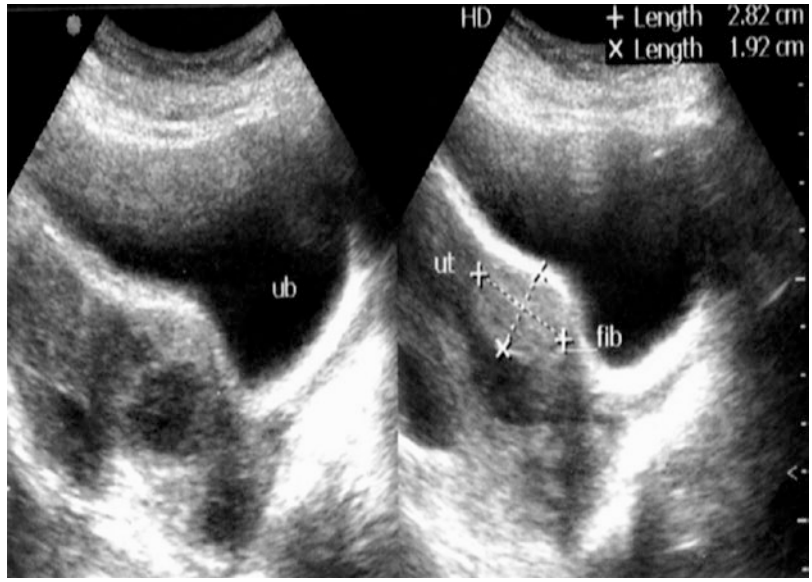

Fig. 3.45 Caesarean scar pregnancy mimicking a fibroid with a bulge in the anterior wall of the lower portion of the uterus

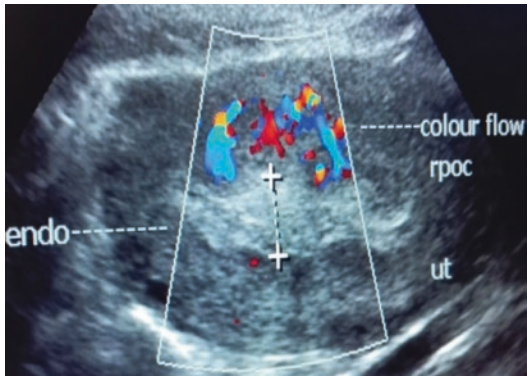

Fig. 3.46 Retained products of conception after incomplete evacuation

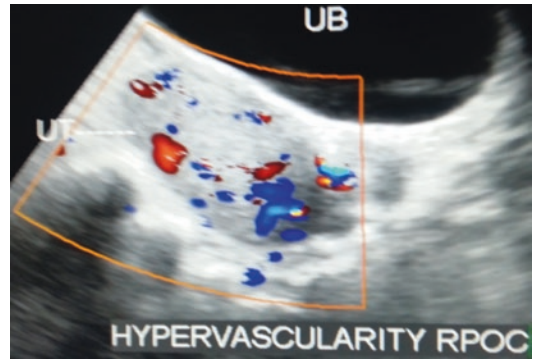

Fig. 3.47 Hypervascularity in the uterus post D and E

ments favour malignancy [30] (Figs. 3.48, 3.49 and 3.50).

Absence of flow within a lesion usually indicates a benign lesion; Weiner et al. [31] have shown absent flow within malignant lesions. It is suggested that Doppler studies should be done between the third and tenth day of menstrual cycle to avoid confusion with normal luteal flow.

Mucinous cystadenomas constitute 20–25% of all benign ovarian neoplasms, and mucinous cystadenocarcinomas make up 5–10% of all primary malignant ovarian neoplasms [7].

The normal fallopian tube is difficult to identify by trans-abdominal or transvaginal sonography. The lumen is not seen unless it is fluid filled [32].

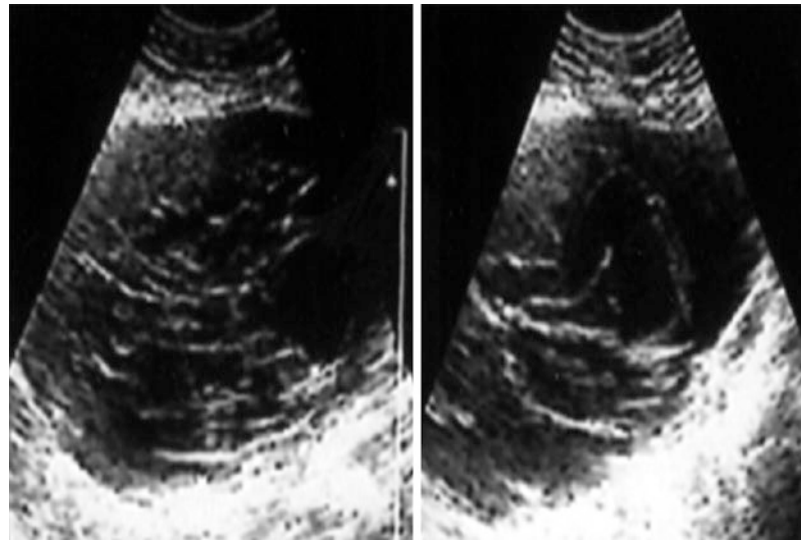

Fig. 3.48 Mucinous cystadenoma of ovary

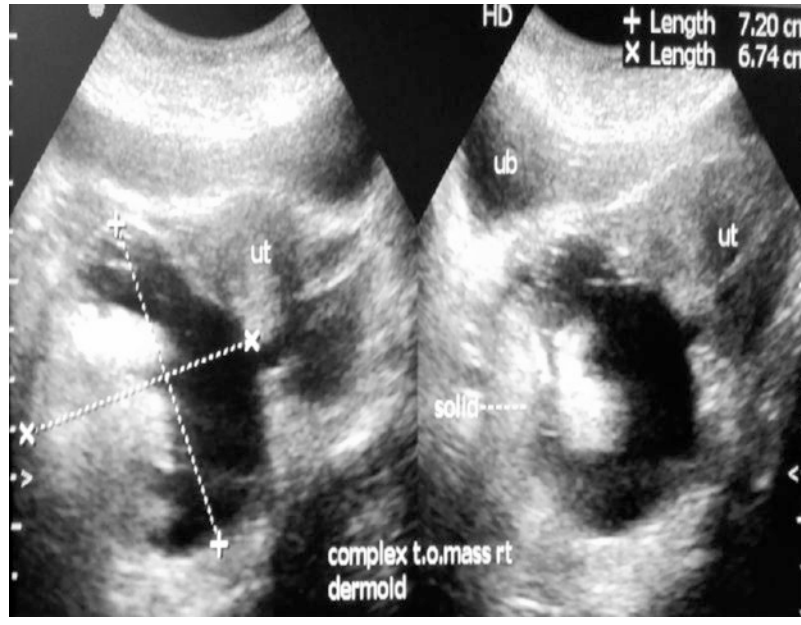

Fig. 3.49 Dermoid cyst right ovary containing hyper-echogenic solid area with posterior shadow

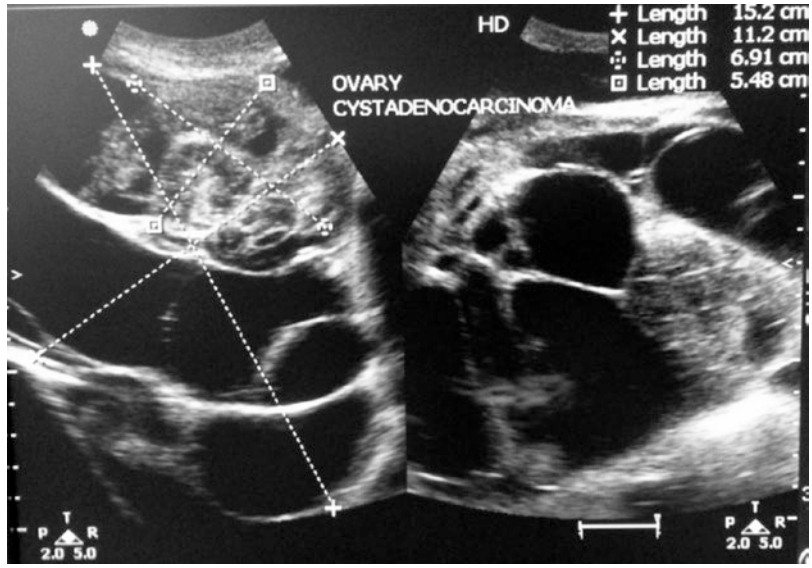

Fig. 3.50 Mucinous cystadenoma right ovary

References

1. Sample WF, Lippe BM, Gyepes MT. Gray-scale ultrasonography of the normal female pelvis. Radiology. 1977;125:477–83.
2. Callen PW. Ultrasonography in obstetrics and gynaecology. Philadelphia: WB Saunders; 2007.
3. Andolf E, Jorgensen C. A prospective comparison of trans-abdominal and trans-vaginal ultrasound with surgical findings in gynaecologic diseases. J Ultrasound Med. 1990;9:71–5.
4. Platt JF, Bree RL, Davidson D. Ultrasound of the normal non-gravid uterus: correlation with gross and histopathology. J Clin Ultrasound. 1990;18:15–9.
5. Fleischer AC, Kalemeris GC, Entman SS. Sonographic depiction of the endometrium during normal cycles. Ultrasound Med Biol. 1986;12:271–7.
6. Rumack CM, Wilson SR, Charboneau JW. Diagnostic ultrasound, Chap. 15. In: Salem S, editor. The uterus and adnexa. 2nd ed. St. Louis: Mosby-Year Book; 1998. p. 535.
7. Kurman RJ. Blaustein's pathology of the female genital tract. 4th ed. New York: Springer; 1994.
8. Jones HW III, Wentz AC, Burnett LS. Novak's textbook of gynecology. 11th ed. Baltimore: Williams & Wilkins; 1988.
9. Toshagi K, Ozasa H, Konishi I, et al. Enlarged uterus: differentiation between adenomyosis and leiomyoma with MR imaging. Radiology. 1989;171:531–4.
10. Reinhold C, Atri M, Mehio A, et al. Diffuse uterine adenomyosis: morphologic criteria and diagnostic accuracy of endovaginal sonography. Radiology. 1995;197:609–14.
11. Cullinan JA, Fleischer AC, Kepple DM, et al. Sonohysterography: a technique for endometrial evaluation. Radiographics. 1995;15:501–14.
12. Kupfer MC, Schwimmer SR, Lebovie J. Transvaginal sonographic appearance of endometriomata: spectrum of findings. J Ultrasound Med. 1992;11:129–33.
13. Kupfer MC, Schiller VL, Hansen GC, et al. Transvaginal sonographic evaluation of endometrial polyps. J Ultrasound Med. 1994;13:535–9.
14. Davis JA, Gosnik BB. Fluid in the female pelvis: cyclic patterns. J Ultrasound Med. 1986;5:75–9.
15. Wilson DA, Stacy TM, Smith EI, et al. Ultrasound diagnosis of hydrocolpos and hydrometrocolpos. Radiology. 1978;128:451–4.
16. Fogel SR, Slasky BS. Sonography of nabothian cysts. AJR. 1982;138:927–30.
17. Boortz HE, Margolis DJ, et al. Migration of intrauterine devices: radiologic findings and implications for patient care. Radiographics. 2012;32(2) doi:10.1148/rg.322115068.
18. Cohen HL, Tice HM, Mandel FS. Ovarian volume measured by US: bigger than we think. Radiology. 1990;177:189–92.
19. Hann LE, Hall DA, McArdle CR, et al. Polycystic ovarian disease: sonographic spectrum. Radiology. 1984;150:531–4.
20. Pache TD, Wladimiroff JW, De Jong FH, et al. Growth patterns of non-dominant follicles during the normal menstrual cycle. Fertil Steril. 1994;54(4):638–42.
21. Lenz S. Ultrasonic study of follicular maturation, ovulation and development of corpus luteum during normal menstrual cycles. Acta Obstet Gynecol Scand. 1985;64(1):15–9. 3883689

22. Laing FC. US analysis of adnexal masses: the art of making the correct diagnosis. Radiology. 1994;191:21–2.
23. Stein SM, Laifer-Narin S, Johnson MB, et al. Differentiation of benign and malignant adnexal masses: relative value of gray-scale, colour Doppler and spectral Doppler sonography. AJR. 1995;164: 381–6.
24. Levine D, Gosink BB, Johnson LA. Change in endometrial thickness in postmenopausal women undergoing hormone replacement therapy. Radiology. 1995;197:603–8.
25. Quinn SF, Erickson S, Black WC. Cystic ovarian teratoma: the sonographic appearance of dermoid plug. Radiology. 1985;155:477–8.
26. Guttmann PH Jr. In search of the elusive benign cystic ovarian teratoma: application of the ultrasound "tip of the iceberg" sign. J Clin Ultrasound. 1977;5:403–6.
27. Malde HM, Kedar RP, Chadha D, et al. Dermoid mesh: a sonographic sign of ovarian teratoma. AJR Am J Roentgenol. 1992;159:1349–50.
28. Campbell S. Ultrasound in obstetrics and gynaecology: recent advances. clinics in obstetrics and gynecology. Philadelphia: WB Saunders; 1983. p. 10.
29. Hertzberg BS, Bowie JD. Ultrasound of the postpartum uterus: prediction of retained placental tissue. J Ultrasound Med. 1991;10:451–6.
30. Moyle JW, Rochester D, Sider L, et al. Sonography of ovarian tumours: predictability of tumour type. AJR Am J Roentgenol. 1983;141:985–91.
31. Weiner Z, Thaler I, Beck D, et al. Differentiating malignant from benign ovarian tumors with transvaginal colour flow imaging. Obstet Gynecol. 1992;79:159–62.
32. Timor-Tritsch IE, Rottem S. Transvaginal ultrasonographic study of the fallopian tube. Obstet Gynecol. 1987;70:424–8.

Obstetric Ultrasound

4

R.K. Diwakar

Abstract

The obstetric ultrasound has provided answer to many basic questions such as the presence of pregnancy in the uterus or in extrauterine location, number of foetuses, whether the embryo/foetus is alive, estimate of gestational age/pregnancy dating and nuchal translucency measurement in the first trimester scan. The foetal death should be confirmed by more than one examination based on the absence of cardiac motion for at least 2–3 min.

The second and third trimester obstetric ultrasound includes evaluation and follow-up of information available from the first trimester scan, confirmation of foetal life, assignment of gestational age, estimation of foetal body weight and amniotic fluid, placental position and maturity, diagnosis of growth restriction in compromised foetuses and detection of foetal development anomalies. In twin gestation, it is important to determine the number of placenta and the gestational sacs (the chorionicity and the amnionicity). One or more USG examinations in pregnancy are done safely with weekly monitoring in growth-restricted foetus. Doppler study and four-chamber view of heart/foetal echocardiography are other dimensions of obstetric ultrasound.

Obstetric ultrasound has provided answer to many questions about pregnancy. The technological advances in ultrasound imaging made it possible to conduct detailed anatomic survey of foetus for detection of chromosomal anomalies and congenital defects. Ultrasound-guided in utero foetal surgery at specialised centres has become a reality. To make the ultrasound examination safe, recommendations from time to time have been issued [1].

The real-time obstetric ultrasound includes confirmation of presence, size, location and numbers of gestational sac; presence or absence of cardiac activity; measurement of CRL if embryo (foetal pole) is present in the sac; position of foetus; evaluation of uterus, adnexa and ovaries; leiomyoma,

R.K. Diwakar
Department of Radio-Diagnosis, C.C.M. Medical College & Hospital, Durg, Chhattisgarh, India
e-mail: rkdiwakar49@yahoomail.co.in

R.K. Diwakar (ed.), *Basics of Abdominal, Gynaecological, Obstetrics and Small Parts Ultrasound*,
https://doi.org/10.1007/978-981-10-4873-9_4

adnexal mass or presence of fluid in cul-de-sac; measurement of foetal biometry such as BPD, HC, AC, FL, humerus/radius length for estimation of gestational age and interocular distance; nuchal translucency measurement; placental location, appearance, maturity grades and its relationship with internal os; assessment of amniotic fluid and its volume; etc. The study of foetal anatomy includes cerebral ventricles, posterior cranial fossa, spine, stomach, kidneys, urinary bladder, intactness of anterior abdominal wall, umbilical cord, four-chamber view (4 CH view) of heart, etc.

A 3–5 MHz abdominal transducer or 5–7.5 MHz transvaginal probe for TVS is used. It should be understood that not all malformations can be detected using USG.

4.1 Ultrasound Evaluation of First Trimester Pregnancy

Since there is no visible landmark to announce conception, the radiologist and obstetrician continue to use menstrual age or gestational age for pregnancy dating.

The first sign of pregnancy using sonography is the demonstration of the gestational sac [2]. Three dimensions of the GS are measured to calculate the mean sac diameter (MSD) (i.e. the mean of long, transverse and anteroposterior diameter). The mean sac diameter (MSD), 2–3 mm, can be observed first (Figs. 4.1 and 4.2). Yolk can be seen when MSD ranges from 6 to 12 mm. A thick ring of trophoblastic reaction is seen around the gestational sac of 7.5 weeks (Fig. 4.3).

One week after the missed period, a gestational sac of 5 mm corresponding to 5 weeks of gestation can be detected by TVS to indicate the presence of pregnancy. However, transabdominal sonography can detect a gestational sac of 6 weeks. Simple formula to calculate gestational age (GA) in days is MSD in mm + 30 [2]. The normal sac grows by 1 mm/day (Table 4.1).

From Hellman LM, Kobayashi M, Fillisti L, et al.: Growth and development of the human foetus prior to the twentieth weeks of gestation. Am J Obstet Gynaecol. 103:789. 1969 [3]

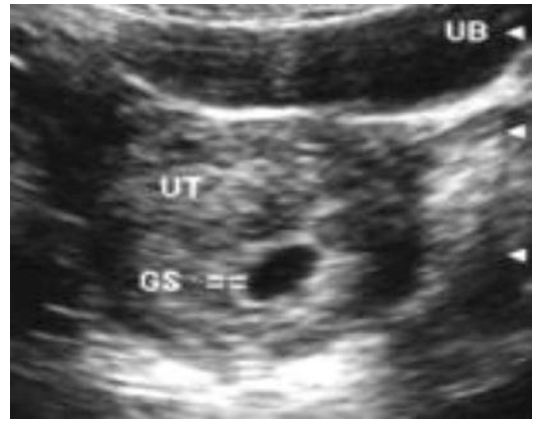

Fig. 4.1 Gestational sac of 6 weeks, no embryo or yolk sac

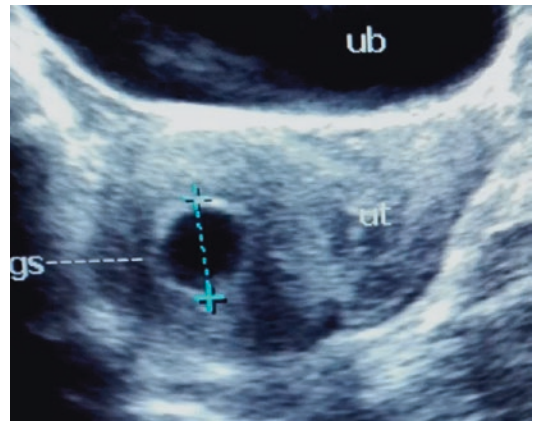

Fig. 4.2 Six week's gestational sac without embryo or yolk sac

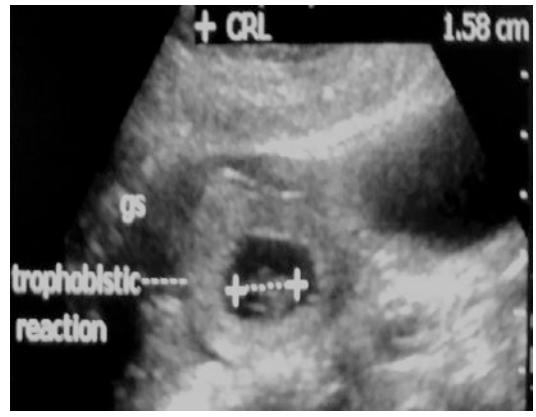

Fig. 4.3 Trophoblastic reaction is seen as an echogenic ring around gestational sac (GS) in 7.5 week's pregnancy

Table 4.1 Gestational sac measurement

GS (cm)	GA (weeks)	GS (cm)	GA (weeks)
1.0	5.0	4.5	10
1.5	5.8	4.7	10.3
2.0	6.5	5.0	10.7
2.5	7.2	5.2	11.0
3.0	7.9	5.5	11.5
3.5	8.6	5.9	12.0
4.0	9.3	6.0	12.2

The embryo in the sac, i.e. foetal pole, can be visualised in 6 weeks, and as small as 2 mm can be detected with transvaginal transducer. The measurement of foetal pole, i.e. CRL, provides clue to the age of foetus. GA in days can also be estimated by adding 42 to the embryonic length in millimetres for pregnancies between 43 and 67 days [4]. The crown rump length (CRL) (Fig. 4.4) measures 30 mm by the end of tenth week (Table 4.2).

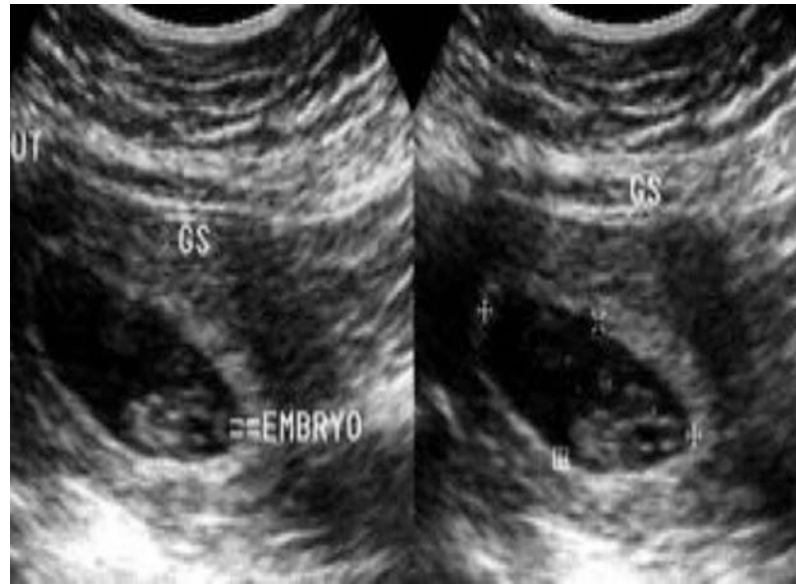

Fig. 4.4 CRL measurement in the first trimester

Table 4.2 Crown rump length in cm

CRL	MA	CRL	MA	CRL	MA	CRL	MA	CRL	MA
0.2	5.7	2.2	8.9	4.2	11.1	6.2	12.6	8.2	14.2
0.4	6.1	2.4	9.1	4.4	11.2	6.4	12.8	8.4	14.3
0.6	6.4	2.6	9.4	4.6	11.4	6.6	12.9	8.6	14.5
0.8	6.7	2.8	9.6	4.8	11.6	6.8	13.1	8.8	14.7
1.0	7.2	3.0	9.9	5.0	11.7	7.0	13.2	9.0	14.9
1.2	7.4	3.2	10.1	5.2	11.9	7.2	13.4	9.2	15.1
1.4	7.7	3.4	10.3	5.4	12.0	7.4	13.5	9.4	15.3
1.6	8.0	3.6	10.5	5.6	12.2	7.6	13.7	9.6	15.4
1.8	8.3	3.8	10.7	5.8	12.3	7.8	13.8	9.8	15.6
2.0	8.6	4.0	10.9	6.0	12.5	8.0	14.0	10.0	15.9

From Hadlock FP, Shah YP, Kanon DJ, Lindsey JV: Foetal crown-rump length: Re-evaluation of relation to menstrual age (5–18 weeks) with high-resolution real-time US. Radiology. 182:501–505, 1992 [5].

Yolk sac (YS) is seen at 5.5 weeks in transvaginal sonography [6]. In abdominal sonography, the earliest detection of yolk sac is at seventh week of gestation [7]. The normal yolk sac is 5–6 mm in diameter at about 10 weeks' GA [8] (Figs. 4.5, 4.6 and 4.7). It disappears by the end of the first trimester [8]. However, patients with a large yolk sac are at increased risk for spontaneous abortion.

The primordial heartbeats can be seen from sixth week onwards [9]. The earliest detection of heart rate by abdominal USG is by 7.5 to 8th week. It is 137–144 beats per minute after ninth week GA [10].

Colour flow imaging depicts the presence of flow in the foetal heart (Fig. 4.8).

MSD of 10 mm or more with distorted sac shape, less than 2 mm thin weakly echogenic trophoblastic reaction and absence of double decidual sac [11] suggest failed pregnancy. It is suggested by Bradley et al. [12] that the origin of only one of the double rings is from decidua,

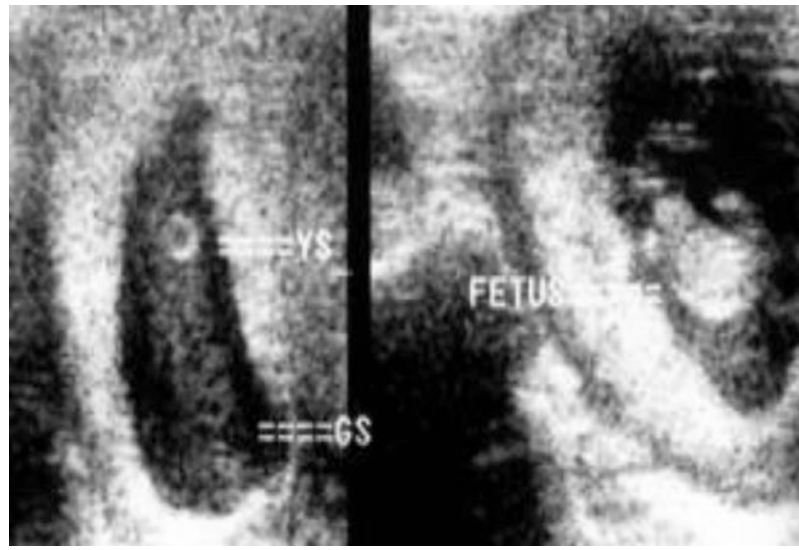

Fig. 4.5 Gestational sac with a foetus of 9 weeks and yolk sac

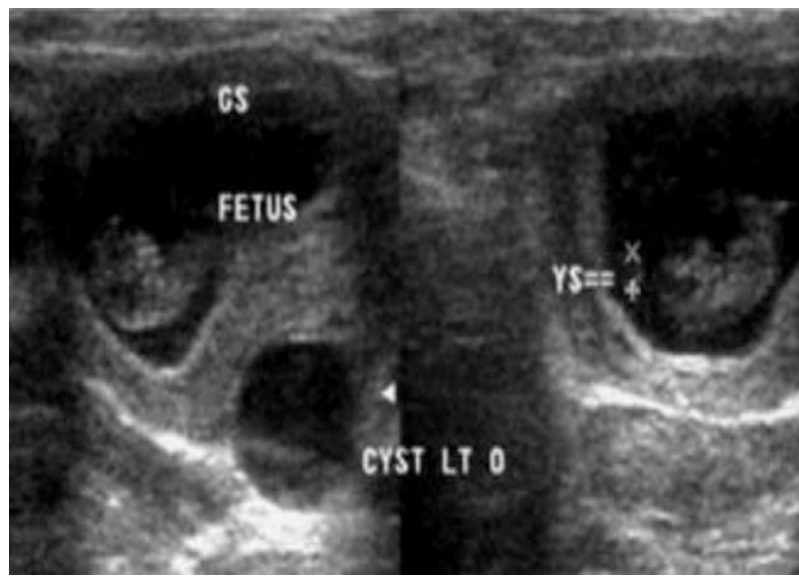

Fig. 4.6 Yolk sac and foetus in normal early pregnancy

while the origin of the inner of the double ring is from proliferating chorionic villi.

Anembryonic gestation (absence of embryo) or blighted ovum is an abnormal pregnancy with a gestational sac but no visible embryo beyond 8 weeks' GA. In the presence of a nonliving embryo in early pregnancy, the term foetal demise should be used instead of missed abortion [13]. In case of any doubt, quantitative level of HCG is complimentary to ultrasound.

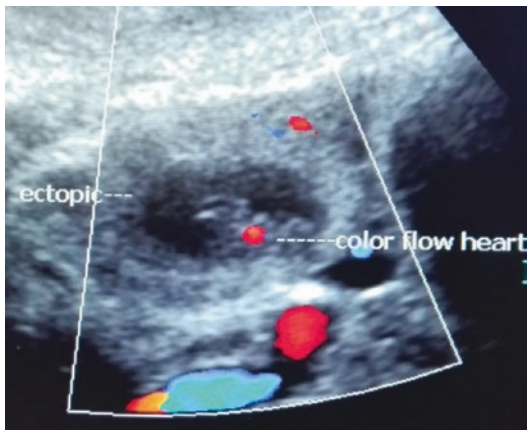

Fig. 4.7 Early pregnancy associated with a cyst in the left ovary

Sonography in the first trimester of pregnancy is carried out to confirm the presence of gestational sac in intrauterine or extrauterine location, to estimate gestational age, to confirm number of gestational sac, to confirm viability of embryo or foetus, to find out the cause of vaginal bleeding and to detect associated pelvis masses and uterine abnormalities. It is also used as an adjunct to chorionic villi sampling, amniocentesis, embryo transfer and IUD localisation and removal.

Transvaginal scan should be done whenever possible, if transabdominal USG fails to provide definite information about the gestational sac, embryo or foetus.

USG criteria of abnormal sac include MSD of >25 mm or greater without cardiac activity in the embryo, MSD of >20 mm or greater without yolk sac and failure to detect a double decidual sac when the MSD is 10 mm or greater [11].

4.1.1 Complications in the First Trimester of Pregnancy

Vaginal spotting or frank bleeding is a common experience during the first few weeks of pregnancy

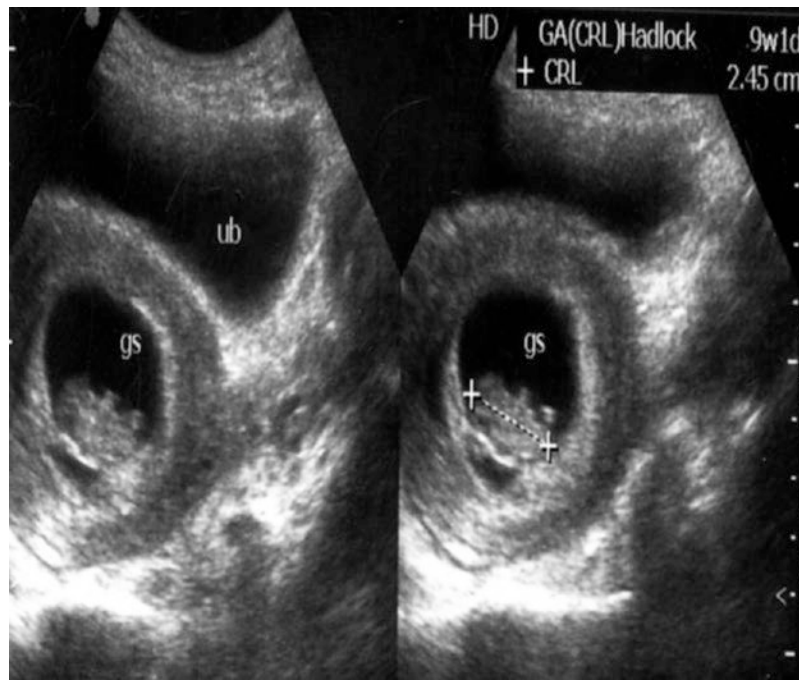

Fig. 4.8 Colour flow in foetal heart in 8 weeks in the right tubal ectopic pregnancy

in approximately 25% of patients [14]. Often the bleeding is self-limited and temporary.

Nyberg et al. [15] suggested the following as the sonographic findings of threatened abortion and abnormal intrauterine pregnancy:

1. Threatened abortion: a gestational sac of 5–6.5 weeks with or without embryo (Fig. 4.9)
2. Complete abortion: empty uterus or empty one gestational sac in twin pregnancy (Fig. 4.10)
3. Incomplete abortion: typical thickened endometrium or fluid within endometrial cavity
4. Embryonic demise: discrete embryo without cardiac activity (Fig. 4.11)
5. Blighted ovum: discrepancy between gestational sac and embryonic development with little or no embryonic remnant

Retained products after the first trimester abortion can be diagnosed when a gestational sac

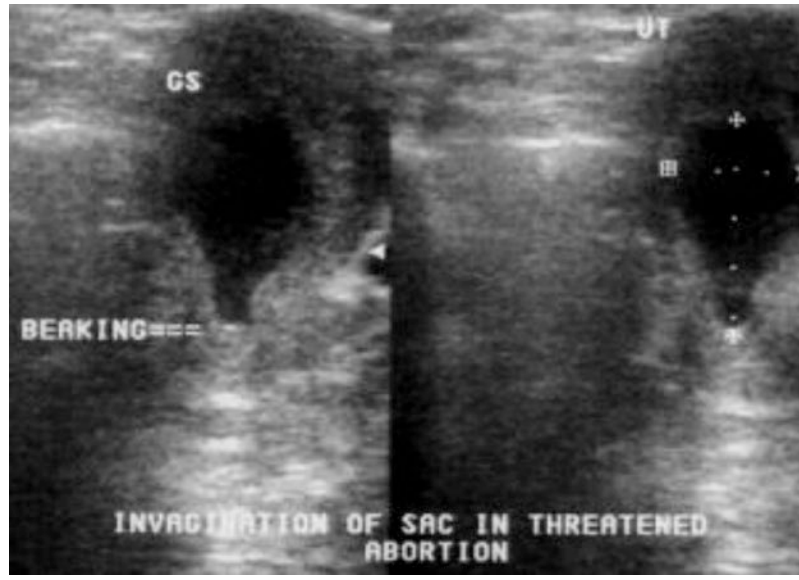

Fig. 4.9 Invagination of gestational sac in endocervical canal in threatened abortion

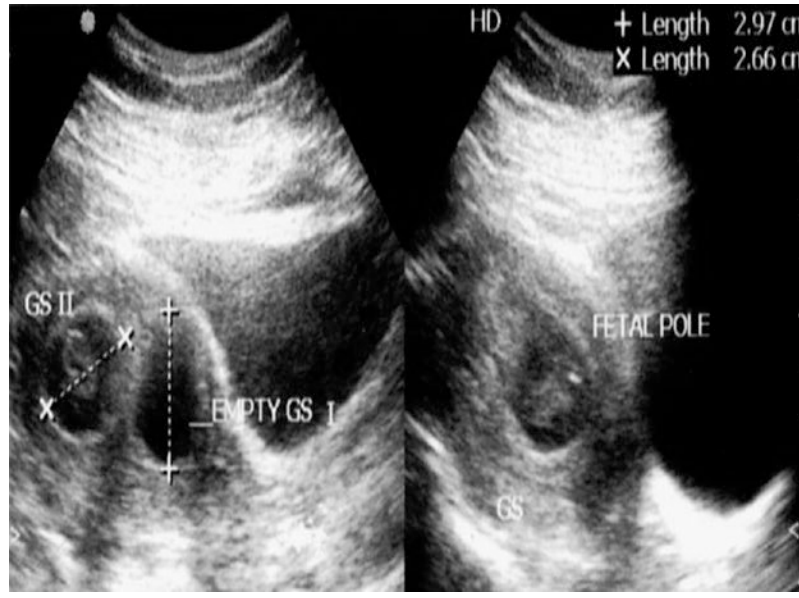

Fig. 4.10 Abortion of a member of twin pregnancy GS

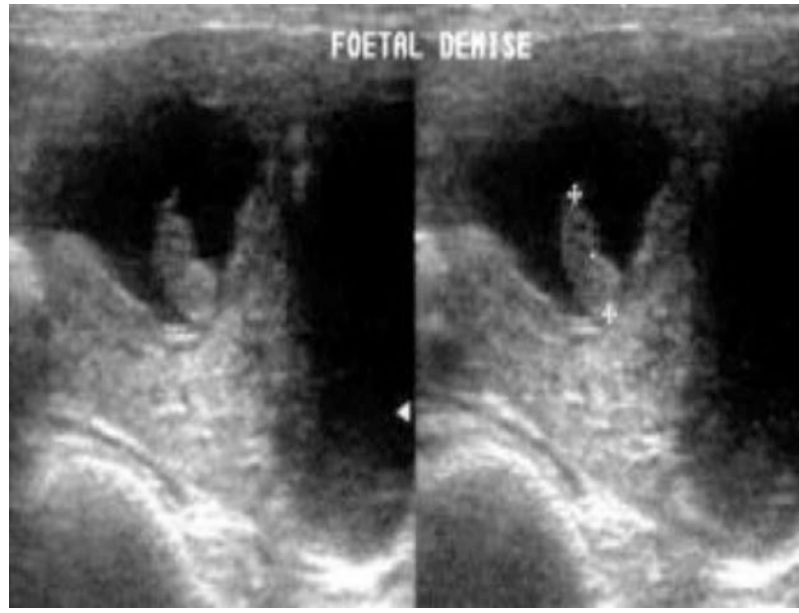

Fig. 4.11 Nonliving foetus (no heart pulsations) lying in the bottom of irregular-shaped gestational sac in missed abortion

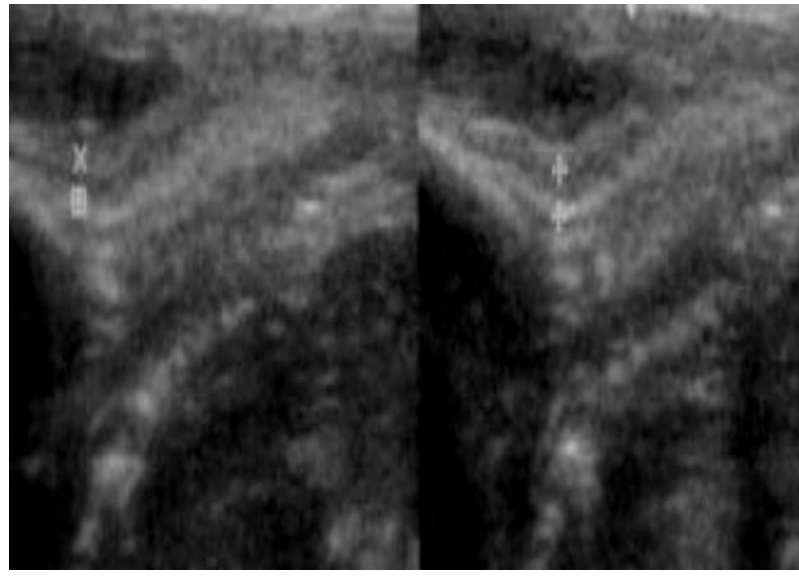

Fig. 4.12 Nuchal translucency of 3 mm

or collection or an endometrium greater than 5 mm thickness is seen.

The posterior nuchal translucency of 3 mm or more in AP dimension at 10 weeks' GA is considered abnormal [16] (Fig. 4.12).

Weeks 6 through 10 constitute the embryonic phase, during which time all major internal and external structures begin to form [17]. The final 2 weeks of the first trimester, i.e. 11th and 12th, begin the foetal period during which there is continued rapid growth and ongoing organ development [17].

Definitive placenta is seen after 10–12 weeks' GA.

Pregnancy may be associated with fibroid (Figs. 4.13, 4.14 and 4.15).

Ectopic Pregnancy: GS as small as 2 mm can be visualised with transvaginal USG. The double decidual sac (DDS) [12] sign is a highly reliable indicator of an intrauterine pregnancy.

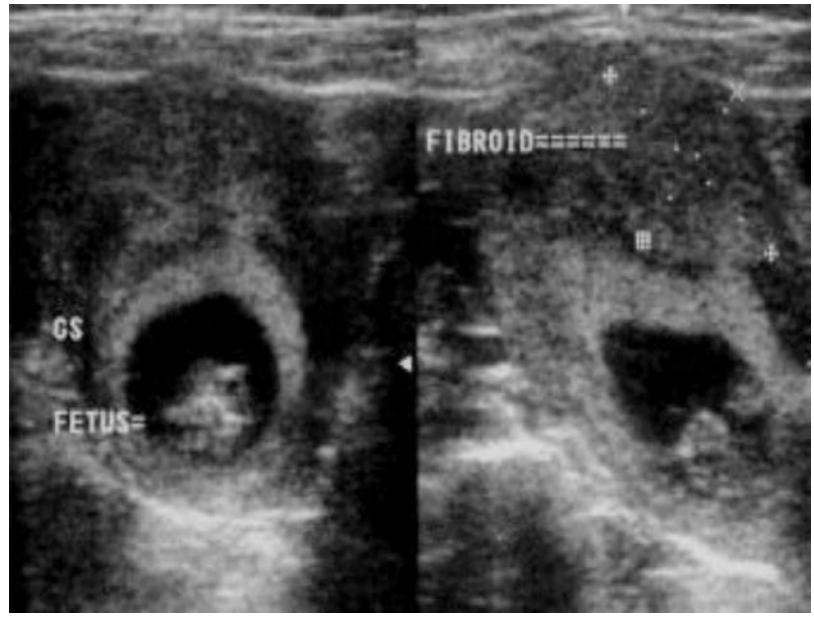

Fig. 4.13 Viable foetus with fibroid in anterior wall of uterus

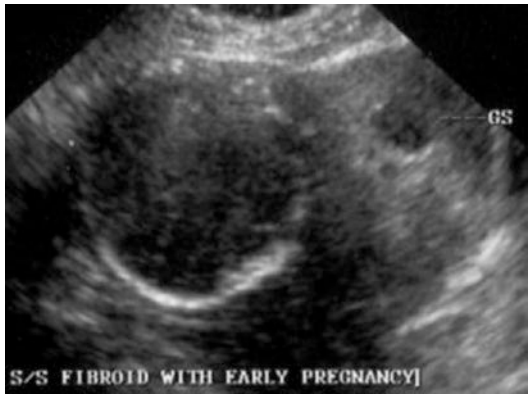

Fig. 4.14 A large fibroid near uterine fundus and GS in the lower segment of the uterus

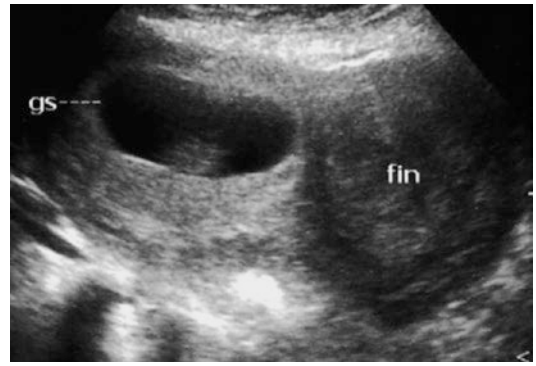

Fig. 4.15 Early pregnancy with viable embryo and a fibroid in lower segment of the uterus

The DDS sign is a highly reliable indicator of an intrauterine pregnancy and is caused by the inner rim of chorionic villi surrounded by a thin crescent of fluid in the endometrial cavity which in turn is surrounded by the outer echogenic rim of the decidua basalis [12].

The presence of intrauterine pregnancy markedly decreases the risk of ectopic pregnancy; all patients should have evaluation of adnexa to identify other gestations (Fig. 4.16).

The pseudo-gestational sac in ectopic pregnancy is seen due to fluid collection in the endometrial cavity mimicking a GS. It is visualised in 20% of ectopic pregnancy [18].

It should always be remembered that about 26% of patients with ectopic pregnancy may have normal USG finding. In such situation transvaginal sonography (TVS) and monitoring of HCG levels should be done. Colour Doppler study in ectopic pregnancy due to absence of blood flow does not offer any additional advantage.

Molar changes (gestational trophoblastic disease) can be detected between 9 and 12 weeks of amenorrhea.

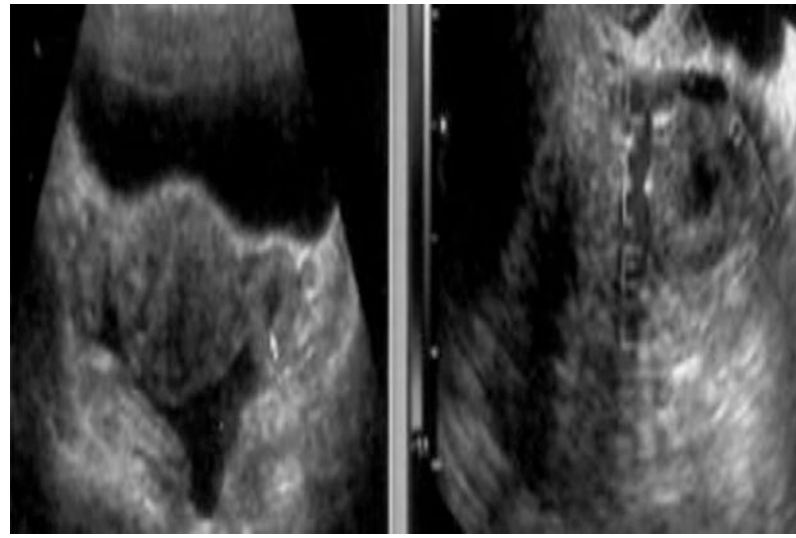

Fig. 4.16 Ectopic gestational sac in the left tube with blood collection in cul-de-sac

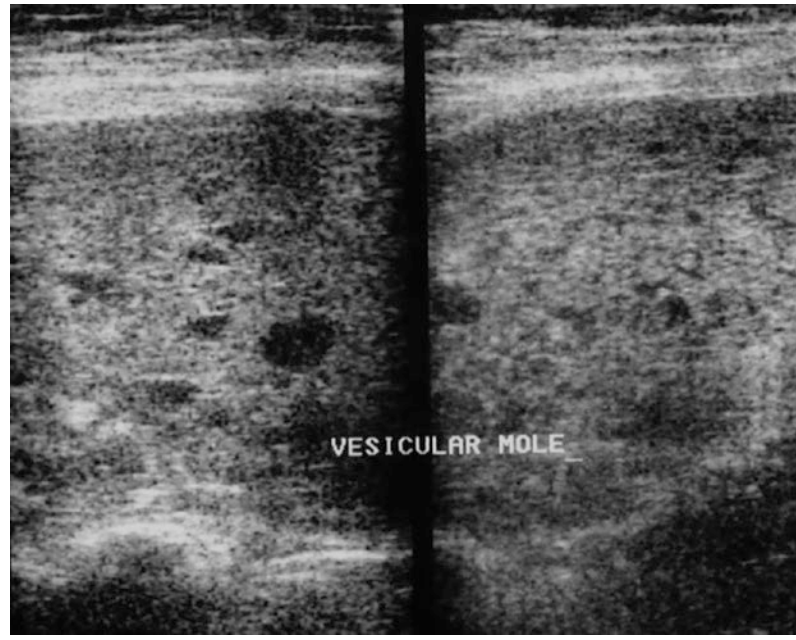

Fig. 4.17 Areas of hyperechogenicity mixed with hypoechogenic areas in a molar pregnancy (Swiss cheese appearance)

The uterine cavity is typically filled with multiple echolucent areas of varying size and shape and uterine size is greater than expected for GA (Figs. 4.17 and 4.18). Complete hydatidiform mole (CHM) with coexisting foetus is diagnosed at 15–20 weeks' GA. Partial hydatidiform mole (PHM) refers to combination of a foetus with enlarged placenta (thickness >4 cm at 18–22 weeks) containing multicystic (avascular echo-free) spaces [19].

Choriocarcinoma is a highly malignant tumour arising from trophoblastic epithelium. It may occur a few weeks to few months or few years after the last pregnancy. The sonographic features include hypoechoic areas (blood lacunae) surrounded by numerous hyperechogenic

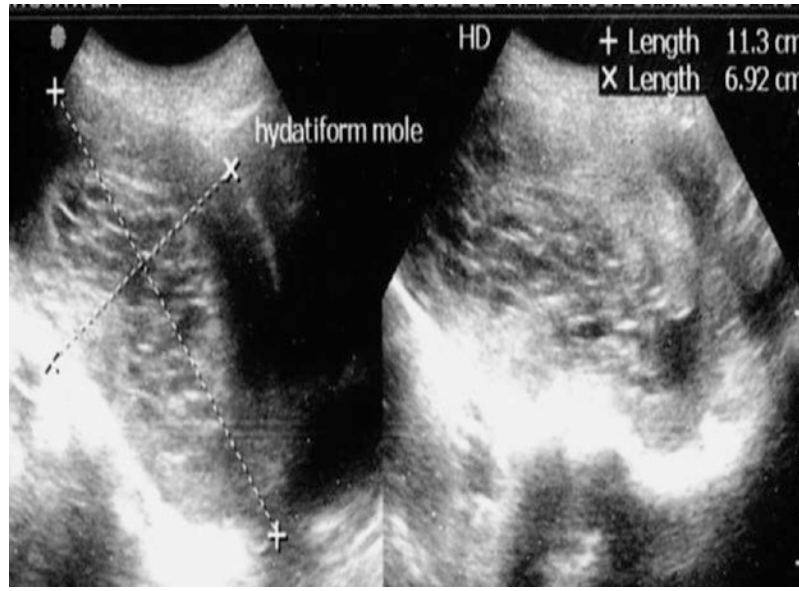

Fig. 4.18 Multiple cystic (avascular echo-free) spaces in hydatidiform mole

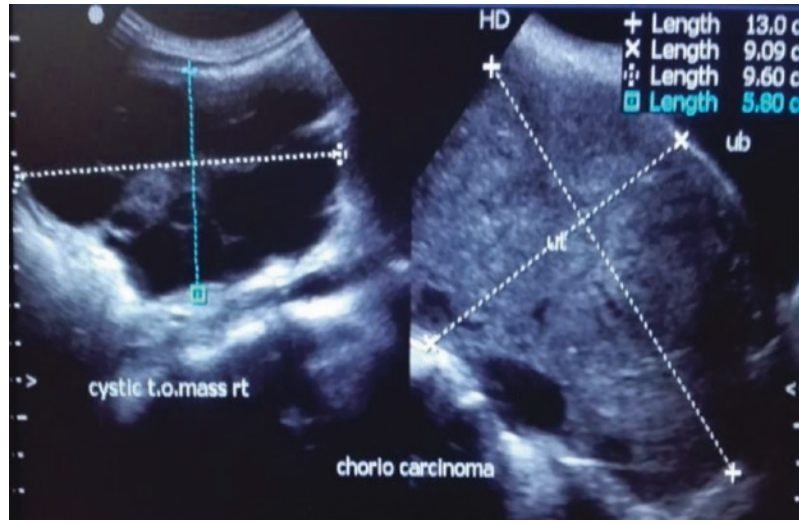

Fig. 4.19 Multiple nodules of increased echogenicity and hypoechoic cystic areas with multicystic T.O. mass right

areas (trophoblastic nodules) and numerous intramyometrial vascular shunts (Figs. 4.19 and 4.20).

Approximately 50% of choriocarcinoma follows a molar pregnancy. Thirty percent occur after a miscarriage and 20% occur after an apparently normal pregnancy [20].

Cervical incompetence [21] affects 1% of pregnancy patients in the second trimester. The USG signs include short cervix (<20 mm length) [22].

Cervical length measured by transabdominal sonography is directly proportional to bladder fullness. TVS is the preferred method for cervical measurements.

Cervical length is the distance between the internal os and external os as measured with electronic callipers (Fig. 4.21). An inverse relationship between cervical length measurement and relative risk of preterm birth has been demonstrated. Three potential risk measurements are identified: 30, 25 and 20 mm.

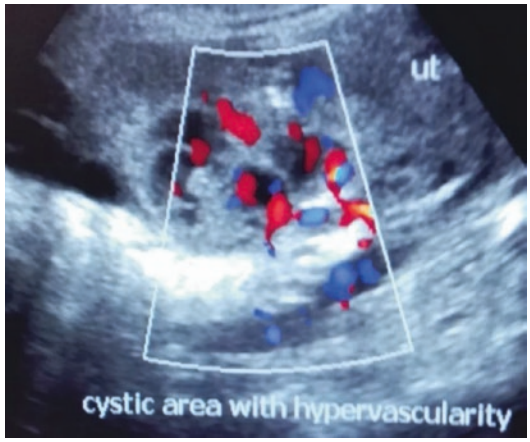

Fig. 4.20 Multiple intra-tumoural vessels on colour Doppler imaging in choriocarcinoma

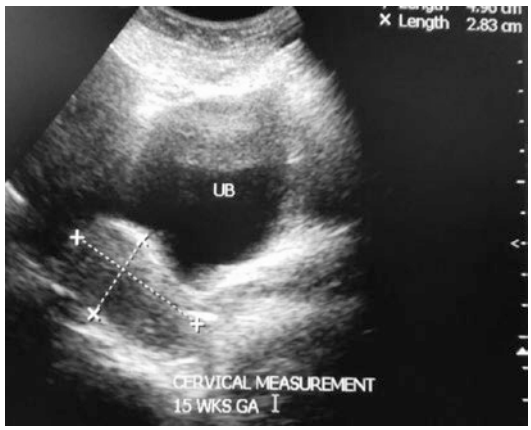

Fig. 4.21 Cervical measurement

Funnelling of internal os and wide internal os diameter [23] of more than 50%, before 25 weeks, has a high incidence of preterm delivery. The cerclage operation is performed at 12–15 weeks' gestation.

Criteria to define funnelling of cervix [23] are as follows:

1. Funnel width (dilatation of internal os) = *C*
2. Residual or functional cervical length (cervical length distal to funnel) = *B*
3. Funnel length (length of an imaginary line that connects the apex of the funnel to the cranial-most edge of the base of the funnel) = *A*

Table 4.3 USG findings in the first trimester of pregnancy

Sonographic finding	Gestational age in weeks
Mean sac diameter of 5 mm	5 weeks (increases at 1.13 mm/day)
Double decidual sac sign, MSD 10 mm	6 weeks (at least 2 mm thickness)
Yolk sac MSD 8 mm	5.5 weeks (transvaginal US)
Yolk sac MSD 20 mm	7 weeks (transabdominal US)
Cardiac activity, MSD 25 mm	8 weeks (transabdominal)
CRL	8–12 weeks (increases at 1 mm/day)
Anembryonic pregnancy/ blighted ovum	MSD >16 mm, no embryo, no yolk sac, no cardiac activity

Percentage of funnelling = $A/A + B$ is most predictive of preterm birth. 50% funnelling may have 75% of preterm birth.

$$\text{Cervical index} : A + 1/B$$

USG findings in the first trimester of pregnancy are summarised in Table 4.3.

4.2 Ultrasound in Second and Third Trimester of Pregnancy

Since the foetus has grown sufficient in size, many structures can be identified and measured. The foetal position is first ascertained by localising the foetal head in lower uterine segment in cephalic position, while in breech position, the foetal head is located in the upper abdomen (near uterine fundus). In breech, the presenting part as foot or buttock should be mentioned. In transverse lie, the foetal head is located in the abdomen on the right/left side and the foetal rump in opposite side of maternal abdomen, and foetal spine is seen at right angle to maternal spine and the shoulder as the presenting part. Radiograph of abdomen should be advised in late second and third trimester in case of any doubt especially in transverse lie. Since the foetus has grown sufficient in size, many structures can be identified and measurement can be recorded.

Ultrasound in the second and third trimester of pregnancy includes evaluation of foetus and its surrounding, biophysical profile, follow-up of suspected foetal anomalies, association of uterine fibroid or adnexal mass and Doppler parameters, etc. It is also used as an adjunct to amniocentesis, percutaneous umbilical blood sampling or cerclage placement.

Readers may refer to ACR/AIUM guidelines for obstetric ultrasound examination [1].

Foetal Biometry:

It is an important part of obstetric sonography. It may vary or be operator dependent because the measurement will depend on the section/plane in which the image has been obtained and the placement of cursors.

The multiple foetal growth parameters [24, 25] are used for foetal biometry:

Biparietal Diameter (BPD): It is measured through a plane traversing the third ventricle and thalami (Fig. 4.22). Cursors are placed on the middle of the skull wall and not on the skin surface. Skull oval in shape with well-demarcated skull wall as sharp bright echo should be selected for measurement.

Cephalic index = BPD/OFD (occipitofrontal diameter) × 100. Dolichocephalic skull is seen in breech presentation, oligohydramnios and meningomyelocele. The measurement of BPD will tend to underestimate the GA.

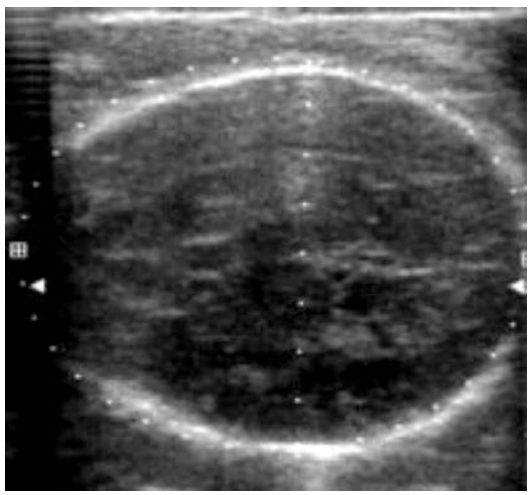

Fig. 4.22 BPD and HC measurement in the second trimester of pregnancy

The menstrual age can be determined using a standard reference table for BPD [24], HC [27], AC [28], femur length [26], transverse cerebellar diameter and interocular distance. The modern instruments immediately compute an age as the measurement is obtained.

Head Circumference (HC): It is measured on the image taken for BPD by placing the ellipse over the skull outline.

The ratio of HC to AC remains above 1 before 35–36 weeks of gestation, and in foetuses with normal growth, it becomes 1 or less than one, after 35–36 weeks of gestation. This is used to predict intrauterine growth restriction (IUGR) of the foetus.

Abdominal Circumference: It is measured at a plane where the junction of the right and left portal vein is seen (Figs. 4.23 and 4.24). The shape of abdomen should be as round as possible. AC has been reported having the largest variability.

Femur Length: This measurement is taken at a plane where both ends of the femur are clearly visualised. It is considered to be the most accurate parameter in predicting GA. A foetus with shortening of femur greater than 2 SD below the mean for GA suggests a skeletal dysplasia. Absence or hypoplasia of radius is seen in many syndromes and conditions including tracheo-oesophageal fistula, anorectal atresia, trisomy 18, etc.

It should be remembered that if age is known by conception data, the menstrual age is established. Foetal biometry has a variability of 8%. CRL is the most accurate parameter taken in the first trimester of pregnancy. Multiple parameters should be used to determine GA. In later part of the third trimester, sole reliability on measurement-based GA assessment is invalid as it is more reliable for foetal weight and growth rather than an index of GA.

Estimation of Foetal Weight: BPD, AC and FL are used for estimation of foetal weight [29].

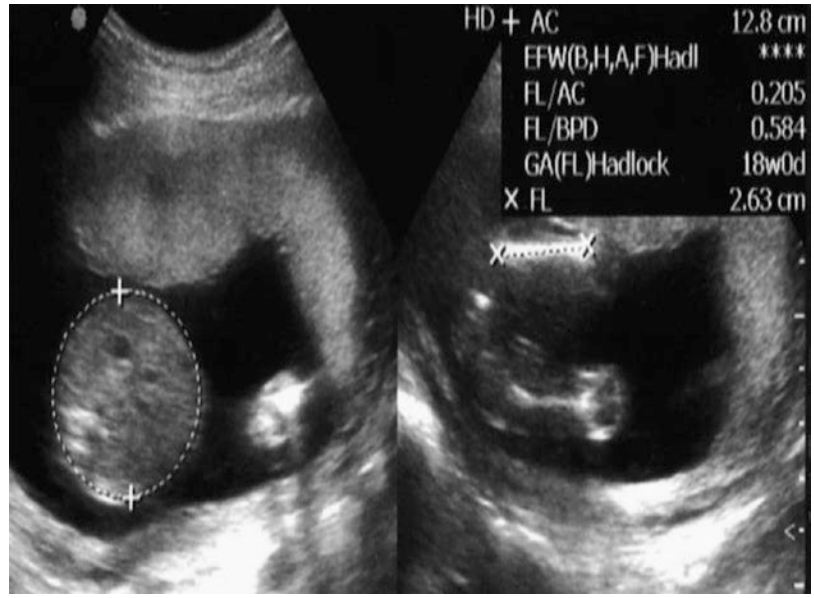

Fig. 4.23 AC and femur length measurements

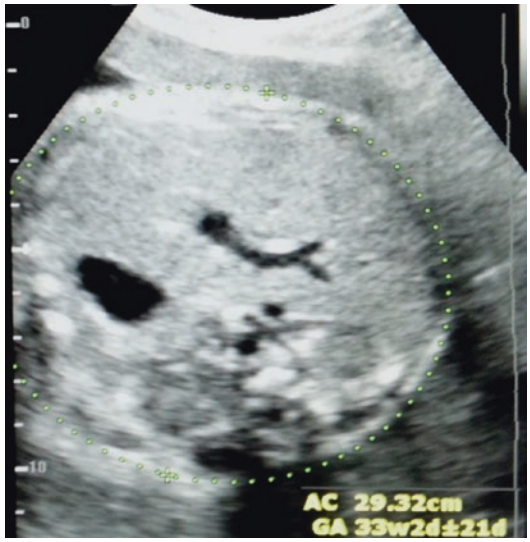

Fig. 4.24 Measurement of AC

4.2.1 Ultrasound in Twin/ Multifoetal Gestations

Twin gestation results from fertilisation of two separate ova (dizygotic) or a single ovum which subsequently divides (monozygotic) (Fig. 4.25). Approximately two-thirds of twin pregnancies are dizygotic and one-third monozygotic. The number of placenta depends on when the zygote divides: division of zygote prior to day 4 (before blastocyst formation) results in dichorionic diamniotic gestation; between 4 and 8 days after fertilisation, it results in a monochorionic diamniotic gestation; and cleavage after 8 days of fertilisation results in a monochorionic-monoamniotic gestation [30].

Conjoined twins are seen in monochorionic-monoamniotic twin pregnancy. Preterm birth and low birth weight are contributing factors for increased morbidity and mortality in multifoetal gestation. The inter-foetal dividing membrane is identified and its thickness (1 mm) should be evaluated (Fig. 4.26). There is thinning of the membranes as pregnancy progresses [31].

The membrane rules out monoamnionicity. The number of placenta should be determined. Two separate placentae confirm dichorionicity. Two heads and two abdomens are visualised (Fig. 4.27). By definition, all monoamniotic twin gestations are also monochorionic.

In the first trimester, demise of co-twin has negligible effect on the remaining gestation

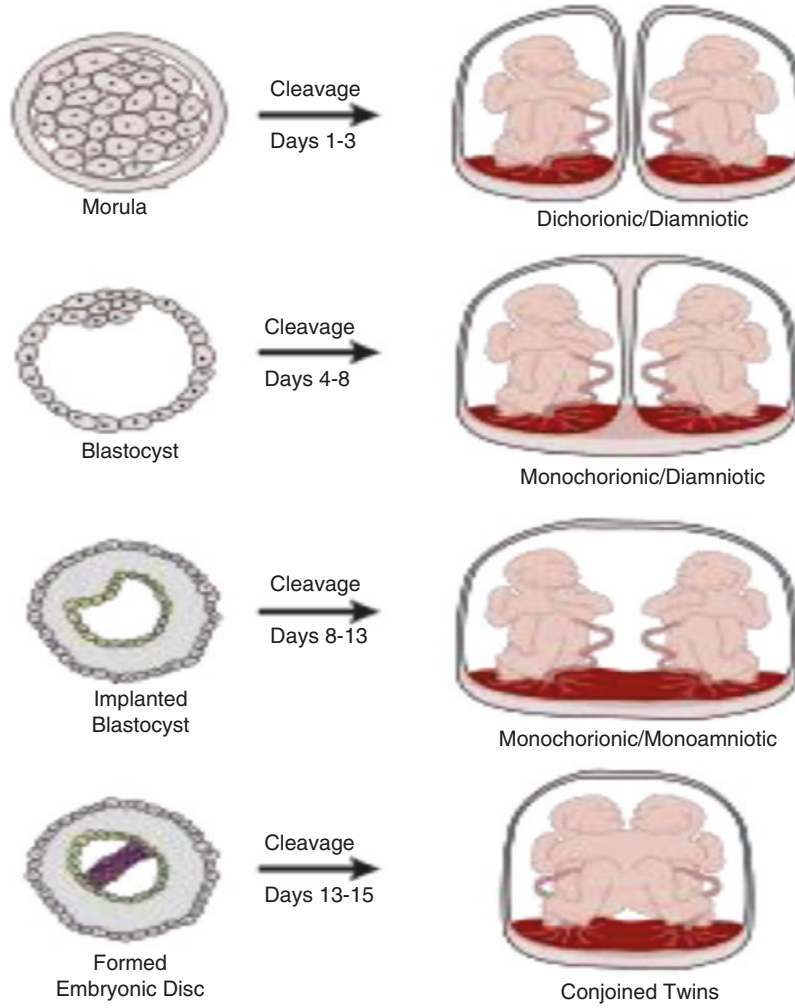

Fig. 4.25 Various types of chorionicity and amnionicity in monozygotic (one egg/identical) twins (from: Wikipedia, free encyclopaedia)

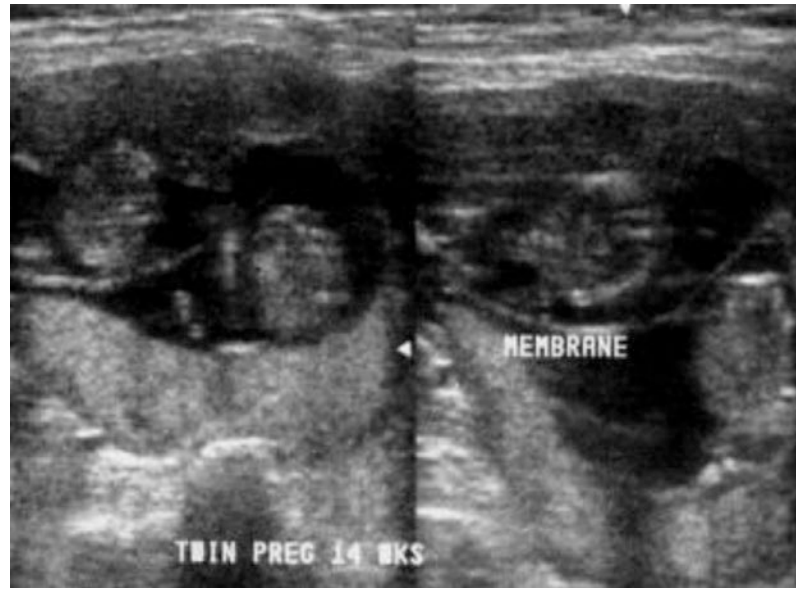

Fig. 4.26 Two sacs separated by inter-foetal dividing membrane and two placentas

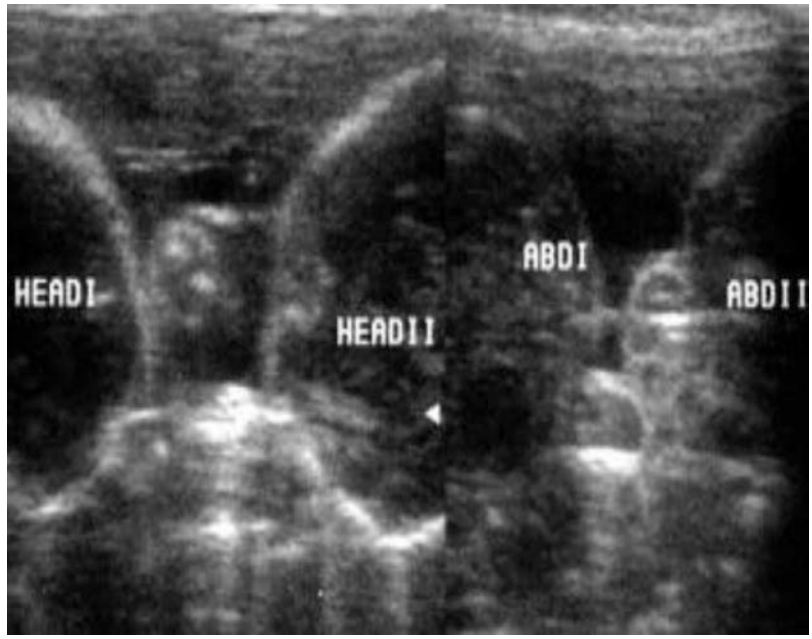

Fig. 4.27 Two heads and two abdomens in dichorionic-diamniotic twin pregnancy

which should be allowed to proceed. Evans et al. [32] found that the overall pregnancy loss rate was 12% and early premature deliveries were only 4.5%.

Reduction of multiple pregnancies (triplet and above) is considered safe nowadays and is done to improve the outcome. Selective foetal reduction may be done in the late second trimester if lethal anomaly is present especially in association with polyhydramnios.

Conjoined Twins

The word pagus (the Greek term for fastened) is used to describe fused anomalies. The fusion may be anterior, posterior or side to side (lateral) or at the head or buttock.

The word pagus (the Greek term for fastened) is used to describe fused anomalies (conjoined twin). The fusion may be anterior, posterior or side to side (lateral) or at the head or buttock. For example, craniopagus refers to head-to-head fusion; thoragopagus, chest-to-chest fusion; and omphalopagus, abdomen-to-abdomen fusion [33].

TRAP (twin reversed arterial perfusion) sequence is suspected when a severely malformed foetus is seen in a monochorionic twin gestation. This is also called acardiac twin. Abnormal placental vascular communications between the twins lead to perfusion of the malformed acardiac twin. Diffuse oedema and cystic hygroma are usually present in the acardiac twin [34].

TTTS (twin-to-twin transfusion syndrome) is a complication unique to monochorionic gestation. There are arteriovenous communications deep in the placenta so that one twin is growth restricted, hypovolemic and anaemic and the other (the recipient twin) is larger, hypervolemic and plethoric, and both are at serious risk for increased mortality and morbidity [35].

TOPS (Twin Oligohydramnios Polyhydramnios Sequence) in which one twin is stuck with oligohydramnios [36].

4.2.2 Ultrasound of Placenta and Umbilical Cord

Placenta

Definitive placenta is well seen only after 10–12 weeks. By 14–15 weeks, placenta is well established and a prominent hypoechoic area

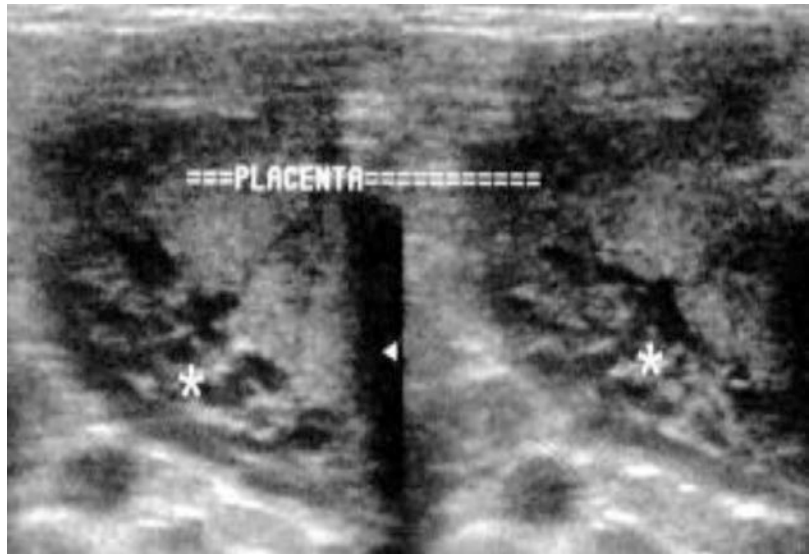

Fig. 4.28 Normal retro-placental complex (*asterisk*)

"retro-placental complex" is seen (Fig. 4.28). It is composed of the decidua, myometrium and uterine vessels [37].

The thickness of the placenta is equal to GA in weeks +10 mm. The term placenta is usually 4 cm in thickness. A thin placenta (placentomalacia) is often a marker for small-for-gestational-age (SGA) foetus or IUGR [37].

Placentomegaly (thickening of placenta) may be with heterogenous or homogenous echotexture. Heterogenous placentomegaly is seen in molar pregnancy, triploidy, placental haemorrhage and mesenchymal dysplasia. Homogenous placentomegaly is seen in diabetes mellitus, anaemia, hydrops, infection and aneuploidy [37]. In circumvallate placenta, the membranes insert from the placental edge towards the centre: it may be partial or complete [x]. Succenturiate placenta or accessory lobe of placenta has high incidence of placental infarction and velamentous insertion of umbilical cord [37].

Placental calcifications (USG sign of aging of placenta) and its co-relation with foetal lung maturity could not be established. It was in vogue but currently has little clinical value.

Cystic/hypoechoic lesions (venous lakes) in the placenta are rarely significant (Fig. 4.29).

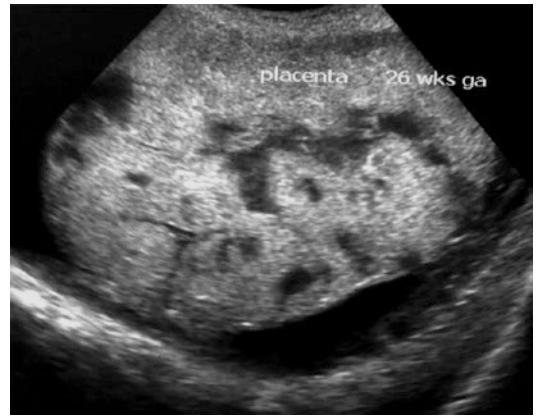

Fig. 4.29 Multiple hypoechoic lakes in the placenta with normal outcome of pregnancy

Placenta praevia refers to a placenta that is in front of or previous to the foetus relative to the birth canal (Fig. 4.30). Complete placenta praevia covers the internal os totally. The term marginal or partial placenta praevia is used to describe the edge of placental tissue within 2 cm of the internal os (Fig. 4.31). If the placental edge is more than 2 cm away from the internal os, it is described as low-lying placenta (Fig. 4.32). Ninety-five percent of low-lying placenta seen in

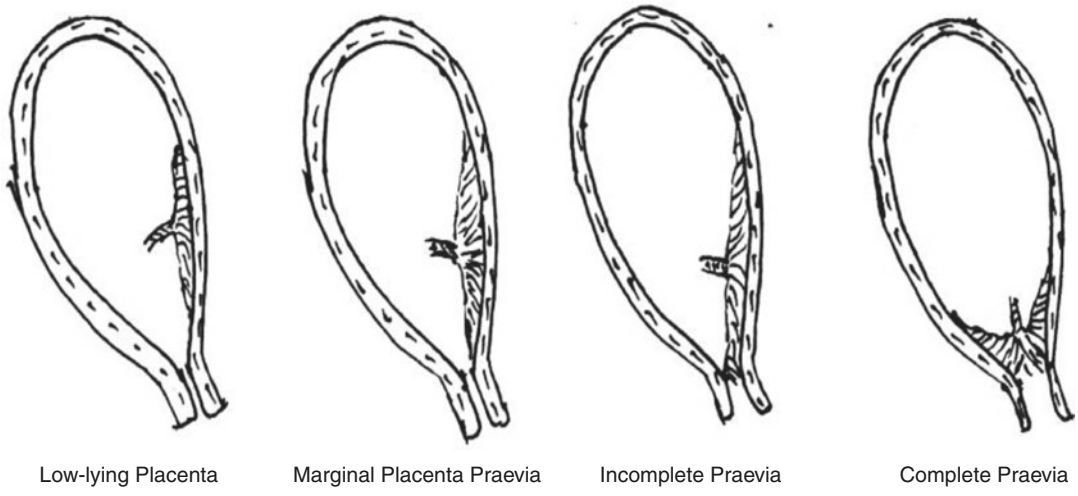

Fig. 4.30 Different types of placenta praevia

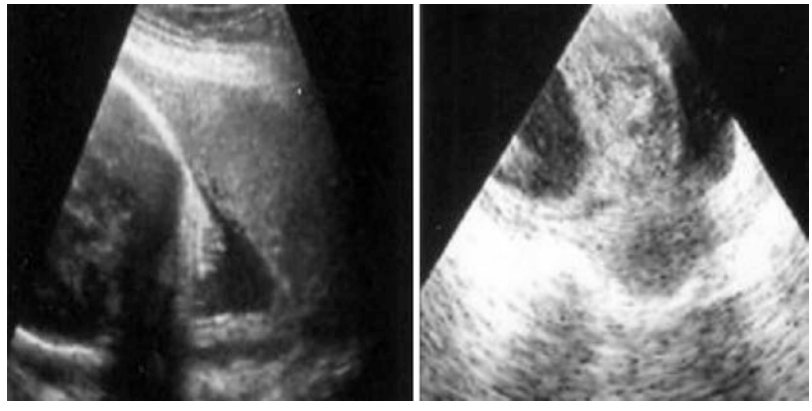

Fig. 4.31 Placenta interposed between the foetal head and urinary bladder (incomplete placenta praevia)

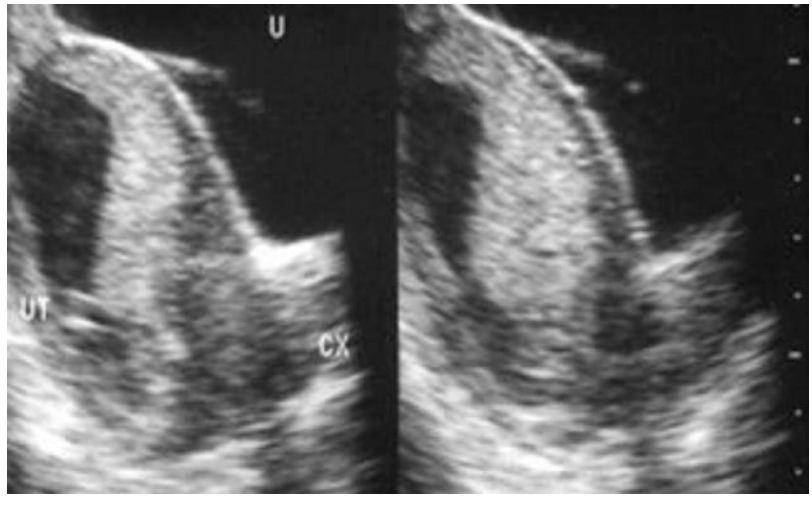

Fig. 4.32 Commonly seen low-lying placenta in early pregnancy

the second trimester is converted into non-praevia by the third trimester [38].

Placental abruption may be seen as retro-placental haemorrhage more than 3 cm thickness and more rounded in shape than the normal "retro-placental complex". The retro-placental haematoma are hyperechoic (initial 0–48 h) (Fig. 4.33) and become hypoechogenic after 1 week (Fig. 4.34). Retro-placental haemorrhage resulting in 30–40% detachment may end in IUGR or foetal demise [38].

Placenta accreta refers to abnormal adherence of placenta to the uterus with subsequent failure separate after delivery of the foetus.

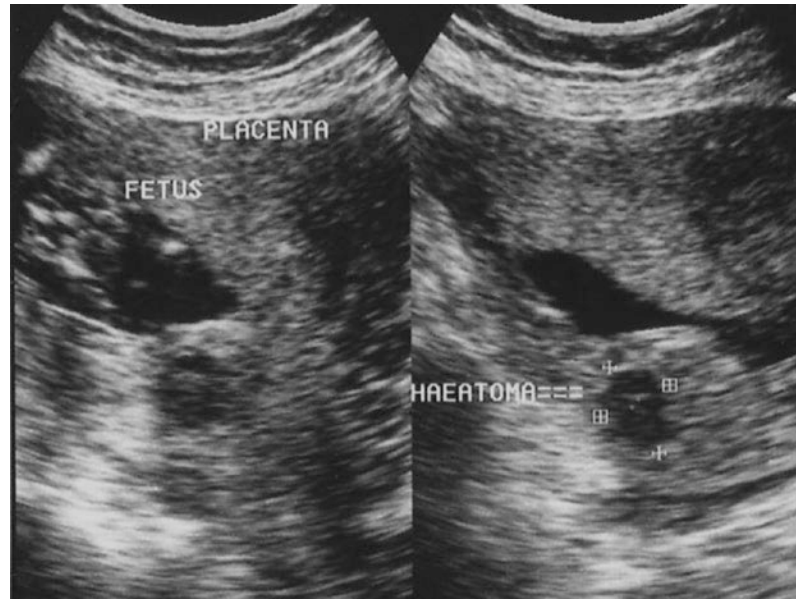

Fig. 4.33 Retro-placental haematoma in early pregnancy

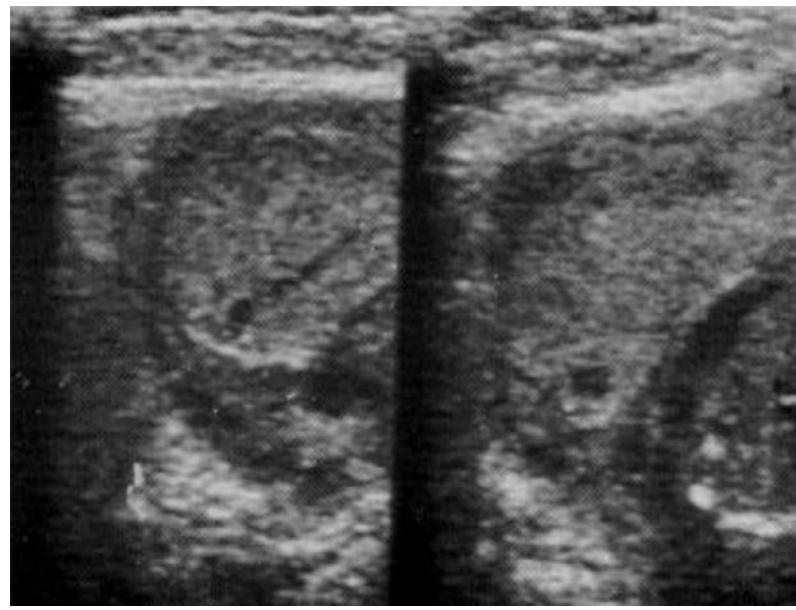

Fig. 4.34 Resolving retro-placental haematoma

It may/may not invade the myometrium. Colour Doppler or power Doppler should be performed**.**

Evaluation of Placental Maturity [39]

Grade 0: Homogenous appearance of placental tissue with smooth chorionic plate (Fig. 4.35) prior to 29–30 weeks' gestational age.

Grade 1: Echogenic areas randomly dispersed in the placenta with subtle indentations of chorionic plate (Fig. 4.36) between 30 and 33 weeks' gestational age.

Grade 2: Echogenic densities near the uterine wall and comma-like densities near placental margin (Fig. 4.37) at 33–35 weeks' gestational age.

Grade 3: Echo-free or fall-out areas, indentations of chorionic plate and irregular densities with acoustic shadowing (Fig. 4.38) beyond 35 weeks' gestational age.

Umbilical cord can be visualised as early as 8 weeks onwards (Fig. 4.39). The diameter is usually less than 2 cm. It has two arteries and one vein (Fig. 4.40). The length remains the same throughout the pregnancy.

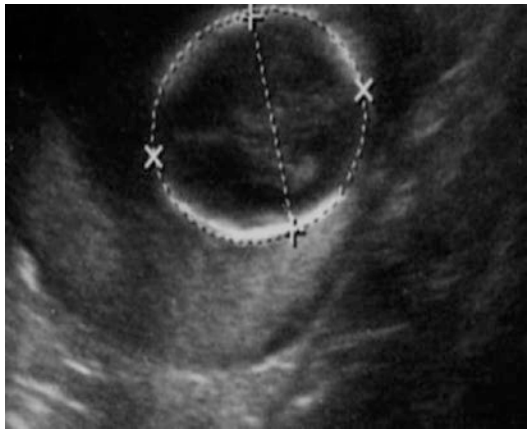

Fig. 4.35 Homogenous appearance of Grade 0 placenta

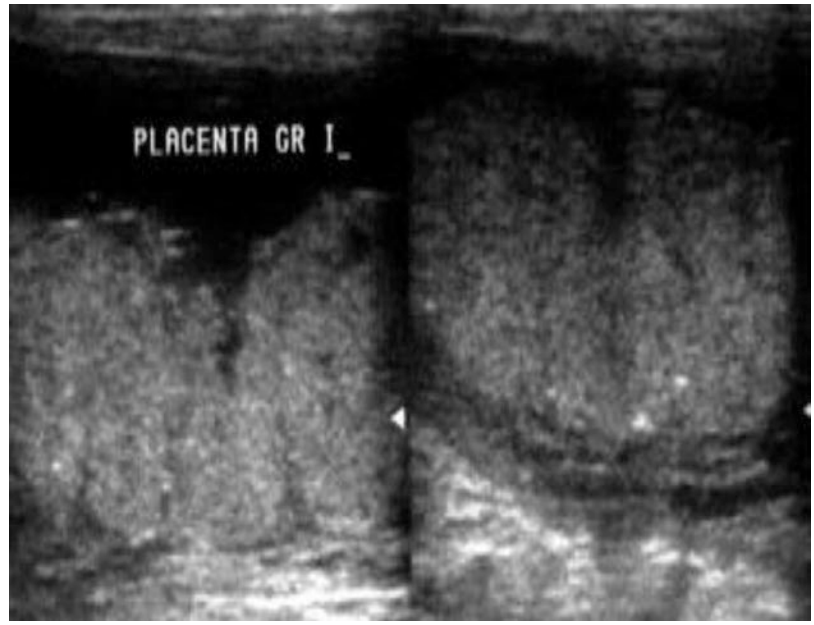

Fig. 4.36 Grade I posterior placenta

Normal umbilical cord is coiled (Figs. 4.41 and 4.42).

Umbilical cord index (normal values 0.13–0.21) is calculated 1/distance in centimetres between a pair of coils, i.e. intercoil distance of the cord [40]. Uncoiled or hypocoiled umbilical arteries (Figs. 4.43 and 4.44) are associated with increased foetal morbidity including small-for-gestational-age foetuses [41].

The insertion of cord is usually central in the placenta (Fig. 4.45). However, it may be in eccentric location (Battledore placenta) and have no clinical significance.

Cord around neck: A single loop near the foetal neck is not associated with foetal morbidity or mortality (Fig. 4.46). However, two or more tight loops around the foetal neck in sagittal or axial images are associated with foetal mortality.

Umbilical cord presentation may occasionally be encountered (Fig. 4.47).

Uterine rupture is a recognised complication of vaginal birth after caesarean section.

(VBAC). The scar thickness cut-off used was 3.5 cm by Rosenberg [42]. Bujold [43] found increased chances of uterine rupture (21.8 times

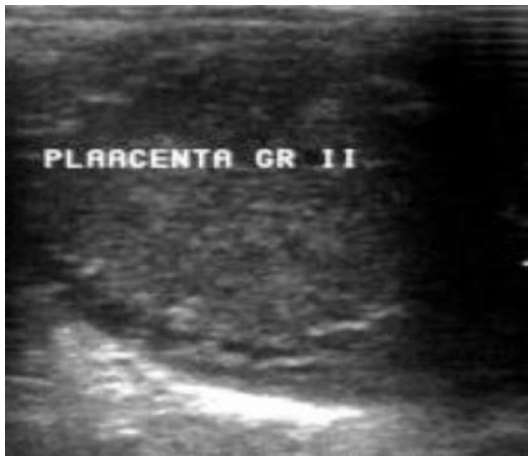

Fig. 4.37 Grade II placental maturity

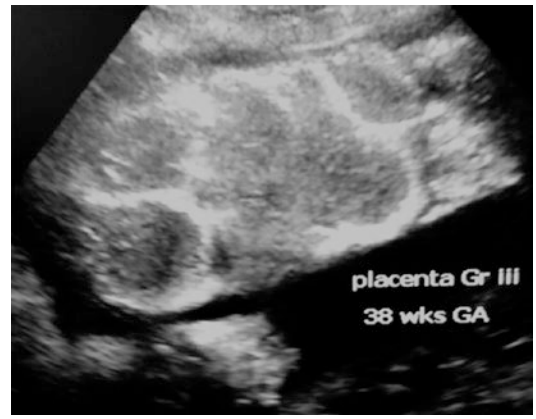

Fig. 4.38 Placental maturation Grade III

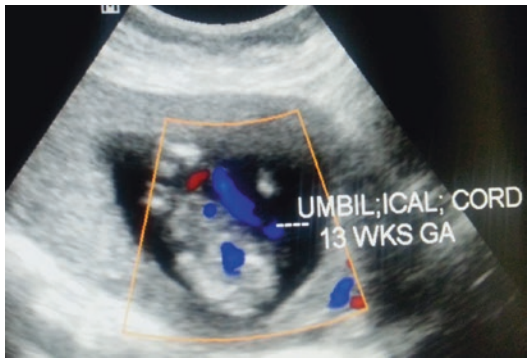

Fig. 4.39 Visualisation of umbilical cord in 10–12 weeks of pregnancy

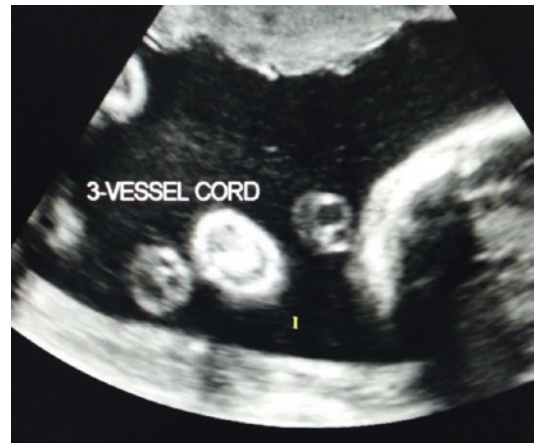

Fig. 4.40 Normal triple vessel umbilical cord

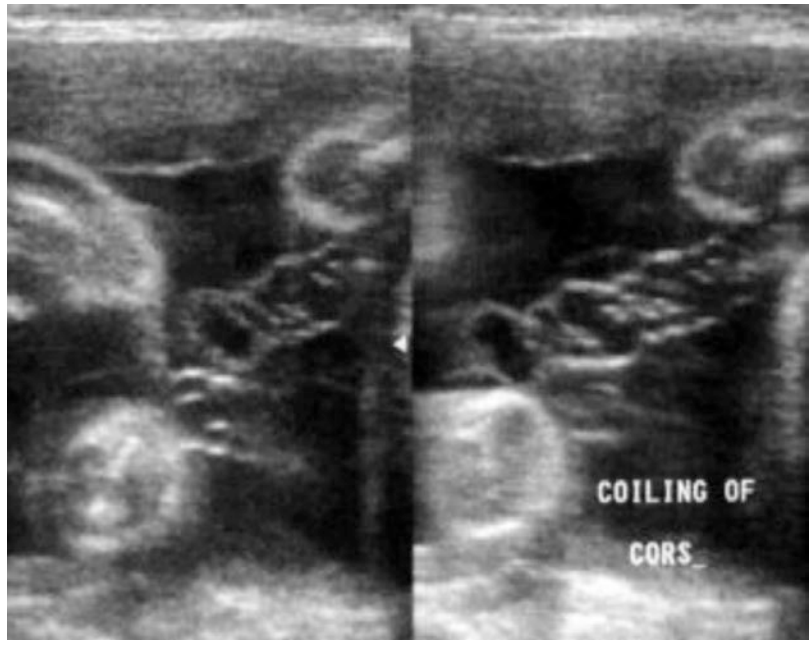

Fig. 4.41 Normal coiling of umbilical cord

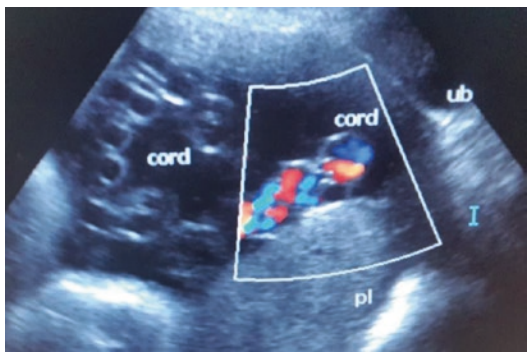

Fig. 4.42 Normal coiling of umbilical cord after 28 weeks' gestation

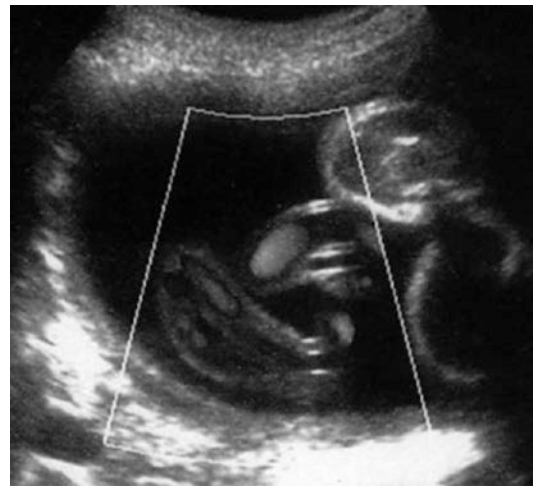

Fig. 4.43 Absence of coiling in cord is common before 26–28 weeks' gestation

the risk) in patients having a scar thickness less than 2.3 mm and a single-layer repair.

A 5 MHz linear probe is used for measurement of normal scar thickness (Figs. 4.48 and 4.49). A bulge in LSCS scar (Fig. 4.50) or layering effect in the scar needs caution [44].

Gretchen Humphries, Director of International Caesarean Awareness Network, advised that *caution should remain the byword in the use of ultrasound to predict the risk of uterine rupture* to avoid misuse of LSCS scar thickness to manage risk in women with a prior caesarean.

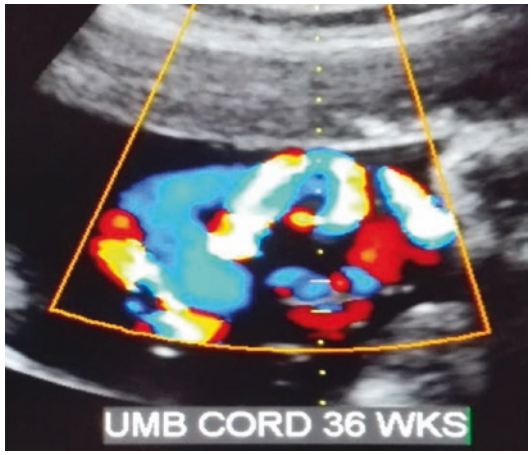

Fig. 4.44 Hypocoiled cord in 36 weeks of pregnancy with IUGR

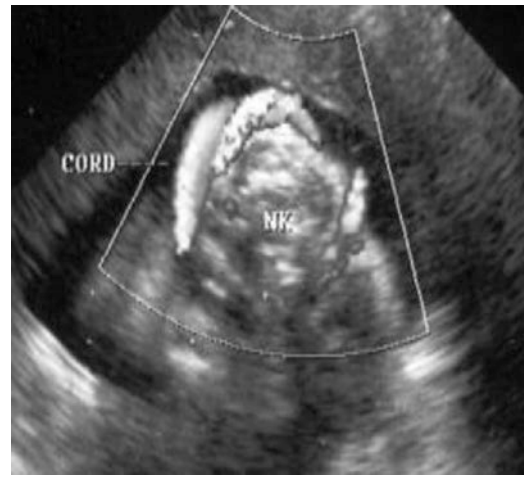

Fig. 4.46 Cord around foetal neck

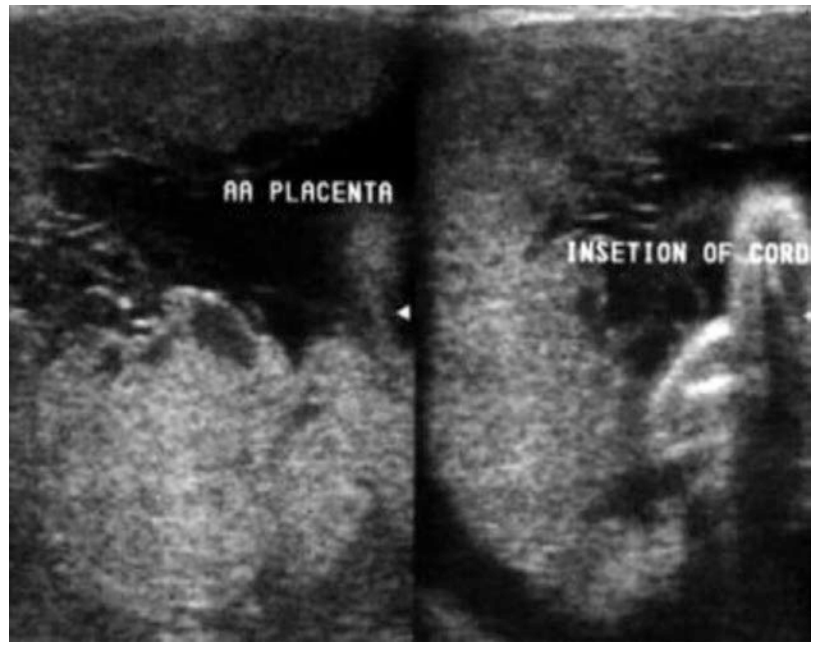

Fig. 4.45 Central insertion of cord onto placenta

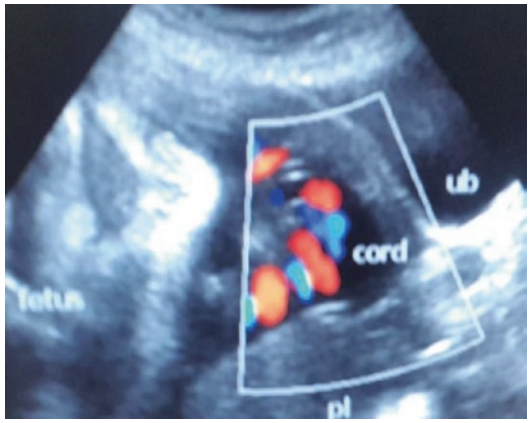

Fig. 4.47 Cord presentation in the third trimester of pregnancy

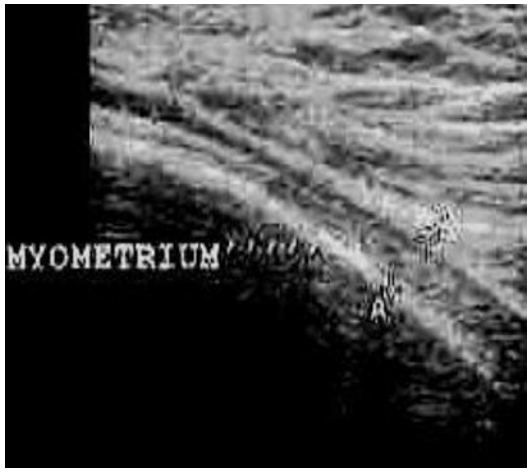

Fig. 4.48 Normal thickness of scar in post-caesarean pregnancy at 35–36 weeks' gestation

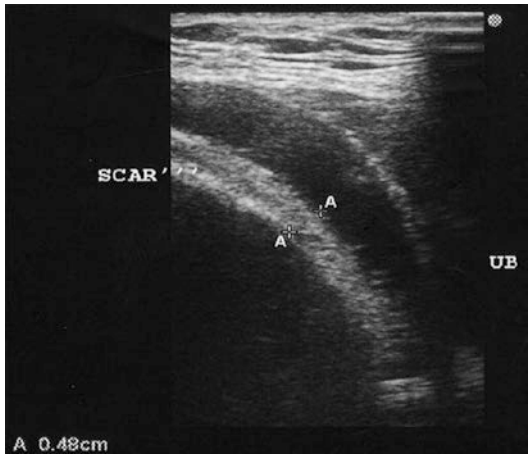

Fig. 4.49 Normal thickness of LSCS scar

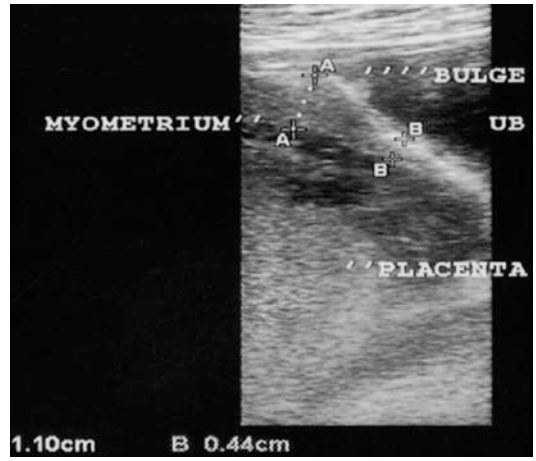

Fig. 4.50 Thinning of lowermost portion with a bulge in upper portion of LSCS scar in 36 weeks' pregnancy

4.3 Amniotic Fluid

The amniotic fluid volume (AFV) depends on the balance between its production and removal [45].

The presence of normal AFV in the second and third trimester implies that at least one functioning kidney must be present. The removal of amniotic fluid throughout pregnancy is largely a result of foetal swallowing. At term the foetus may swallow as much as 50% of the total AFV. Foetal urine production is 7–17 mL/day at 18 weeks' GA [46] and 600–1200 mL/day at term [47]. The AFV increases until about 30 weeks of gestation and then appears to decline.

Amniotic fluid index (AFI) [48] is determined by dividing the uterus into four equal quadrants. The vertical depth of the largest amniotic fluid pocket in millimetres is measured in each quadrant to find out the average of the four measurements.

Another method is to take vertical measurement of the largest amniotic fluid pocket (mean vertical pocket/MVP) as is used in foetal biophysical profile score. MVP of less than 1–2 cm and two diameter pockets of less than 15 cm^2 and AFI of less than 5 cm suggest oligohydramnios [49].

Assessment of amniotic fluid is summarised in Table 4.4.

Oligohydramnios is defined as obvious lack of amniotic fluid, i.e. less than 300–500 mL. Foetal body surface is in close proximity to the placenta

Table 4.4 Assessment of amniotic fluid

Index	Normal (cm)	Low (oligohydramnios) (cm)	High (polyhydramnios) (cm)
AFI (28–36 weeks)	15	<5–6	>20–24
AFI (36–40 weeks)	8–18	5–8	>18
MVP	5–8	1–2	>8

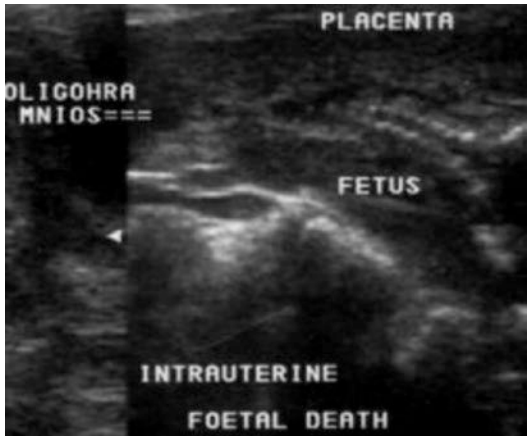

Fig. 4.51 Foetal spine in close proximity to placental margin in oligohydramnios

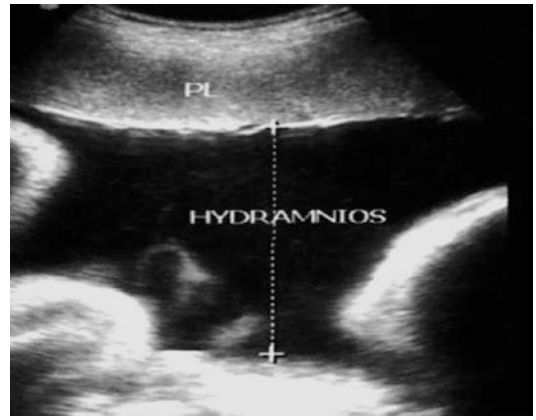

Fig. 4.53 Maximum vertical pocket (MVP) in polyhydramnios

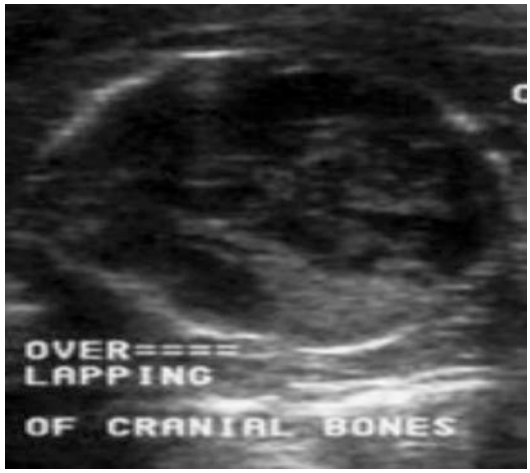

Fig. 4.52 Spalding's sign in foetal death and the presence of oligohydramnios

or uterine wall with hardly any amniotic fluid in between them, resulting sometimes into deformity of foetal parts (Figs. 4.51 and 4.52).

Polyhydramnios is defined as amniotic fluid more than 1500–2000 mL [45]. In this situation, excessive foetal movements may make interrogation of an organ or structure difficult. Also, placental thickness may be reduced. AFI of greater than 24 cm and the deepest pocket greater than 8 cm suggest polyhydramnios (Fig. 4.53) [50].

Amnioreduction (therapeutic amniocentesis) is done to reduce abdominal pain, PROM and preterm delivery to improve perinatal outcome [51].

Post-term pregnancy is defined as the one lasting for more than 294 days (42 weeks). The oligohydramnios is the result of the aging of maternal-placental-foetal unit, dehydration of foetus, diminished oxygen supply to the foetus (hypoxia) and deterioration of foetal cardiac function due to decreased FHR variation.

The presence of echogenic foci of 5–7 mm size slightly curved in shape moving with foetal movements is due to vernix (Fig. 4.54). It is a normal occurrence in near-term pregnancy [52].

Meconium peritonitis: In utero bowel perforation results in a sterile chemical peritonitis. The USG findings include bowel dilatation, ascites, meconium pseudocyst and polyhydramnios [53]. The ascites frequently has echogenic debris [54]. Calcification in the peritoneal cavity is detected 8 days after meconium has escaped into the peritoneal cavity [55].

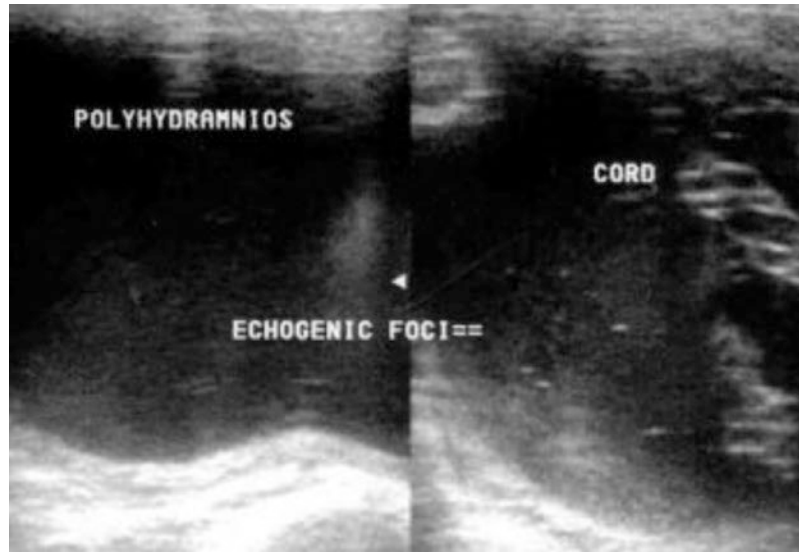

Fig. 4.54 Echogenic foci in amniotic fluid in near-term pregnancy

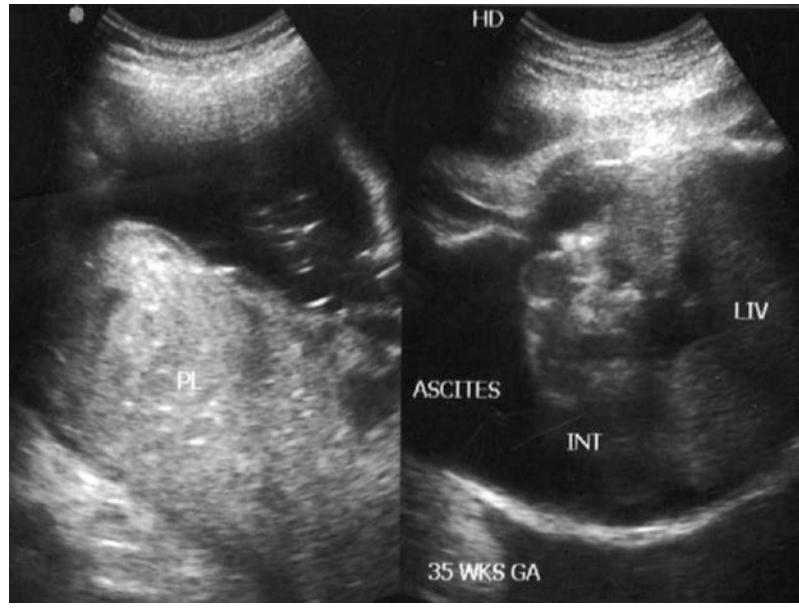

Fig. 4.55 Ascites in foetal abdomen with floating bowel loops in Rh sensitisation

Hydrops fetalis [56] is described as an abnormal interstitial accumulation of fluid in body cavities (pleural, pericardial and peritoneal), ascites, subcutaneous oedema and placental oedema (placental thickness > 5 cm). Immune hydrops fetalis results from Rh incompatibility.

The term non-immune hydrops fetalis (NIHF) is used if there is no evidence of blood group incompatibility (Fig. 4.55). To diagnose NIHF, fluid accumulation in at least two foetal sites or a single serous effusion and anasarca should be detected. The causes of NIHF are numerous.

The sonography in the second trimester of pregnancy is summarised in Table 4.5.

Table 4.5 Sonography in the second trimester of pregnancy

Growth parameter	Sonographic criteria
BPD	1. Plane that passes through the thalami and third ventricle 2. Bilaterally symmetrical and smooth calvaria with cursor at the middle of calvarial wall
HC	Same as for BPD but should include cavum septum pellucid anteriorly and tentorial hiatus posteriorly The entire perimeter of calvaria need not to be demonstrated
Femur length	Measure only the ossified portion of the diaphysis and metaphysis in the same plane, exclude cartilaginous ends
AC	At the plane where the right and left portal veins are continuous with one another or at a plane where the AP and transverse diameter of abdomen are equal
Placenta	Definite placenta seen after 10–12 weeks Placental thickness in mm equal to GA in weeks +10 mm Term placenta 4 cm in thickness Thin placenta is a marker for growth restriction Placenta haematoma causing 30–40% placenta away from myometrium has clinical significance. Low-lying placenta: placental edge within 2 cm of internal os but not covering it
Umbilical cord	Can be seen after 8 weeks' GA Diameter is less than 2 cm, 3-vessel cord, single loop of cord around neck is an incidental finding Eccentric insertion of cord into placenta has no clinical significance
Amniotic fluid	Umbilical cord filled with amniotic fluid pocket should not be used for assessment of AFV MVP 3–5 cm normal AFI 5–8 cm normal
Oligohydramnios	MVP of less than 1–2 cm, 2 diameter pocket of less than 15 cm^2, AFI less than 5 cm
Polyhydramnios	MVP >8 cm AFI > 24 cm
Inter-twin membrane	Seen by tenth week Thickness 1–2 mm "Twin peak" sign in dichorionic gestation Twins usually have birth weight < 2500 g
IUGR	Foetal weight below tenth percentile AC less than tenth percentile HC, AC ratio > 2 standard deviation Birth weight < 2.5 kg No increase in AC or HC performed at 2 weeks' interval
Doppler criteria for IUGR	Uterine arcuate artery RI >0.58 S/D ratio > 95th percentile PI >2 SD above mean

4.4 The Foetal Biophysical Profile

The non-stress test (NST) and the contraction stress test (CST) have limited value in detecting unhealthy (asphyxiated) foetus.

The foetal biophysical profile is used to evaluate foetal well-being to distinguish between the healthy (non-asphyxiated) and unhealthy (asphyxiated) foetus (Table 4.6).

The normal BPS of 8–10 is associated with perinatal mortality of 1 per thousand, and abnormal score of 0–4 may have perinatal mortality of 200 per thousand.

In abnormal foetal growth, sonography should be repeated every 2 weeks.

From: Intrauterine Growth Retardation. Robert C. Vandenbosche and Jeffrey T. Kirchner, Am Fam Physician. 1998 Oct 15;58(6):1384–1390. [1] "*Archived copy*" (PDF). Archived from *the original* (PDF) on 2013–05-13. *Retrieved 2012–08-02* [58]

Table 4.6 Foetal biophysical profile scoring

Variable	Score 2	Score 0
Foetal breathing movements	Presence of at least 30 s of sustained foetal breathing movements in 30 min	Less than 30 s of foetal breathing movements in 30 min
Foetal movements	Three or more gross body movements in 30 min	Two or less gross body movements in 30 min
Foetal tone	At least one episode of motion of a limb from a position of flexion to extension and rapid return to flexion	Foetus in a position of semi- or full-limb extension with no return to flexion/ absence of foetal movements
Foetal reactivity	Presence of two or more FHR accelerations of at least 15 beats/min and lasting at least 15 s and associated with foetal movements in 40 min	No acceleration or less than two accelerations of the foetal heart rate in 40 min
Qualitative amniotic fluid volume	A pocket of amniotic fluid that measures at least 1 cm in two perpendicular planes	Largest pocket of amniotic fluid <1 cm in two perpendicular planes

Table V: From: Manning FA, Platt LD, Sipos L: Antepartum Foetal evaluation. Development of a foetal biophysical profile score. Am J Obstet Gynaecol 136:787,1980 [57]

Table 4.7 Recommended management based on the biophysical profile

BPP	Recommended management
<2	• Labour induction
4	• Labour induction if gestational age >32 weeks • Repeating test same day if <32 weeks, then delivery if BPP <6
6	• Labour induction GA >36 weeks if favourable cervix and normal AFI • Repeating test in 24 h if <36 weeks and cervix unfavourable; then delivery if BPP <6, and follow-up if >6
8	• Labour induction if presence of oligohydramnios

Table 4.8 Growth of interocular distance (mm) in percentile

Age (weeks)	5th	50th	95th
16	6	10	15
18	7	11	16
20	8	12	17
22	9	13	18
24	10	14	19
26	11	15	20
28	12	16	21
30	13	17	22
32	14	18	23
34	15	19	24
36	16	20	25
38	17	21	26
40	18	22	26

From: Romero R, Pilu G, Jeanty P et al. Prenatal Diagnosis of Congenital Anomalis. Norwalk,CT, Appleton and Lange,1988 p 83 [82]

4.4.1 Intrauterine Growth Restriction

IUGR and macrosomia are associated with increased risk for perinatal morbidity and mortality; therefore its prenatal diagnosis can aid in decision-making for the timing and route of delivery to reduce perinatal risk.

IUGR (small for gestation age/SGA) is defined as foetal weight below tenth percentile for GA [59]. The other parameters used are abnormal biophysical profile or abnormal Doppler waveform of the umbilical artery.

IUGR can be of two types:

1. Symmetric IUGR where all body parts are decreased in size, i.e. all growth parameters are smaller.
2. Asymmetric IUGR (sparing the foetal head) where the foetal abdomen is small resulting in HC/AC ratio to persist above 1 beyond 35–36 weeks' GA. This is more commonly seen in cases of placental insufficiency.

The GA assessment at initial USG becomes important to diagnose IUGR at a later date and to find out interval growth. Diagnosis of IUGR may be erroneous if it is done on the basis of USG done for the first time in the late second trimester or third

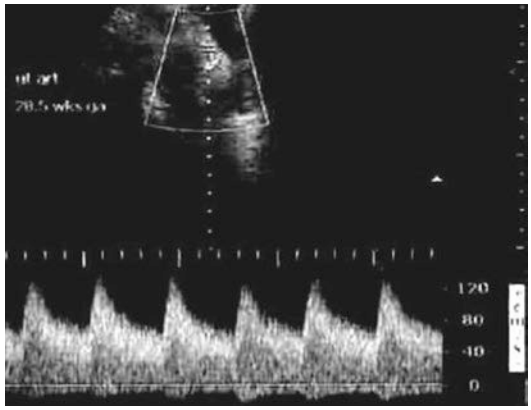

Fig. 4.56 Normal uterine Doppler waveform with good diastolic flow in 28.5 weeks' pregnancy

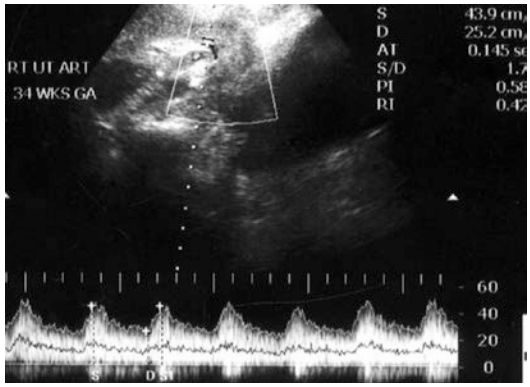

Fig. 4.57 Normal uterine artery waveform with PI of 0.58 and RI of 0.42 in 34 weeks' pregnancy

trimester pregnancy. GA should be assigned at the time of first sonogram during pregnancy [60].

The presence of oligohydramnios and advanced placental grade may be helpful for the diagnosis of IUGR. *In general, Doppler criteria are not as good as non-Doppler US criteria for IUGR* [59, 60].

No single sonographic criteria permit confident diagnosis of IUGR. The criteria used include weight below the tenth percentile for gestational age, elevated HC/AC ratio, elevated FL/AC ratio, presence of oligohydramnios without rupture of membranes, presence of advanced placental grade and others.

Normal uterine waveform in 29 weeks' GA (Fig. 4.56) and at 34 weeks' GA (Fig. 4.57) with good diastolic flow and normal RI and PI are helpful excluding possible IUGR.

Doppler criteria for diagnosis of IUGR [61] include >0.58 RI in uterine artery; S/D ratio > 3, absent or reverse diastolic flow in umbilical artery; and umbilical vein flow < tenth percentile.

IUGR can be diagnosed most accurately using a combination of three parameters: estimated weight percentile, amniotic fluid volume and maternal blood pressure status (normotensive versus hypertensive) [62].

Growth-restricted foetuses have a four- to eightfold increased risk for perinatal mortality compared with appropriate-sized foetus [63].

The role of colour Doppler imaging of the uterine arteries at 20 weeks' gestation in stratifying antenatal care has been described by Kurdi et al. [64] as follows:

- Uterine arteries RI > 0.55 + bilateral notches = preeclampsia, SGA, any complication
- UA RI > 0.65 + unilateral notch = preeclampsia, SGA, any complication
- UA RI >0.7 + no notches = preeclampsia, SGA, any complication

Macrosomia: The term is applied to foetus having body weight more than 4000 g or weight above the 90th percentile for gestational age. Antenatal sonographic diagnosis can prompt caesarean section preventing complications such as shoulder dystocia, soft tissue trauma and fracture of humerus or skull, brachial plexus and facial palsies, meconium aspiration, prolonged labour and asphyxia injuries. Perinatal mortality is elevated in these foetuses [65].

4.5 Ultrasound Evaluation of Normal Foetal Anatomy

Ultrasound evaluation of foetal anatomy has undergone a transformation in the past few decades. To examine every patient for all anomalies would be highly impractical; a targeted examination by large is possible for anomaly detection. A scan at 14–16 weeks followed by a scan at 22–24 weeks' gestation is considered ideal. It is recommended that if a single ultrasound or a targeted (level 2) examination is performed, it should be done at a gestational age of

19–20 weeks. High-resolution real-time scanners with their flexible approach to imaging are mandatory for modern foetal sonography [66].

The evaluation of foetal anatomy by real-time sonographic system enables the sonographer to perform a quick survey of the foetus in different planes. The foetal position, maternal body habitus and the amount of amniotic fluid may limit the ability to see foetal anatomy; still a large number of foetal structures are visible in sonography [67, 68].

Nowadays targeted foetal anatomy scan is in practice, but ultrasound study of foetal anatomy is the integral part of the routine second trimester obstetric sonography. A sonologist with gradually improved understanding of foetal anatomy and availability of multi-frequency transducer has led to improved foetal imaging by transabdominal transducer in foetuses beyond 14 weeks. Three-dimensional imaging (3D) depends on "volume imaging". The data from the volume of tissue is gathered in the processing computer, and from this, 3D images are generated. 3D images of the foetal face can pick up various abnormalities of foetal face, lip and palate [69] (Figs. 4.58, 4.59, 4.60 and 4.61).

A systematic approach to evaluate foetal anatomy should be used from the foetal skull, brain including cerebral ventricles, midline structures (Figs. 4.58 and 4.60), posterior fossa and cisterna magna (Fig. 4.59), Circle of Willis (Fig. 4.61), foetal spine from neck to sacrum, foetal thorax, foetal abdomen, lower limbs, upper limbs and anterior abdominal wall. Since it will not be possible to describe detection of all the abnormali-

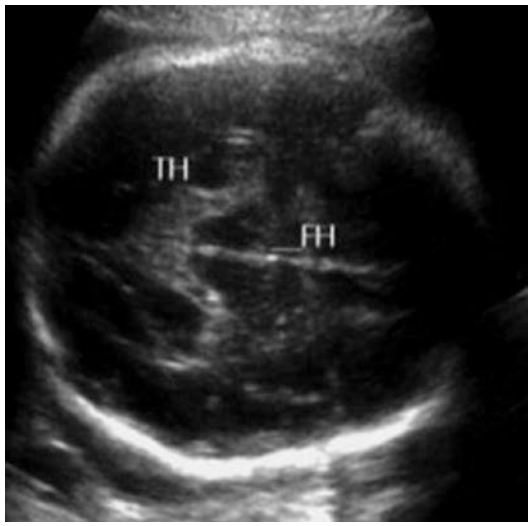

Fig. 4.58 Normal midline echo of falx with frontal horns on sides

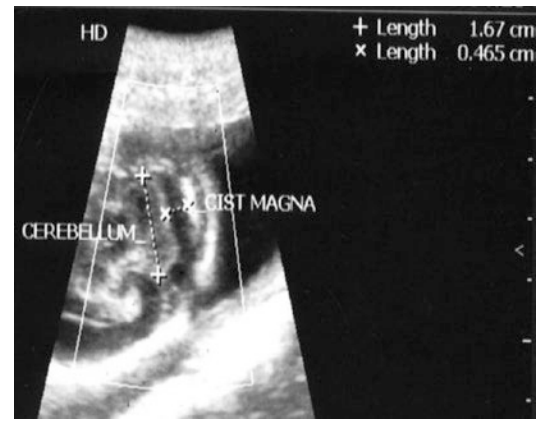

Fig. 4.59 Depth measurement of normal cisterna magna (0.46 cm) and transverse diameter of cerebellum (1.67 cm)

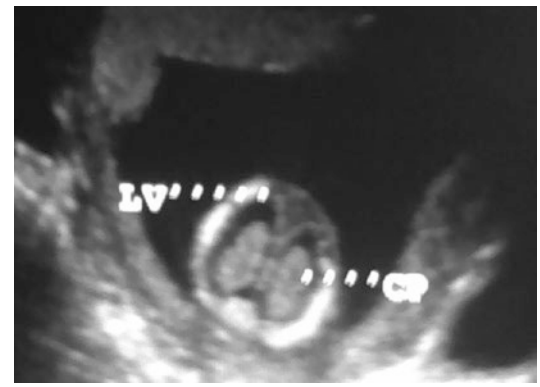

Fig. 4.60 Lateral ventricle filled with choroid plexus in early pregnancy

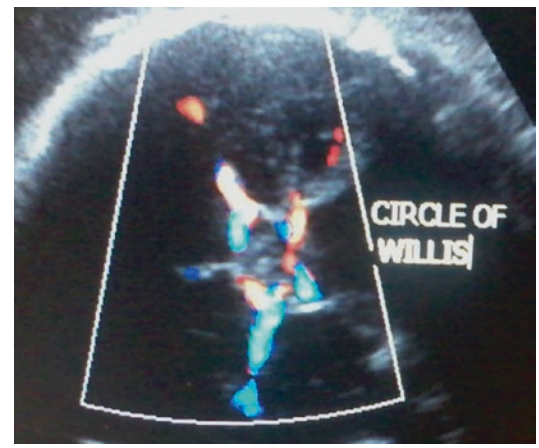

Fig. 4.61 Circle of Willis in colour flow mapping

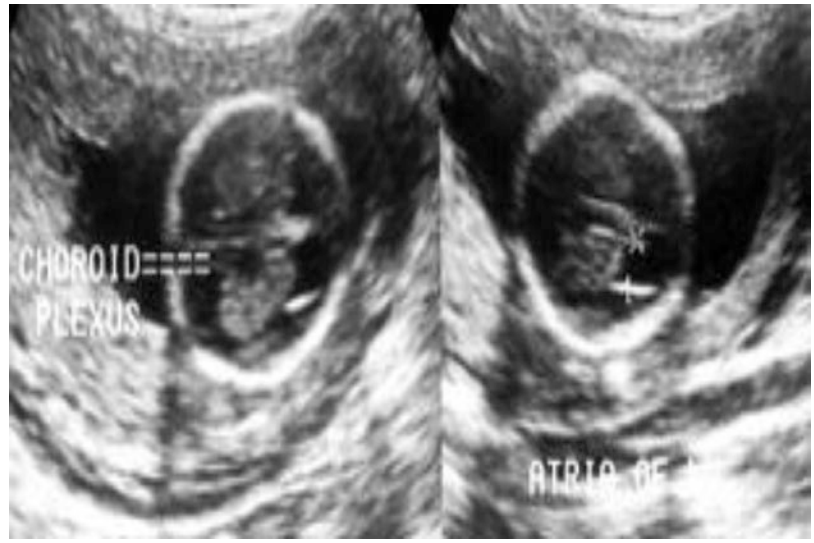

Fig. 4.62 Measurement of width of atria of left ventricle

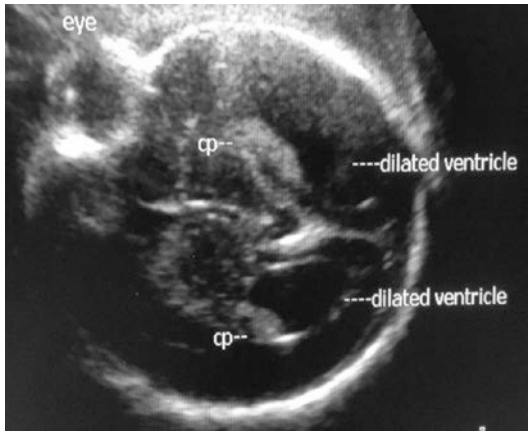

Fig. 4.63 Mild bilateral ventriculomegaly in the second trimester of pregnancy

ties and foetal syndromes here, only a few of them which should be picked up by basic ultrasonography work will be included.

The CNS is probably the first organ system investigated in utero by diagnostic ultrasound because CNS anomalies are frequent and often have a severe prognosis. Coronal and sagittal views in targeted examination become necessary for proper evaluation of the midline structures and to assess the symmetry of the two hemispheres.

The transverse diameter of the ventricular atrium at the level of the glomus of the choroid plexus measuring more than 10 mm suggests ventricular enlargement (ventriculomegaly) [70]. Mild unilateral ventriculomegaly is suggested to be a benign finding. Infants with isolated mild ventriculomegaly are at increased risk for developmental delay. Hydrocephalus is defined on the basis of an atrial width of more than 15 mm in the second and third trimester (Fig. 4.62). Markedly dilated venricles (Hydrocephalus) poses no problem in diagnosis (Figs. 4.63 and 4.64) [38].

Anencephaly is seen as an absence of the cranial vault. Necrotic remnants of the brain stem are covered by a vascular membrane (Fig. 4.65) [71]. Commonly associated abnormalities are spina bifida, cleft lip/palate, clubfoot and omphalocele. Polyhydramnios is frequently present. Frog's eye view or "Mickey Mouse sign" is the appearance described in anencephaly (Fig. 4.66) [71].

Microcephaly should not be considered as a single clinical entity but rather as a symptom of many etiologic disturbances [72].

Many difficulties arise in the identification of microcephaly [73]. Only the head measurement is incorrect. A comparison of HC/AC ratio and FL/BPD ratio has false-positive and false-negative diagnoses, and the small head size does not necessarily mean mental retardation. Large subarachnoid spaces and a rudimentary shape of the lateral ventricles in foetuses beyond 20 weeks are suggested to diagnose undersized cerebral hemispheres.

The nasal bone is absent at 11 weeks. Therefore, scan should be repeated in 1 week. The nasal bone is seen as distinct three lines in a

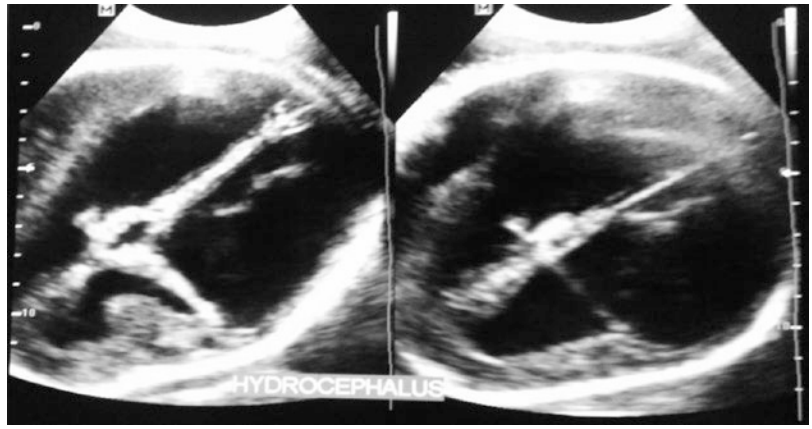

Fig. 4.64 Marked hydrocephalus in near-term pregnancy with thin rim of cortex

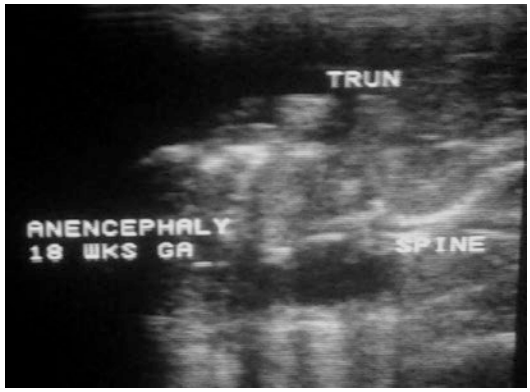

Fig. 4.65 Anencephaly in pregnancy of 18 weeks' gestation

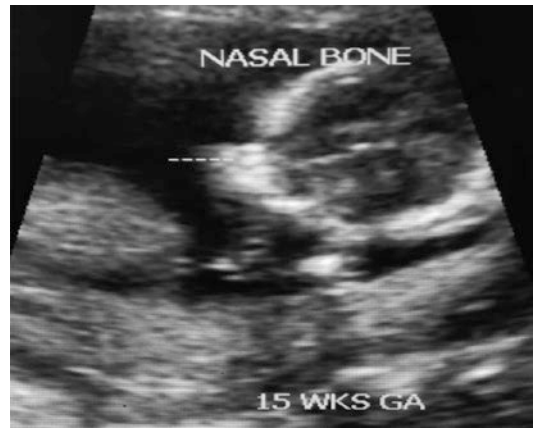

Fig. 4.67 Normal nasal bone

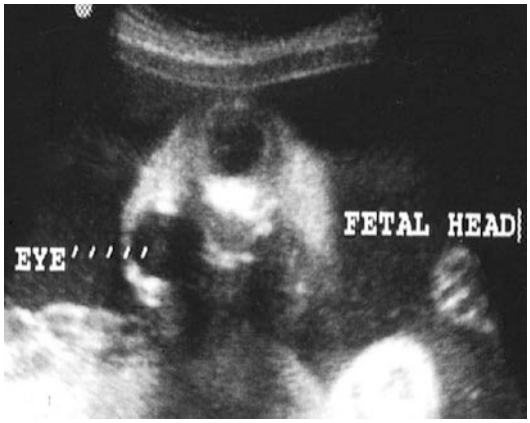

Fig. 4.66 Frog's eye sign in anencephaly in the second trimester of pregnancy

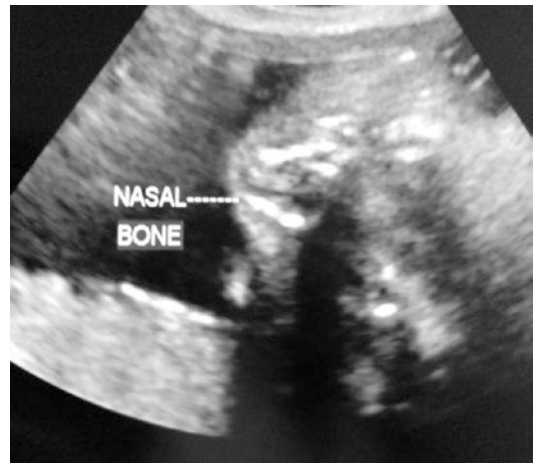

Fig. 4.68 Nasal bone in near term pregnancy

midsagittal view of the face (Fig. 4.67). The 90 degree angle between the hard palate and outer surface of frontal bone is considered to be normal (Fig. 4.68). The skin fold thickness over nasal bone (Fig. 4.69) 2.4 mm at 16 weeks and 4.6 mm at 24 weeks gestation is normal. Presence of lens within eye globe rules out aphakia (Fig. 4.70).

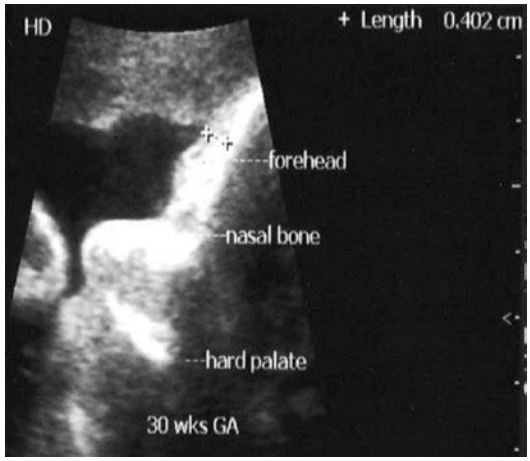

Fig. 4.69 Skin fold thickness over forehead and nasal bone

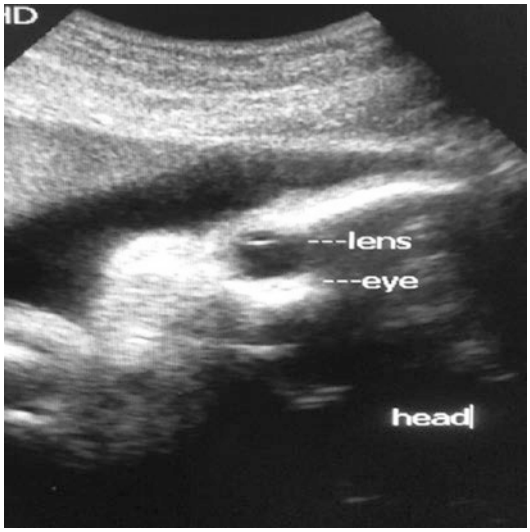

Fig. 4.70 Presence of lens in eye globe

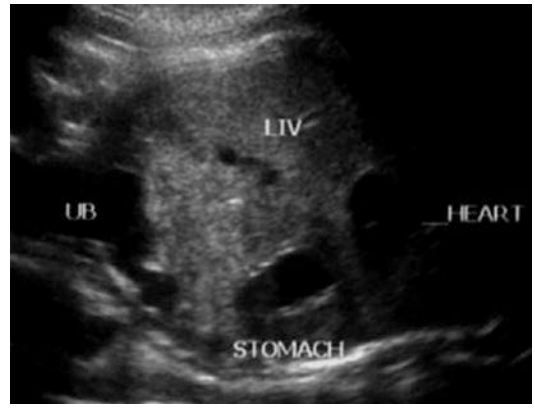

Fig. 4.71 Foetal urinary bladder (UB), liver (Liv), stomach and heart

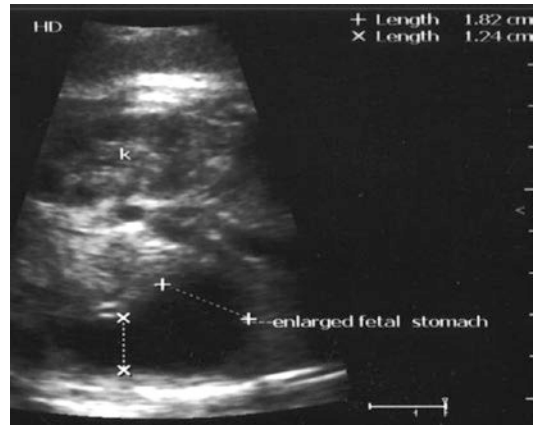

Fig. 4.72 Gastric dimension of 1.8 cm suggests enlargement of stomach

Stomach, liver, gall bladder and urinary bladder are visualized in foetal abdomen (Fig. 4.71). Usually one kidney is visualized in sonography (Fig. 4.75). Foetal stomach varies in size; therefore, a prominent stomach should not be mistaken for obstruction (Fig. 4.73) [74]. If there is persistent nonvisualisation of stomach after 19 weeks' gestation, oesophageal atresia should be the first diagnosis for consideration.

Gastric outlet obstruction is associated with enlarged stomach (Figs. 4.72 and 4.73) and polyhydramnios which may be seen as early as 22 weeks' gestation [75]. However, in duodenal atresia or stenosis, the double bubble sign gives the clue for diagnosis [76].

In the late second and early third trimester, the bowel loops can be seen (Fig. 4.74). They are more easily visualised when they are dilated.

Echogenic bowel is associated with a high incidence of poor perinatal outcome and an increased risk of IUGR, prematurity and foetal demise [77]. One should keep in view that high-frequency transducer of ultrasound equipment may accentuate the echogenicity of the foetal bowel (Fig. 4.76). Echogenic bowel is divided into two grades: grade I, echogenicity of small bowel is more than liver (Fig. 4.77) and grade II when it has the echogenicity equal to bone [78].

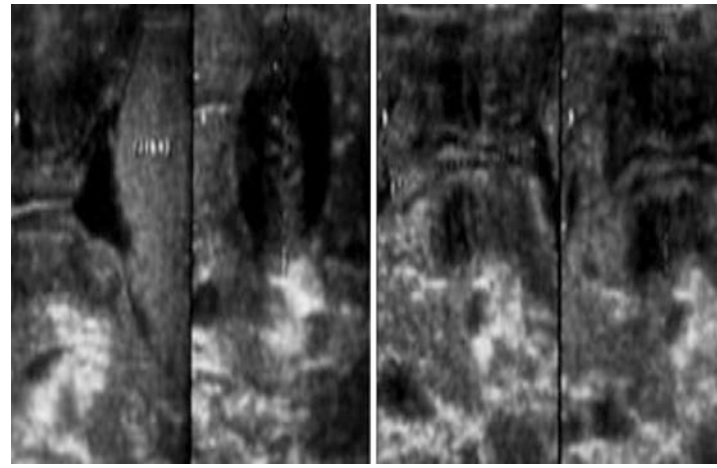

Fig. 4.73 Pyloric canal in hypertrophic pyloric stenosis

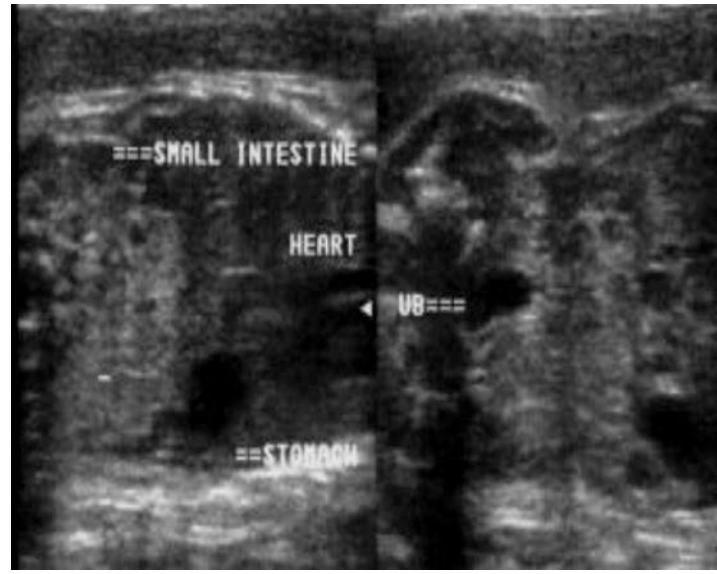

Fig. 4.74 Normal intestine is seen as a few ring shadows

In term pregnancy, mildly dilated intestinal loops containing echogenic fluid may be seen (Figs. 4.78 and 4.84). In the presence of foetal ascitesfloating bowel loops are clearly visualized (Fig. 4.79). In Rh-sensitization foetal ascites around liver is seen (Fig. 4.80). In meconium ileus, USG reveals echogenic second trimester small bowel, dilated fluid-filled loops of bowel and echogenic dilated bowel [79]. Foetal ascites and pericardial effusion are relatively easy to identify.

Foetal abdominal cystic mass (Fig. 4.81) may be difficult to differentiate from distended foetal urinary bladder (Fig. 4.82) in bladder outlet obstruction.

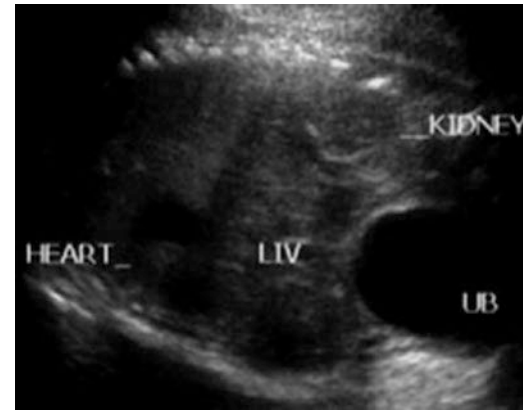

Fig. 4.75 Usually only one kidney can be seen in the foetal abdomen

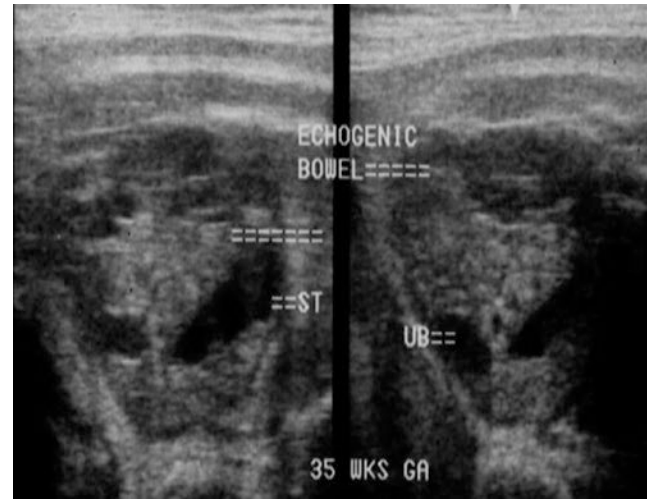

Fig. 4.76 Echogenic bowel in 35 weeks' pregnancy

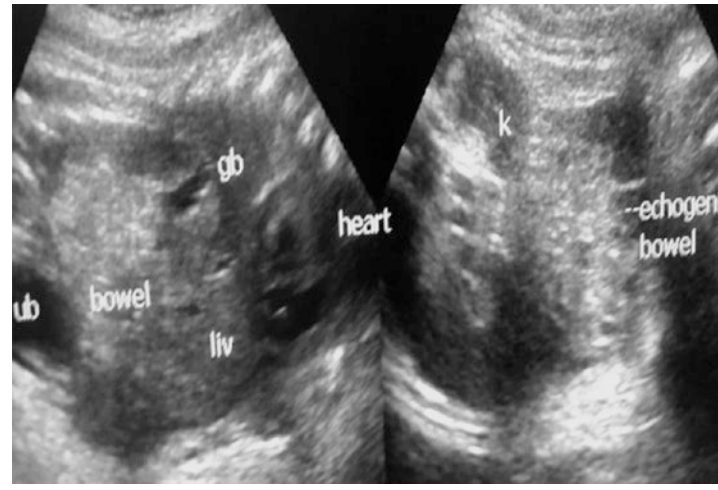

Fig. 4.77 Echogenic bowel grade I is seen between liver and UB

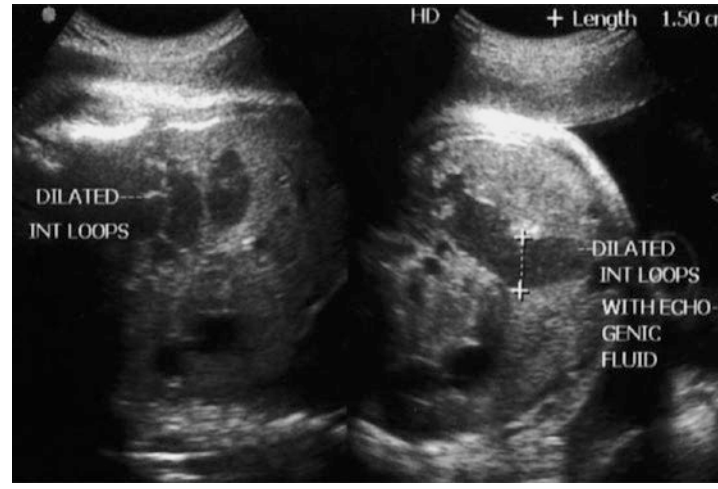

Fig. 4.78 Dilated intestinal loops containing echogenic fluid in near-term pregnancy

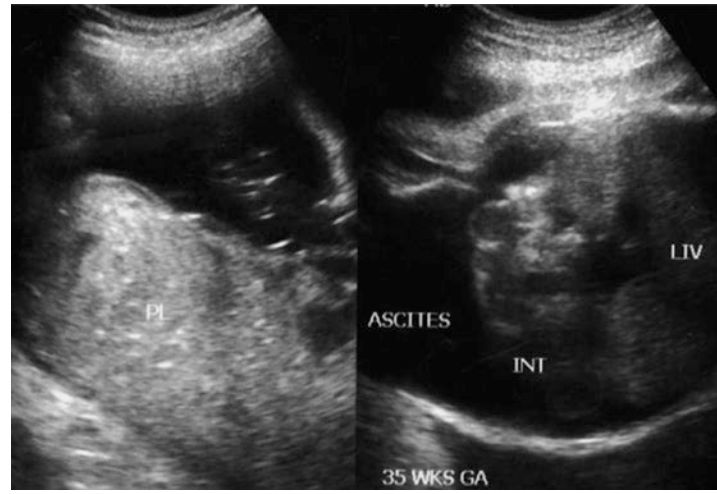

Fig. 4.79 Floating intestinal loops on top of foetal ascitic fluid

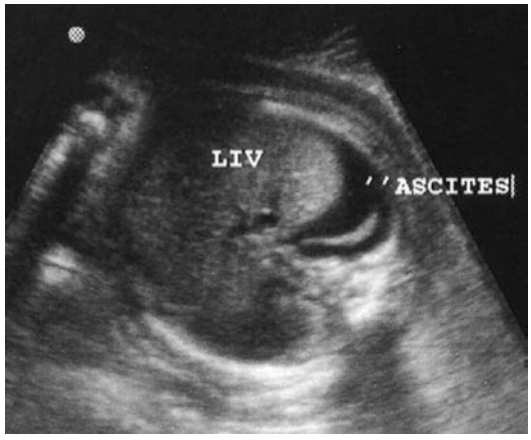

Fig. 4.80 Foetal ascites in a case of Rh sensitisation

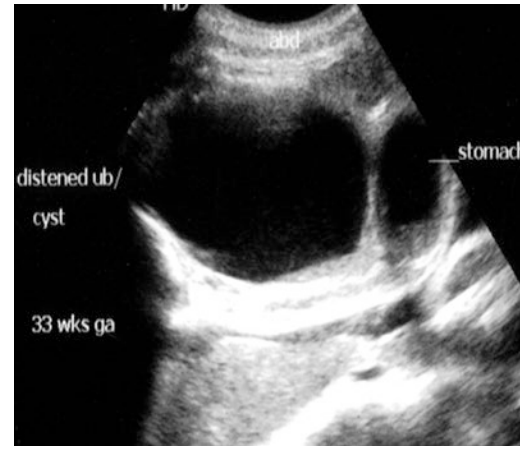

Fig. 4.82 Distended foetal UB in 33 weeks' pregnancy

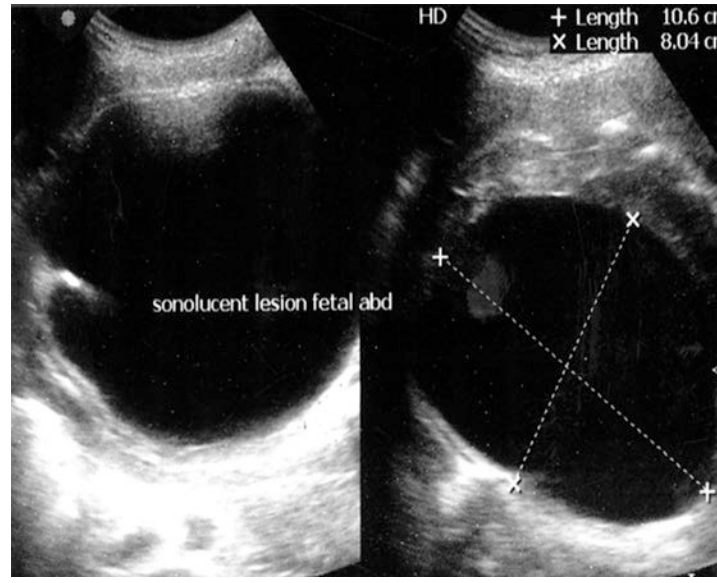

Fig. 4.81 A large cystic mass in foetal abdomen

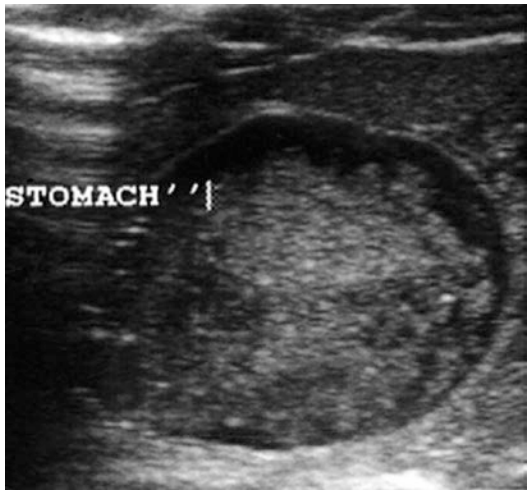

Fig. 4.83 Imaging of abdomen in newborn showing enlarged stomach containing echogenic milk in hypertrophic pyloric stenosis (same case shown in Fig. 4.72)

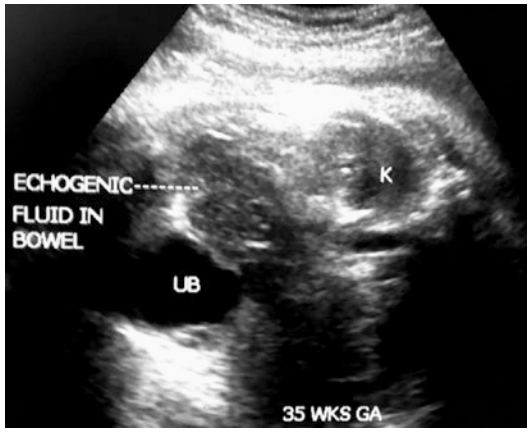

Fig. 4.84 Echogenic fluid in the bowel, newborn was normal

However, normal bladder on subsequent examination may reveal emptying.

Imaging of newborn abdomen (Fig. 4.83) with distended stomach containing echogenic milk in infantile pyloric senosis. Foetal spine is well seen from 15 to 16 weeks onwards. Two parallel lines (rail-track appearance) represent normal spine (Fig. 4.85). The spinal cord inside these two parallel lines can be seen as bright linear echo.

Familiarity with this appearance is very helpful to identify spina bifida and myelomeningocele. Spina bifida occulta is difficult to predict by USG. The lumbar, thoracolumbar and lumbosacral areas are most common sites. Meningocele is

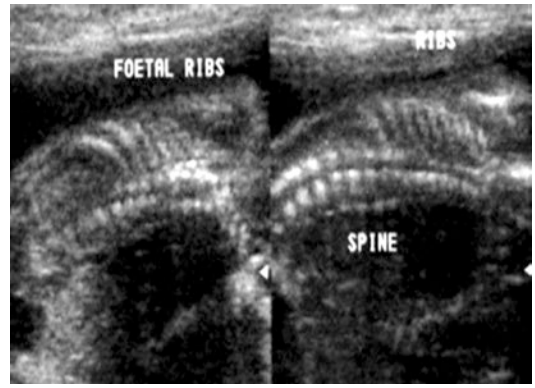

Fig. 4.85 Foetal spine and ribs

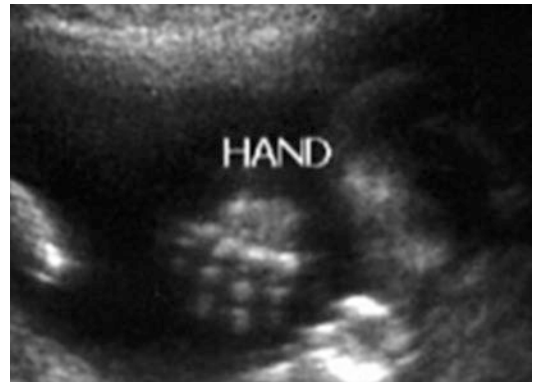

Fig. 4.86 Foetal hand with phalanges

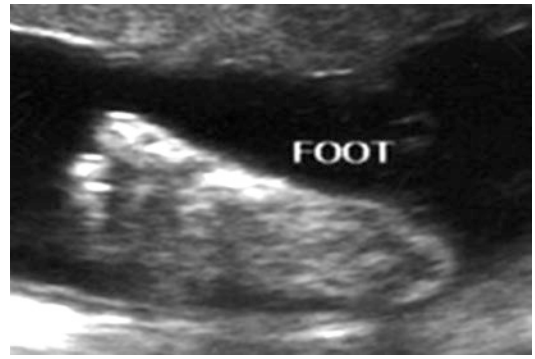

Fig. 4.87 Foetal foot

seen as thin-walled cyst in the soft tissue at the level of the defect.

Foetal hand malformations may be isolated or may be associated with a large number of abnormalities. The normal foetal hand is most often in a resting position with loosely curled fingers which the foetus periodically opens (Fig. 4.86) [80].

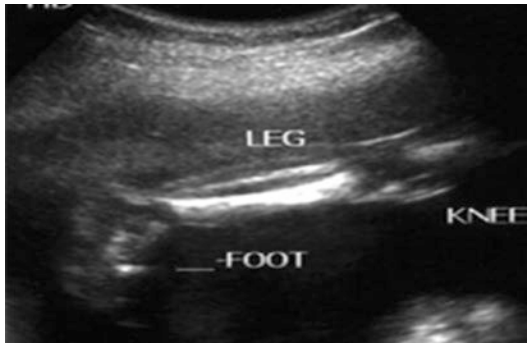

Fig. 4.88 Extended foetal leg and foot

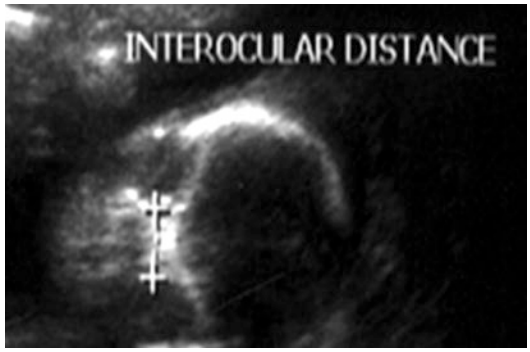

Fig. 4.89 Measurement of interocular distance

Occasionally foetal foot and digits may be seen during routine ultrasound examination (Fig. 4.87).

The perpendicular relationship of the lower leg bones and sole of the foot is helpful in prenatal diagnosis of clubfoot (Fig. 4.88) [81].

Interocular distance can be measured (Fig. 4.89), and if it falls below the fifth percentile for the expected GA, it is defined as hypotelorism. In hypertelorism, this distance is greater than 95th percentile (Table 4.8) [82].

Foetal anterior abdominal wall is considered to be present if any organ except the small bowel is seen outside the abdomen. The small bowel physiologic umbilical hernia is seen before 12 weeks' GA; after 12 weeks' GA, the small bowel returns into the abdomen.

Gastroschisis is a paraumbilical defect including all layers of the abdominal wall involving mostly the small bowel, but stomach or other organs may be involved.

Omphalocele (exomphalos) is a defect in the anterior abdominal wall with extrusion of abdominal contents into the base of the umbilical cord.

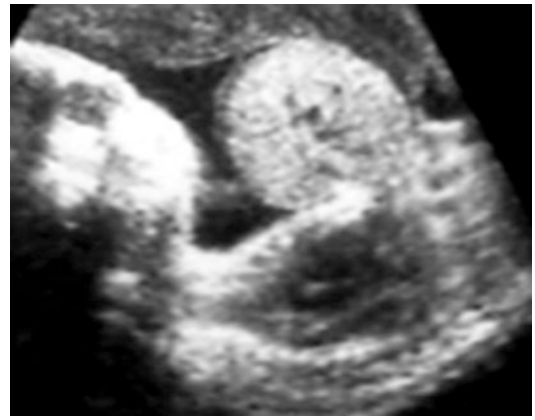

Fig. 4.90 Normal chorion should not to be confused with amniotic band

The liver may or may not be a part of the herniation (Fig. 4.90).

4.5.1 Foetal Limbs

Limb shortening in the second trimester should raise the suspicion of foetal abnormality. Mild humeral shortening (length < 90% of the predicted humeral length) is even more specific than femoral shortening in predicting trisomy 21. Detection of bone lengths measuring less than 2 SD (standard deviation) below the mean for gestational age indicates foetus at risk for skeletal dysplasia. The foetus is at risk for lethal skeletal dysplasia if limb shortening is greater than 4 SD below the mean [83].

Skeletal dysplasia is classified in terms of which portions of the limbs are shortened:

- Micromelia means shortening of all portions of a limb.
- Rhizomelia denotes shortening of the proximal limb namely humerus and femur.
- Mesomelia indicates shortening of the middle portion of the limb, i.e. forearm/lower leg bone.
- Acromelia is the shortening of the hand and foot bones.

Foetal foot length (FL) is approximately equal to the femur length throughout gestation. Foot length (FL) ratio is <0.9; skeletal dysplasia is possible.

Foetal liver and gallbladder can be visualised easily from 14 weeks onwards.

Foetal kidneys can be visualised persistently after 20 weeks. The expected normal size (length) of kidney is as follows: 2.6 cm at 20 weeks, 4 cm at 33 weeks and 4.5 cm at 41 weeks.

Mild pyelectasis or dilatation of renal pelvis is considered as evidence of hydronephrosis if AP diameter of pelvis is greater than 10 mm at or above 30 weeks, or the ratio of the AP diameter of pelvis to kidney is more than 0.5. A number of pathologies may result in the multicystic dysplastic kidney: adult and infantile polycystic disease. Enlarged kidneys with increased echogenicity, cysts and oligohydramnios are the usual findings seen in USG.

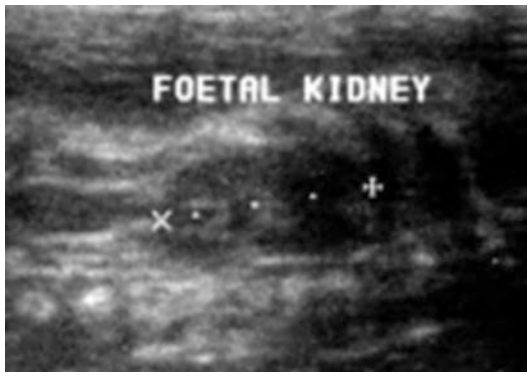

Fig. 4.91 Herniation of the liver through anterior abdominal wall defect (exomphalos)

Renal ectopia is a relatively common congenital anomaly. Common forms are pelvic and horseshoe kidneys. More often than not, only one kidney is visualised in ultrasonography. The visualisation of foetal urinary bladder rules out bilateral renal agenesis.

Amniotic band syndrome (ABS) [84] describes a wide range of abnormalities including minor constriction rings to complex and bizarre multiple congenital anomalies such as annular grooves, congenital amputation, cephaloceles, syndactyly, clubfoot, spinal scoliosis, ambiguous genitalia, etc. A more descriptive term of ADAM complex (amniotic deformities, adhesions and mutilation) is preferred to use in place of ABS. Chromosomal abnormalities have not been shown with ABS.

Four-chamber view (4 CH) of the heart is obtained (two-dimensional images), and the heart rate is calculated in M-mode by measuring the distance between the two peaks. The four-chamber view is easily obtained in most foetuses between 16 and 20 weeks (Fig. 4.97). Foetal echocardiography including the study of great vessels and outflow tracts (Figs. 4.98 and 4.99) in a low-risk population as well as in patients with a family history or maternal disease may be able

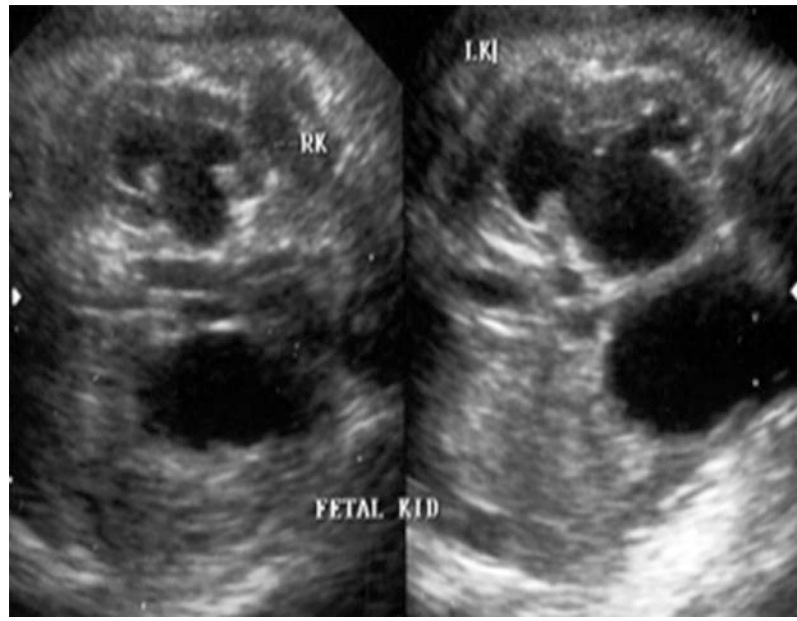

Fig. 4.92 Usually one kidney is seen in foetal anatomical survey

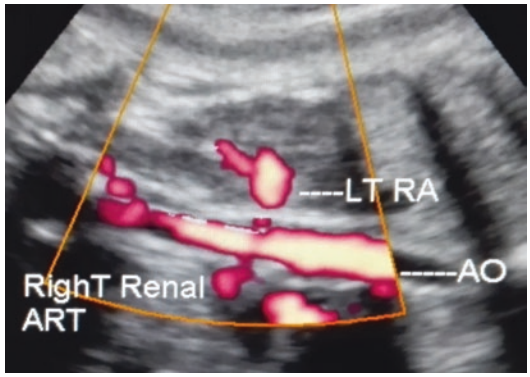

Fig. 4.93 Bilateral foetal hydronephrosis

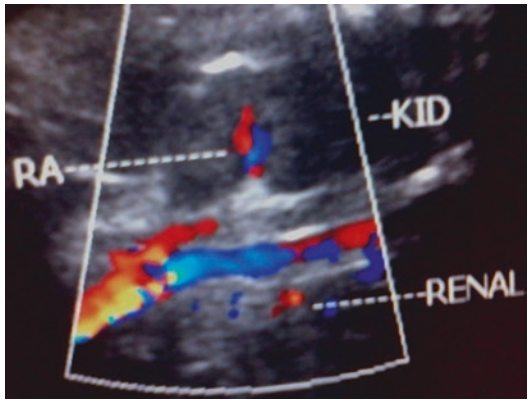

Fig. 4.94 Visualisation of both renal arteries in power Doppler

to detect approximately two-thirds of foetuses with congenital heart disease [85]. Real-time echocardiography allows evaluation of foetal ventricular cavity and wall thickness or valve and wall motion as well as cardiac arrhythmias.

Pulsed Doppler ultrasonography demonstrates the direction and characteristics of blood flow within foetal heart and the great vessels. High pulse repetition frequency or continuous-wave ultrasonography allows to measure high velocities.

Foramen ovale (Fig. 4.100) and its flap opening into left atrium can be seen (Fig. 4.101).

The structural abnormalities of the heart are not being described here. The foetal heart rate (FHR) is slow (bradycardia) with <100 beats per minutes (beats per minute/bpm) or fast (tachycardia) with >200 bpm. The foetal heart rate after 9 weeks' GA is 140–160 bpm. The heart rate gradually decreases with advancing GA and remains at 140 beyond 36 weeks' GA. In post-

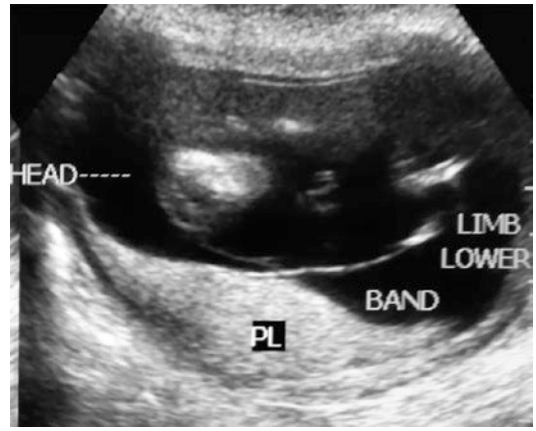

Fig. 4.95 Visualisation of both renal arteries rules out renal agenesis

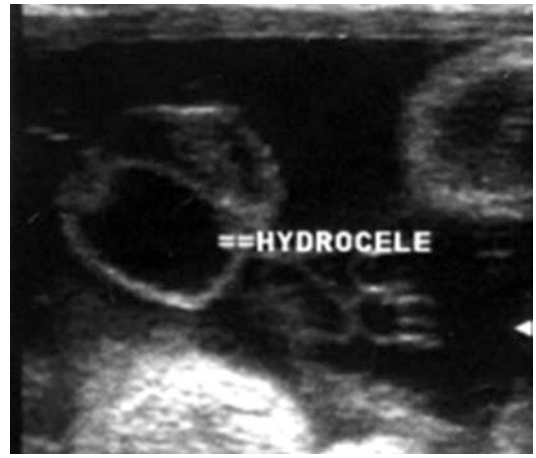

Fig. 4.96 Unilateral hydrocele in a foetus near term

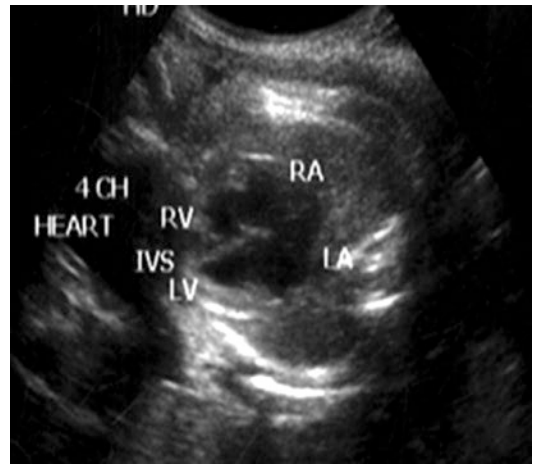

Fig. 4.97 Four-chamber view of foetal heart

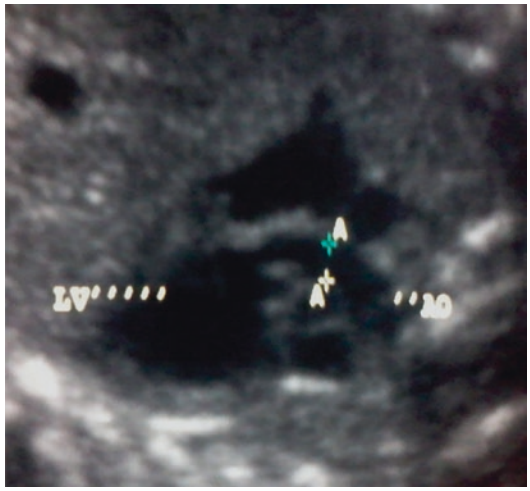

Fig. 4.98 Left ventricular outflow tract and aorta

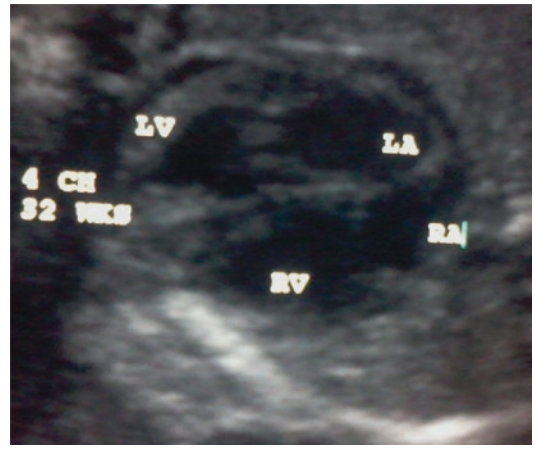

Fig. 4.100 Four-CH view of foetal heart with patent foramen ovale between RA and LA

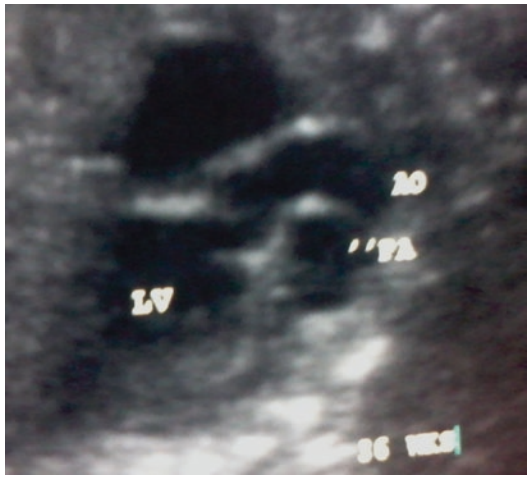

Fig. 4.99 Pulmonary artery (PA) located posterior to the aorta

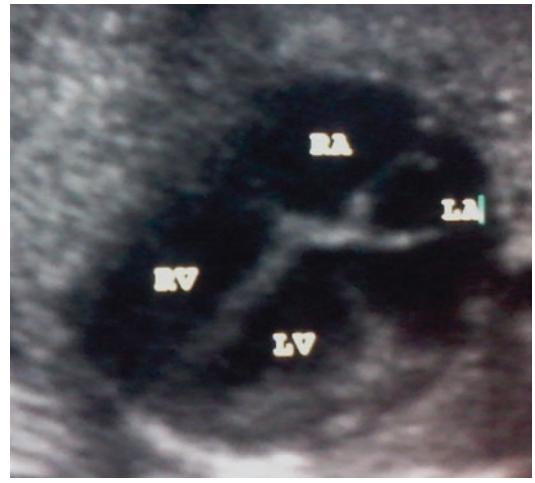

Fig. 4.101 Flap of foramen ovale opening into the left atrium

dated pregnancies it may remain at 110–120 bpm. Foetal cardiac arrhythmia can be detected.

References

1. Guidelines for performance of the antepartum obstetrical ultrasound examination. J Ultrasound Med. 1996;15:185.
2. Nyberg DA, Laing FC, Filly RA, et al. Ultrasonographic differentiation of the gestational sac of early intrauterine pregnancy from the pseudogestational sac of ectopic pregnancy. Radiology. 1983;146:755.
3. Hellman LM, Kobayashi M, Fillisti L, et al. Growth and development of the human foetus prior to the twentieth weeks of gestation. Am J Obstet Gynaecol. 1969;103:789.
4. Goldstein SR, Wolfson R. Transvaginal ultrasonography measurement 0f early embryonic as a means of assessing gestational age. J Ultrasound Med. 1994;13:27–31.
5. Hadlock FP, Shah YP, Kanon DJ, Lindsey JV. Foetal crown-rump length: re-evaluation of relation to menstrual age(5–18 weeks) with high resolution real-time US. Radiology. 1992;182:501–5.
6. Levi CS, Lyons EA, Lindsay DJ. Early diagnosis of non-viable pregnancy with transvaginal US. Radiology. 1988;167:383–5.

7. Nyberg DA, Mack LA, Laing FC, Patten RM. Distinguishing normal from abnormal gestational sac growth in early pregnancy. J Ultrasound Med. 1987; 6:23–7.
8. Nyberg DA, Hill LM. Normal early intrauterine pregnancy: sonographic development and hCG correlation. In: Nyberg DA, Hill LM, Bohm-Velez M, Mendelson EB, editors. Transvaginal ultrasound. Mosby-Year Book: St. Louis; 1992. p. 65–84.
9. Moore KL. The cardiovascular system. In: Moore KL, editor. The developing human: clinically oriented embyology. 4th ed. Philadelphia: W.B. Saunders; 1988. p. 294.
10. Hertberg BS, Mahony BS, Bowie JD. First trimester foetal cardiac activity: sonographic documentation of a progressive early rise in heart rate. J Ultrasound Med. 1988;7:573–5.
11. Nyberg DA, Laing FC, Filly RA. Threatened abortion: sonographic distinction of normal and abnormal gestational sacs. Radiology. 1986;158:397–400.
12. Bradley WG, Fiske CE, Filly RA. The double sac sign of early intrauterine pregnancy used in exclusion of ectopic pregnancy. Radiology. 1982;143: 223–6.
13. Fleishner AC, James AE, Karuse DA, et al. Sonographic patterns in trophoblastic disease. Radiology. 1978; 126:215.
14. Scott JR. Early pregnancy loss. In: Scott JR, Di Saia PJ, Hammond CB, Spellacy WN, editors. Danforth's obstetrics and gynaecology. 8th ed. Philadelphia: Lippincott-Raven; 1999. p. 143–53.
15. Nyberg DA, Laing FC. Threatened abortion and abnormal first-trimester intrauterine pregnancy. In: Nyberg DA, Hill LM, Bohm-Velez M, Mendelson EB, editors. Transvaginal ultrasound. St. Louis: Mosby-Year Book; 1992. p. 85–103.
16. Nocolaides KH, Brizol ML, Snijders RJM. Foetal nuchal translucency: ultrasound screening for trisomy in the first trimester of pregnancy. Br J Obstet Gynaecol. 1994;101:782.
17. Moore KL, Persaud TVN. Organogenic period: the fourth to eighth weeks. Inr system. In: Moore KL, Persaud TVN, editors. The developing human: clinically oriented embyology. 6th ed. Philadelphia: W.B. Saunders; 1998. p. 85–100.
18. Braffman BH, Coleman B, Ramchandani P, et al. Emergency department screening for ectopic pregnancy: a prospective US Study. Radiology. 1994;190:797.
19. Jauniaux E, Nicolaides KH. Early ultrasound diagnosis and follow-up of molar pregnancies. Ultrasound Obstet Gynecol. 1997;9:17.
20. Fox H. Pathology of. placenta. 2nd ed. London: W.B. Saunders; 1997.
21. Iams JD, Johnson FF, Sonek J, et al. Cervical incompetence as a continuum: a study of ultrasonographic cervical length and obstetric performance. Am J Obstet Gynaecol. 1995;172:1097.
22. Verma TR, Patel RH, Pillai U. Ultrasonic assessment of cervix in "at risk" patients. Acta Obstet Gynecol Scand. 1986;65:147.
23. Berghella V, Kuhlman K, Weiner S, et al. Cervical funnelling: sonographic criteria predictive of preterm delivery. Ultrasound Obstet Gynecol. 1977;10:161.
24. Hadlock FP, Harrist RB, Shah YP, et al. Estimating foetal age using multiple parameters: A prospective evaluation in a racially mixed population. Am J Obstet Gynaecol. 1987;156:955.
25. Hadlock FP. Sonographic estimation of foetal age & weight. Radiol Clin N Am. 1990;28:39.
26. Hadlock FP, Deter RL, Harrist RB, Park SK. Fetal femur length as a predictor of menstrual age; sonographically measured. AJR Am J Roentgenol. 1982;138:875.
27. Hadlock FP, Deter RL, Harrist RB, Park SK. Foetal head circumference: relation to menstrual age. AJR. 1982;138:649.
28. Hadlock FP, Deter RL, Harrist RB, Park SK. Foetal abdominal circumference as a predictor of menstrual age. AJR. 1982;139:367.
29. Hadlock FP, Harrist RB, Sharman RS, et al. Estimation of foetal weight with the use of head, body and femur measurement-a prospective study. Am J Obstet Gynaecol. 1985;151:333.
30. Afahony BS, Filly RA, Callen PW. Amnionicity & chorionicity in twin pregnancies: prediction using ultrasound. Radiology. 1985;155:205.
31. Hertzberg BS, Kurtz AB, Choi HY, et al. Significance of membrane thickness in the spnographic evaluation of twin pregnancy. AJR Am J Roentgenol. 1987; 148(1):151.
32. Evans MI, Dommergues M, Wapner RJ, et al. International, collaborative experience of 1789 patients having mutifetal pregnancy reduction: a plateauing of risks and outcomes. J Soc Gynecol Invest. 1996;3(1):23.
33. Pattern BM, Corliss CE. Pattern's human embryology. Elements of clinical development. New York: McGraw-Hill; 1976.
34. Van Allen MI, Smith DW, Shepard TH. Twin reversed arterial perfusion (TRAP) sequence: a study of 14 twin pregnancies with acardius. Semin Perinatol. 1983;7(4):285.
35. Lage JM, Vanmarter LJ, Mikhail E. Vascular anastomoses in fused, dichorionic twin placentas resulting in twin transfusion syndrome. Placenta. 1989; 10(1):55.
36. Bruner JP, Rosemond RL. Twin-to-twin transfusion syndrome: a subset of the twin nios-polyhydramnios sequence. Am J Obstet Gynecol. 1993;169(4):925.
37. Harris RD, Alexander RD. Ultrasound of the placenta and umbilical cord. Chap 20. In: Callen PW, editor. Ultrasonography in obstetrics and gynecology. 4th ed. Philadelphia: W. B. Saunders; 2000. p. 598–9.
38. Harris RD, Alexander RD. Ultrasound of the placenta and umbilical cord. Chap 20. In: Callen PW, editor. Ultrasonography in obstetrics and gynecology. 4th ed. Philadelphia: W B Saunders; 2000. p. 607–13.
39. Grannum P, Berkowitz R, Hobbins J. The ultrasonic changes in the maturing placenta and their relationship to foetal pulmonic maturity. Am J Obstet Gynaecol. 1979;133:915.

40. Strong JH Jr, Jarles DL, Vegas JS, Feldman DB. The umbilical coiling index. Am J Obstet Gynaecol. 1995;172(2Pt):718–20.
41. Strong JH, Elliot JP, Radin TG. Non-coiled umbilical blood vessels: a new marker for the foetus at risk. Obstet Gynaecol. 1993;81(3):409–11.
42. Rozenberg P, Goffinet F, Philippe HJ, Nisand I. Ultrasonographic measurement of lower uterine segment to assess risk of defects of scarred uterus. Lancet. 1996;347(8997):281. [PubMed].
43. Bujold E, Jastrow N, Simoneau J, et al. Prediction of complete uterine rupture by sonographic evaluation of the lower uterine segment. Am J Obstet Gynecol. 2009;201:320.el–6.
44. Baker ME, Kay H, Mahony BS, et al. Sonography of the low transverse incision caesarean section: a prospective study. J Ultrasound Med. 1988;7:389–93.
45. Brace RA, Wolf EJ. Normal amniotic fluid volume changes throughout pregnancy. Am J Obstet Gynecol. 1989;161:382.
46. Otterlo L, Wladimiroff J, Wallenberg H. Relationship between fetal urine production and amniotic fluid volume in normal pregnancy complicated by diabetes. Br J Obstet Gynecol. 1977;84:205.
47. Gilbert W, Moore T, Brace R. Amniotic fluid volume dynamics. Fetal Med Rev. 1991;3:89.
48. Moore TR, Cayle JE. The amniotic fluid index in normal human pregnancy. Am J Obtet Gynaecol. 1990;162: 1168.
49. Rutherford SE, Phalen JP, Smith CV, et al. The four quadrant assessment of amniotic fluid volume: an adjunct to antepartum fetal heart rate testing. Obstet Gynecol. 1987;70:353.
50. Goldstein RB, Filly RA. Sonographic estimation of amniotic fluid volume. Subjective assessment versus pocket measurement. J Ultrasound Med. 1988;7:363.
51. Elliot JP, Sawyer AT, Radin TG, et al. Large-volume therapeutic amniocentesis in the treatment of hydramnios. Obstet Gynecol. 1994;84:1025.
52. Gross TL, Wolfson RN, Kuhnert PM, et al. Sonograpgically detected free-floating particles in amniotic fluid predict a mature lecithin-sphingomyelin ratio. J Clin Ultrasound. 1985;13(6):405.
53. Williams J, Nathan RO, Worthen NJ. Sonographic demonstration of the progression of meconium peritonitis. Obstet Gynecol. 1984;64:82.
54. Foster MA, Nyberg DA, Mahoney BS, et al. Meconeum peritonitis: prenatal sonographic findings and their clinical significance. Radiology. 1987;165:66.
55. Pan EY, Chen LY, Zang JZ, et al. Radiographic diagnosis of meconium peritonitis. A report of 200 cases including six fatal cases. Pediatr Radiol. 1983;13:19.
56. Jui SS, Rizos N, Jontsi P, et al. Nonimmune hydrops foetalis. Am J Obtet Gynaecol. 1984;148:566.
57. Manning FA, Platt LD, Sipos L. Antepartum foetal evaluation: development of a foetal biophysical profile. Am J Obstet Gynaecol. 1980;136:787.
58. Vandenbosche RC, Kirchner JT. Intrauterine growth retardation. Am Fam Physician. 1998;58(6):1384–90.
59. Chang TC, Robson SC, Boys RJ, et al. Prediction of the small for gestation age infant: which ultrasonic measurement is best? Obstet Gynecol. 1992;80:1030.
60. Benson CB, Doubilet PM. Foetal measurements: normal and abnormal foetal growth. In: Rumack CM, Wilson SR, Charboneau JW, editors. Diagnostic ultrasound. St. Louis: Mosby-Year Book; 1991. p. 723.
61. Benson CB, Doubilet PM. Doppler criteria for intrauterine growth retardation: predictive values. J Ultrasound Med. 1988;7:655.
62. Harris RD, Alexander RD. Ultrasound of the placenta and umbilical cord. Chap 8. In: Callen PW, editor. Ultrasonography in obstetrics and gynecology. 4th ed. Philadelphia: W. B. Saunders; 2000. p. 211.
63. Hadlock FP, Deter RL, Harrist RB, et al. A date independent predictor of intrauterine growth retardation: femur length/abdominal circumference ratio. AJR Am J Roentgenol. 1983;141:979.
64. Kurdi W, Campbell S, Acquilina J, et al. The role of colour Doppler imaging of the uterine arteries at 20 weeks' gestation in stratifying antenatal care. Ultrasound Obstet Gynecol. 1998;12:339.
65. Golditch IM, Kirkman K. The large foetus. Management and outcome. Obstet Gynecol. 1978;52:26.
66. Callen PW. Chap 1, The obstetric ultrasound examination. In: Callen PW, editor. Ultrasonography in obstetrics and gynecology. 4th ed. Philadelphia: W. B. Saunders; 2000. p. 14.
67. Hattan RA, Rees GK, Johnson ML. Normal foetal anatomy. Radiol Clin N Am. 1982;20:271.
68. Filly RA, Golbus MS. Ultrasonography of normal and pathological foetal skeleton. Radiol Clin N Am. 1982;20:311.
69. Filly RA, Feldstein VA. Ultrasound evaluation of normal foetal anatomy. Chap 9. In: Callen PW, editor. Ultrasonography in obstetrics and gynecology. 4th ed. Philadelphia: W. B. Saunders; 2000. p. 222.
70. Denkhaus H, Winsberg F. Ultrasonic measurement of the foetal ventricular system. Radiology. 1979;131:781.
71. Chatzipapas IK, Whitlow BJ, Economides DL. The 'Mickey Mouse' sign and the diagnosis of anencephaly in early pregnancy. Ultrasound Obstet Gynecol. 1999;13:196–9.
72. Book J, Schut J, Reed S. A clinical and genetical study of microcephaly. Am J Ment Defic. 1953;57:637.
73. Bromley B, Benacerraf BR. Difficulties in the prenatal diagnosis of microcephaly. J Ultrasound Med. 1995;14:303.
74. Pritchard JA. Foetal swallowing and amniotic fluid volume. Obstet Gynecol. 1966;28:606.
75. Weissman A, Achiron R, Kuint J, et al. Prenatal diagnosis of congenital gastric outlet obstruction. Prenatal Diagn. 1994;14:88.
76. Nelson LH, Clark CE, Fishburne JI. Value of serial sonography in the in-utero detection of duodenal atresia. Obstet Gynecol. 1982;59:657.
77. MacGregor SN, Tamura R, Sabbagha R, et al. Isolated hyperechoic foetal bowel: significance and

implications for management. Am J Obstet Gynecol. 1995;173:1254.
78. Hill LM, Fries J, Hecker J, et al. Second trimester echogenic small bowel: an increased risk for adverse perinatal outcome. Prenat Diagn. 1994;14:84.
79. Goldstein RB, Filly RA. Sonographic diagnosis of meconium ileus in utero. J Ultrasound Med. 1987;6:66.
80. Budorick NE, Pretorius DH, Johhson DD, et al. Three-dimensional ultrasound examination of the foetal hands: normal and abnormal. Ultrasound Obstet Gynecol. 1998;12:227.
81. Jeanty P, Romero R, d'Alton M, et al. In utero sonographic detection of hand & foot deformities. J Ultrasound Med. 1985;4:595.
82. Romero R, Pilu G, Jeanty P, et al. Prenatal diagnosis of congenital anomalis. Appleton & Lange: Norwalk; 1988. p. 83. [40]
83. Romero R, Athanassiadis AP, Jeanty P. Fetal skeletal anomalies. Radiol Clin N Am. 1989;28:75.
84. Burton DJ, Filly RA. Sonographic diagnosis of amniotic band syndrome. AJR. 1991;156:555.
85. Kirk JS, Comstock CH, Lee W, et al. Sonographic screening to detect foetal cardiac anomalies: a 5-year experience with 111 abnormal cases. Obstet Gynecol. 1997;89:227.

Colour Doppler Sonography in Obstetrics

5

M.K. Dwivedi

Abstract

The minimum frequency of transducer should be 7.5 MHz in early pregnancy (up to 8 weeks) and 5 MHz in 9–13 weeks of pregnancy. A duplex Doppler or a triplex Doppler capability is essential for displaying Doppler waveforms and for calculating the resistance index (RI) and pulsatility index (PI) and also the A/B ratio (peak systolic/end diastolic ratio). Doppler ultrasound is a non-invasive method of evaluating blood flow in the feto-placental and utero-placental circulation in normal and complicated pregnancy.

Uterine Artery: Diastolic notch of the uterine artery (Fig. 5.1) disappears from 24 weeks (Fig. 5.2) and RI drops from 0.84 to 0.56 (Figs. 5.3 and 5.4) [1]. If the notch does not disappear by 24 weeks, most women will develop a hypertensive complication of pregnancy.

Impaired uterine artery flow velocity is identified by (a) a persistent abnormal index, (b) a persistent notch and (c) significant differences between the indices in two vessels.

The commonly used PI with cut-off value of 1.5 is proved to be the best.

5.1 Umbilical Artery [2]

End diastolic flow is present in all pregnancies by 20 weeks. A mature umbilical artery flow velocity waveform is achieved by 28–30 weeks (Fig. 5.5). Indices mid cord or placental insertion are clinically more reliable. Normal RI ranges from 0.5 to 0.7 and S/D ratio ≤ 3.

Absent end diastolic velocity is clearly abnormal.

Decreased diastolic flow (RI > 0.7) indicates early placental insufficiency (Fig. 5.6). When there is reversal of flow, it may be a clinical emergency because most of the foetuses die within 2 weeks.

The ratio of intraplacental/UA PI and RI of more than one is associated with increased incidence of IUGR, preeclampsia, foetal distress and neonatal intensive care unit admissions.

M.K. Dwivedi
Department of Radio-Diagnosis, C.C.M. Medical College & Hospital, Durg, Chhattisgarh, India
e-mail: mahendra_van@yahoo.com

R.K. Diwakar (ed.), *Basics of Abdominal, Gynaecological, Obstetrics and Small Parts Ultrasound*,
https://doi.org/10.1007/978-981-10-4873-9_5

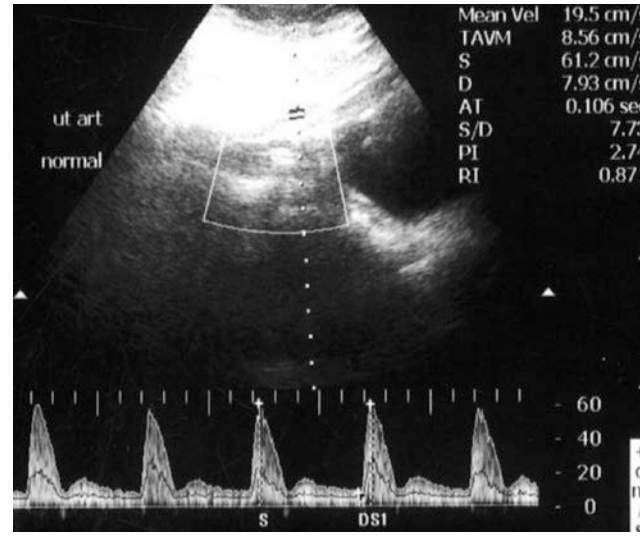

Fig. 5.1 Flow velocity waveform of a uterine artery in a non-pregnant woman showing diastolic notch and RI of 0.8

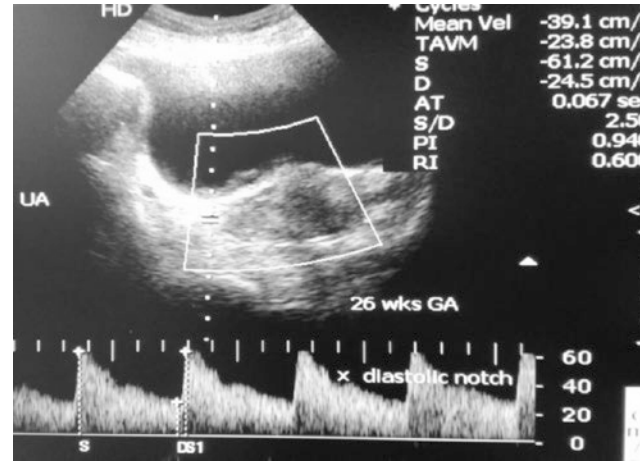

Fig. 5.2 Diastolic notch in 26 weeks of pregnancy

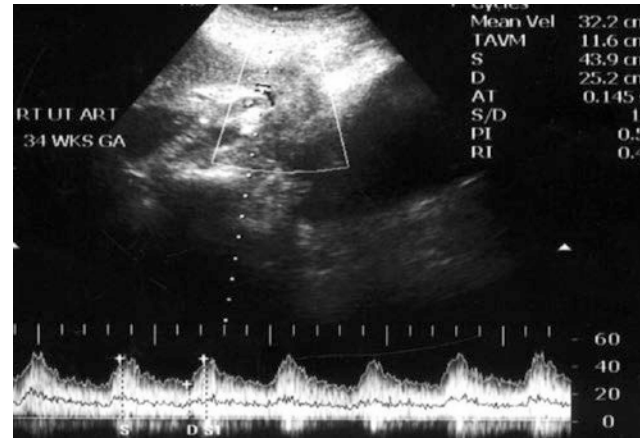

Fig. 5.3 FVW of uterine artery in normal 34 pregnancy weeks with disappearance of diastolic notch and RI of 0.4

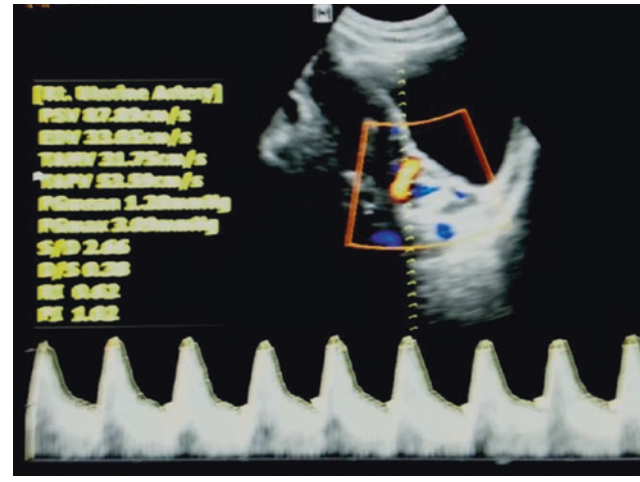

Fig. 5.4 Right uterine artery VF with normal RI, PI and diastolic flow

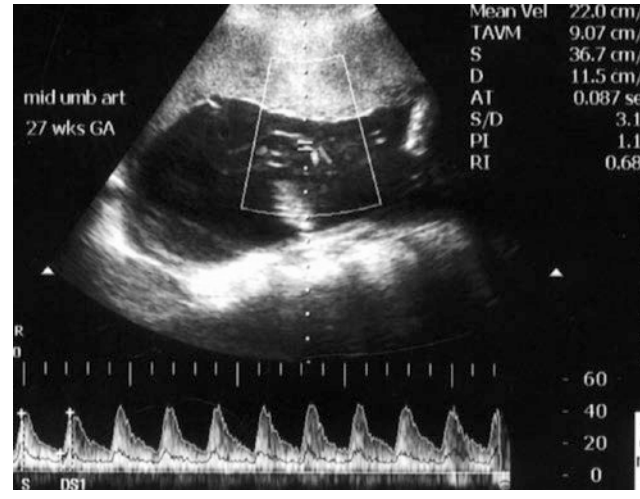

Fig. 5.5 Normal FVW of UA displays forward flow with PI of 1.1

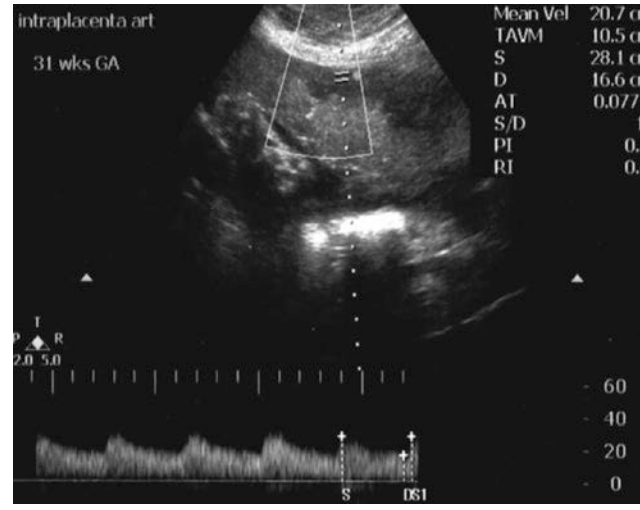

Fig. 5.6 Normal FVW in spiral branch of placenta with normal RI of 0.4

5.2 Foetal Descending Thoracic Aorta

Normal flow wave pattern (Fig. 5.7) shows RI = 0.82 + 0.1 and PI = 1.83 + 0.3.

There is increase in RI and PI of growth retarded foetuses. High PI is suggestive of foetal academia.

Absent end diastolic flow is suggestive of perinatal complications such as respiratory distress syndrome, necrotising enterocolitis and renal failure.

5.3 Foetal Middle Cerebral Artery [3]

Normal RI of MCA is less than 0.7 and PI is >1.3 (Fig. 5.8). Foetus with mild hypoxia shows reduced umbilical artery flow velocity. The preterminal flow pattern shows absent diastolic flow in the umbilical artery, aorta, vena cava and umbilical vein pulsations. The PI of MCA is significantly lower and the mean systolic velocity is higher in small-for-gestational-age foetuses than the normal foetuses.

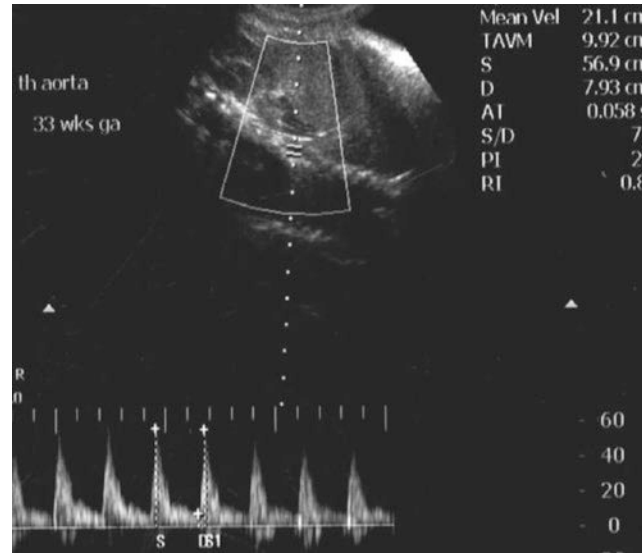

Fig. 5.7 TA FVW with PI of 2.3 indicates normal blood flow

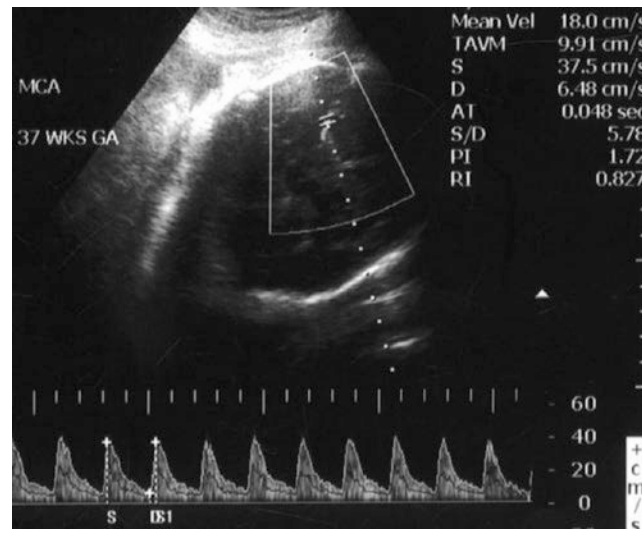

Fig. 5.8 The FVW of MCA displays a continuous forward flow and a high PI of 1.72

Whether growth retarded foetus is normal, it is determined by the state of umbilical and uterine circulation, and foetal hypoxaemia is determined by MCA Doppler. In growth restriction, a rise in PI of UA precedes changes in the MCA and TA.

5.4 Foetal Venous Circulation [4]

Doppler evaluation of the ductus venosus (Fig. 5.9), hepatic veins and umbilical veins (Fig. 5.9) gives an idea of foetal hypoxic and acidotic state. Absent diastolic velocities and reversal of blood flow in ductus venosus are an absolute indication of delivery.

The umbilical venous flow when measured at an extra-abdominal level displays regular pulsations up to 15 weeks of gestation. Thereafter, venous pulsations gradually disappear (Fig. 5.10). Occurrence of venous pulsations in UV later in pregnancy is a sign that indicates congestive heart failure in compromised foetuses.

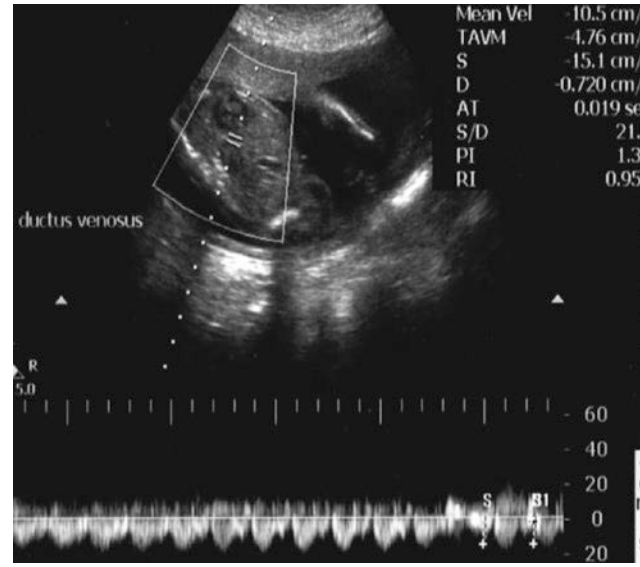

Fig. 5.9 FVW of DV displaying continuous forward flow with two surges of velocity peaks and no reverse flow

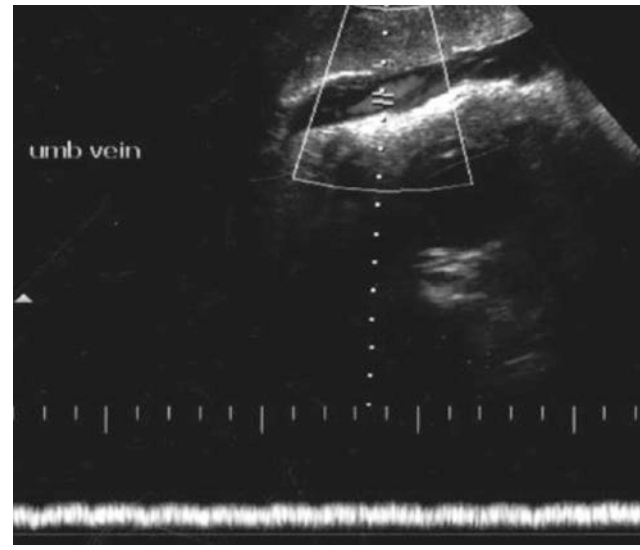

Fig. 5.10 Normal UV FVW with its steady flow and no venous pulsations

References

1. Farrel T, Chien PF, Mires GJ. The reliability of the detection of an early diastolic notch with uterine artery Doppler velocimetry. Br J Obstet Gynecol. 1998;105:1308.
2. Trudinger BJ, Cook CM, Giles WB, et al. Foetal umbilical artery velocity waveforms and subsequent neonatal outcome. Br J Obstet Gynaecol. 1991; 98:378.
3. Mari G, Deter RL. Middle cerebral artery flow velocity waveforms in normal and small-for-gestational foetuses. Am J Obstet Gynaecol. 1992;166:1262.
4. Nishio J, Nakai Y, Mine M, et al. Characteristics of blood flow in intrauterine growth-restricted foetuses with hypocoiled cord. Ultrasound Obstet Gynecol. 1999;13:171.

Chromosomal Abnormalities

6

M.K. Dwivedi

Abstract

Chromosomal abnormality increases with advancing maternal age. However, Turner syndrome is not related to age. Birth defects such as clubfoot, cleft lip and neural tube defects (NTDs) may result due to genetic and environmental factors. Many of the foetal structural anomalies can be detected with prenatal ultrasound. Triple marker screening with AFP, uE3 and HCG is now routinely carried out for screening and detection of chromosomal abnormalities.

The incidence of birth defect varies from 3 to 4%. It will not be possible to include the description of all of them; therefore only some of the chromosomal abnormalities are described. However, a systematic careful evaluation of foetal anatomy and growth parameters by ultrasound will prove to be the key factors.

The total number of chromosomes, spoken of as diploid number, is 46 in males (23 pairs). Twenty-two pairs of these are homologous and known as autosomes. The remaining pairs are known as sex chromosomes. The term "gene" is used to describe the factor at a particular point or locus on the chromosomes which represent individual hereditary characteristics. The capacity of the genes for identical replication is due to the unique structure of the DNA molecule.

Aneuploidy is the failure of separation of a pair of chromosomes. The fertilisation of such gamete with one from the fertilising gamete results in trisomy.

The risk for many chromosomal abnormalities increases with advancing maternal age [1].

Down syndrome, the most common chromosomal abnormality, was found in 80% of foetuses born to women younger than 35 years [2].

Nuchal translucency (Fig. 6.1) is measured in the late first trimester and early second trimester (11.3–13.6 weeks) [3–5]. The nuchal fold thickness is measured (3 mm early and 6 mm later) in 18–20 weeks' gestation in second trimester of pregnancy [6] (Fig. 6.2).

Nicolaides and co-workers, who have been instrument in demonstrating the association between the thickened nuchal translucency and chromosomal anomalies [3], indicated that a cut-off

M.K. Dwivedi
Department of Radio-Diagnosis, C.C.M. Medical College & Hospital, Durg, Chhattisgarh, India
e-mail: mahendra_van@yahoo.com

R.K. Diwakar (ed.), *Basics of Abdominal, Gynaecological, Obstetrics and Small Parts Ultrasound*,
https://doi.org/10.1007/978-981-10-4873-9_6

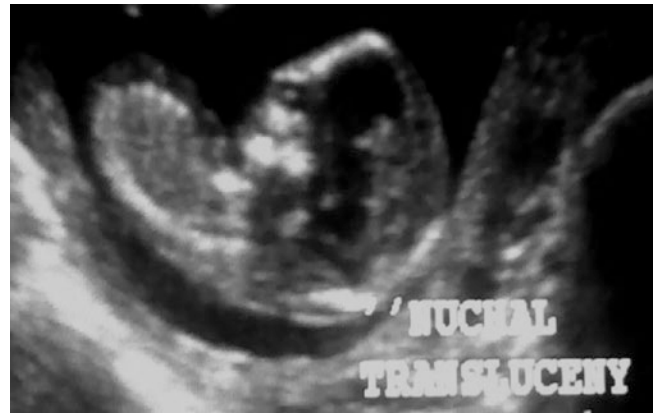

Fig. 6.1 Nuchal translucency

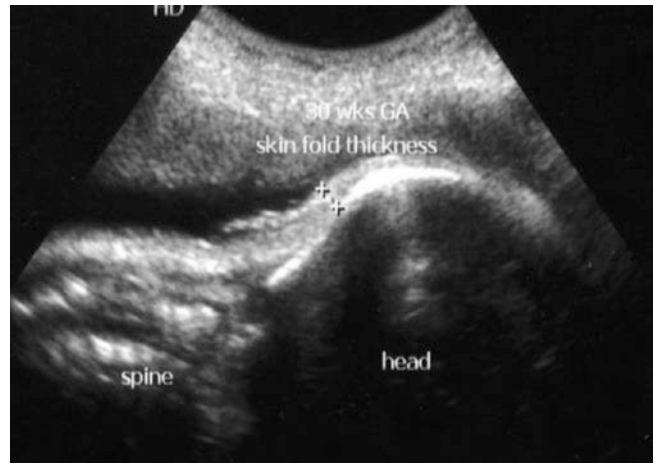

Fig. 6.2 Nuchal fold thickness in third trimester

of >/−3 mm could be used as a screening method to detect foetuses with abnormal karyotype with a relatively low false-positive rate. The measurement can be done using the trans-abdominal or transvaginal approach between 10 and 13 weeks.

Whitlow and Economides suggested that the optimal age to examine the nuchal translucency as well as the foetal anatomy in the first trimester is 13 weeks [4]. Pandya et al. [7] assessed the repeatability of the nuchal translucency measurement between 10 and 14 weeks' gestation. Braithwaite and Economides showed that the measurement of the nuchal translucency can be done using the trans-abdominal or transvaginal approach between 10 and 13 weeks [8].

The common sonographic findings in Down syndrome include major anomaly, nuchal fold >6 mm [9], short humerus/femur [10], pyelectasis (separation of the wall of calices >4 mm) [9] and hyper-echogenic bowel [11].

Triple marker screening, i.e. AFP, uE3 (unconjugated estriol) and human chorionic gonadotrophin (HCG) has higher sensitivity than MSAFP screening alone to detect Down syndrome [12].

Alpha fetoprotein in amniotic fluid (AFAFP) and maternal serum (MSAFP) at higher levels are in foetuses with anencephaly and spina bifida (when the lesions are open) [13].

Trisomy 13 includes cardiac defects, cystic hygroma, IUGR, facial clefts, microcephaly, neural tube defects, omphalocele, polycystic kidneys, polydactyl and ventriculomegaly [14].

Trisomy 18 includes agenesis of corpus callosum, single umbilical artery, cardiac defects, etc. [15].

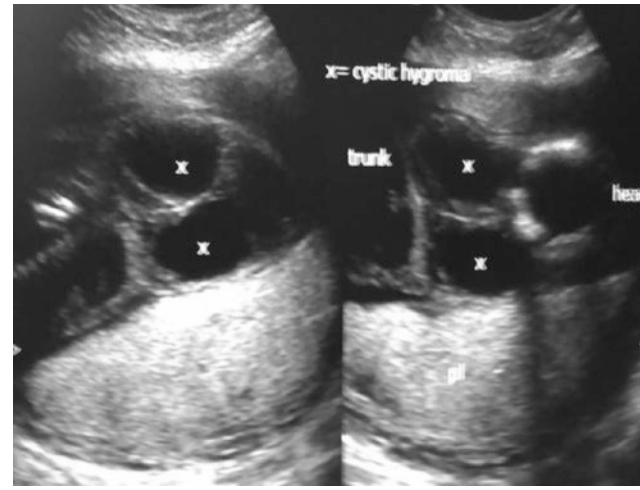

Fig. 6.3 Cystic swelling on both sides of foetal neck in cystic hygroma

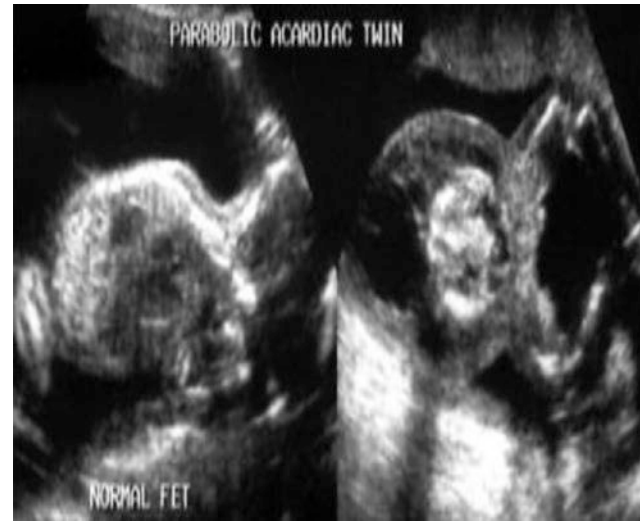

Fig. 6.4 Acardiac twin, normal on left/donor on right

Cystic hygroma is seen as cystic area containing fluid on posterior aspect of foetal neck (Fig. 6.3).

Turner syndrome shows the entire foetal body swollen resembling a space suit. Cardiac and renal anomalies are common. Spontaneous abortion is the most common outcome in such cases [16].

Foetal cytomegalovirus (*CMV*) *infection* is characterised by NIHF, ascites, ventriculomegaly and other findings associated with transplacental transmission of CMV to the foetus [17]. The associated findings could be microcephaly, splenomegaly, right heart overload, IUGR, brain atrophy, oligohydramnios, etc.

Foetal rubella syndrome is characterised by cardiac malformations (septal defects), eye defects (cataract, microphthalmia), microcephaly, hepato-splenomegaly and IUGR. Deafness and mental retardation are expected after birth.

Foetal toxoplasmosis syndrome. The findings include chorio-retinitis, microcephaly, hydrocephalus, ascites, hepato-splenomegaly, etc.

Prune belly syndrome. It is more common in males and consists of a deficiency in abdominal wall muscles which may be absent or hypoplastic. Ultrasound reveals large abdominal masses, bladder obstruction, cryptorchidism and oligohydramnios (Fig. 6.4).

Syndrome is a pattern of multiple anomalies which does not represent a single sequence [18].

6.1 Surgical Therapy for Foetal Anomalies

Accurate ultrasonography and fast MRI can identify a number of disorders at an early stage of development to be amenable to prenatal intervention in an institution equipped with appropriate resources. Foetal therapy or foetal treatment is part of foetal medicine which is performed on a "sick" foetus with the aim of achieving foetal well-being. It includes medical (i.e. non-invasive) and surgical procedures [19].

Congenital malformations that may benefit from foetal surgery include urinary tract obstruction, congenital diaphragmatic hernia, sacrococcygeal teratoma, meningomyelocele, placental vascular anomalies, congenital cystic adenomatoid malformation, congenital high airway obstruction syndrome, foetal hydrothorax and amniotic band syndrome (from Table 27.1; p. 764) [19].

Foetal intervention involves in utero surgical treatment of a foetus that includes open foetal surgery, the most invasive and the less invasive video-endoscopic foetal surgery (FETEENDO) and foetal image-guided surgery (FIGS). The surgical techniques for hysterotomy and foetal surgery have been developed and refined [20].

Surgical intervention may involve either a direct operation of the foetus or it may be performed as exutero intrapartum treatment (EXIT) procedure [21].

The video-endoscopic foetal surgery (FETEENDO) techniques are now common for foetal intervention. The congenital malformations that may benefit from foetal surgery include urinary tract obstruction, congenital diaphragmatic hernia, sacrococcygeal teratoma, myelomeningocele, placental vascular anomalies (twin-twin transfusion, TRAP sequence), congenital cystic adenomatoid malformation, congenital higher airway obstruction syndrome, foetal hydrothorax and amniotic band syndrome [22].

Three approaches to foetal surgery have been developed: percutaneous ultrasound-guided, fetoscopic and open foetal surgery.

Skarsgard et al. [22] have successfully developed fetoscopic techniques for treatment of severe congenital diaphragmatic hernia, TTTS, umbilical cord ligation and division, myelomeningocele, urinary tract decompression, chronic foetal vascular access and foetal tracheostomy for high airway obstruction syndrome.

All ultrasound examinations should include a detailed report on anatomic features for patients at higher risk for foetal anomalies. A referral for a high-detail scan to a tertiary centre having increased accuracy in detection may allow for optimising perinatal care.

References

1. Hook EB, Cross PK, Schreinemachers DM. Chromosomal abnormality rate at amniocentesis and in live-born infants. JAMA. 1983;249:2034.
2. Adams MM, Erickson JD, Layde PM, et al. Down's syndrome: recent trends in the United States. JAMA. 1981;246(7):758.
3. Nicolaides KH, Snijders RJ, Gosden CM, et al. Ultrasonographically detectable markers of foetal chromosomal abnormalities. Lancet. 1992;340:704.
4. Whitlow BJ, Economides DL. The optimal gestational age to examine foetal anatomy and measure nuchal translucency in the first trimester. Ultrasound Obstet Gynecol. 1998;11:258.
5. Nocolaides KH, Brizol ML, Snijders RJM. Foetal nuchal translucency: ultrasound screening for trisomy in the first trimester of pregnancy. Br J Obstet Gynaecol. 1994;101:782.
6. Borell A, Costa D, Martinez JM, et al. Criteria for foetal nuchal thickness cut-off: a re-evaluation. Prenat Diagn. 1997;17:23.
7. Pandya PP, Atman DG, Brizot ML, et al. Repeatability of measurement of foetal nuchal translucency thickness. Ultrasound Obstet Gynaecol. 1995;5:334.
8. Braithwaite JM, Economides DL. The measurement of nuchal translucency with transabdominal and transvaginal sonography-success rates, repeatability and levels of agreement. Br J Radiol. 1995;68:720.
9. Benacerraf BR, Barss VA, Laboda LA. A sonographic sign for the detection in the second trimester of the foetus with Down's syndrome. Am J Obstet Gynaecol. 1985;151:1078.
10. Nyberg DA, Resta RG, Luthy DA, et al. Humerus and femur length shortening in the detection of Down syndrome. Am J Obstet Gynaecol. 1993;168:534.

11. Nyberg DA, Resta RG, Luthy DA. Prenatal sonographic findings of Down syndrome: review of 94 cases. Obstet Gynaecol. 1990;76:370.
12. JMG VV, van Zalen-Sprock RM, Kostense PJ. First trimester nuchal translucency: a risk analysis on foetal chromosome abnormality. Radiology. 1996; 200:537.
13. Haddow JE. Prenatal screening for open neural tube defects, Down's syndrome and other major foetal disorders. Semin Perinatol. 1990;14:488.
14. Lehman CD, Nyberg DA, Winter TC III, et al. Trisomy 13 syndrome: Prenatal US findings in a review of 33 cases. Radiology. 1995;194:217.
15. Ginsberg N, Cadkin A, Pergament E, et al. Ultrasonographic detection of the second-trimester fetus with trisomy 18 and trisomy 21. Am J Obstet Gynecol. 1990;163:1186.
16. Garden AS, Benzie RJ, Miskin M, et al. Foetal cystic hygroma colli. Antenatal diagnosis, significance, and management. Am J Obstet Gynaecol. 1986;154:221.
17. Hagoy ZJ, Birang G, Ornoy A, et al. Congenital Cytomegalovirus infection: a long standing problem still seeking a solution. Am J Obstet Gynaecol. 1996;174:241.
18. Silva SR, Jeanty P. Chapter 4: Foetal syndromes. In: Callen PW, editor. Ultrasonography in obstetrics and gynecology. 4th ed. Philadelphia: W.B. Saunders; 2000. p. 68–104.
19. Albanese CT, Harrison MR, Paek B, Jennings RW. Chapter 27: Surgical therapy for foetal anomalies. In: Callen PW, editor. Ultrasonography in obstetrics and gynecology. 4th ed. Philadelphia: W.B. Saunders; 2000. p. 763–80.
20. Albanese CT, Harrison MR. Surgical treatment for foetal disease. The state of the art. Ann N Y Acad Sci. 1998;847:74.
21. Hirose S, Farmer DL, Lee H, et al. The ex-utero intrapartum treatment procedure: Looking back at the EXIT. J Pediatr Surg. 2004;39(3):375–80; discussion 375–80.
22. Skarsgard ED, Bealer JF, Meuli M, et al. Fetal endoscopic ('Fetendo') surgery: the relationship between insufflating pressure and the fetoplacental circulation. J Pediatr Surg. 1995;30(8):1165.

Ultrasound of Small Parts and Superficial Organs

7

R.K. Diwakar

Abstract

Sonography plays an important role in diagnostic evaluation of small parts and superficial organs. FNAC is an important adjunct to sonography in making the diagnosis. High-frequency transducers (7.5–15 MHz) provide penetration up to 5 cm and high-definition images with a resolution of 0.7–1.0 mm. Linear array transducers are preferred to sector transducer because of the wider near field of view and the capability to combine high-frequency greyscale and colour Doppler images. High-frequency transducers (7.5–10 MHz) provide both deep penetration up to 5 cm and high-definition images with a resolution of 0.7·10·1.0 mm. Linear array transducer is preferably used than the sector transducer because of the wider near field of view and capability of combining colour Doppler images.

7.1 US Imaging of Breast [1]

Sonography has become an important diagnostic tool in the management of breast diseases. Two types of instruments, automated and hand-held, are used for sonography of breast [2]. The lesion in the breast is described as in the anterior/middle/posterior third of the breast, in the axillary tail or retro-areolar in location. In USG, the breast glandular parenchyma appears homogenously echogenic having hypoechoic zones caused by fatty tissue (Fig. 7.1). Breast sonography is an important supplement to mammography. The American College of Radiology's BI-RADS categorization of mammographic abnormalities [3] is:

1. Negative
2. Benign finding
3. Probably benign (short-term follow-up suggested)
4. Suspicious abnormality (consider biopsy)
5. Highly suggestive of malignancy

Breast sonography has become indispensable in the diagnosis and management of benign and malignant process [4]. The mammographic study and interventional procedures should be supplemented with ultrasound.

R.K. Diwakar
Department of Radio-Diagnosis, C.C.M. Medical College & Hospital, Durg, Chhattisgarh, India
e-mail: rkdiwakar49@yahoomail.co.in

R.K. Diwakar (ed.), *Basics of Abdominal, Gynaecological, Obstetrics and Small Parts Ultrasound*,
https://doi.org/10.1007/978-981-10-4873-9_7

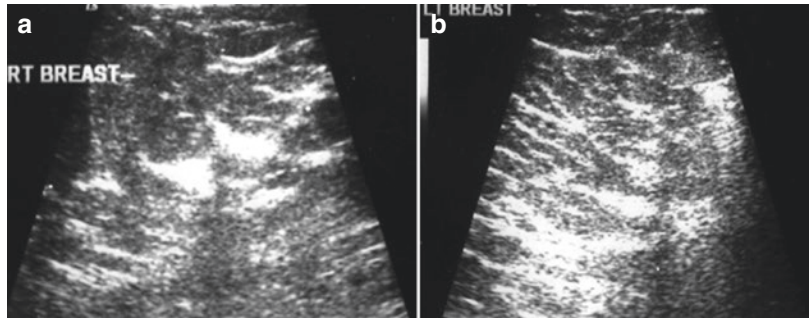

Fig. 7.1 Normal echotexture of breast. (**a**) Right breast. (**b**) Left breast

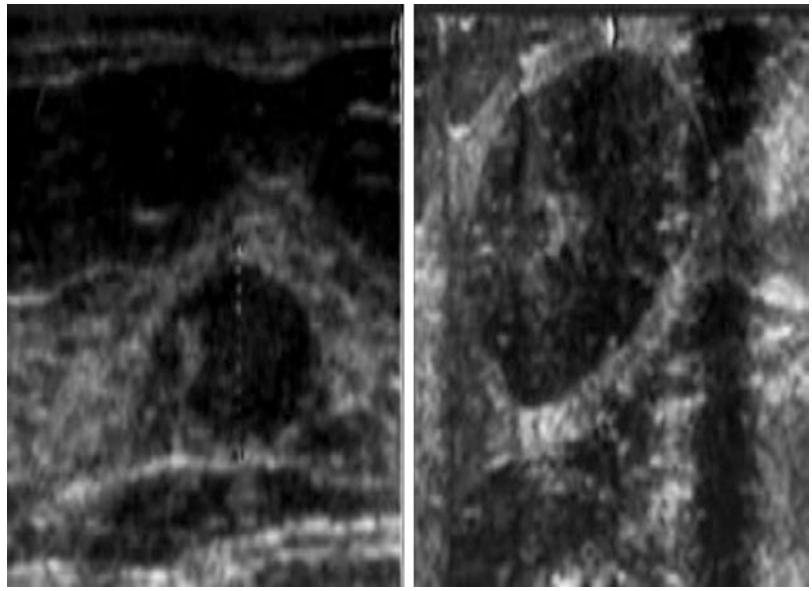

Fig. 7.2 Fibroadenoma of breast

Indications for Breast Sonography [5]

1. To characterize mammographic or palpable masses as solid or cystic
2. To evaluate palpable masses in young (under the age of 30 years), pregnant and lactating patients
3. To evaluate nonpalpable abnormalities for which the mammographic diagnosis is uncertain
4. To evaluate a mass causing asymmetric density in mammography
5. To confirm or better visualize a lesion seen in mammography
6. To guide interventional procedures

Fibroadenoma is the most common benign mass in a woman of 30–35 years of age, and it may be multiple in 10–30% of cases. They are hypoechoic than fibro-glandular parenchyma and isoechoic with fat lobules in the breast (Figs. 7.2 and 7.3).

Cysts in the breast are fairly common between 35 and 50 years of age. Sono-mammography provides confident diagnosis of cyst (Fig. 7.4).

Breast abscess may have sonographic features of complex mass with irregular margins or well-circumscribed oval lesions with low-level internal echoes and posterior acoustic enhancement (Figs. 7.5 and 7.6).

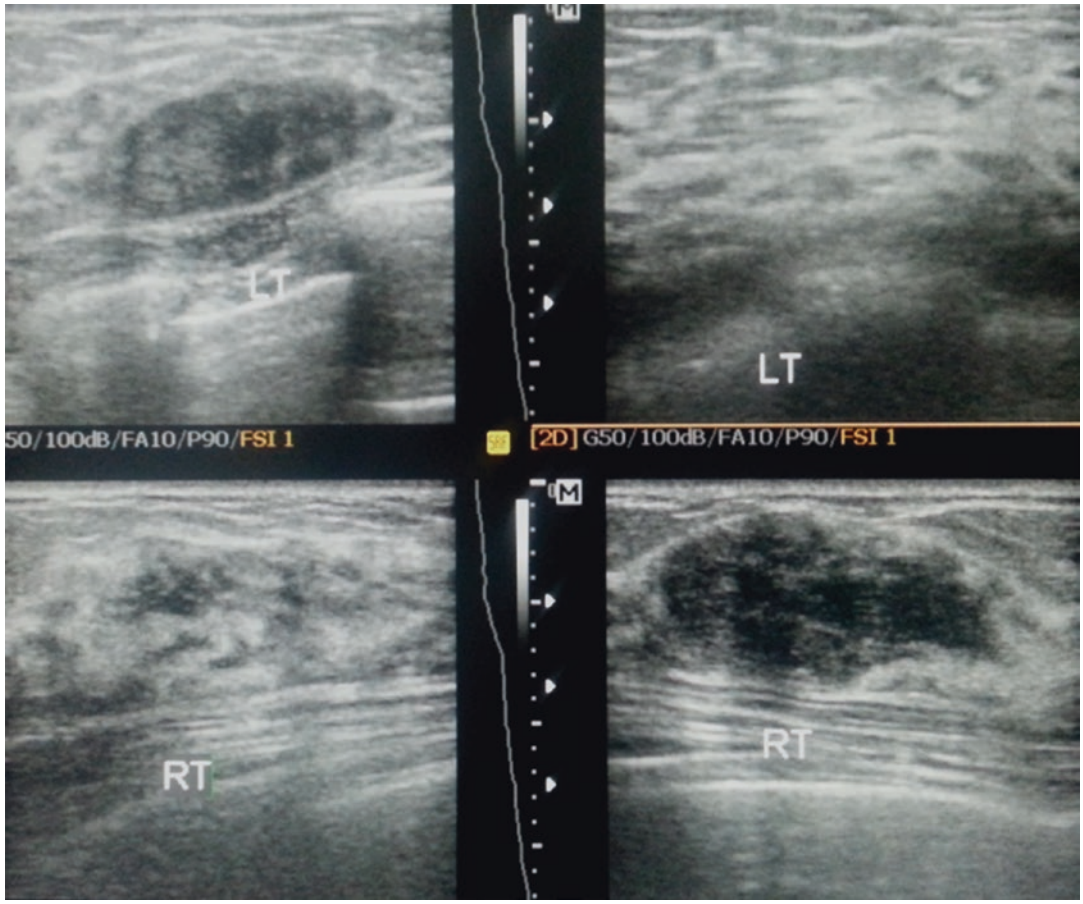

Fig. 7.3 Fibroadenoma in both breasts

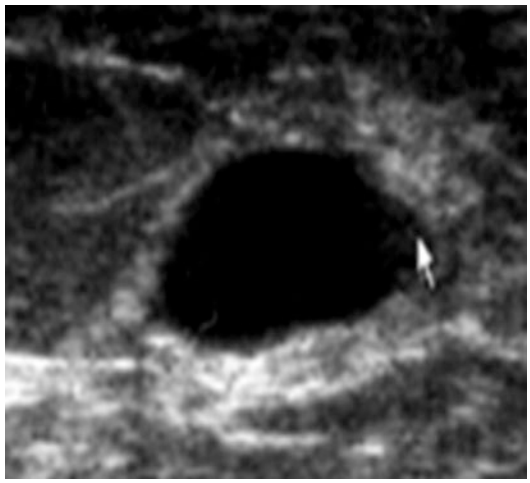

Fig. 7.4 Cystic breast lesion

Carcinoma of the breast is one of the leading causes of cancer in women. The sonographic features include marginal irregularity, irregular shape, hypoechogenicity relative to fibroglandular tissue, long axis of the mass perpendicular to the skin, an echogenic ring of variable thickness and posterior acoustic shadowing (Figs. 7.7, 7.8 and 7.9).

Colour flow mapping may reveal hyper- and neo-vascularity (Fig. 7.10).

Galactocele: Prominent and dilated mammary ducts seen as tubular hypoechoic structures which widen as they approach the nipple

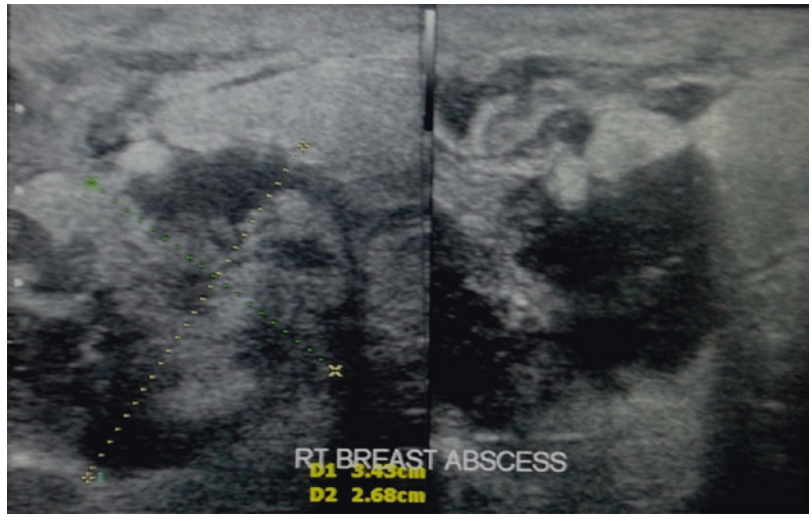

Fig. 7.5 Multiple hyperechogenic and hypoechoic areas in breast abscess with ill-defined margins

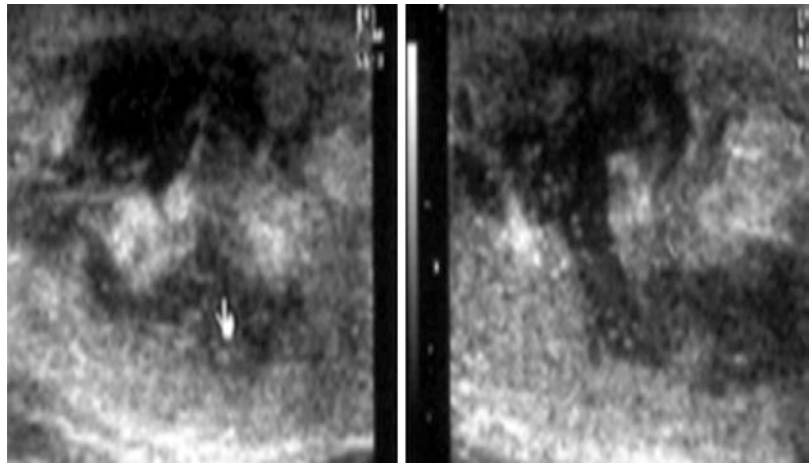

Fig. 7.6 Complex echotexture in breast abscess

Fig. 7.7 Irregular margins in breast carcinoma

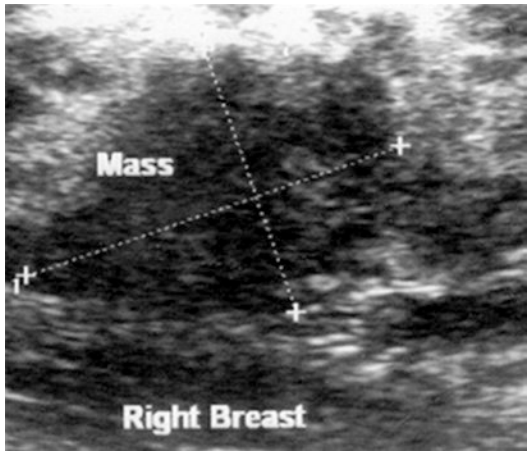

Fig. 7.8 Breast carcinoma with lobulated margins

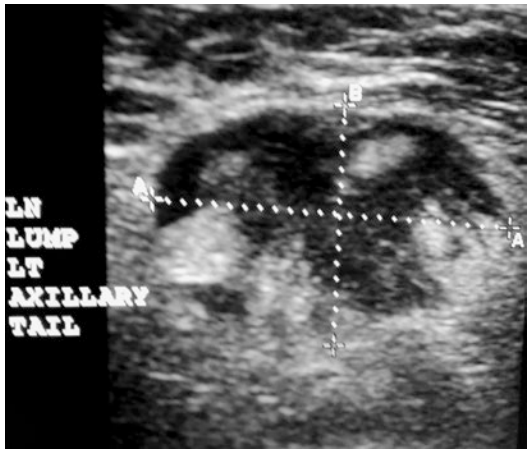

Fig. 7.9 Heterogenous texture of lump in axillary tail of left breast

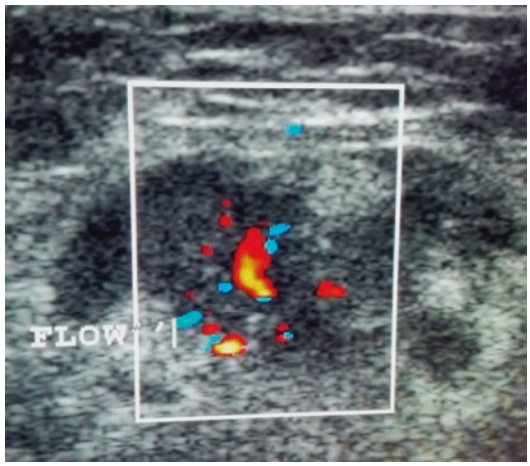

Fig. 7.10 Carcinoma of left breast with colour flow and heterogenous texture of mass

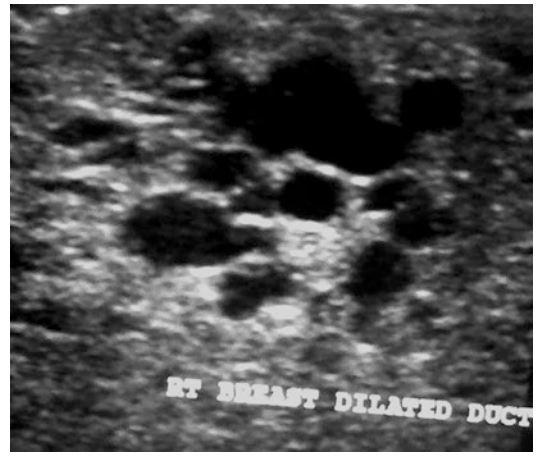

Fig. 7.11 Dilated lactiferous ducts 1 year after last delivery

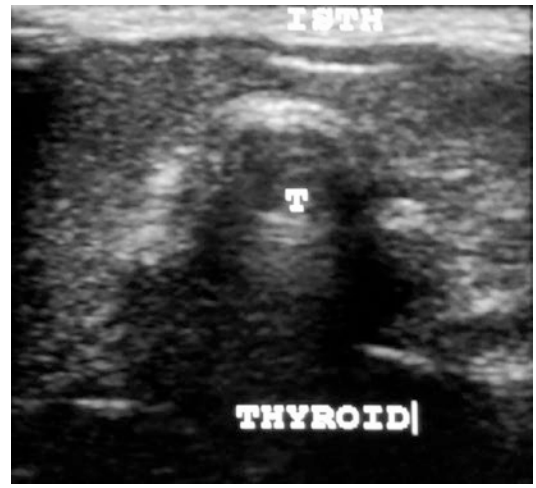

Fig. 7.12 Both lobes and isthmus of thyroid in coronal plane

(Fig. 7.11). It is also referred to as a lactocele. Majority of them have ultrasound appearance of cystic/multicystic lesion but may be solid also. They occur typically in young lactating women and are benign lesion (BI-RADS II).

7.2 Thyroid Gland

Size and shape of thyroid gland vary widely in normal patients. In adults the mean length of the lobe is about 40–60 mm and the mean thickness (AP diameter) is 13–18 mm. The mean thickness of the isthmus is 4–6 mm (Fig. 7.12). The AP

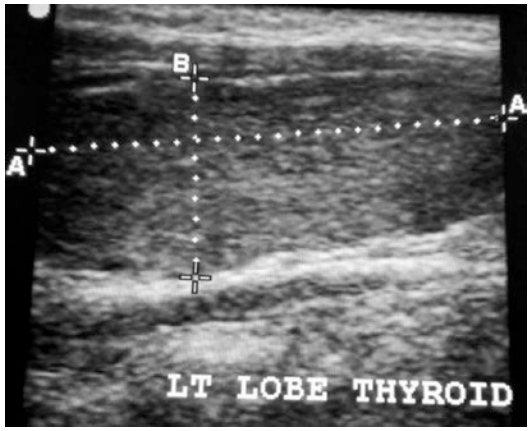

Fig. 7.13 Measurements of left lobe of thyroid

diameter of a lobe more than 2 cm suggests its enlargement [6]. Normal thyroid parenchyma has a homogenous medium- to high-level echogenicity (Fig. 7.13).

The most common application of USG thyroid is to differentiate between solid and cystic lesion (Figs. 7.14, 7.15, 7.16 and 7.17) and benign nodule from the malignant lesion. Occasionally haemorrhage in the cyst may be visualized (Fig. 7.18).

Colour Doppler application is quite useful in such situations. Also, USG guided aspiration cytology from a precise location is possible.

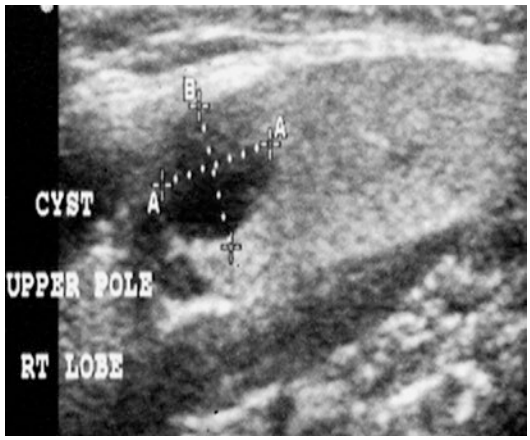

Fig. 7.14 Small cyst upper pole the right lobe of thyroid

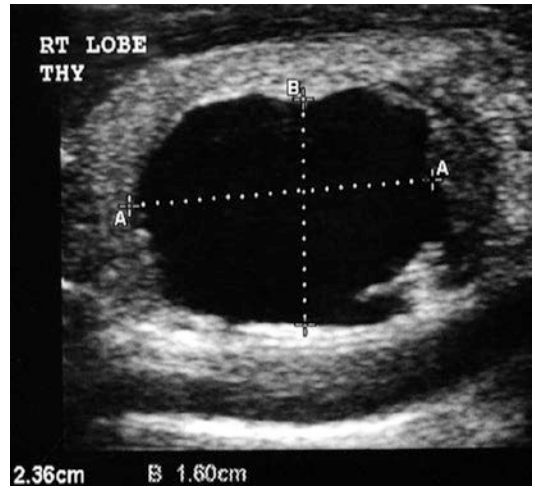

Fig. 7.15 Cystic lesion in the right lobe of thyroid

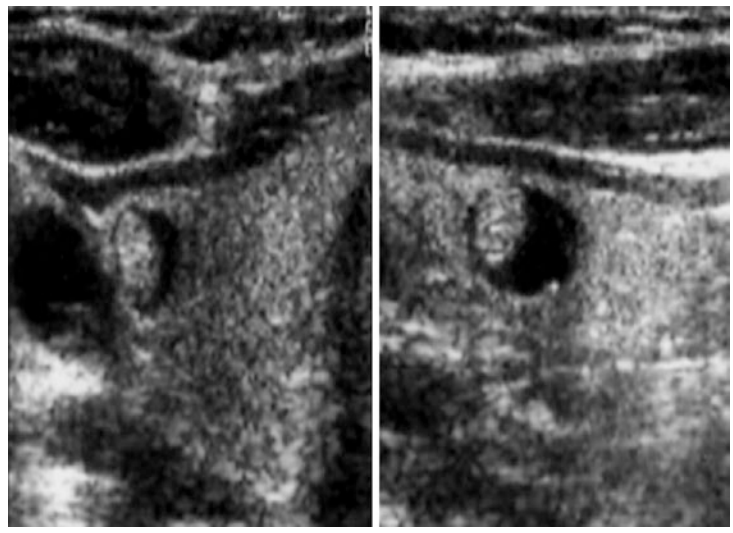

Fig. 7.16 Cystic lesion with solid nodule in the right lobe of thyroid

Diffuse enlargement of both lobes of thyroid with inhomogenous echogenicity of parenchyma is seen in sonography (Fig. 7.19). The isthmus of thyroid may be 1 cm or more in thickness.

A study [7] suggests that hypervascularity occurs when hypothyroidism develops (Fig. 7.20).

For differentiation of benign and malignant thyroid nodule, certain features which may be helpful are:

1. Purely cystic component is likely to be benign.
2. Cystic as well as hyperechogenic nodules may be benign/malignant.
3. Peripheral sonolucent halo in benign lesion.
4. Well-defined margins in benign, while irregular margins in malignant.
5. Peripheral or egg-shell calcification in benign lesion, while fine and punctuate calcifications in malignant.
6. Peripheral vascularity in benign and internal vascularity with/without peripheral component in malignant lesion.

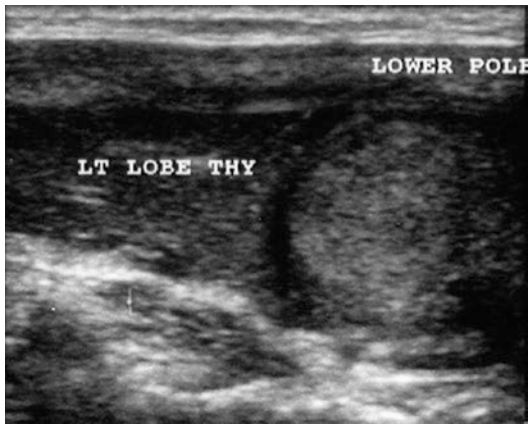

Fig. 7.17 Solid nodule in the left lobe of thyroid

Any nodule of >1.5 cm with sonographic features of irregular margin, microcalcifications, thick halo and internal flow pattern should undergo US-guided FNAC.

The normal parathyroid glands are difficult to image. However, the echogenicity of the majority of parathyroid adenomas is less than that of thyroid tissue. Thyroid adenomas are about 0.8–1.5 cm in size.

The thyroid and parathyroid glands are examined with patient in supine posture with neck extended by keeping a pillow beneath the shoulders and upper portion of back.

The superior parathyroid glands are located posterior to mid-portion of the thyroid, while the inferior parathyroid gland has variable position but is usually located near the caudal end of the lower pole of the thyroid. The parathyroid adenoma are 0.8–1.5 cm in size and may be as large

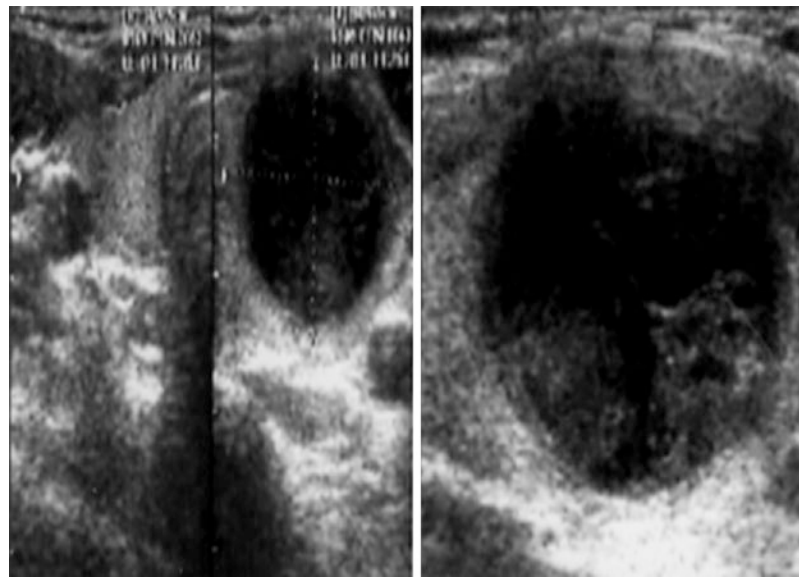

Fig. 7.18 Haemorrhagic cyst in the left lobe of thyroid

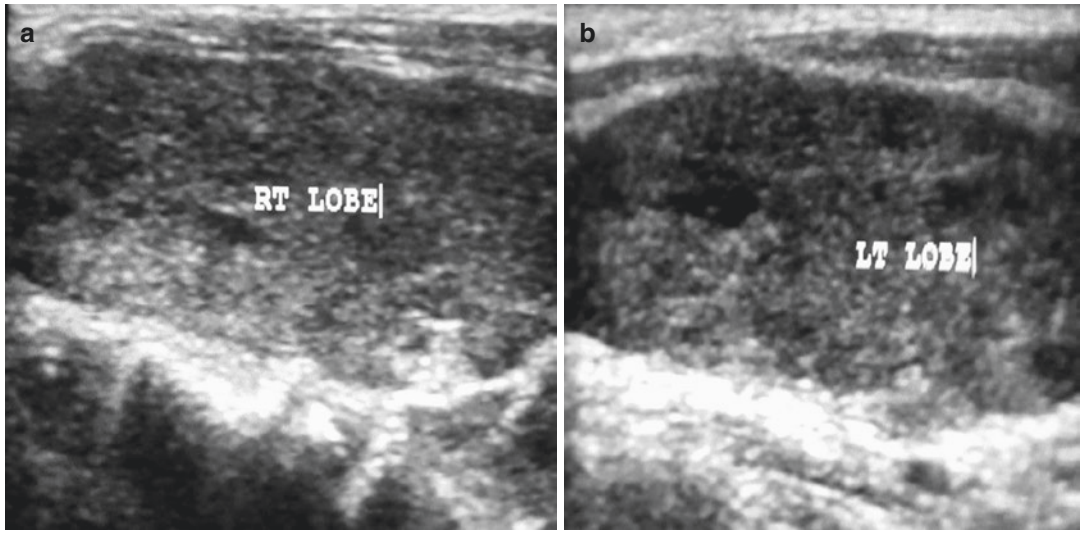

Fig. 7.19 (**a**, **b**) Coarse heterogenous texture of enlarged lobes of thyroid in chronic thyroiditis

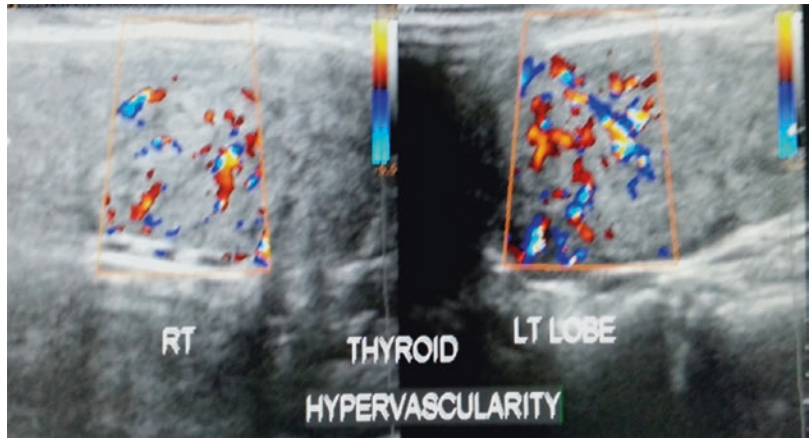

Fig. 7.20 Hypervascularity in thyroiditis

as 5 cm. FNA and PTH assay are valuable adjunct to ultrasound examination [6].

7.3 USG of the Salivary Gland

7.3.1 Parotid and Submandibular Gland

Parotid gland has superficial lobe anterior to tragus of the ear and the deep lobe underneath the angle of mandible (Fig. 7.21).

Submandibular gland is located below second molar tooth (Fig. 7.22).

High-frequency 7–14 linear probe is used. Colour Doppler is used to differentiate a vessel from dilated duct.

The commonest examination is done to detect mass (localization for intra-glandular or extra-glandular lesion), abscess and complications after mumps, which is more often seen in children. Abnormality seen in previous X-rays, CT or sialogram may be evaluated by sonography.

US-guided FNAC is usually done for cytologic diagnosis.

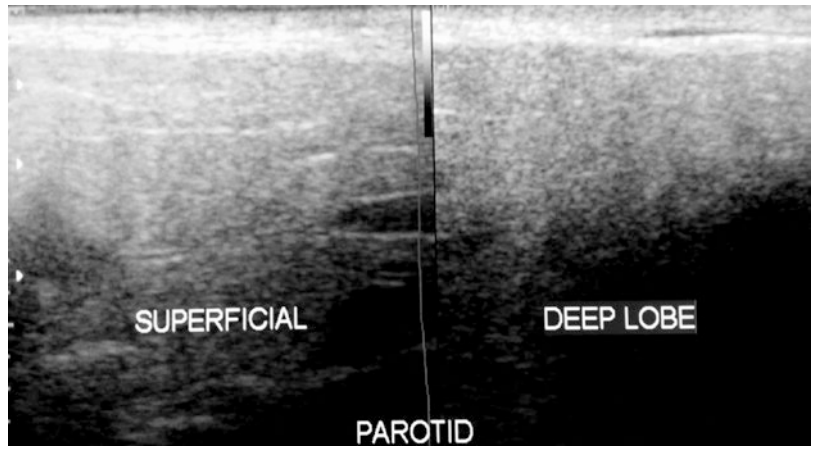

Fig. 7.21 Normal parotid gland

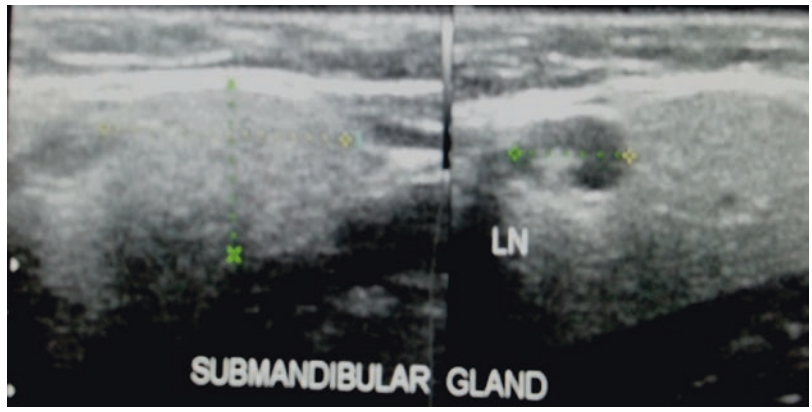

Fig. 7.22 Normal submandibular gland

7.4 Ultrasound of Scrotum

The adult testis measures 3–5 cm length × 2–4 cm width × 3 cm AP dimension. It has a homogenous granular echotexture (Fig. 7.23). The epididymis is 6–7 cm in length lying posterolateral to the testis. The mediastinum testis seen as a linear echogenic band extending craniocaudally within the testis (Fig. 7.24) provides support for the entering and existing testicular vessels and ducts [7].

Hydrocele. Serous fluid, blood, pus or urine may accumulate in the space between the parietal and visceral layer of the tunica vaginalis lining the scrotum (Figs. 7.25 and 7.26).

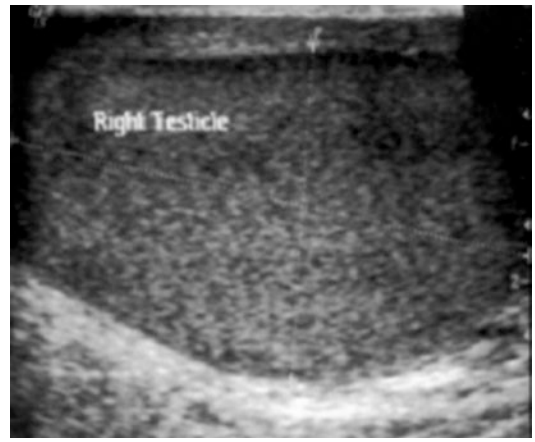

Fig. 7.23 Normal echogenicity of the right testes

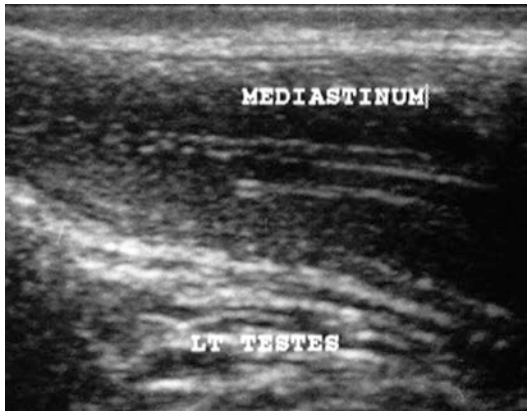

Fig. 7.24 Mediastinum testes seen as linear echogenic band

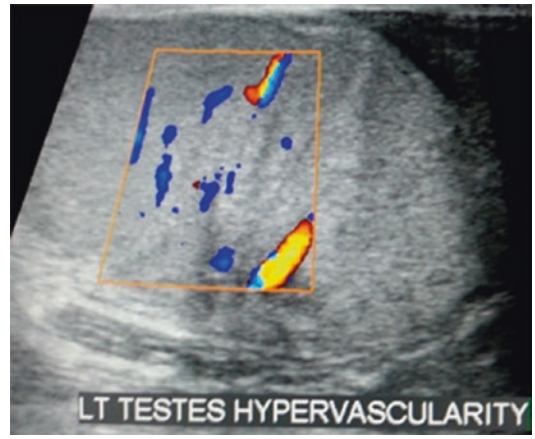

Fig. 7.26 Hypervascularity in testes in epididymo-orchitis

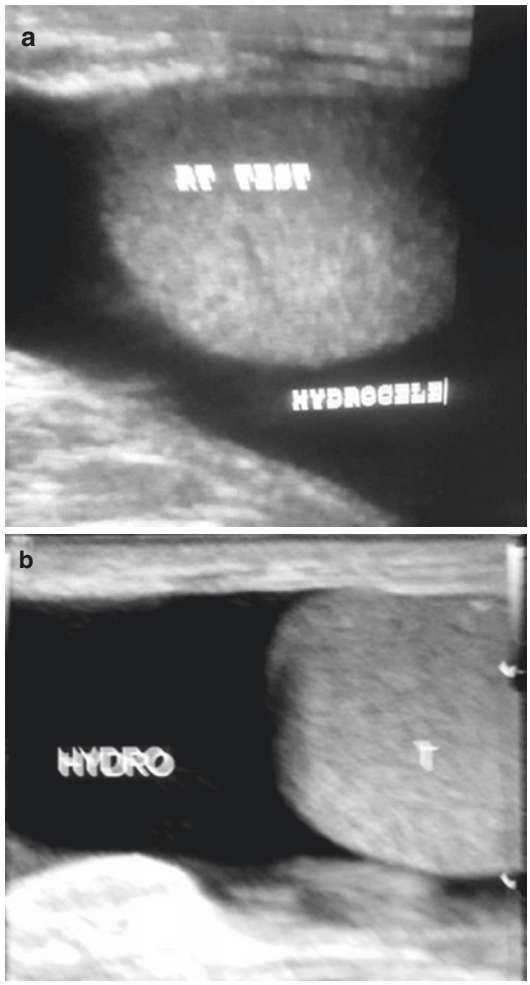

Fig. 7.25 (**a**) Hydrocele right (**b**) Hydrocele left

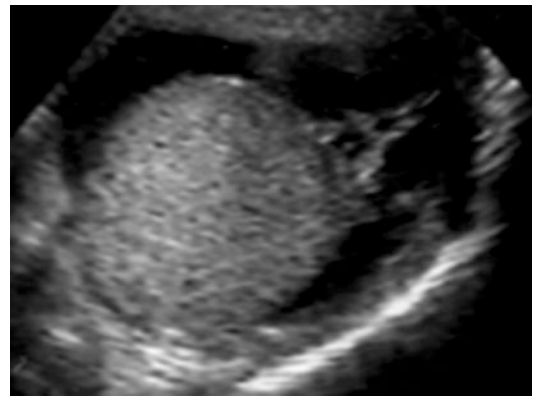

Fig. 7.27 Haematocele with septations in scrotal haematoma

Colour flow Doppler ultrasound usually demonstrates increased blood flow in the epididymis and/or testis (Fig. 7.26).

7.4.1 Haematoma Testis

Ultrasonography plays a profound role in early diagnosis of rupture, torsion and dislocation of testis as surgical intervention within 72 h after the injury increases the salvage rate and prevents ischaemic atrophy of the testis. US findings include haematocele, testicular rupture (break in tunica albuginea) and testicular haematoma (Fig. 7.27). Haematoma may mimic tumour; hence follow-up is recommended.

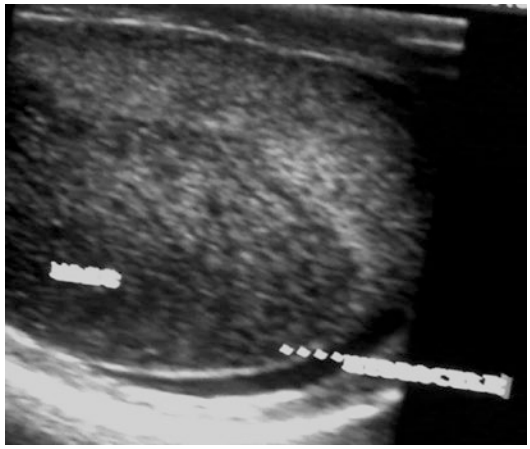

Fig. 7.28 Poorly defined growth (seminoma) in testes with small hydrocele

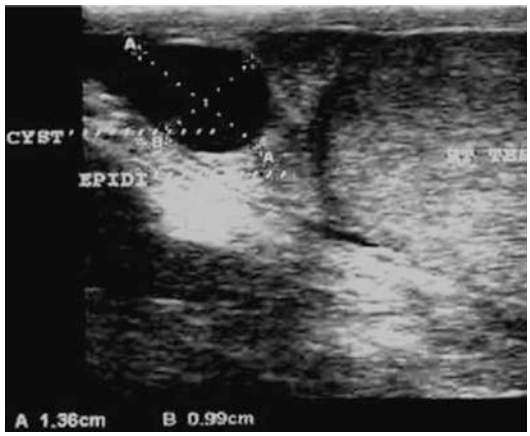

Fig. 7.29 Cyst in epididymis

Scrotal mass. USG plays a major role in the evaluation of scrotal masses because of its accuracy. Virtually all testicular masses should be considered malignant until proven otherwise (Fig. 7.28).

Cysts in epididymis or testis are discovered incidentally on ultrasound in 8–10% of the population (Fig. 7.29). The differentiation between a benign cyst and a cystic neoplasm is of utmost clinical importance [8].

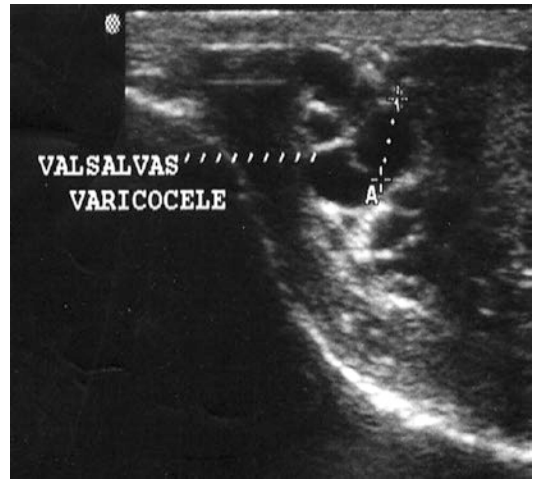

Fig. 7.30 Dilated veins within spermatic cord (varicocele) after Valsalva's manoeuvre

Varicocele is a collection of abnormally dilated, tortuous and elongated veins of the pampiniform plexus located posterior to testis accompanying the epididymis and vas deferens within the spermatic cord. Dilated veins measure more than 2 mm in diameter. The venous flow can be augmented by Valsalva's manoeuvre (Fig. 7.30) or patient in the upright position [9]. Colour Doppler sonography with low flow Doppler settings should be used. High resolution realtime sonography facilitate visualisation of varicocele [10].

Torsion of testis: The presence of normal or increased blood flow within testis in colour Doppler study excludes the diagnosis of acute torsion. Five hundred and forty degree of torsion is necessary to completely occlude testicular blood flow.

Epididymitis: Colour flow Doppler ultrasound demonstrates increased blood flow in the epididymis and/or testis as compared with the asymptomatic side.

Cryptorchidism: The undescended testis may be located anywhere along the pathway of its descent from the retro-peritoneum to the scrotum. The incidence varies 30% in premature

infants and 100% in neonates weighing less than 1 kg at birth.

7.4.2 Sonography of Inguinal Region

Inguinal sonography is useful in detecting the presence of intestine and/or omentum in a hernia sac (Fig. 7.31). Direct hernia is seen medial to inferior epigastric artery, whereas indirect hernia is seen lateral to the inferior epigastric artery.

A cystic lesion may be seen (Fig. 7.32) or an encysted effusion of spermatic cord (Fig. 7.33) or an encysted effusion with multiple septations (Fig. 7.34).

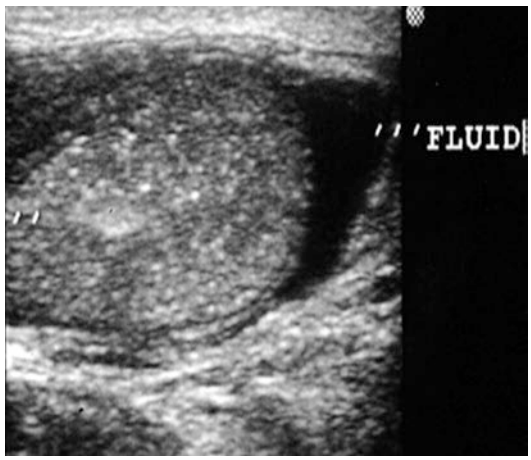

Fig. 7.31 Omental fat and fluid in inguinal hernia sac

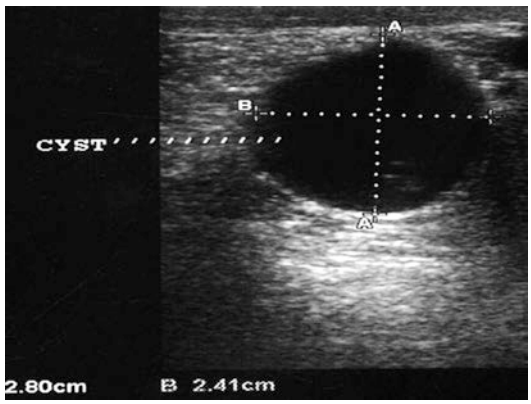

Fig. 7.32 Cystic lesion in right inguinal canal

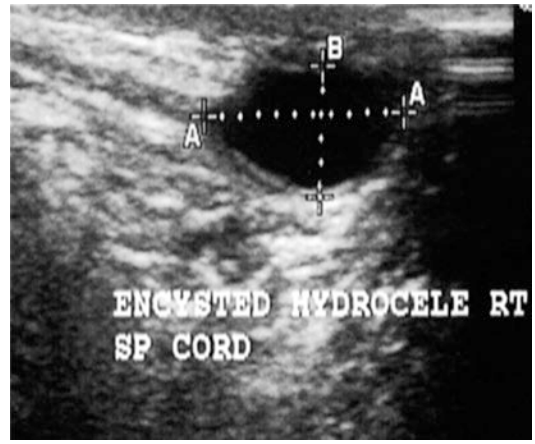

Fig. 7.33 Encysted hydrocele right spermatic cord

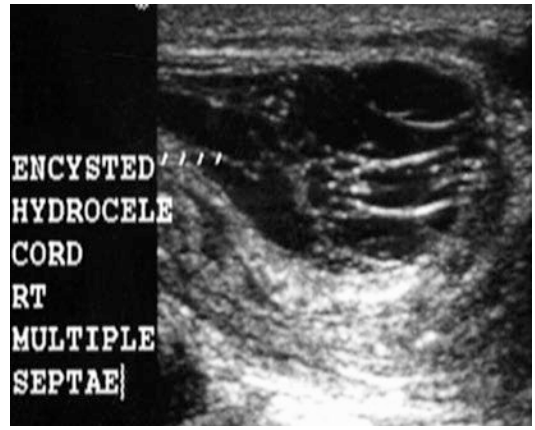

Fig. 7.34 Encysted hydrocele of spermatic cord with multiple septae

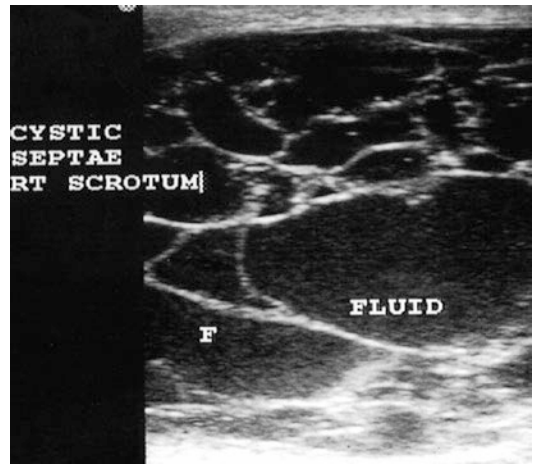

Fig. 7.35 Lymphangiectasis scrotal sac post-operative

Complications of inguinal herniorrhaphy include haematoma, hydrocele, epididymo-orchitis and disturbance of lymphatic drainage (Fig. 7.35).

References

1. Mendelson EB. The breast, Chap. 23. In: Diagnostic ultrasound, vol. 1. 2nd ed. Missouri: Mosby–Year Book; 1998. p. 751–62.
2. Jackson VP. Role of US breast imaging. Radiology. 1990;177:305–11.
3. Breast Imaging Reporting and Data System (BI-RADSTM). Reston: American College of Radiology; 1993. p. 15.
4. Jackson VP. Benign breast lesions. In: Bassett LW, Jackson VP, Jahan R, Fu YS, Gold RH, editors. Diagnosis of diseases of breast. Philadelphia: WB Saunders; 1997. p. 402.
5. Feig SA. The role of ultrasound in a breast imaging centre. Semin Ultrasound CT MR. 1989;10:90–105.
6. Gooding GA. Sonography of the thyroid and parathyroid. Radiol Clin N Am. 1993;31:967–89.
7. Lagalla R, Caruso G, Benza I, et al. Echo-color Doppler in the study of hypothyroidism in the adult (Ital). Radiol Med. 1993;86:281–3.
8. Krone KD, Carroll BA. Scrotal ultrasound. Radiol Clin North Am. 1985;23:121–39.
9. Hamn B, Fobbe F, Loy V. Testicular cysts: differentiation with ultrasound and clinical findings. Radiology. 1988;168:19–23.
10. Wolverson MK, Houttium E, Heiberg E, et al. High resolution real-time sonography of scrotal varicocele. AJR. 1983;141:681–4.

Neonatal Cranial Ultrasound

8

R.K. Diwakar

Abstract

The imaging of brain in neonates is done with 5–7.5 MHz probe placed on the anterior fontanel. Images are obtained in sagittal as well as coronal plane. Normal lateral ventricles are seen as a slitlike hypo-echogenic curved area anterior to the thalamus in sagittal plane. Haemorrhage in the germinal matrix of choroid plexuses or sub-ependymal location is seen as an area of increased echogenicity in premature infants. Ventriculomegaly (hydrocephalus), cerebral parenchymal solid/cystic lesion or calcifications can be identified.

8.1 Ultrasound of Neonatal Brain

Neuroimaging or transfontanellar neonatal brain scanning is an important test in the diagnosis of haemorrhage and other acquired and congenital brain pathologies of the newborn. It does not involve ionizing radiation and can be done without the problems of sedation. USG findings at different days of ultrasound examination of neonatal brain are shown in Table 8.1.

Table 8.1 Cranial USG findings in premature newborn

Day of USG scanning	USG findings
1	Normal
3–5	Haemorrhage
7	Periventricular leukomalacia
30	Cystic changes

The cranial ultrasound examination is performed with a linear array transducer. Six to eight coronal plane images are taken through the

R.K. Diwakar
Department of Radio-Diagnosis, C.C.M. Medical College & Hospital, Durg, Chhattisgarh, India
e-mail: rkdiwakar49@yahoomail.co.in

R.K. Diwakar (ed.), *Basics of Abdominal, Gynaecological, Obstetrics and Small Parts Ultrasound*,
https://doi.org/10.1007/978-981-10-4873-9_8

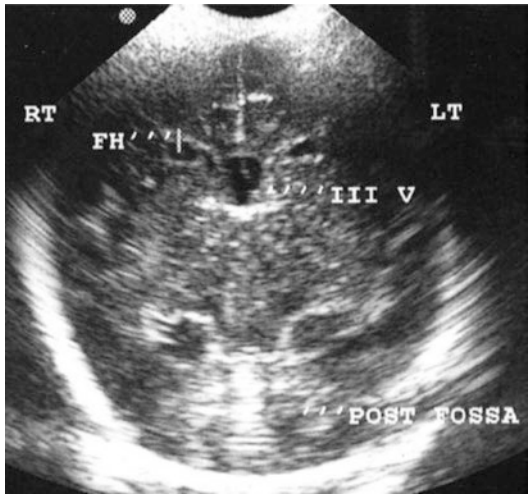

Fig. 8.1 Normal frontal horn, third ventricle, hippocampus and posterior fossa in axial scan

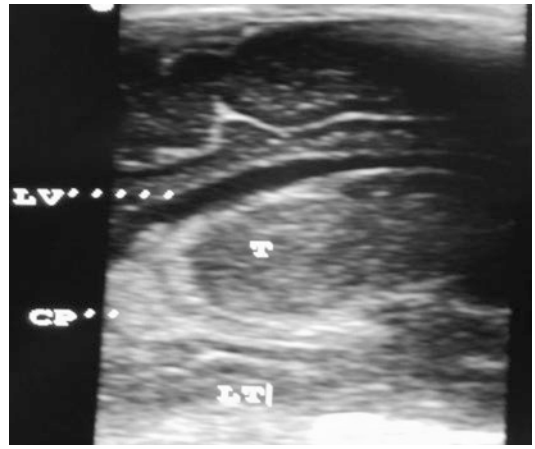

Fig. 8.3 Lateral ventricle (LV), choroid plexus (CP) and thalamus (T) in parasagittal image

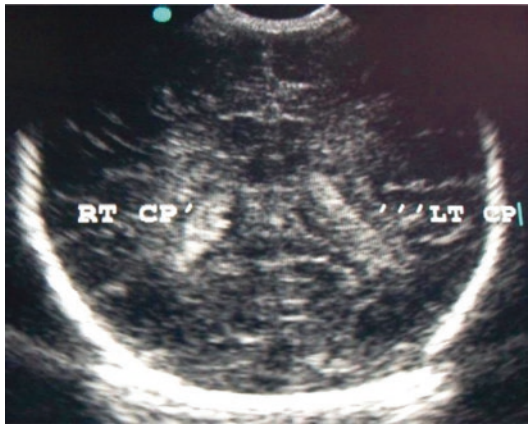

Fig. 8.2 Choroid plexus in lateral ventricles in coronal image

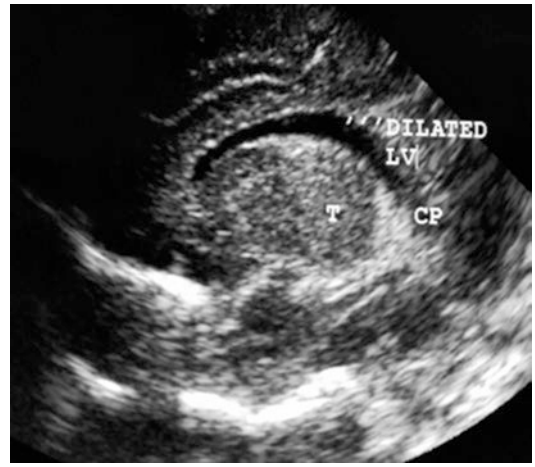

Fig. 8.4 Parasagittal image showing lateral venricle and thalamus with choroid plexus

anterior fontanel beginning in the frontal lobes anterior to the frontal horns and progressing posteriorly to the occipital lobes past the trigones of the lateral ventricles (Figs. 8.1 and 8.2) [1, 2].

Next, the transducer is turned 90° on the anterior fontanel, and five more images are acquired in the sagittal and parasagittal planes (Figs. 8.3 and 8.4).

The echogenic structures in the midline that form the choroid plexus and cerebellar vermis have an appearance that, with one's imagination, looks like a woman in a Victorian-era dress, the "lady in the dress" sign (Fig. 8.5) [1].

Mastoid or posterior fontanels are also used for improved visualization of posterior fossa.

Sub-ependymal/germinal matrix haemorrhage is seen in caudo-thalamic notch (CTN) (Fig. 8.6).

Up to 40 weeks of gestational age, the Levene index should be used for ventricular measurement [3].

After 40 weeks, the ventricular index (Fig. 8.7) should be used, i.e. the ratio of the distance between the lateral sides of the ventricles and the biparietal diameter in axial plane (7/2.6 = 2.7).

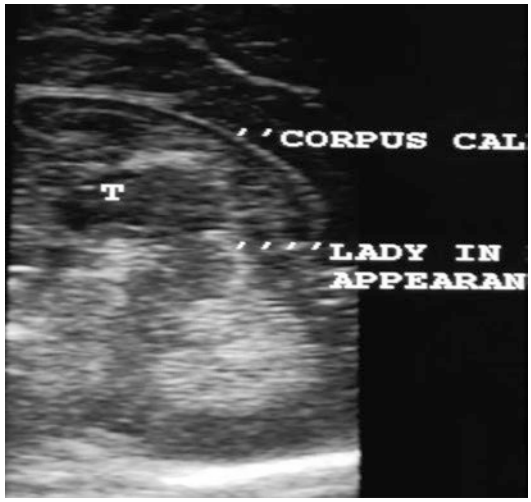

Fig. 8.5 Lady-in-the-dress appearance in coronal plane

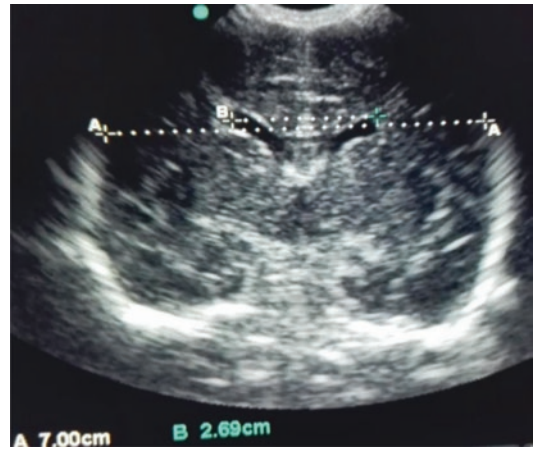

Fig. 8.7 Measurements for ventricular index in coronal image

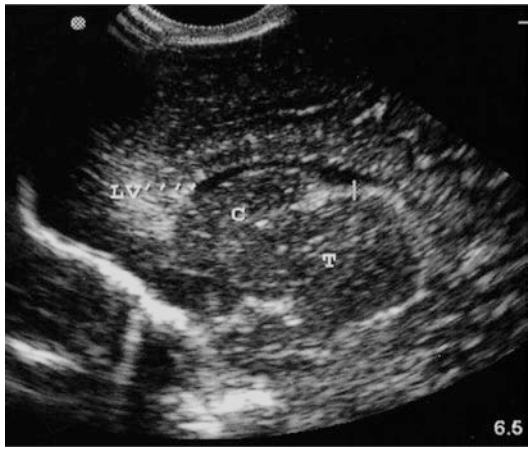

Fig. 8.6 Normal caudo-thalamic notch (I), caudate nucleus (c), thalamus (T), lateral ventricle (LV)

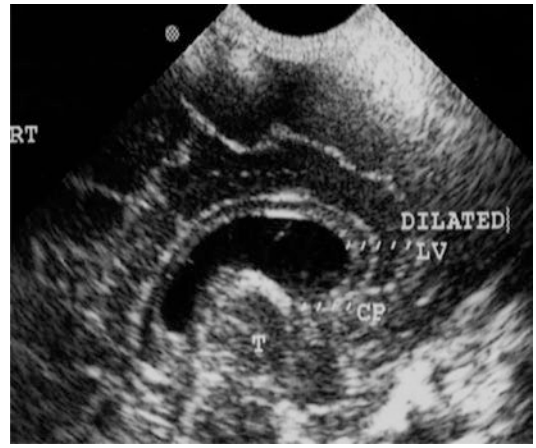

Fig. 8.8 Mildly dilated right lateral ventricle in a newborn of 32 weeks of GA

Ventricular diameters/hemispheric diameters ≤ 1/3 (Figs. 8.8, 8.9, 8.10, 8.11, 8.12, 8.13).

Cranial USG findings in HIE or periventricular leukomalacia in premature newborn born at less than 33 weeks of gestation and less than 1500 g birth weight.

Grades of PVL

Grade 1—Increased periventricular echogenecity persisting more than 7 days

Grade 2—Development of small periventricular cysts resulting in "Swiss-cheese"-like appearance of the parenchyma

Grade 3—Extensive cysts in periventricular, occipital and fronto-parietal region

Grade 4—Cysts in deep white matter and subcortical region

A value of 0.6–0.9 is used to estimate a normal RI in premature and full-term infants. Lower values may indicate acute hypoxia or ischaemia while higher values may suggest cerebral swelling [4].

Intracranial haemorrhage (ICH) is the leading cause of serious mortality and morbidity in the premature neonate of less than 32 weeks of gestational age. It has been divided into four grades:

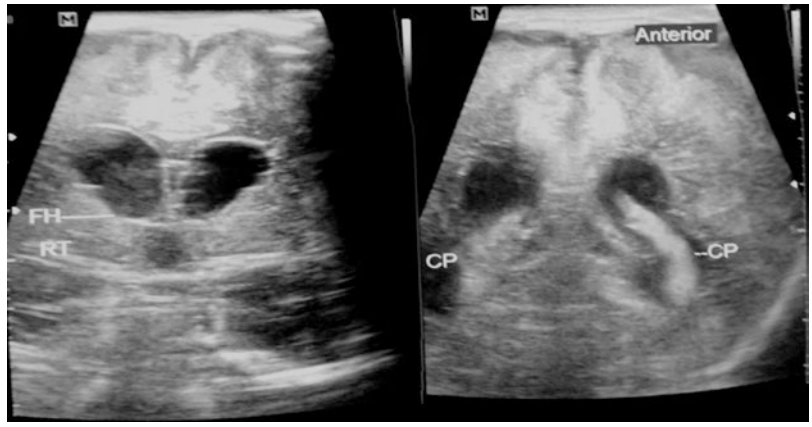

Fig. 8.9 Choroid plexuses visualized in atria of lateral ventricles in the presence of hydrocephalus

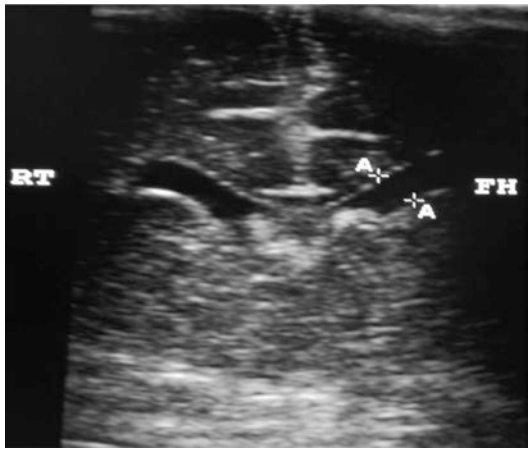

Fig. 8.10 Choroid plexus/haemorrhage in frontal horn in a premature (32 weeks of GA) newborn

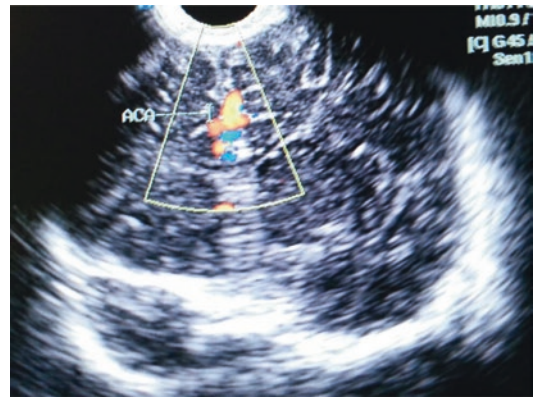

Fig. 8.12 Colour flow in anterior cerebral artery

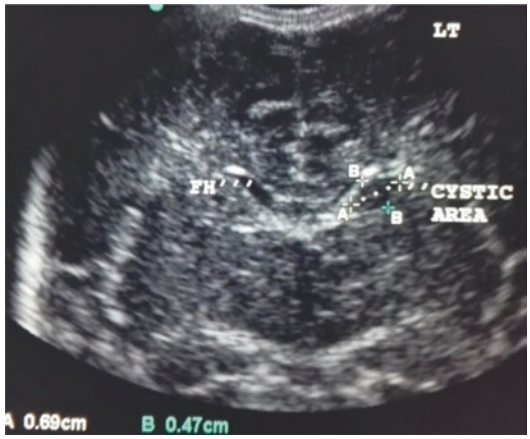

Fig. 8.11 Cystic area (venous infarction) postero-lateral to left frontal horn in a premature newborn

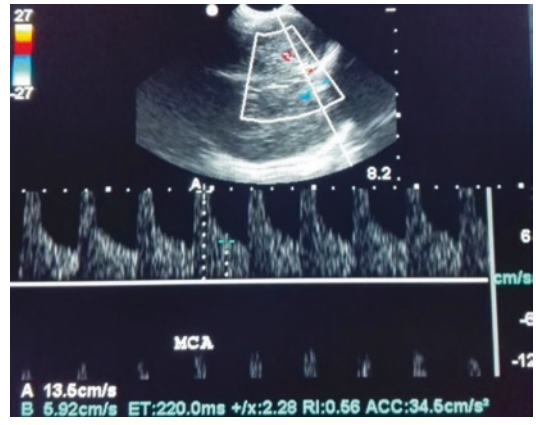

Fig. 8.13 Normal waveform MCA in a newborn of 31 weeks of gestational age

Grade I—Sub-ependymal germinal matrix haemorrhage
Grade II—Germinal matrix haemorrhage and intraventricular haemorrhage without ventricular dilatation
Grade III—Germinal matrix haemorrhage and intraventricular haemorrhage with ventricular dilatation
Grade IV—Intraparenchymal haemorrhage and intraventricular haemorrhage (IVH)

The germinal matrix is highly susceptible to hypoxic damage. It is located infero-lateral to the frontal horns at a level just posterior to the foramen of Monro. The haemorrhage may occur unilaterally or bilaterally.

The IVH is seen as bright echoes within the ventricle and may be difficult to identify in the absence of ventricular dilatation.

The haemorrhage, as it resolves, may lead to cyst formation.

Hypoxic–Ischaemic Encephalopathy (HIE)
In preterm infant, germinal matrix–intraventricular haemorrhage is the most common manifestation of hypoxic brain injury. Significant ischaemic component may result in infarction. Periventricular leukomalacia and haemorrhage are the primary manifestations of HIE in premature infant.
Anomalies of the posterior brain such as Dandy Walker and Dandy Walker variants may be seen.

Chiari Malformation
Type I—It consists of inferior displacement of tonsil and cerebellum without displacement of fourth ventricle or medulla.
Type II—It includes a small posterior fossa, elongation of pons and fourth ventricle and downward displacement of medulla, fourth ventricle and cerebellum into the cervical spinal canal. Spina bifida and meningomyelocele are the associated findings.

Limitations of Cranial USG
1. Limited overview in posterior fossa and convexity of the brain
2. Absence of US signs in ischaemia in full terms in the first 24 h
3. Difficulty in detecting migration disorders, cortical dysplasia

See better with sound, use colour to improve images, explore the third and fourth dimension, practise better medicine with better images and scan the patient yourself in a difficult case.

References

1. Traci BF. Sonography of the neonatal brain. J Diagn Med Sonogr. 2009;25:331–48.
2. Lisa HL, Zachary B. State-of-the-art cranial sonography: part 1, modern techniques and image interpretation. AJR. 2011;196(5):1028–33.
3. Levene MI. Measurement of the growth of the lateral ventricles in preterm infants with real-time ultrasound. Arch Dis Child. 1981;56(12):900–4.
4. North K, Lowe L. Modern head ultrasound: normal anatomy, variants and pitfalls that may simulate disease. Ultrasound Clin. 2009;4:497–512.

9 Ultrasound-Guided Biopsy, Aspiration and Fine Needle Aspiration Cytology

M.K. Dwivedi

Abstract

Ultrasound-guided percutaneous biopsy, drainage of abdominal abscess and aspiration of cyst and fluid have become routine diagnostic procedures nowadays. It is an accurate, safe and widely accepted cost-effective technique for management of superficial as well as deeply located solid or cystic masses.

9.1 US-Guided Biopsy and Aspiration and Drainage of Abscess and Cyst

Ultrasonography is preferred for guided procedures because of the availability of portable machine. It is relatively inexpensive and uses no ionising radiation. Real-time ultrasound provides guidance in multiple planes, i.e. longitudinal, transverse or oblique.

The real-time visualisation of needle into target area through tissue planes avoiding important intervening vascular structures is the greatest advantage. Colour Doppler may be used to avoid puncture of major blood vessels such as inferior vena cava and portal vein [1].

Downey et al. have shown an accuracy as high as 91% for US-guided biopsy of small (<2.5 cm) abdominal masses [2].

A variety of needle with broad-spectrum calibres, lengths and tip designs are commercially available for use in percutaneous biopsy [3].

Modalities such as sonography and CT allow for precise needle placement for superficial and deep abdominal fluid collection or abscesses [4].

Although rare, haemorrhage is the most common complication of solid organ biopsy. Nolsoe et al. [5] found a major complication rate of 0.187%.

Informed consent should be obtained, and the patient should be under observation for 1–2 hours after the procedure. Biopsy in deep structures requires special attention to coagulation indices.

Uncorrected coagulopathy, a major contraindication for needle biopsy, is to be assessed from the patient's medical history [6].

M.K. Dwivedi
Department of Radio-Diagnosis, C.C.M. Medical College & Hospital, Durg, Chhattisgarh, India
e-mail: mahendra_van@yahoo.com

R.K. Diwakar (ed.), *Basics of Abdominal, Gynaecological, Obstetrics and Small Parts Ultrasound*,
https://doi.org/10.1007/978-981-10-4873-9_9

References

1. Longo JM, Bilbao JI, Barettino MD, et al. Percutaneous vascular and nonvascular puncture under US guidance: role of colour Doppler imaging. Radiographics. 1994;14:959–72.
2. Downey DB, Wilson SR. Ultrasonographically guided biopsy of small intra-abdominal masses. Can Assoc Radiol J. 1993;44:350–3.
3. Hagga JR, LiPuma JP, Bryan PJ, et al. Clinical comparison of small and large calibre cutting needles for biopsy. Radiology. 1983;146:665–6.
4. Mcgahan JP, Hanson F. Ultrasonographic aspiration and biopsy techniques. In: Dublin AB, editor. Outpatient invasive radiologic procedures: diagnosis and therapeutic. Philadelphia: WB Saunders; 1989. p. 79–113.
5. Nolsoe C, Nielson L, Torp-Pederson S, et al. Major complications and deaths due to interventional ultrasonography: a review of 8000 cases. J Clin Ultrasound. 1990;18:179–84.
6. Rapaport SI. Preoperative hemostatic evaluation: which tests, if any? Blood. 1983;61:229–31.

Appendix A

Points to Remember

1. A-mode: Peaks and distances, used in ophthalmic scanner.
2. B-mode: Two-dimensional images in which the echo amplitude is depicted as dots of different brightness.
3. Real time: Shows movement as it occurs.
4. M-mode: Shows movement as a function of time; used in cardiac scanning.
5. Doppler: Demonstrates and measures blood flow.
6. Colour Doppler: Shows different flow velocities in different colours.
7. Know the equipment and the use of its control and read instructions in the manual.
8. Keep in view the gain setting, the use of the thick layer of ultrasound jelly, the proper preparation of the patient such as empty stomach, good distension of urinary bladder or empty urinary bladder for transvaginal sonography.
9. Make yourself familiar with the artefacts and the manoeuvre to avoid them to obtain clear image.
10. Use the probe of proper frequency according to patient body habitus or the ultrasound examination.
11. Fluid-filled structures such as distended urinary bladder, portal vein and IVC should be seen black with proper TGC setting.
12. Develop good knowledge and orientation of normal ultrasound anatomy of abdominal and pelvic organs and important landmarks by scanning normal individuals.
13. In case GB, kidney etc. are not visualised properly due to colonic gases/faecal matter, change the patient position or do the scanning in sitting/standing posture.
14. Avoid giving opinion in GB pathology if the patient has not done overnight fasting. If the problem still persists, the patient may be asked to have fat-free diet for 24–48 h and the repeat examination of GB should be done.
15. If renal sonography is done on the posterior aspect of the body, do not comment on the echogenicity of the renal cortex.
16. To make a correct diagnosis, scanning should be done in multiple planes to allow enough information.
17. Diagnosis of hepatomegaly may not be accurate; be careful in commenting on it if the AP measurement of the right lobe of the liver in the mid-clavicular line is 14 cm or less than that.
18. Liver cirrhosis is not excluded even if the US scan of the liver appears normal.
19. Differentiation of liver abscess, haematoma, metastasis or lymphoma may not be easy on US examination.
20. Aspiration of hydatid cyst may be dangerous. Avoid it.
21. GB stones may be asymptomatic (silent stones); rule out other existing diseases.
22. Ultrasound is not reliable in recognising stones in the bile ducts especially when they are not dilated.
23. Ultrasound is very useful in differentiating between obstructive and nonobstructive jaundice.

R.K. Diwakar (ed.), *Basics of Abdominal, Gynaecological, Obstetrics and Small Parts Ultrasound*,
https://doi.org/10.1007/978-981-10-4873-9

24. Imaging of the pancreas may be difficult in a seriously ill patient. In blunt abdominal trauma, tear in the liver/spleen may not be reliably identified, affecting the reliability of the examination; hence, go for CT/MRI.
25. Ultrasound cannot distinguish between ascites, blood, bile or pus; hence aspiration should be advised.
26. Feeding 2–3 h before abdominal USG should be avoided to have a good distension of GB in neonates and infants.
27. Experience is needed to diagnose hypertrophic pyloric stenosis and intussusceptions.
28. Renal pyramid may appear prominent in small children and thin adults.
29. Make sure that both the poles of the kidneys have been clearly visualised.
30. Ureteric calculi may not be seen if there is no dilatation of ureters; always advice X-ray KUB in a suspected case of nephrolithiasis.
31. Function of the kidney cannot be evaluated by US.
32. Failure to see adrenals does not exclude abnormality; use CT/MRI.
33. Search the entire abdomen to look for ectopic kidney when the kidney is not visualised on any sides in its normal location.
34. Inadequate distension of UB may restrict proper evaluation of the pelvic organs; ask the patient to take 2–3 glasses of water and then do the US.
35. Endovaginal sonography may be misleading if the operator is not well trained.
36. A small carcinoma of the cervix cannot be recognised by ultrasound.
37. Ovarian cystic lesion with nodules is likely to be malignant.
38. Obstetric ultrasound need not be performed on every antenatal visit.
39. Pelvic US can pick up 6 weeks pregnancy and TVS of 5 weeks pregnancy at the earliest.
40. Foetal heart activity is demonstrated at/after 8 weeks pregnancy.
41. Inform the patient about variations in gestational age estimate and EDD.
42. Make sure that the table used for the assessment of gestational age is appropriate for your patient and not derived from some quite different population.
43. When in doubt, serial measurements should be made with at least 2 or 3 weeks interval.
44. In symmetric growth retardation, all measurements are reduced, while in asymmetrical IUGR, abdominal circumference is less than normal.
45. In suspected IUGR, interval growth should be assessed after 2 or 3 weeks.
46. CRL measurement in early pregnancy, if available, should be used to define gestational age and for EDD.
47. Anomaly scan should be done at 18–20 weeks of gestation.
48. Shortening of femur length should be kept in view if both ends of the bone are not included in the image.
49. Caution should be exercised when making a difficult diagnosis of microcephaly.
50. Oligohydramnios is a poor prognostic feature when there is foetal renal anomaly because it is associated with pulmonary insufficiency.
51. Overdistension of the bladder can sometimes produce a false impression of placenta praevia; hence, repeat the examination after partial emptying of the bladder.
52. In early pregnancy, placenta covering the internal os does not necessarily mean placenta praevia as the placenta moves upwards with the enlargement of the uterus subsequently.
53. Usually two ultrasound scans are required for good antenatal care.
54. In twin pregnancy, two sacs separated by a membrane rule out possible conjoined twins.
55. Two placentae may be difficult to demonstrate especially in late stages of twin pregnancy.
56. Ultrasound is not a reliable way to exclude a parathyroid tumour.
57. A large thyroid with internal calcifications may or may not be malignant.
58. US-guided needle punctures should be carried out in strictly sterile conditions.
59. In US-guided aspiration, make sure to see the tip of the needle and not the entire length of the needle.
60. Avoid making overdiagnosis in overenthusiasm.

Appendix B

Measurements and Formulae for Calculations

1. Menstrual age = From first day of LMP
2. GA By GS MSD = MSD in mm + 30
3. Trophoblastic reaction ≥ 2 mm
4. GA By CRL = CRL in cm + 6.2
5. Yolk sac = 3–7 mm diameter
6. Amniotic fluid (MVP) = 3–5 cm
7. Amniotic fluid index = 5–8 cm
8. Cephalic index = BPD/OFD × 100
9. Atrial width ≤ 10 mm + 2 SD
10. Nuchal translucency = 3 mm
11. Interocular distance = 7–8 mm (18–20 weeks GA)
12. Depth of cisterna magna ≥ 10 mm
13. Hepatomegaly ≥ 13 cm in AP RT lobe in MCL
14. PV diameter = 12–15 mm
15. CBD AP diameter = 2–3 mm
16. Spleen = 11 × 7 × 4 cm
17. Splenic vein diameter = 2–3 mm
18. Aortic diameter = 19–22 mm
19. Pancreas
    head ≤ 3.5 cm (AP diameter)
    body ≤ 3 cm
    tail = 2.5 cm
20. Kidney = 10–12 cm (*L*) × 4–6 cm (*w*)
21. Volume of UB, ovaries = *L* × *W* × AP × 0.52
22. Bladder wall thickness = 3 mm (distended UB), 5 mm (empty)
23. Prostatic volume (weight) = *L* × *W* × AP × 0.52 (mL/g)
24. Uterus (adult) = 8 cm (*L*) × 5 cm (*W*) × 4 cm (AP)
25. Ovary volume
    =5.5–10 cm^3 (premenopausal)
    =2.5–3.5 cm^3 (postmenopausal)
26. Endometrial thickness
    ≤15 mm (premenopausal)
    ≤8 mm (postmenopausal)
27. IUD to fundus distance = 2 cm